بسم الله الرحيم

In the name of Allah,
the Most Beneficent,
the Most Merciful

Development of Mathematical Models for Peristalsis with Rheological Characteristics

QUAID-I-AZAM UNIVERSITY

By

Syed Irfan Shah

Department of Mathematics
Quaid-I-Azam University
Islamabad, Pakistan
2016

Development of Mathematical Models for Peristalsis with Rheological Characteristics

By

Syed Irfan Shah

Supervised By

Prof. Dr. Tasawar Hayat

Department of Mathematics
Quaid-I-Azam University
Islamabad, Pakistan
2016

Development of mathematical models for peristalsis with rheological characteristics

By

Syed Irfan Shah

A THESIS SUBMITTED IN THE PARTIAL FULFILLMENT OF THE REQUIREMENT

FOR THE DEGREE OF

DOCTOR OF PHILOSOPHY

IN

MATHEMATICS

Supervised By

Prof. Dr. Tasawar Hayat

Department of Mathematics
Quaid-I-Azam University
Islamabad, Pakistan
2016

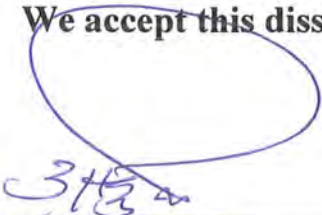# Development of mathematical models for peristalsis with rheological characteristics
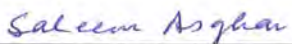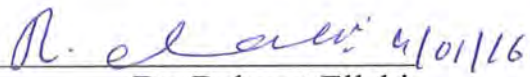
By

Syed Irfan Shah

CERTIFICATE

A THESIS SUBMITTED IN THE PARTIAL FULFILLMENT OF THE REQUIREMENTS FOR THE DEGREE OF THE DOCTOR OF PHILOSOPHY

We accept this dissertation as conforming to the required standard

1. _____
Prof. Dr. Tasawar Hayat
(Chairman)

2. _____
Prof. Dr. Tasawar Hayat
(Supervisor)

3. _____
Prof. Dr. Saleem Asghar
(External Examiner)

4. _____
Dr. Rahmat Ellahi
(External Examiner)

Department of Mathematics
Quaid-I-Azam University
Islamabad, Pakistan
2016

DEDICATED
TO

MY LOVING PARENTS

&

MY SUPERVISOR, PROF. DR. TASAWAR HAYAT

Acknowledgement

My special thanks is for **Dr. Mazhar Husain**, Head Department of Science and Humanities NU-FAST Islamabad for being my well wisher in whole course of journey.

My sincerest thanks goes to **Dr. Sabir Ali Shehzad, Dr. Fahad Munir Abbasi, Dr. Qamar Hussain, Dr. Humaira Yasmin** and **Dr. M. Farooq** for their valuable suggestions and prolific discussions.

I feel obligated to pay great debt of thanks to my dear family members specially my **parents** and my **wife** whose intellectual and moral support enabled me to achieve my goals. I look forward for their love and support in future.

Lastly, I offer my regards and blessings to all of those who supported me in any respect during the completion of thesis.

Syed Irfan Shah

Preface

In recent years the study of peristalsis of non-Newtonian fluids has attracted the attention of many investigators due to its extensive applications in engineering and physiology. The non-Newtonian fluids do not obey the Newton's law of viscosity and cannot be described by using the Navier-Stokes equations. Therefore, various constitutive equations have been proposed due to the diversity in the physical structure of non-Newtonian fluids. Most of them are empirical or semi-empirical and give rise to equations which are much more non-linear, higher order and more complicated than the Navier-Stokes equations. Peristaltic flows are of fundamental importance in processes such as swallowing food through the esophagus, vasomotion of small blood vessels such as arterioles, venues and capillaries, bile flow from the gall bladder into the duodenum. urine transport from kidney to the bladder through the ureter etc. Devices like roller and finger pumps are also operated on the principle of peristaltic pumping that are used to pump corrosive fluids, slurries, blood and foods in order to avoid their direct contact with the machinery. The design of many modern medical devices are also based upon the principle of peristaltic pumping for instance one may consider the blood in the heart-lung machine. Peristaltic flows with heat transfer analysis have vital role especially in chemical engineering processes. In physiology, the heat transfer is used to analyze the properties of tissues. Radio frequency therapy is helpful in the treatment of diseases like tissue coagulation, the primary living cancer, the lung cancer and the reflux of stomach acid. Moreover heat transfer analysis is also significant in hemodialysis and oxygenation processes. Magnetohydrodynamic fluid flow in a channel/tube with elastic and rhythmically contracting walls is of great interest with certain problems of the movement of conductive physiological fluids and for operating peristaltic MHD compressor. Flows in presence of magnetic field are significant in MHD power generators, MHD pumps and accelerators etc. Specific examples in this direction may include flow of nuclear fuel slurries, flow of liquid metals and alloys, flow of plasma, flow of mercury amalgams, lubrications of heavy oils and greases. In medical sciences the effect of magnetic field is used in the development of magnetic devices for cell separation, magnetic wounds and cancer tumor treatment, reduction of bleeding during surgeries. However, very little has

been reported yet on the peristaltic flows in the presence of magnetic field with Hall effect. Such effect cannot be over looked when flow subject to high magnetic field is considered. Hall effect can be taken into account when the Hall parameter (the ratio between the electron-cyclotron frequency and the electron-atom-collision frequency) is high. This happens, when the magnetic field is high or when the collision frequency is low. Also the current trend in the application of magnetohydrodynamics is towards a strong magnetic field, therefore one has to consider the influence of Hall current as it has great effect on the magnitude and direction of the current density and consequently on the magnetic-force term. However it is noted that scarce literature is available for MHD peristaltic flow of non-Newtonian fluids with Hall effect. Motivated by all such facts we structure the present dissertation as follows:

In chapter one we presented some definitions, fundamental equations and existing literature review regarding peristaltic flow in various flow configurations.

Chapter two discusses the peristaltic flow of Johnson Segalman fluid with nanoparticles. Johnson Segalman fluid is useful for explaining 'spurt' phenomenon. Experimentalists associate 'spurt' with slip at wall. The problem is first non-dimensionalized and then solved by homotopy perturbation method (HPM) under long wavelength and low Reynolds number approximation. A net flow due to the travelling wave is obtained up to second order approximation. The results of this chapter are published in **Journal of Aerospace Engineering 27 (2013) 404-413.**

The influence of heat and mass transfer on peristaltic flow of Jeffrey six-constant fluid with nanoparticles in an asymmetric channel has been discussed in chapter three. Asymmetry in the flow is induced by sinusoidal wave with different amplitudes and phases. Flow is induced by peristaltic wave along the length of channel walls. The analysis for axial velocity, pressure gradient and stream functions are carried out under lubrication approximation. The resulting non-linear equations are then solved for the series solutions. Graphical results are obtained to see the effect of various parameters of interest. The contents of this chapter have been submitted in **"Meccanica".**

Chapter four investigates the effect of velocity slip on the peristaltic transport of Powell-Eyring fluid. Powell-Eyring fluid model deserves attention due to the fact that its stress constitutive relation is deduced from kinetic theory of liquids rather than the empirical

relation as in the case of power-law model. It also correctly reduces to Newtonian model for high shear rate. The channel is assumed symmetric. The governing equations are presented in a wave frame. Solutions for stream function and pressure gradient are derived by employing long wavelength and low Reynolds number assumptions. It is found that the magnitude of shear stress decreases for velocity slip parameter. The contents of this chapter are published in **Applied Bionics and Biomechanics 11(2014) 69-79.**

Chapter five discloses the effect of Hall current on peristaltic flow of an electrically conducting Powell-Eyring fluid. The motion is induced by a sinusoidal wave traveling along the flexible walls of the channel. The flow is analyzed in a wave frame of reference moving with the velocity of wave. The equations governing the flow are solved by adopting lubrication approach. Series solution for stream function and axial pressure gradient are obtained. Impact of rheological parameters, Hartman number and Hall parameter on the flow quantities of interest are analyzed. It is noted that Hall parameter assists the flow. Moreover effect of Hall parameter is quite opposite to that of Hartman number. Main observations of this chapter are submitted in **J. Magnetism and Magnetic Materials.**

Chapter six looks at the peristaltic motion of an incompressible third order fluid in a symmetric channel. This study is performed in the presence of applied magnetic field and the effect of Hall currents is also considered. The third order fluid described shear thinning/shear thickening effect but it lacks the stress relaxation and retardation effects. Mathematical formulation is given in a wave frame of reference. Series solutions up to first order for small Deborah number are obtained for the stream function, longitudinal velocity and pressure gradient. Numerical integration is carried out for the pressure rise and frictional forces. Influence of emerging parameters on the pressure rise, frictional forces, axial pressure gradient, velocity profile and trapping are discussed. It is observed that pressure rise is a decreasing function of Hall parameter. The outcome of this chapter is submitted for publication in **Int. J. Numerical Methods for Heat and Fluid flow.**

Hall and ion-slip effects on the peristaltic flow of hyperbolic fluid are reported in chapter seven. Long wavelength and low Reynolds number assumptions are employed in the problem formulation. The governing nonlinear problem is solved using perturbation approach. Graphical results are reported and discussed for various parameters of interest. It is found that effect of Hall and ion-slip parameters on velocity is quite similar. Findings of this chapter have been submitted for publication in **Journal of Aerospace Engineering.**

Heat transfer analysis for the peristaltic transport of an incompressible Williamson fluid with Hall and ion-slip effects is carried out in chapter eight. Joule heating effects is also taken in to account. The flow analysis is modeled in a frame moving with the velocity of the wave. Lubrication approach is adopted in the mathematical formulation. Series solutions for stream function, pressure gradient and temperature profile are constructed for small values of Weissenberg number. Variations of emerging physical parameters on the axial velocity, shear stress, pressure gradient and temperature are analyzed graphically. Increase in Weissenberg number leads to an enhancement in the pressure rise. It is also noted that pressure rise is a decreasing function of Hall and ion-slip parameters. The results of this chapter have been submitted for publication in **"Applied Bionics and Biomechanics".**

Chapter nine contains the study of peristaltic flow of Phan-Thein-Tannar (PTT) fluid with Joule heating. The fluid is electrically conducting in the presence of uniform applied magnetic field. Hall and ion-slip effects are considered. PTT model is derived from the Lodge-Yamamoto network theory and is known as the simple best differential model which exhibits viscoelastic and shear thinning properties of polymer solution. The problem formulation is developed in a wave frame of reference. The resulting problem is solved for the stream function, longitudinal pressure gradient and temperature. The phenomena of pumping and trapping are discussed. The contents of this chapter have been submitted for publication in **"Applied Bionics and Biomechanics".**

Chapter ten is devoted to study the peristaltic flow of a MHD Prandtl fluid with Hall and ion-slip effects. Flow configuration is taken asymmetric. Asymmetry in the flow is induced by sinusoidal wave with different amplitudes and phases. Flow is induced by

peristaltic wave along the length of channel walls. Both the magnetic field and channel are inclined. Mathematical modeling of the governing equations is developed. Series solutions for stream function and pressure gradient are obtained under the assumption of small wave number. Results of pressure rise are analyzed through numerical integration. Main results of this chapter are submitted for publication in **"Applied Mathematics and Mechanics"**.

Contents

3

Chapter 1

Preliminaries with some basic laws

This chapter includes the relevant review of peristaltic transport phenomenon with some basic law regarding mathematical formulation.

1.1 Peristaltic transport and pumping

Peristalsis is a mechanism that transport fluid in a channel or tube by means of pressure gradient which is induced by progressive sinusoidal waves. The contraction and expansion of the wave pushed the fluid along the tube/channel. Such type of transport phenomenon is useful in the situations where one avoid the use of external source like piston. In physiology the peristalsis is used by the body to propel the fluid and transport it from part of the body to an other part. peristalsis play key role in the processes like urine transport from kidney to bladder, chyme movement in the digestive tract, vasomotion of blood vessels in capillaries and arterioles, movement of spermatozoa in the ductus afferents of male reproductive tract and movement of ovum in the female fallopian tube. Some worms also use peristalsis for their locomotion. In addition devices like roller and finger pumps are also operated on the principle of peristaltic pumping that are used to pump corrosive fluids, slurries, blood and foods in order to avoid their direct contact with the machinery. Furthermore the occurrence of peristaltic pumping is quite prevalent in several applications associated with the biomedical systems. The design of many modern medical devices are also based upon the principle of peristaltic pumping for instance one may consider the blood in the heart-lung machine. At present, different aspects of

peristaltic transport of fluids in channels and tubes have been investigated thoroughly by many researchers in the field.

1.2 Literature review

The fundamental study for the peristaltic flow of viscous fluid was made by Latham [1]. Shapiro [2] examined the peristaltic phenomenon in a two-dimensional flexible tube under small wave number and considered the flow to be inertia free. Under these assumptions there is a steady flow in a wave frame and the obtained solution of velocity profile is similar to that of poiseuille flow. The work of shapiro has good agreement with the experimental work of Latham. Barton and Raynor [3] use the concept of peristaltic motion to calculate the time elapsed for the chyme movement in the small intestine. Shapiro et al. [4] discussed the peristaltic flow of viscous fluid for both planar and axisymmetric cases under long wavelength and zero Reynolds number approximation. They suggested that physiological significance of reflux phenomenon is true in ureter. Another study for the mechanics of peristaltic pumping in planar channel and axisymmetric tube under small wavelength and low Reynolds number approximation is presented by Yin and Fung [5]. Lew et al. [6] analyzed the peristaltic motion of carrying and mixing chyme in small intestine under long wavelength approximation. They obtained two solutions of the problem, peristaltic pumping without net pressure gradient and peristaltic compressions with net transport of the fluid. The total solution consist the linear combination of the two solutions. In another attempt Lew and Fung [7] investigated the peristaltic flow with low Reynolds number in a valved vessel with special reference to the flow in a valved vessel lie in lymphatic ducts and veins. Jaffrin [8] analyzed the inertia and streamline curvature effects in peristaltic pumping. Such effects can be predicted in gastrointestinal tracts and in roller pumps. Jaffrin and Shapiro [9] looked at a review on peristalsis in view of different flow regimes. Mittra and Prasad [10] analyzed the interaction of peristalsis with poiseuille flow and investigated the peristaltic motion in the presence of pressure gradient. A mathematical model which describes the mechanism for swimming of spermatozoa in the cervix is presented by Semleser et al. [11]. Asymptotic solution for peristaltic flow at low Reynolds number in an axisymmetric case is studied by Manton [12]. Takabatake and Ayukawa [13] obtained numerical

solutions for peristaltic flow of two-dimensional problem. In another attempt Takabatake et al. [14] solved the problem for the peristaltic pumping in circular cylindrical tubes by generalizing the numerical method suggested in ref. [13]. Vries et al. [15] noted that the intra uterine fluid flow induced by myometrial contractions occur in both symmetric and asymmetric directions. Eytan et al. [16] disclosed that contraction of non-pregnant woman uterine are composed of variable amplitudes, range of frequencies and different wavelengths. Mathematical model for peristaltic transport in an asymmetric channel is presented by Eytan and Elad [17]. Mishra and Rao [18] investigated the flow of incompressible viscous fluid in an asymmetric channel. The channel asymmetry is produced through waves that propagates on the walls having different amplitudes and phases. Rao and Mishra [19] examined the curvature effects of Newtonian fluid in an asymmetric channel with peristalsis. Mekheimer [20] reported the peristaltic transport of Newtonian fluid through uniform and non-uniform annulus.

The above mentioned studies deals with the peristaltic flow of viscous fluid with different flow geometries and aspects. However there are many fluids in nature that violate linear relationship between stress and deformation rate and are classified as the non-Newtonian fluids. Examples of such fluids include clay suspension, personal care products, polymers, shampoo, ketchup, blood flow at low shear rate, chyme etc. The non-Newtonian fluids are completely different form Newtonian fluids. Infact the equations which governs the flow of non-Newtonian fluids are more complicated and subtle when compared with the Newtonian fluids. Therefore to compute solutions (Analytic or numerical) of such equations under one or more simplified assumptions are not easy. The resulting equations of non-Newtonian fluids are in general higher order than the viscous fluid and thus require additional boundary conditions for the unique solution. Therefore peristaltic transport of non-Newtonian fluids is hot topic of research for the mathematicians, engineers, physicists, modelers and numerical simulists. Extensive literature are now available on peristaltic flow of non-Newtonian fluids. Chaturani and Samy [21] discussed the non-Newtonian aspect of blood flow through stenosed arteries. Raju and Devanathan [22] reported the analytical properties of power law fluid in a tube with peristalsis. In another attempt Radhakrishnamacharya [23] analyzed the peristaltic transport of power law fluid in a two-dimensional channel. Johnson and Segalman [24] presented a model for the behavior of viscoelastic fluid with non-affine deformations. Thien and Tanner [25] suggested

new constitutive equations for polymeric fluids that are driven from Lodge-Yamamoto network theory. Soon after Thein [26] revealed a viscoelastic model resembling physiological fluids. Srivastava and Srivastava [27] examined the peristaltic flow of power-law fluid and associated the study with pragmatic flow rates in the vas deferens and small intestine. The peristaltic flow of third order fluid is analyzed by Siddiqui and Schwarz [28]. They considered the flow in a planar channel and computed analytical solution for small Deborah number. Also Siddiqui and Schwarz [29] studied the peristaltic transport of a second order fluid in an axisymmetric duct when the wave number is small. The rheological properties of couple-stresses with peristaltic transport is stated by Shehawey and Mekheimer [30]. Tsiklauri and Beresnev [31] discussed the viscoelastic properties of Maxwell fluid in a circular porous tube. Hayat et al. [32, 33] investigated the peristaltic flow of Johnson-Segalman and Oldroyd-B fluids in a planar channel. Vajravelu et al. [34] have examined the peristaltic transport of a Herschel-Bulkley fluid with long wavelength approximation in an inclined circular tube. Peristaltic motion of a Burger's fluid in a planar channel is analyzed by Hayat et al. [35]. Haroun [36] studied the peristaltic transport of a third-order fluid. Nguyen et al. [37] presented an experimental model for a peristaltic pump with low cost and high quality performance. Ali et al. [38] discussed the peristaltic flow in a curved channel under consideration of lubrication approximation. Hayat and Javed [39] obtained an exact solution to the peristaltic motion of power-law fluid in a channel with compliants walls. Maiti and Misra [40] and Rao and Rao [42] investigated the peristaltic flow of couple stress fluid in a porous medium. Peristaltic motion of Walter's B fluid in an endoscope is presented by Nadeem et al. [41]. Modeling of peristaltic flow for non-Newtonian fluid with a new approach is proposed by Yazdanpanh-Ardakani and Niroomand-Oscuii [43]. Hayat et al. [44] considered the flow of P.T.T fluid in a planar channel with peristalsis. Numerical study for non-Newtonian fluids in a curved channel is presented by Kalantari et al. [45]. Flow of the fourth grade fluid with suction and injection between porous walls under peristaltic action is examined by Hari Prabakaran et al. [46]. Ellahi et al. [47] investigated the three dimensional flow of Williamson fluid in a rectangular duct.

The peristaltic transport of fluid with heat and mass transfer plays a vital role especially in chemical engineering processes. In physiology, the heat transfer is used to analyze the properties of tissues. Radio frequency therapy is helpful in the treatment of diseases like tissue

coagulation, the primary living cancer, the lung cancer and the reflux of stomach acid. Moreover heat transfer analysis is also significant in hemodialysis and oxygenation processes. It plays an important role in many industrial sectors like power plants, electronic devices and chemical processing plants. Having such usefulness in mind Vajravelu et al. [48] studied the peristaltic motion of viscous fluid with heat transfer in a vertical annulus. Srinivas and Kothandapani [49] and Hayat et al. [50] canvassed the effect of heat transfer on peristaltic flow of viscous fluid in an asymmetric channel. Nadeem and Akbar [51, 52] considered the influence of heat transfer phenomenon on peristaltic motion of Jhonson-Segalman and Jeffrey-six constant fluids in non-uniform axisymmetric tubes. In another study Nadeem [53] illustrated the effect of heat with mass transfer on peristaltic motion of third order fluid. Mekheimer et al. [54] and Vasudev et al. [55] analyzed the heat transfer analysis on peristaltic flows containing viscous fluid with porosity. Peristaltic motion of viscoelastic fluid with heat transfer effects is observed by Sobh et al. [56]. Hayat et al. [57] scrutinized effect of heat transfer with slip condition on peristalsis. Srinivas et al. [58] considered the mixed convective peristaltic flow with heat and mass transfer. Effect of wall slip on peristalsis along with heat and mass transfer is analyzed by Srinivas et al. [59]. Hayat et al. [60] discussed the heat transfer analysis on peristaltic motion of an Oldroyd-B fluid with compliant walls. In another attempt Hayat et al. [61] investigated the effects of heat and mass transfer on Maxwell fluid in the presence of slip condition. A mathematical model for swallowing of food bolus under influence of heat transfer is proposed by Tripathi [62]. Ellahi et al. [63] analyzed heat transfer analysis in non-uniform rectangular duct with peristalsis. Now a days, the flows of nanofluid is an active area of research. In fact, the nanofluids are a suspension of nanosized solid particles in a base fluid having higher thermal conductivity than base fluid. Concept of nanofluids is employed to increase the heat transfer rate. The traditional base fluids employed in heat transfer processes that includes water, mineral oils, toluene and ethylene glycol has low thermal conductivity. Now, various inexpensive combinations of liquid/particles are available because of growing advancement in nano manufacturing. Aluminum, gold, iron, copper and titanium or their oxides are worth pointing amongst such particles of metals and possesses high thermal conductivity than the base fluids. Extensive attempts are now available on the flows of nanofluids. Few recent researches on the topic of nanofluids are presented through studies [64 - 72].

Literature survey also indicates that there are several attempts describing the impact of applied magnetic field on peristaltic transport of viscous and non-Newtonian fluids. Flows in presence of magnetic field are significant in MHD power generators, MHD pumps and accelerators etc. Specific examples in this direction may include flow of nuclear fuel slurries, flow of liquid metals and alloys, flow of plasma, flow of mercury amalgams, lubrications of heavy oils and greases. Magnetohydrodynamic fluid flow in a channel with elastic and rhythmically contracting walls is of great interest with certain problems of the movement of conductive physiological fluids and for operating peristaltic MHD compressor. In medical sciences the influence of magnetic field is used in surgeries to reduce bleeding and cancer tumors. Mekheimer [73] analyzed the peristaltic transport of blood under the influence of magnetic field. Peristaltic flow of MHD Newtonian fluid with slip effects in an asymmetric channel is examined by Yildirim and Sezer [74]. Hayat and Hina [75] discussed the effect of wall properties on the magnetohydrodynamic flow of Maxwell fluid with peristalsis. Impact of induced magnetic field with peristalsis on third order fluid is investigated by Hayat et al. [76]. Srinivas and Muthuraj [77] discussed the effects of chemical reaction and space porosity on MHD mixed convective flow in a vertical asymmetric channel with peristalsis. Impact of induced magnetic field with peristalsis in an annulus is analyzed by Elmaboud [78]. Combined influence of slip, temperature and concentration jump conditions on MHD peristaltic flow of a Carreau fluid is examined by Vajravelu et al. [79]. It has been noted that peristalsis in presence of Hall effects has given very less attention. Such effects cannot be over looked when flow subject to high magnetic field is considered. Hall effect can be taken into account when the Hall parameter (the ratio between the electron-cyclotron frequency and the electron-atom-collision frequency) is high. This happens, when the magnetic field is high or when the collision frequency is low. Also the current trend in the application of magnetohydrodynamics is towards a strong magnetic field, therefore one has to consider the influence of Hall current as it has great impact on the magnitude and direction of the current density and consequently on the magnetic-force term. However it is noted that scarce literature is available for MHD peristaltic flow of non-Newtonian fluids with Hall and ion-slip effects. Saha et al. [80] investigated the effect of Hall currents on the MHD laminar natural convection flow from a vertical permeable flat plate with uniform surface temperature. Hayat et al. [81] examined the impact of Hall currents on peristaltic transport of a Maxwell fluid in a porous

medium. Hall and ion-slip effects on three-dimensional flow of second grade fluid is analyzed by Hayat and Nawaz [82]. Effect of Hall parameter on interaction of pulsatile and peristaltic transport induced flows of a particle–fluid suspension is studied by Gad [83]. Nowar et al. [84] investigated the peristaltic pumping of Johnson-Segalman fluid in an asymmetric channel under the effects of Hall and ion-slip currents. Hall effects on peristalsis of Maxwell fluid in porous space is explored by Koumy et al. [85].

1.3 Some definitions regarding peristaltic pumping

This section enclosed some decisive terminology used in peristaltic flows. We let ΔP_λ that represents the pressure rise per wavelength and Θ as the mean flow rate.

1.3.1 Peristaltic pumping

It occurs when the pressure rise at the ends of the channel or tube and the mean flow rate both are positive i.e. $\Delta P_\lambda > 0$ and $\Theta > 0$.

1.3.2 Retrograde pumping

The case when the pressure rise per wavelength is positive but the corresponding flow rate is negative is named as Retrograde pumping i.e. $\Delta P_\lambda > 0$ and $\Theta < 0$.

1.3.3 Free pumping

For free pumping the pressure rise is zero however the flow rate is positive i.e. $\Delta P_\lambda = 0$ and $\Theta > 0$.

1.3.4 Augmented pumping

The case where the pressure rise is negative and the mean flow rate is positive is designated as augmented pumping. Here $\Delta P_\lambda < 0$ and $\Theta > 0$.

1.3.5 Trapping

A phenomenon in which the stream lines split under certain conditions and enclosed a bolus is known as Trapping. The trapped bolus is pushed ahead along with the peristaltic wave.

1.4 Necessary fundamental equations

This section includes the general form of equations that governs the flow mechanism of the fluid.

1.4.1 The law of mass conservation

Compressible fluid

$$\frac{\partial \rho_f}{\partial t} + \text{div}\left(\rho_f \mathbf{V}\right) = 0.$$

Incompressible fluid

$$\text{div}\left(\mathbf{V}\right) = 0.$$

1.4.2 The linear momentum equation

$$\frac{\rho_f d\mathbf{V}}{dt} = \text{div}\,\mathbf{T} + \rho b,$$

where

$$\mathbf{T} = -p\mathbf{I} + \mathbf{S}.$$

1.4.3 Energy equation

$$\rho_f c_p \frac{dT}{dt} = k\nabla^2 T.$$

1.4.4 Concentration equation

$$\frac{dC}{dt} = D\nabla^2 C.$$

1.4.5 Ohm's law

$$\mathbf{J} = \sigma \left(\mathbf{E} + \mathbf{V} \times \mathbf{B} \right).$$

In above equations ρ_f is the density of the fluid, $\mathbf{T}$ the Cauchy stress tensor, p the pressure, $\mathbf{S}$ the extra stress tensor, $\mathbf{V}$ the velocity vector, b the body force, d/dt the material time derivative, t the time, c_p the specific heat, $\overline{T}$ the temperature, k the thermal conductivity, C the concentration, D the mass diffusivity, $\mathbf{E}$ and $\mathbf{B}$ are the electric and magnetic fields, $\mathbf{J}$ the current density and σ the electrical conductivity.

Chapter 2

Peristaltic flow of Johnson Segalman fluid with nanoparticles

This work investigates the peristaltic transport of Johnson-Segalman fluid with nanoparticles. The fluid is considered in an asymmetric channel. The relevant nonlinear equations are modeled by employing mass, momentum, energy and concentration laws. The solutions for velocity, temperature, nanoparticle phenomenon and pressure gradient are derived. Results obtained are analyzed for various parameters of interest entering into the problem.

2.1 Basic equations with fluid model

The governing equations of motion for incompressible fluid flow in terms of mass, momentum, temperature and nanoparticle volume fraction are:

$$\text{div}\,\bar{V} = 0, \tag{2.1}$$

$$\rho_f \frac{d\bar{V}}{d\bar{t}} = \text{div}\,\bar{\mathbf{T}} + \rho_f g\alpha_t\left(\bar{T} - T_0\right) + \rho_f g\alpha_c\left(\bar{C} - C_0\right), \tag{2.2}$$

$$\frac{d\bar{T}}{d\bar{t}} = \alpha^*\nabla^2\bar{T} + \Upsilon^*\left[D\nabla\bar{C}.\nabla\bar{T} + \left(D_{\bar{T}}/\bar{T}_m\right)\nabla\bar{T}.\nabla\bar{T}\right], \tag{2.3}$$

$$\frac{d\bar{C}}{d\bar{t}} = D\nabla^2\bar{C} + \left(D_{\bar{T}}/\bar{T}_m\right)\nabla^2\bar{T}. \tag{2.4}$$

Here ρ_f is the density of fluid, $\bar{V}$ the velocity vector, $d/d\bar{t}$ the material time derivative, $\bar{\mathbf{T}}$ the Cauchy stress tensor and $\bar{C}$ the nanoparticle phenomenon, D the Brownian diffusion coefficient, $D_{\bar{T}}$ the thermophoretic diffusion coefficient, α_t the coefficient of thermal expansion, α_c the coefficient of expansion with concentration $\alpha^* \left(= k/\left(\rho c\right)_f\right)$ the thermal diffusivity, $\Upsilon^* = \left(\left(\rho c\right)_p / \left(\rho c\right)_f\right)$ the ratio of effective heat capacity of nanoparticle phenomenon to heat capacity of fluid and $\bar{T}_m$ the average temperature

The Cauchy stress tensor $\bar{\mathbf{T}}$ in a Johnson-Segalman fluid is given by

$$\bar{\mathbf{T}} = -\bar{P}\bar{\mathbf{I}} + 2\mu\bar{\mathbf{D}} + \bar{\mathbf{S}}, \tag{2.5}$$

$$\bar{\mathbf{S}} + \lambda_1[\frac{d\bar{\mathbf{S}}}{dt} + \bar{\mathbf{S}}(\bar{\mathbf{W}} - l\bar{\mathbf{D}}) + (\bar{\mathbf{W}} - l\bar{\mathbf{D}})^\top \bar{\mathbf{S}}] = 2\eta\bar{\mathbf{D}}, \tag{2.6}$$

where $\bar{P}$ is the pressure, μ and η are viscosities, λ_1 the relaxation time and l the slip parameter. The definitions of $\bar{\mathbf{D}}$ and $\bar{\mathbf{W}}$ are

$$\bar{\mathbf{D}} = \frac{1}{2}\left(\bar{\mathbf{L}} + \bar{\mathbf{L}}^\top\right), \quad \bar{\mathbf{W}} = \frac{1}{2}\left(\bar{\mathbf{L}} - \bar{\mathbf{L}}^\top\right), \tag{2.7}$$

where $\bar{\mathbf{L}} = \operatorname{grad}\bar{V}$ and $\top$ in the superscript shows the transpose of a matrix. Note that for $l = 1$ the current model reduces to Oldroyd-B model. when $l = 1$ and $\mu = 0$ then it represents the Maxwell model and for $\lambda_1 = 0$ it reduces to the viscous fluid model.

2.2 Definition of mathematical problem

We examine the peristaltic flow of Johnson-Segalman fluid with nanoparticle in an asymmetric channel. Different amplitudes and phases of wave propagating along the channel walls induce asymmetry. The geometry of walls satisfies the following relations

$$Y = \bar{H}_1 = d_1 + a_1 \cos\left(\frac{2\pi}{\lambda}\left(\bar{X} - c\bar{t}\right)\right), \quad \text{Upper wall} \tag{2.8}$$

$$Y = \bar{H}_2 = -d_2 - b_1 \cos\left(\frac{2\pi}{\lambda}\left(\bar{X} - c\bar{t}\right) + \bar{\phi}\right). \quad \text{Lower wall} \tag{2.9}$$

The values of $\bar{T}$ and $\bar{C}$ as $\bar{y}$ tend to $\bar{H}_1$ are denoted by T_0 and C_0 respectively. In above equations a_1 and b_1 show the waves amplitudes, λ is the wave length, $d_1 + d_2$ the channel width, c the

15

wave speed, $\bar{t}$ the time and the phase difference $\tilde{\phi}$ ranges $0 \leq \tilde{\phi} \leq \pi$. For $\tilde{\phi} = 0$ and $\tilde{\phi} = \pi$, the waves are out of phase and in phase respectively. Further, a_1, b_1, d_1, d_2 and $\tilde{\phi}$ satisfy

$$a_1^2 + b_1^2 + 2a_1 b_1 \cos \tilde{\phi} \leq (d_1 + d_2)^2. \tag{2.10}$$

For the unsteady, two-dimensional velocity field we have

$$\bar{\mathbf{V}} = \left[\bar{U}(\bar{X}, \bar{Y}, \bar{t}), \; \bar{V}(\bar{X}, \bar{Y}, \bar{t}), 0 \right]. \tag{2.11}$$

Inserting the constitutive relations (2.5) and (2.6) along with Eq. (2.11), the Eqs. (2.1 - 2.4) take the following forms:

$$\overline{U}_{,\overline{X}} + \overline{V}_{,\overline{Y}} = 0, \tag{2.12}$$

$$\begin{aligned}
\rho_f(\bar{U}_{,\bar{t}} + \overline{U}\bar{U}_{,\overline{X}} + \overline{V}\bar{U}_{,\overline{Y}}) &= -\bar{P}_{,\overline{X}} + \overline{S}_{\overline{XX}},_{\bar{X}} + \overline{S}_{\overline{XY}},_{\bar{Y}} + \rho_f g \alpha_t \left(\bar{T} - T_0\right) \\
&\quad + \rho_f g \alpha_c \left(\bar{C} - C_0\right),
\end{aligned} \tag{2.13}$$

$$\rho_f(\overline{V}_{,\bar{t}} + \overline{UV}_{,\overline{X}} + \overline{VV}_{,\overline{Y}}) = -\bar{P}_{,\overline{Y}} + \overline{S}_{\overline{YX}},_{\bar{X}} + \overline{S}_{\overline{YY}},_{\bar{Y}}, \tag{2.14}$$

$$\begin{aligned}
\overline{T}_{,\bar{t}} + \overline{UT}_{,\overline{X}} + \overline{VT}_{,\overline{Y}} &= \alpha^*(\bar{T}_{,\overline{XX}} + \bar{T}_{,\overline{YY}}) + \Upsilon^*[D\{\bar{C}_{,\bar{X}}\, \bar{T}_{,\bar{X}} + \bar{C}_{,\bar{Y}}\, \bar{T}_{,\bar{Y}}\} \\
&\quad + \left(D_{\bar{T}}/\bar{T}_m\right)\{(\bar{T}_{,\bar{X}})^2 + (\bar{T}_{,\bar{Y}})^2\}],
\end{aligned} \tag{2.15}$$

$$(\overline{C}_{,\bar{t}} + \overline{U}\bar{C}_{,\overline{X}} + \overline{V}\bar{C}_{,\overline{Y}}) = D(\bar{C}_{,\overline{XX}} + \bar{C}_{,\overline{YY}}) + \left(D_{\bar{T}}/\bar{T}_m\right)(\bar{T}_{,\overline{XX}} + \bar{T}_{,\overline{YY}}), \tag{2.16}$$

where

$$\begin{aligned}
2\eta \bar{U}_{,\overline{X}} &= \overline{S}_{\overline{XX}} + \lambda_1(\overline{S}_{\overline{XX}},_{\bar{t}} + \overline{U}\overline{S}_{\overline{XX}},_{\bar{X}} + \overline{V}\overline{S}_{\overline{XX}},_{\bar{Y}}) - 2l\lambda_1 \overline{S}_{\overline{XX}}\bar{U}_{,\overline{X}} \\
&\quad + \lambda_1[(1-l)\overline{V}_{,\overline{X}} - (1+l)\bar{U}_{,\overline{Y}}]\overline{S}_{\overline{XY}},
\end{aligned} \tag{2.17}$$

$$\begin{aligned}
\eta(\bar{U}_{,\overline{Y}} + \overline{V}_{,\overline{X}}) &= \overline{S}_{\overline{XY}} + \lambda_1(\overline{S}_{\overline{XY}},_{\bar{t}} + \overline{U}\overline{S}_{\overline{XY}},_{\bar{X}} + \overline{V}\overline{S}_{\overline{XY}},_{\bar{Y}}) + \frac{\lambda_1}{2}[(1-l)\bar{U}_{,\overline{Y}} \\
&\quad - (1+l)\overline{V}_{,\overline{X}}]\overline{S}_{\overline{XX}} + \frac{\lambda_1}{2}[(1-l)\overline{V}_{,\overline{X}} - (1+l)\bar{U}_{,\overline{Y}}]\overline{S}_{\overline{YY}},
\end{aligned} \tag{2.18}$$

16

$$2\eta\bar{V},_{\overline{Y}} = \overline{S}_{\overline{YY}} + \lambda_1(\overline{S}_{\overline{YY}},_{\bar{t}} + \overline{U}S_{\overline{YY}},_{\bar{X}} + \overline{V}S_{\overline{YY}},_{\overline{Y}}) - 2l\lambda_1\overline{S}_{\overline{YY}}\bar{U},_{\overline{X}}$$

$$+\lambda_1[(1-l)\bar{U},_{\overline{Y}} - (1+l)\overline{V},_{\overline{X}}]\overline{S}_{\overline{XY}}. \tag{2.19}$$

Note that the subscripts are used to represent the partial derivatives. We now introduce the transformations

$$\bar{x} = \bar{X} - c\bar{t}, \ \bar{y} = \bar{Y}, \ \bar{u} = \bar{U} - c, \ \bar{v} = \bar{V}, \ \bar{p}(\bar{x},\bar{y}) = \bar{P}(\bar{X},\bar{Y},\bar{t}), \tag{2.20}$$

in which $(\bar{x},\bar{y})$, $(\bar{u},\bar{v})$ and $\bar{p}$ are the coordinates, velocity components and pressure in the wave frame where as $(\bar{X},\bar{Y})$, $(\bar{U},\bar{V})$ and $\bar{P}$ are the respective coordinates, velocity components and pressure in the fixed frame.

Setting the non-dimension variables as

$$x = \frac{2\pi\bar{x}}{\lambda}, \ y = \frac{\bar{y}}{d_1}, \ u = \frac{\bar{u}}{c}, \ v = \frac{\bar{v}}{c}, \ \delta = \frac{2\pi d_1}{\lambda}, \ d = \frac{d_2}{d_1}, \ p = \frac{2\pi d_1^2\bar{p}}{\mu c\lambda},$$

$$h_1 = \frac{\bar{H}_1}{d_1}, \ h_2 = \frac{\bar{H}_2}{d_2}, \ \mathrm{Re} = \frac{\rho c d_1}{\mu}, \ a = \frac{a_1}{d_1}, \ b = \frac{a_2}{d_1}, \ d = \frac{d_2}{d_1}, \ S = \frac{\bar{S}d_1}{\mu c},$$

$$\theta = \frac{\bar{T} - T_0}{T_1 - T_0}, \ \Phi = \frac{\bar{C} - C_0}{C_1 - C_0}, \ N_b = \frac{\Upsilon^* D(C_1 - C_0)}{\nu}, \ N_t = \frac{\Upsilon^* D_{\bar{T}}(T_1 - T_0)}{\bar{T}_m\nu}$$

$$G_r = \frac{g\alpha_t d_1^2(T_1 - T_0)}{\nu c}, \ B_r = \frac{g\alpha_c d_1^2(C_1 - C_0)}{\nu c}, \ W_e = \frac{\lambda_1 c}{d_1}, \ \gamma^* = \frac{\mu}{\eta}. \tag{2.21}$$

and letting the stream function by Ψ such that

$$u = \frac{\partial\Psi}{\partial y} \text{ and } v = -\delta\frac{\partial\Psi}{\partial x}, \tag{2.22}$$

the incompressibility condition is automatically satisfied and Eqs. (2.13) to (2.19) reduces to

$$\delta\,\mathrm{Re}\left[\left(\frac{\partial\Psi}{\partial y}\frac{\partial}{\partial x} - \frac{\partial\Psi}{\partial x}\frac{\partial}{\partial y}\right)\frac{\partial\Psi}{\partial y}\right] = -\left(\frac{1+\gamma^*}{\gamma^*}\right)\frac{\partial p}{\partial x} + \delta\frac{\partial S_{xx}}{\partial x} + \frac{\partial S_{xy}}{\partial y} + G_r\theta + B_r\Phi \tag{2.23}$$

$$\delta^3\,\mathrm{Re}\left[\left(\frac{\partial\Psi}{\partial y}\frac{\partial}{\partial x} - \frac{\partial\Psi}{\partial x}\frac{\partial}{\partial y}\right)\frac{\partial\Psi}{\partial x}\right] = -\left(\frac{1+\gamma^*}{\gamma^*}\right)\frac{\partial p}{\partial y} + \delta^2\frac{\partial S_{xy}}{\partial x} + \delta\frac{\partial S_{yy}}{\partial y} \tag{2.24}$$

17

$$\frac{2\delta}{\gamma^*}\frac{\partial^2 \Psi}{\partial x \partial y} = S_{xx} + W_e\delta\left(\frac{\partial \Psi}{\partial y}\frac{\partial}{\partial x} - \frac{\partial \Psi}{\partial x}\frac{\partial}{\partial y}\right)S_{xx} - 2lW_e\delta S_{xx}\frac{\partial^2 \Psi}{\partial x \partial y}$$
$$-W_e\left[\delta^2(1-l)\frac{\partial^2 \Psi}{\partial x^2} + (1+l)\frac{\partial^2 \Psi}{\partial y^2}\right]S_{xy}, \qquad (2.25)$$

$$\frac{1}{\gamma^*}\left(\frac{\partial^2 \Psi}{\partial y^2} - \delta^2\frac{\partial^2 \Psi}{\partial x^2}\right) = S_{xy} + W_e\delta\left(\frac{\partial \Psi}{\partial y}\frac{\partial}{\partial x} - \frac{\partial \Psi}{\partial x}\frac{\partial}{\partial y}\right)S_{xy}$$
$$+\frac{W_e}{2}\left[(1-l)\frac{\partial^2 \Psi}{\partial y^2} + \delta^2(1+l)\frac{\partial^2 \Psi}{\partial x^2}\right]S_{xx}$$
$$-\frac{W_e}{2}\left[\delta^2(1-l)\frac{\partial^2 \Psi}{\partial x^2} + (1+l)\frac{\partial^2 \Psi}{\partial y^2}\right]S_{yy}, \qquad (2.26)$$

$$-\frac{2\delta}{\gamma^*}\frac{\partial^2 \Psi}{\partial x \partial y} = S_{yy} + W_e\delta\left(\frac{\partial \Psi}{\partial y}\frac{\partial}{\partial x} - \frac{\partial \Psi}{\partial x}\frac{\partial}{\partial y}\right)S_{yy} + 2lW_e\delta S_{yy}\frac{\partial^2 \Psi}{\partial x \partial y}$$
$$+W_e\left[(1-l)\frac{\partial^2 \Psi}{\partial y^2} + (1+l)\delta^2\frac{\partial^2 \Psi}{\partial x^2}\right]S_{xy}, \qquad (2.27)$$

$$\delta\,\mathrm{Re}\left[\left(\frac{\partial \Psi}{\partial y}\frac{\partial}{\partial x} - \frac{\partial \Psi}{\partial x}\frac{\partial}{\partial y}\right)\theta\right] = \delta^2\frac{\partial^2 \theta}{\partial x^2} + \frac{\partial^2 \theta}{\partial y^2} + N_b\left(\delta^2\frac{\partial \Phi}{\partial x}\frac{\partial \theta}{\partial x} + \frac{\partial \Phi}{\partial y}\frac{\partial \theta}{\partial y}\right)$$
$$+N_t\left[\delta^2(\frac{\partial \theta}{\partial x})^2 + (\frac{\partial \theta}{\partial y})^2\right], \qquad (2.28)$$

$$\delta\,\mathrm{Re}\left[\left(\frac{\partial \Psi}{\partial y}\frac{\partial}{\partial x} - \frac{\partial \Psi}{\partial x}\frac{\partial}{\partial y}\right)\Phi\right] = \delta^2\frac{\partial^2 \Phi}{\partial x^2} + \frac{\partial^2 \Phi}{\partial y^2} + \frac{N_t}{N_b}\left(\delta^2\frac{\partial^2 \theta}{\partial x^2} + \frac{\partial^2 \theta}{\partial y^2}\right). \qquad (2.29)$$

Here W_e, N_b, N_t, G_r and B_r are respectively used for the Weissenberg number, the Brownian motion parameter, the thermophoresis parameter, the local temperature Grashof number and the local nanoparticle Grashof number. Further, Re, δ, θ, Φ are the Reylonds number, wave number, dimensionless temperature and nonoparticle phenomenon respectively.

Note that the solutions of Eqs. (2.23), (2.24), (2.28) and (2.29) for all values of parameters are impossible, therefore we carried out our analysis under long wave-length and low Reylonds number approximation. For that we set $\delta = 0$ by which Eqs. (2.23 - 2.29) yield

$$\left(\frac{1+\gamma^*}{\gamma^*}\right)\frac{\partial p}{\partial x} = \frac{\partial S_{xy}}{\partial y} + G_r\theta + B_r\Phi, \qquad (2.30)$$

18

$$-\frac{\partial p}{\partial y} = 0, \tag{2.31}$$

$$S_{xx} - W_e \left[(1 + l) \frac{\partial^2 \Psi}{\partial y^2} \right] S_{xy} = 0, \tag{2.32}$$

$$\frac{1}{\gamma^*} \frac{\partial^2 \Psi}{\partial y^2} = S_{xy} + \frac{W_e}{2} \left[(1 - l) \frac{\partial^2 \Psi}{\partial y^2} \right] S_{xx} - \frac{W_e}{2} \left[(1 + l) \frac{\partial^2 \Psi}{\partial y^2} \right] S_{yy}, \tag{2.33}$$

$$S_{yy} + W_e \left[(1 - l) \frac{\partial^2 \Psi}{\partial y^2} \right] S_{xy} = 0. \tag{2.34}$$

$$\frac{\partial^2 \theta}{\partial y^2} + N_b \frac{\partial \theta}{\partial y} \frac{\partial \Phi}{\partial y} + N_t \left(\frac{\partial \theta}{\partial y} \right)^2 = 0, \tag{2.35}$$

$$\frac{\partial^2 \Phi}{\partial y^2} + \frac{N_t}{N_b} \left(\frac{\partial^2 \theta}{\partial y^2} \right) = 0. \tag{2.36}$$

With the use of Eqs. (2.32) and (2.34), Eq. (2.33) becomes

$$S_{xy} = \frac{\frac{1}{\gamma^*} \frac{\partial^2 \Psi}{\partial y^2}}{1 + W_e^2 (1 - l^2) \left(\frac{\partial^2 \Psi}{\partial y^2} \right)^2}. \tag{2.37}$$

Applying binomial expansion about W_e, Eq. (2.37) takes the form

$$S_{xy} = \frac{\partial^2 \Psi}{\partial y^2} + \frac{W_e^2 (l^2 - 1)}{(1 + \gamma^*)} \left(\frac{\partial^2 \Psi}{\partial y^2} \right)^3 + O(W_e)^4. \tag{2.38}$$

Invoking Eq. (2.38) in Eq. (2.30), we have

$$\frac{dp}{dx} = \frac{\partial}{\partial y} \left(\frac{\partial^2 \Psi}{\partial y^2} + \frac{W_e^2 (l^2 - 1)}{(1 + \gamma^*)} \left(\frac{\partial^2 \Psi}{\partial y^2} \right)^3 \right) + G_r \theta + B_r \sigma. \tag{2.39}$$

Cross differentiation of Eqs. (2.31) and (2.39) give the compatibility equation as follows:

$$\frac{\partial^2}{\partial y^2} \left(\frac{\partial^2 \Psi}{\partial y^2} + \frac{W_e^2 (l^2 - 1)}{(1 + \gamma^*)} \left(\frac{\partial^2 \Psi}{\partial y^2} \right)^3 \right) + G_r \frac{\partial \theta}{\partial y} + B_r \frac{\partial \Phi}{\partial y} = 0, \tag{2.40}$$

The appropriate dimensionless boundary conditions can be written as:

19

$$\Psi = \frac{F}{2}, \ \frac{\partial \Psi}{\partial y} = -1, \ at \ y = h_1 = 1 + a\cos x, \qquad (2.41)$$

$$\Psi = -\frac{F}{2}, \ \frac{\partial \Psi}{\partial y} = -1, \ at \ y = h_2 = -d - b\cos\left(x + \tilde{\phi}\right), \qquad (2.42)$$

$$\theta = 0, \ at \ y = h_1, \ \theta = 1, \ at \ y = h_2, \qquad (2.43)$$

$$\Phi = 0, \ at \ y = h_1, \ \Phi = 1, \ at \ y = h_2. \qquad (2.44)$$

Here F is the flux in wave frame and a, b, ϕ and d satisfy

$$a^2 + b^2 + 2ab\cos\phi \leq (1 + d)^2. \qquad (2.45)$$

The flux at any axial station in fixed frame is

$$\bar{Q} = \int_{h2}^{h1} (u + 1)\, dy = \int_{h2}^{h1} u\, dy + \int_{h2}^{h1} dy = F + h_1 - h_2. \qquad (2.46)$$

The average volume flow rate over one period $\left(\tilde{T} = \frac{\lambda}{c}\right)$ of the peristaltic wave is defined as follows:

$$Q = \frac{1}{\tilde{T}} \int_0^{\tilde{T}} \bar{Q}\, dt = \frac{1}{\tilde{T}} \int_0^{\tilde{T}} (q + h_1 - h_2)\, dt, \qquad (2.47)$$

$$\Theta = F + 1 + d. \qquad (2.48)$$

Where Θ and F are the dimensionless time-mean flows in the laboratory and wave frames respectively with

$$F = \int_{h_1}^{h_2} \frac{\partial \tilde{\Psi}}{\partial y}\, dy = \Psi(h_2) - \Psi(h_1), \qquad (2.49)$$

20

2.3 Analytical solution

2.3.1 Solution by homotopy perturbation method

By using Homotopy Perturbation Method (HPM) Eqs. (2.40), (2.35) and (2.36) can be expressed as

$$
\begin{aligned}
H\left(q,\Psi\right) \;=\; & \left(1-q\right)\left[L_\Psi\left(\Psi\right)-L_\Psi\left(\Psi_0\right)\right]+q\left(L_\Psi\left(\Psi\right)+\frac{W_e^2\left(l^2-1\right)}{\left(1+\gamma^*\right)}\frac{\partial^2}{\partial y^2}\left(\frac{\partial^2\Psi}{\partial y^2}\right)^3\right. \\
& \left.+G_r\frac{\partial\theta}{\partial y}+B_r\frac{\partial\Phi}{\partial y}\right),
\end{aligned} \tag{2.50}
$$

$$
H\left(q,\theta\right)=\left(1-q\right)\left[L_\theta\left(\theta\right)-L_\theta\left(\theta_0\right)\right]+q\left(L_\theta\left(\theta\right)+N_b\frac{\partial\theta}{\partial y}\frac{\partial\Phi}{\partial y}+N_t\left(\frac{\partial\theta}{\partial y}\right)^2\right), \tag{2.51}
$$

$$
H\left(q,\Phi\right)=\left(1-q\right)\left[L_\Phi\left(\Phi\right)-L_\Phi\left(\Phi_0\right)\right]+q\left(L_\Phi\left(\Phi\right)+\frac{N_t}{N_b}\left(\frac{\partial^2\theta}{\partial y^2}\right)\right). \tag{2.52}
$$

With $L_\Psi=\dfrac{\partial^4}{\partial y^4}$ and $L_\theta=L_\Phi=\dfrac{\partial^2}{\partial y^2}$ are the linear operators. The initial guesses are selected in the forms

$$
\Psi_0\left(x,y\right) \;=\; L_1+L_2y+L_3y^2+L_4y^3, \tag{2.53}
$$

$$
\theta_0\left(x,y\right) \;=\; \Phi_0\left(x,y\right)=K_1+K_2y. \tag{2.54}
$$

Where

$$
\begin{aligned}
L_1 \;=\; & -\frac{(h_1+h_2)\left(2h_1h_2(-h_1+h_2)+F\left(h_1^2-4h_1h_2+h_2^2\right)\right)}{2(h_1-h_2)^3}, \quad L_2=\frac{-h_1^3-3h_1(2F+h_1)h_2+3h_1h_2^2+h_2^3}{(h_1-h_2)^3}, \\
L_3 \;=\; & \frac{3(F+h_1-h_2)(h_1+h_2)}{(h_1-h_2)^3}, \quad L_4=\frac{-2(F+h_1-h_2)}{(h_1-h_2)^3}, \quad k_1=\frac{h_1}{h_1-h_2}, \quad k_2=\frac{-1}{h_1-h_2}.
\end{aligned}
$$

Expanding

$$
\Psi\left(y,q\right) \;=\; \Psi_0+q\Psi_1+q^2\Psi_2, \tag{2.55}
$$

$$
\theta\left(y,q\right) \;=\; \theta_0+q\theta_1+q^2\theta_2, \tag{2.56}
$$

$$
\Phi\left(y,q\right) \;=\; \Phi_0+q\Phi_1+q^2\Phi_2, \tag{2.57}
$$

21

and following the methodology of HPM the results of stream functions(Ψ), temperature (θ), nanoparticle phenomenon (Φ) and longitudinal pressure gradient (dp/dx) by setting $q = 1$ are

$$\Psi = L_{23} + L_{24}y + L_{25}y^2 + L_{26}y^3 + L_{27}y^4 + L_{28}y^5 + L_{13}y^6 + L_{14}y^7$$
$$+ L_{15}y^8 + L_{16}y^9 + L_{17}y^{10} + L_{18}y^{11}, \tag{2.58}$$

$$\theta = k_1 + k_3 + k_5 + (k_2 + k_4 + k_6)\,y - (k_2^2/2)\,(N_b + N_t)\,y^2 - N_t$$
$$- \left(k_4 - k_2^2(N_b + N_t)y\right)^4 / 12k_2^4\,(N_b + N_t)^2, \tag{2.59}$$

$$\Phi = k_1 + k_7 + (k_2 + k_8)\,y + N_t^2 k_2\,(N_b + N_t)\,y^2/2N_b. \tag{2.60}$$

$$\frac{dp}{dx} = (k_1 + k_7)\,B_r + 6L_{26} + G_r(k_1 + k_3 + k_5 - k_4^4 N_t/12k_2^4\,(N_b + N_t)^2)$$
$$- (72(-1 + l^2)k_{25}^2 L_{26}W_e^2)/(1 + \gamma^*), \tag{2.61}$$

in which

$$L_5 = \frac{1}{24(1+\gamma)}(-k_2 B_r - k_2 G_r - 432 L_3 L_4^2 W_e^2(1 - l^2) - k_2 B_r \gamma^* - k_2 G_r \gamma^*),$$

$$L_6 = \frac{54(-1+l^2)L_4^3 W_e^2}{5(1+\gamma^*)}, \quad L_7 = \frac{h_1^2 h_2^2 (L_5 + 2L_6(h_1+h_2))}{l}, \quad L_8 = -h_1 h_2(2L_5\,(h_1 + h_2) + L_6(4h_1^2 + 7h_1 h_2 + 4h_2^2)),$$

$$L_9 = L_5\left(h_1^2 + 4h_1 h_2 + h_2^2\right) + 2\left(h_1 + h_2\right)\left(h_1^2 + 3h_1 h_2 + h_2^2\right) L_6,$$

$$L_{10} = -2\left(h_1 + h_2\right) L_5 - \left(3h_1^2 + 4h_1 h_2 + 3h_2^2\right) L_6,$$

$$L_{11} = \frac{-K_4 G_r}{24} + \frac{6(-1+l^2)L_9(3L_{10}^2 + 2L_5 L_9)W_e^2}{1+\gamma^*}, \quad L_{12} = \frac{(144(-1+l^2)(9L_{10}^3 + 36L_{10}L_5 L_9 + 10L_6 L_9^2)W_e^2 + k_2^2 G_r(N_b+N_t)(1+\gamma^*))}{120(1+\gamma^*)},$$

$$L_{13} = \frac{24(-1+l^2)(9L_{10}^2 L_5 + 6L_5^2 L_9 + 10L_{10}L_6 L_9)W_e^2}{5(1+\gamma^*)},$$

$$L_{14} = \frac{24(-1+l^2)(3L_{10}(6L_5^2 + 5L_{10}L_6) + 20L_5 L_6 L_9)W_e^2}{7(1+\gamma^*)}, \quad L_{15} = \frac{12(-1+l^2)(18L_5^3 + 90L_{10}L_5 L_6 + 25L_6^2 L_9)W_e^2}{7(1+\gamma^*)},$$

$$L_{16} = \frac{20(-1+l^2)(6L_5^2 L_6 + 5L_6^2 L_{10})W_e^2}{1+\gamma^*}, \quad L_{17} = \frac{160(-1+l^2)L_5 L_6^2 W_e^2}{1+\gamma^*}, \quad L_{18} = \frac{800(-1+l^2)L_6^3 W_e^2}{11(1+\gamma^*)},$$

22

$$L_{19} = h_1^2 h_2^2 (L_{11} + 8h_1^7 L_{18} + 7h_1^6 (L_{17} + 2h_2 L_{18}) + 6h_1^5 (L_{16} + 2h_2 L_{17} + 3h_2^2 L_{18}) + 5h_1^4$$
$$(L_{15} + 2h_2 L_{16} + 3h_2^2 L_{17} + 4h_2^3 L_{18}) + 4h_1^3 (L_{14} + 2h_2 L_{15} + 3h_2^2 L_{16} + 4h_2^3 L_{17}$$
$$+ 5h_2^4 L_{18}) + 3h_1^2 (L_{13} + 2h_2 L_{14} + 3h_2^2 L_{15} + 4h_2^3 L_{16} + 5h_2^4 L_{17} + 6h_2^5 L_{18}) + 2h_1$$
$$(L_{12} + 2h_2 L_{13} + 3h_2^2 L_{14} + 4h_2^3 L_{15} + 5h_2^4 L_{16} + 6h_2^5 L_{17} + 7h_2^6 L_{18}) + h_2 (2L_{12}$$
$$+ 3h_2 L_{13} + 4h_2^2 L_{14} + 5h_2^3 L_{15} + 6h_2^4 L_{16} + 7h_2^5 L_{17} + 8h_2^6 L_{18})),$$

$$L_{20} = -h_1 h_2 (16h_1^8 L_{18} + h_1^7 (14L_{17} + 37h_2 L_{18}) + h_1^4 (8L_{14} + 22h_2 L_{15} + 36h_2^2 L_{16} + 50h_2^3 L_{17}$$
$$+ 64h_2^4 L_{18}) + 4h_1^6 (3L_{16} + h_2 (8L_{17} + 13h_2 L_{18})) + h_1^5 (10L_{15} + h_2 (27L_{16} + 44h_2 L_{17}$$
$$+ 61h_2^2 L_{18})) + h_1^3 (6L_{13} + h_2 (17L_{14} + 28h_2 L_{15} + 39h_2^2 L_{16} + 50h_2^3 L_{17} + 61h_2^4 L_{18}))$$
$$+ 4h_1^2 (L_{12} + h_2 (3L_{13} + 5h_2 L_{14} + 7h_2^2 L_{15} + 9h_2^3 L_{16} + 11h_2^4 L_{17} + 13h_2^5 L_{18})) + 2h_2$$
$$(L_{11} + h_2 (2L_{12} + 3h_2 L_{13} + 4h_2^2 L_{14} + 5h_2^3 L_{15} + 6h_2^4 L_{16} + 7h_2^5 L_{17} + 8h_2^6 L_{18})) + h_1$$
$$(2L_{11} + h_2 (7L_{12} + 12h_2 L_{13} + 17h_2^2 L_{14} + 22h_2^3 L_{15} + 27h_2^4 L_{16} + 32h_2^5 L_{17} + 37h_2^6 L_{18}))),$$

$$L_{21} = 8h_1^9 L_{18} + h_1^8 (7L_{17} + 32h_2 L_{18}) + h_1^7 (6L_{16} + 28h_2 L_{17} + 50h_2^2 L_{18}) + h_1^6 (5L_{15} + h_2 (24L_{16}$$
$$+ 43h_2 L_{17} + 62h_2^2 L_{18})) + 4h_1^5 (L_{14} + h_2 (5L_{15} + 9h_2 L_{16} + 13h_2^2 L_{17} + 17h_2^3 L_{18})) + h_1^4$$
$$(3L_{13} + h_2 (16L_{14} + 29h_2 L_{15} + 42h_2^2 L_{16} + 55h_2^3 L_{17} + 68h_2^4 L_{18})) + 2h_1^3 (L_{12} + h_2 (6L_{13}$$
$$+ 11h_2 L_{14} + 16h_2^2 L_{15} + 21h_2^3 L_{16} + 26h_2^4 L_{17} + 13h_2^5 L_{18})) + 4h_1 h_2 (L_{11} + h_2 (2L_{12}$$
$$+ 3h_2 L_{13} + 4h_2^2 L_{14} + 5h_2^3 L_{15} + 6h_2^4 L_{16} + 7h_2^5 L_{17} + 8h_2^6 L_{18})) + h_2^2 (L_{11} + h_2 (2L_{12}$$
$$+ 3h_2 L_{13} + 4h_2^2 L_{14} + 5h_2^3 L_{15} + 6h_2^4 L_{16} + 7h_2^5 L_{17} + 8h_2^6 L_{18})) + h_1^2 (L_{11} + h_2 (8L_{12}$$
$$+ 15h_2 L_{13} + 22h_2^2 L_{14} + 29h_2^3 L_{15} + 36h_2^4 L_{16} + 43h_2^5 L_{17} + 50h_2^6 L_{18})),$$

$$L_{22} = -9h_1^8 L_{18} - 8h_1^7(L_{17} + 2h_2 L_{18}) - 7h_1^6(L_{16} + h_2(2L_{17} + 3h_2 L_{18})) - 6h_1^5(L_{15} + h_2(2L_{16}$$

$$+3h_2 L_{17} + 4h_2^2 L_{18})) - 5h_1^4(L_{14} + h_2(2L_{15} + 3h_2 L_{16} + 4h_2^2 L_{17} + 5h_2^3 L_{18})) - 4h_1^3$$

$$(L_{13} + h_2(2L_{14} + 3h_2 L_{15} + 4h_2^2 L_{16} + 5h_2^3 L_{17} + 6h_2^4 L_{18})) - 3h_1^2(L_{12} + h_2(2L_{13}$$

$$+3h_2 L_{14} + 4h_2^2 L_{15} + 5h_2^3 L_{16} + 6h_2^4 L_{17} + 7h_2^5 L_{18})) - 2h_1(L_{11} + h_2(2L_{12}$$

$$+3h_2 L_{13} + 4h_2^2 L_{14} + 5h_2^3 L_{15} + 6h_2^4 L_{16} + 7h_2^5 L_{17} + 8h_2^6 L_{18})) - h_2(2L_{11} + h_2(3L_{12}$$

$$+4h_2 L_{13} + 5h_2^2 L_{14} + 6h_2^3 L_{15} + 7h_2^4 L_{16} + 8h_2^5 L_{17} + 9h_2^6 L_{18})),$$

$$L_{23} = L_1 + L_{19} + L_7, \quad L_{24} = L_2 + L_{20} + L_8, \quad L_{25} = L_{21} + L_3 + L_9,$$

$$L_{26} = L_{10} + L_{22} + L_4, \quad L_{27} = L_{11} + L_5, \quad L_{28} = L_{12} + L_6.$$

$$k_3 = \tfrac{1}{2}\left(-k_2^2 h_1 h_2 N_b - k_2^2 h_1 h_2 N_t\right), \quad k_4 = \tfrac{1}{2}(k_2^2 h_1 N_b + k_2^2 h_2 N_b + k_2^2 h_1 N_t + k_2^2 h_2 N_t),$$

$$k_5 = -\frac{1}{12K_2^4(N_b+N_t)^2}(N_t(-k_4^4 + 6k_2^4 k_4^2 h_1 h_2 (N_b + N_t)^2 - 4k_2^6 k_4 h_1 h_2 (h_1 + h_2)(N_b + N_t)^3$$

$$+k_2^8 h_1 h_2 \left(h_1^2 + h_1 h_2 + h_2^2\right)(N_b + N_t)^4)),$$

$$k_6 = -\frac{1}{12K_2^2(N_b+N_t)}(N_t \left(2k_4 - k_2^2 (h_1 + h_2)(N_b + N_t)\right)(2k_4^2 - 2k_2^2 k_4 (h_1 + h_2)(N_b + N_t)$$

$$+k_2^4 \left(h_1^2 + h_2^2\right)(N_b + N_t)^2)),$$

$$k_7 = \frac{k_2^2 h_1 h_2 N_t (N_b + N_t)}{2N_b}, \quad k_8 = -\frac{k_2^2 (h_1 + h_2) N_t (N_b + N_t)}{2N_b}.$$

The dimensionless pressure rise ΔP is given by

$$\Delta P = \int\limits_0^{2\pi} \left(\frac{dp}{dx}\right) dx. \tag{2.62}$$

2.4   Analysis

This section consists of plots showing the influence of various pertinent parameters appearing in the considered flow problem. Local temperature Grashof number (G_r), thermophoresis parameter (N_t), Weissenberg number (W_e), slip parameter l and viscosity ratio (γ^*) have been varied for the analysis of velocity in Figs. $(2.1 - 2.5)$. Figs. (2.1) and (2.4) show that by increasing G_r and l, the velocity first increases in the interval $-10.5 < y < -4.5$ and then decreases when

24

$-4.5 < y < 1.6$. It is further found that opposite behavior is seen in the case of parameters $\overline{W}_e$ and γ^* (see Figs. (2.2) and (2.3)). Here the velocity first decreases for $-10.5 < y < -4.5$ and then increases when $-4.5 < y < 1.6$. Fig. (2.5) depicts that by increasing N_t, the velocity decreases for $-10.5 < y < -7$ and $-2 < y < 1.6$ and it increases when $-7 < y < -2$. In addition to this the variation is negligible for the case $0 \leq N_t \leq 1$ but a significant variation occurs when $N_t > 1$. Change in pressure rise per wavelength (ΔP_λ) against dimensionless volume flow rate (Θ) for different values of parameters G_r, N_b, N_t and W_e are portrayed in Figs. (2.6 − 2.9). Figs. (2.6) and (2.8) show that by increasing G_r and N_b the pressure rise increases for all values of Θ while ΔP_λ decreases by increasing N_t (see Fig. (2.7)). The mean flow rate Θ in Fig. (2.9) is divided into three regions i.e $\Theta < 0.25$, $\Theta = 0.25$ and $\Theta > 0.25$. The region $\Theta = 0.25$ is called the free pumping region . In the region where $\Theta < 0.25$ the pressure rise increases while pressure rise decreases in the region $\Theta > 0.25$ for larger values of Weissenberg number W_e. Figs. (2.10 − 2.13) are presented to see the effects of B_r, W_e, N_b, and γ^* on the pressure gradient (dp/dx). These Figs. clearly indicate an increase in pressure gradient when B_r, W_e, N_b, and γ^* are increased. Moreover maximum pressure gradient occurs at $x = 2.9$. Figs. (2.14) and (2.15) are constructed to examine the influence of thermophoresis parameter (N_t) and Brownian motion parameter (N_b) on the concentration profile (Φ). These Figs. indicate that the concentration field increases with an increase in parameter N_b and decreases for increasing values of N_t. Physically increase in thermophoresis parameter (N_t) results in a large mass flux due to temperature gradient which decreases the concentration of nanoparticles. Effect of N_t on temperature profile (θ) is shown in Fig. (2.16). This Fig. shows a substantial increase in the temperature for increasing values of N_t. This is due to the fact that when thermophoresis parameter (N_t) is increased it results in an effective movement of nanoparticles from the wall to the fluid and hence the temperature of the fluid increases significantly. Effect of G_r, W_e and N_b on trapping are presented in the Figs. (2.17 − 2.19). In Fig. (2.17) one can see that the trapping increases by increasing G_r, while Figs. (2.18) and (2.19) depict that trapping decreases when there is an appreciable increase in parameters W_e and N_b.
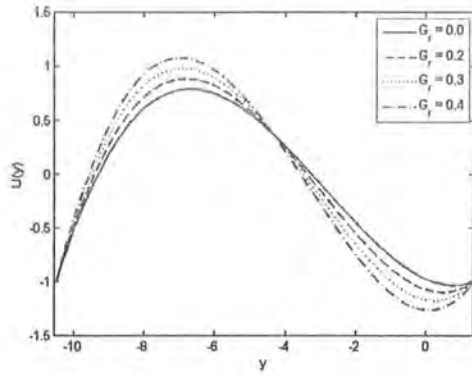
Fig. 2.1
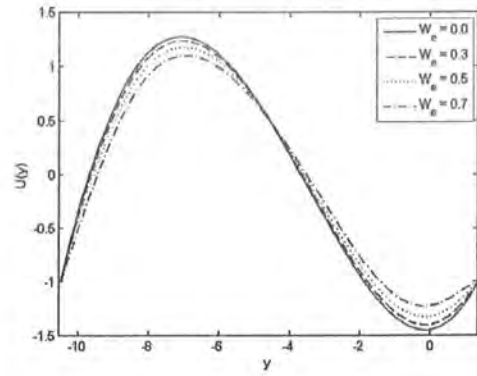

Fig. 2.2

Figs. (2.1 - 2.2): Variation of velocities for different values of G_r with $W_e = 0.3$ and W_e with $G_r = 0.6$, when $\Theta = 5$, $l = 0.4$, $a = 0.4$, $d = 10$, $x = 0.4$, $b = 0.6$, $\phi = 0.2$, $\gamma^* = 2$, $N_t = 0.7$, $N_b = 0.6$, $B_r = 0.5$.
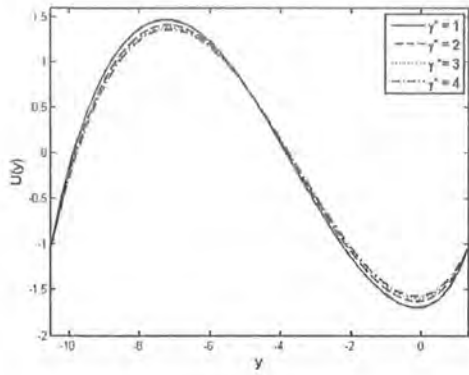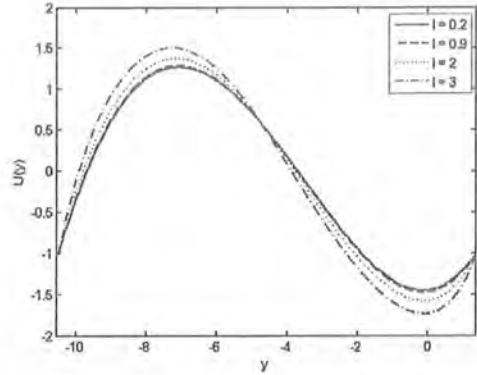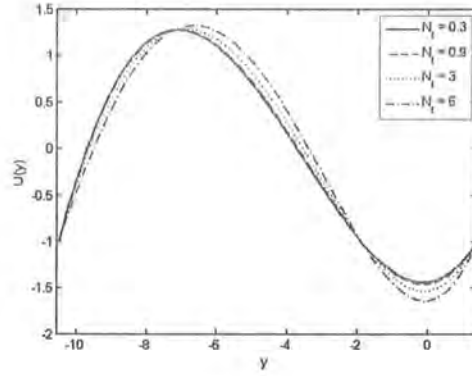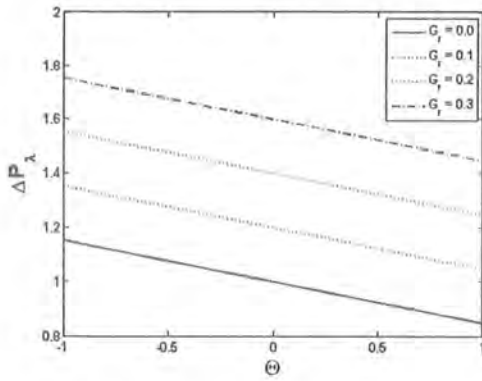

Fig. 2.3

Fig. 2.4

Figs. (2.3 - 2.4): Variation of velocities for different values of γ^* with $l = 0.4$ and l with $\gamma^* = 2$, when $\Theta = 5$, $G_r = 0.6$, $a = 0.4$, $d = 10$, $x = 0.4$, $b = 0.6$, $\phi = 0.2$, $W_e = 0.3$, $N_t = 0.7$, $N_b = 0.6$, $B_r = 0.5$.

26

Fig. 2.5

Fig. 2.5: Variation of velocity for different values of N_t when $\Theta = 5$, $= 0.4$, $a = 0.4$, $d = 10$, $x = 0.4$, $b = 0.6$, $\phi = 0.2$, $\gamma^* = 2$, $l = 0.4$, $N_b = 0.6$, $W_e = 0.3$, $G_r = 0.6$, $B_r = 0.5$.
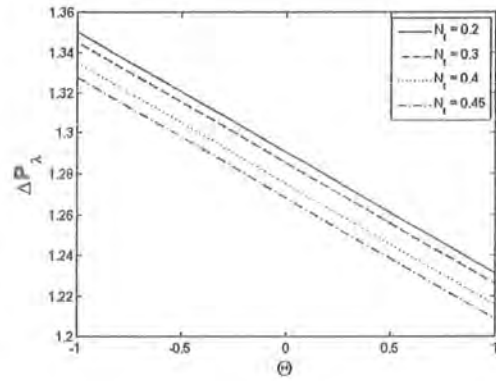

Fig. 2.6   Fig. 2.7

Figs. (2.6 - 2.7): Variation of ΔP_λ for different values of G_r with $N_t = 0.7$ and N_t with $G_r = 0.6$, when $l = 0.4$, $a = 0.4$, $d = 2$, $b = 0.6$, $\phi = 0.2$, $\gamma^* = 2$, $W_e = 0.3$, $N_b = 0.6$, $B_r = 0.5$.
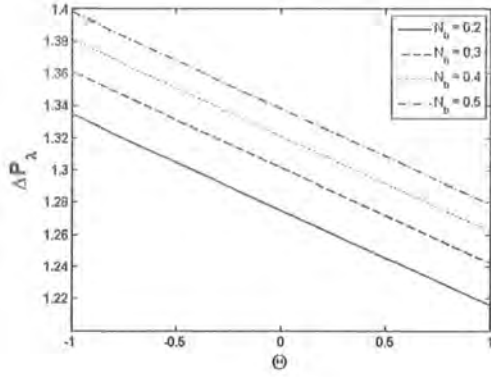
Fig. 2.8
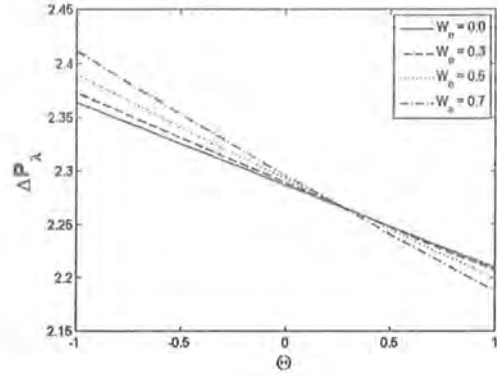
Fig. 2.9

Figs. (2.8 - 2.9): Variation of ΔP_λ for different values of N_b with $W_e = 0.3$ and W_e with $N_b = 0.6$, when $l = 0.4$, $a = 0.4$, $d = 2$, $b = 0.6$, $\phi = 0.2$, $\gamma^* = 2$, $G_r = 0.6$, $B_r = 0.5$, $N_t = 0.7$.
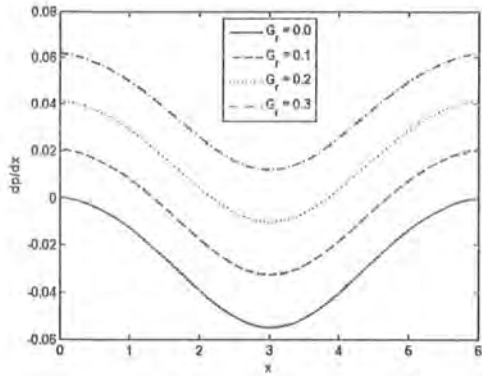
Fig. 2.10
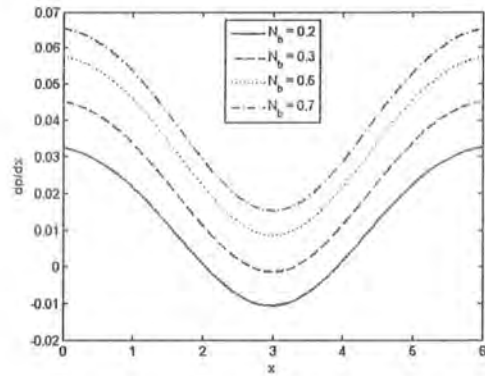
Fig. 2.11

Figs. (2.10 - 2.11): Variation of dp/dx for different values of G_r with $N_b = 0.6$ and N_b with $G_r = 0.2$, when $\Theta = 5$, $l = 0.4$, $a = 0.3$, $d = 2$, $b = 0.4$, $\phi = 0.2$, $\gamma^* = 1$, $N_t = 0.7$, $W_e = 0.3$, $B_r = 0.5$.
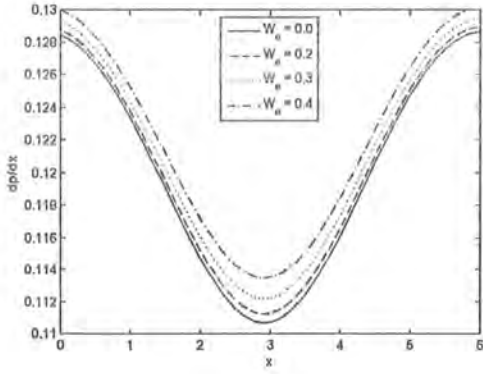
Fig. 2.12
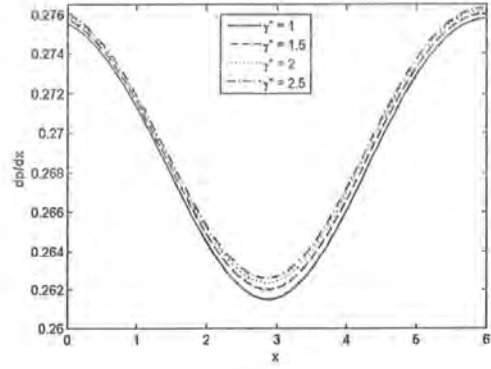
Fig. 2.13

Figs. (2.12 - 2.13): Variation of dp/dx for different values of W_e with $\gamma^* = 1$ and γ^* with $W_e = 0.3$, when $\Theta = 5$, $l = 0.4$, $a = 0.3$, $d = 2$, $b = 0.4$, $\phi = 0.2$, $N_b = 0.6$, $N_t = 0.7$, $G_r = 0.6$, $B_r = 0.5$.
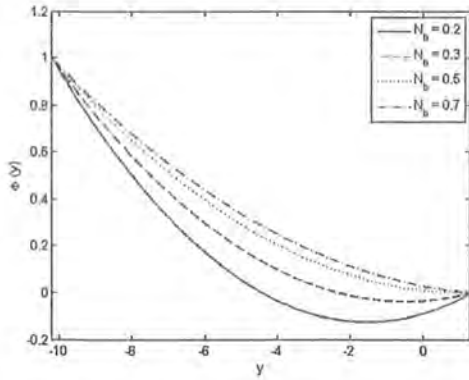
Fig. 2.14
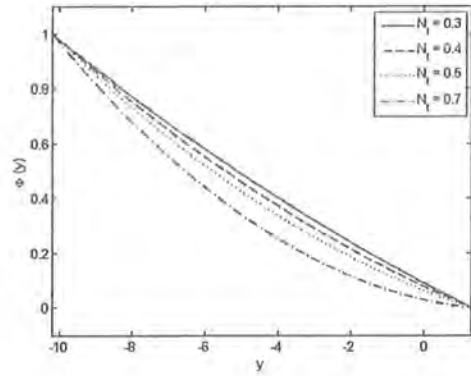
Fig. 2.15

Figs. (2.14 - 2.15): Variation of $\Phi(y)$ for different values of N_b with $N_t = 0.7$ and N_t with $N_b = 0.6$, when $\Theta = 5$, $l = 0.4$, $a = 0.4$, $d = 10$, $x = 0.4$, $b = 0.6$, $\phi = 0.2$, $\gamma^* = 2$, $W_e = 0.3$, $G_r = 0.6$, $B_r = 0.5$.

29
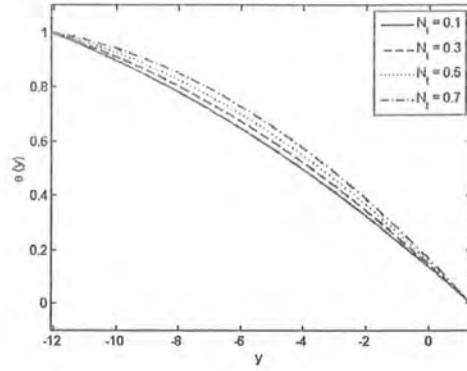
Fig. 2.16

Fig. 2.16: Variation of $\theta(y)$ for different values of N_t when $\Theta = 5$, $l = 0.4$, $a = 0.4$, $d = 10$, $x = 0.4$, $b = 0.6$, $\phi = 0.2$, $\gamma^* = 2$, $W_e = 0.3$, $N_b = 0.6$, $G_r = 0.6$, $B_r = 0.5$.
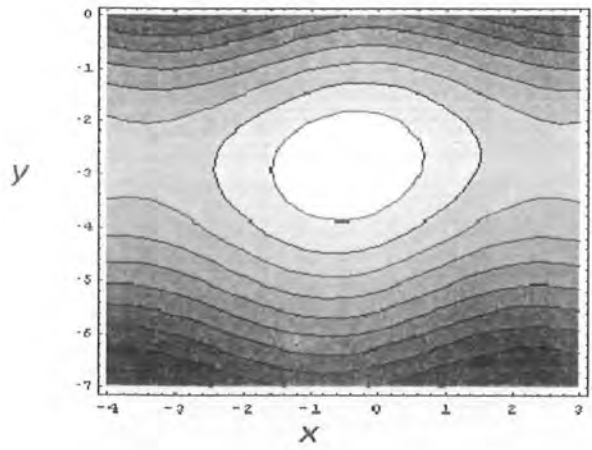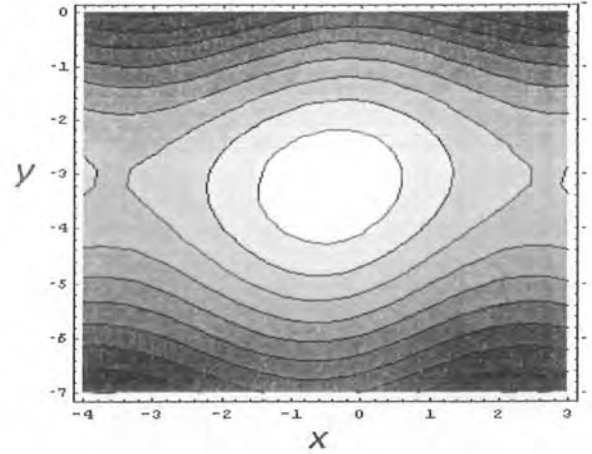

Fig. 2.17(a)   Fig. 2.17(b)

Fig. 2.17: Streamlines for $G_r = 0.1$ (a) and $G_r = 0.6$ (b), when $\Theta = 5$, $l = 0.4$, $a = 0.3$, $b = 0.4$, $d = 2$, $\phi = \pi/4$, $W_e = 0.3$, $\gamma^* = 1$, $N_t = 0.7$, $B_r = 0.3$, $N_b = 0.6$.
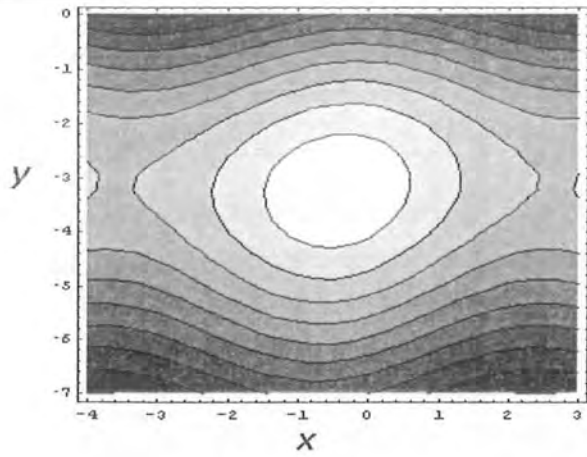
Fig. 2.18(a)   Fig. 2.18(b)
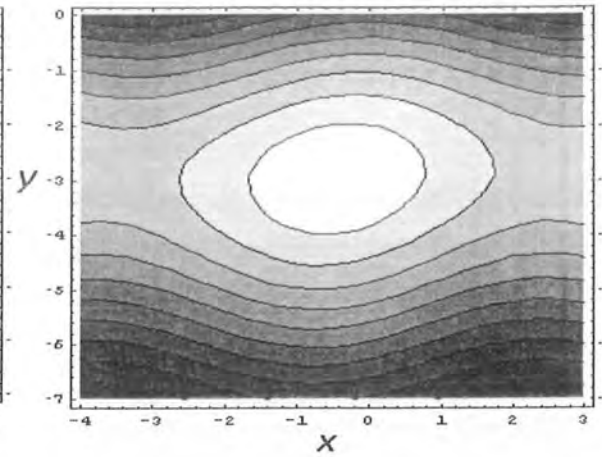
Fig. 2.18: Streamlines for $W_e = 0.2$ (a) and $W_e = 0.9$ (b), when $\Theta = 2$, $l = 0.4$, $a = 0.3$, $b = 0.4$, $d = 2$, $\phi = \pi/4$, $G_r = 0.3$, $\gamma^* = 1$, $N_t = 0.7$, $B_r = 0.3$, $N_b = 0.6$.
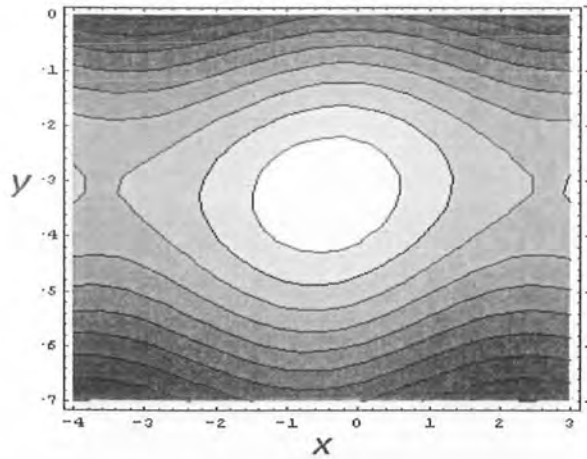

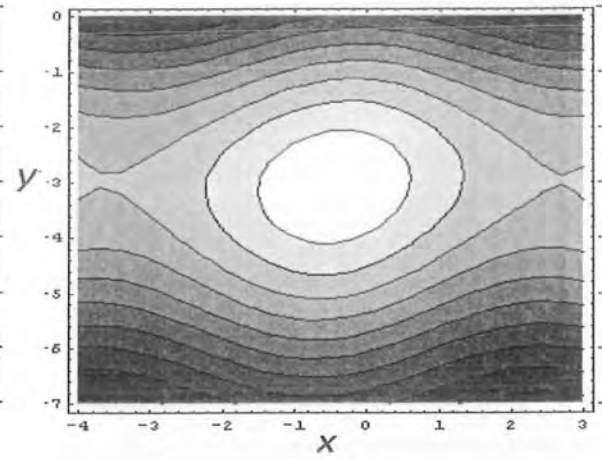Fig. 2.19(a)   Fig. 2.19(b)

Fig. 2.19: Streamlines for $N_b = 0.1$ (a) and $N_b = 0.9$ (b), when $\Theta = 2$, $l = 0.4$, $a = 0.3$, $b = 0.4$, $d = 2$, $\phi = \pi/4$, $W_e = 0.3$, $\gamma^* = 1$, $N_t = 0.7$, $B_r = 0.3$, $G_r = 0.3$.

Chapter 3

Peristaltic transport of Jeffrey six-constant fluid with nanoparticles

This chapter is devoted to investigate the influence of nanoparticles on the peristaltic transport of six constant Jeffrey fluid. Flow is induced by peristaltic wave along the length of channel walls. The analysis for axial velocity, pressure gradient and stream functions are carried out under lubrication approximation. The resulting non-linear equations are then solved for series expressions. Graphical results are obtained to analyze the impact of emerging parameters in the flow problem.

3.1 Governing equations

We consider the peristaltic flow of Jeffrey six-constant fluid with nanoparticle in a vertical asymmetric channel. Asymmetry in the channel is because of propagation of peristaltic waves having different amplitudes and phases along the channel walls. The shape of the channel walls can be expressed as follows:

$$\bar{Y} = \bar{H}_1 = d_1 + a_1 \cos \left(\frac{2\pi}{\lambda} \left(\bar{X} - c\bar{t} \right) \right), \qquad \text{Upper wall} \qquad (3.1)$$

$$\bar{Y} = \bar{H}_2 = -d_2 - b_1 \cos \left(\frac{2\pi}{\lambda} \left(\bar{X} - c\bar{t} \right) + \bar{\phi} \right), \quad \text{Lower wall} \qquad (3.2)$$

Here a_1 and b_1 show the waves amplitudes, λ is the wave length, $d_1 + d_2$ the channel width, c the wave speed, $\bar{t}$ the time and the phase difference $\tilde{\phi}$ ranges $0 \leq \tilde{\phi} \leq \pi$. Further, a_1, b_1, d_1, d_2 and $\tilde{\phi}$ satisfy the relation

$$a_1^2 + b_1^2 + 2a_1 b_1 \cos \tilde{\phi} \leq (d_1 + d_2)^2 . \tag{3.3}$$

The equations of motion that governs the incompressible fluid flow interms of mass, momentum, temperature and nanoparticle volume fraction are:

$$\bar{U}(\bar{X}, \bar{Y}, \bar{t}),_{\bar{X}} + \bar{V}(\bar{X}, \bar{Y}, \bar{t}),_{\bar{Y}} = 0, \tag{3.4}$$

$$
\begin{aligned}
\rho_f \left(\bar{U},_{\bar{t}} + \bar{U}\bar{U},_{\bar{X}} + \bar{V}\bar{U},_{\bar{Y}} \right) &= -\bar{P},_{\bar{X}} + \bar{S}_{\bar{X}\bar{X}},_{\bar{X}} + \bar{S}_{\bar{X}\bar{Y}},_{\bar{Y}} \\
&\quad + \rho_f g \alpha_t \left(\bar{T} - T_0 \right) + \rho g \alpha_c \left(\bar{C} - C_0 \right) ,
\end{aligned} \tag{3.5}
$$

$$\rho_f \left(\bar{V},_{\bar{t}} + \bar{U}\bar{V},_{\bar{X}} + \bar{V}\bar{V},_{\bar{Y}} \right) = -\bar{P},_{\bar{Y}} + \bar{S}_{\bar{X}\bar{Y}},_{\bar{X}} + \bar{S}_{\bar{Y}\bar{Y}},_{\bar{Y}} , \tag{3.6}$$

$$
\begin{aligned}
\bar{T},_{\bar{t}} + \bar{U}\bar{T},_{\bar{X}} + \bar{V}\bar{T},_{\bar{Y}} &= \alpha^*(\bar{T},_{\bar{X}\bar{X}} + \bar{T},_{\bar{Y}\bar{Y}}) + \Upsilon^*[D(\bar{C},_{\bar{X}} \bar{T},_{\bar{X}} + \bar{C},_{\bar{Y}} \bar{T},_{\bar{Y}}) \\
&\quad + \left(D/\bar{T}_m \right) \{ (\bar{T},_{\bar{X}})^2 + (\bar{T},_{\bar{Y}})^2 \}],
\end{aligned} \tag{3.7}
$$

$$\bar{C},_{\bar{t}} + \bar{U}\bar{C},_{\bar{X}} + \bar{V}\bar{C},_{\bar{Y}} = D(\bar{C},_{\bar{X}\bar{X}} + \bar{C},_{\bar{Y}\bar{Y}}) + \left(D_{\bar{T}}/\bar{T}_m \right) (\bar{T},_{\bar{X}\bar{X}} + \bar{T},_{\bar{Y}\bar{Y}}). \tag{3.8}$$

Here $\bar{U}$ is the component of velocity vector in $\bar{X}$ directions whereas $\bar{V}$ is the component of velocity in $\bar{Y}$ direction and the subscripts denotes the partial derivatives. Furthermore α_t, α_c, $\bar{C}$, $\bar{T}$, T_0, C_0, α^*, Υ^*, D, and $D_{\bar{T}}$ are defined in chapter one. Note that expression of Cauchy stress tensor $\bar{\mathbf{S}}$ for six constant Jeffrey's model can be written as

$$
\begin{aligned}
&\bar{\mathbf{S}} + \lambda_1 [\frac{d\bar{\mathbf{S}}}{d\bar{t}} - (\bar{W}\cdot\bar{S} + \bar{S}\cdot\bar{W})\bar{\mathbf{I}} + \tilde{a}(\bar{S}\cdot\bar{D} + \bar{D}\cdot\bar{S})\bar{\mathbf{I}} + \tilde{b}(\bar{S}:\bar{D})\bar{\mathbf{I}} + \tilde{c}\bar{\mathbf{D}}(tr\bar{S})] \\
&= 2\mu[\bar{\mathbf{D}} + \lambda_2(\frac{d\bar{\mathbf{D}}}{d\bar{t}} - (\bar{W}\cdot\bar{D} + \bar{D}\cdot\bar{W})\bar{\mathbf{I}} + 2\tilde{a}\left(\bar{D}\cdot\bar{D}\right)\bar{\mathbf{I}} + \tilde{b}(\bar{D}:\bar{D})\bar{\mathbf{I}}],
\end{aligned} \tag{3.9}
$$

and

$$(\bar{S}:\bar{D}) = \sum_i \sum_j \bar{S}_{ij}\bar{D}_{ji}, \tag{3.10}$$

33

where μ is the viscosity, λ_1 is the relaxation time, λ_2 is the delay time and $\bar{a}$, $\bar{b}$, $\bar{c}$ are material constants of the fluid model. The definitions of $\bar{\mathbf{D}}$ (symmetric part of velocity gradient) and $\bar{\mathbf{W}}$ (antisymmetric part of velocity gradient) are given in chapter two (See Eq. [2.7])

Using the transformations defined in Eq. (2.20) and the dimensionless quantities given in Eq. (2.21) and then writing velocity components in terms of stream function Ψ as

$$u = \frac{\partial \Psi}{\partial y}, \quad v = -\delta \frac{\partial \Psi}{\partial x}, \tag{3.11}$$

the continuity equation (3.4) satisfies automatically, whereas Eqs. (3.5 − 3.8) reduces to

$$\delta \operatorname{Re} \left[\left(\frac{\partial \Psi}{\partial y} \frac{\partial}{\partial x} - \frac{\partial \Psi}{\partial x} \frac{\partial}{\partial y} \right) \frac{\partial \Psi}{\partial y} \right] = \frac{\partial p}{\partial x} + \delta \frac{\partial S_{xx}}{\partial x} + \frac{\partial S_{xy}}{\partial y} + G_r \theta + B_r \Phi, \tag{3.12}$$

$$\delta^3 \operatorname{Re} \left[\left(\frac{\partial \Psi}{\partial y} \frac{\partial}{\partial x} - \frac{\partial \Psi}{\partial x} \frac{\partial}{\partial y} \right) \frac{\partial \Psi}{\partial x} \right] = \frac{\partial p}{\partial y} + \delta^2 \frac{\partial S_{xy}}{\partial x} + \delta \frac{\partial S_{yy}}{\partial y}, \tag{3.13}$$

$$\delta \operatorname{Re} \left[\left(\frac{\partial \Psi}{\partial y} \frac{\partial}{\partial x} - \frac{\partial \Psi}{\partial x} \frac{\partial}{\partial y} \right) \theta \right] = \delta^2 \frac{\partial^2 \theta}{\partial x^2} + \frac{\partial^2 \theta}{\partial y^2} + N_b \left(\delta^2 \frac{\partial \Phi}{\partial x} \frac{\partial \theta}{\partial x} + \frac{\partial \Phi}{\partial y} \frac{\partial \theta}{\partial y} \right)$$
$$+ N_t \left[\delta^2 \left(\frac{\partial \theta}{\partial x} \right)^2 + \left(\frac{\partial \theta}{\partial y} \right)^2 \right], \tag{3.14}$$

$$\delta \operatorname{Re} \left[\left(\frac{\partial \Psi}{\partial y} \frac{\partial}{\partial x} - \frac{\partial \Psi}{\partial x} \frac{\partial}{\partial y} \right) \Phi \right] = \delta^2 \frac{\partial^2 \Phi}{\partial x^2} + \frac{\partial^2 \Phi}{\partial y^2} + \frac{N_t}{N_b} \left(\delta^2 \frac{\partial^2 \theta}{\partial x^2} + \frac{\partial^2 \theta}{\partial y^2} \right), \tag{3.15}$$

The expressions for S_{xx}, S_{xy} and S_{yy} are:

$$S_{xx} + \lambda_1 [\delta \left(\frac{\partial \Psi}{\partial y} \frac{\partial}{\partial x} - \frac{\partial \Psi}{\partial x} \frac{\partial}{\partial y} \right) S_{xx} + \tilde{a} \{ 2\delta \frac{\partial^2 \Psi}{\partial x \partial y} S_{xx} + S_{xy} \left(\frac{\partial^2 \Psi}{\partial y^2} - \delta \frac{\partial^2 \Psi}{\partial x^2} \right) \}$$
$$\times \bar{b} \{ \delta \frac{\partial^2 \Psi}{\partial x \partial y} S_{xx} + S_{xy} \left(\frac{\partial^2 \Psi}{\partial y^2} - \delta^2 \frac{\partial^2 \Psi}{\partial x^2} \right) - \delta S_{yy} \frac{\partial^2 \Psi}{\partial x \partial y} \} + \tilde{c} \{ (S_{xx} + S_{xy} + S_{yy}) \delta \frac{\partial^2 \Psi}{\partial x \partial y} \}]$$
$$= 2[\delta \frac{\partial^2 \Psi}{\partial x \partial y} + \lambda_2 [\delta^2 \left(\frac{\partial \Psi}{\partial y} \frac{\partial}{\partial x} - \frac{\partial \Psi}{\partial x} \frac{\partial}{\partial y} \right) \frac{\partial^2 \Psi}{\partial x^2} + \frac{1}{2} \{ \delta^4 \left(\frac{\partial^2 \Psi}{\partial x^2} \right)^2 - \left(\frac{\partial^2 \Psi}{\partial y^2} \right)^2 \}$$
$$+ 2\tilde{a} \{ \delta^2 \left(\frac{\partial^2 \Psi}{\partial x \partial y} \right) + \frac{1}{4} \left(\frac{\partial^2 \Psi}{\partial y^2} - \delta^2 \frac{\partial^2 \Psi}{\partial x^2} \right)^2 \} + \bar{b} \{ 2\delta^2 \left(\frac{\partial^2 \Psi}{\partial x \partial y} \right)^2$$
$$+ \frac{1}{2} \left(\frac{\partial^2 \Psi}{\partial y^2} - \delta^2 \frac{\partial^2 \Psi}{\partial x^2} \right)^2 \}]], \tag{3.16}$$

34

$$
\begin{aligned}
S_{yy} &+ \lambda_1[\delta\left(\frac{\partial\Psi}{\partial y}\frac{\partial}{\partial x}-\frac{\partial\Psi}{\partial x}\frac{\partial}{\partial y}\right)S_{yy}+\left(\frac{\partial^2\Psi}{\partial y^2}+\delta^2\frac{\partial^2\Psi}{\partial x^2}\right)S_{xy}+\tilde{a}\{-2\delta\frac{\partial^2\Psi}{\partial x\partial y}S_{yy} \\
&+S_{xy}\left(\frac{\partial^2\Psi}{\partial y^2}-\delta^2\frac{\partial^2\Psi}{\partial x^2}\right)\}\times\bar{b}\{\delta\frac{\partial^2\Psi}{\partial x\partial y}S_{xx}+S_{xy}\left(\frac{\partial^2\Psi}{\partial y^2}-\delta^2\frac{\partial^2\Psi}{\partial x^2}\right)-\delta S_{yy}\frac{\partial^2\Psi}{\partial x\partial y}\} \\
&+\bar{c}\{(S_{xx}+S_{yy})\delta\frac{\partial^2\Psi}{\partial x\partial y}\}] \\
=& \ 2[\frac{\partial^2\Psi}{\partial y^2}+\lambda_2[\delta^2\left(-\frac{\partial\Psi}{\partial y}\frac{\partial}{\partial x}+\frac{\partial\Psi}{\partial x}\frac{\partial}{\partial y}\right)\frac{\partial^2\Psi}{\partial x\partial y}+\frac{1}{2}\{\left(\frac{\partial^2\Psi}{\partial y^2}\right)^2-\delta^4\left(\frac{\partial^2\Psi}{\partial x^2}\right)^2\} \\
&+2\tilde{a}\{\delta^2\left(\frac{\partial^2\Psi}{\partial x\partial y}\right)+\frac{1}{4}\left(\frac{\partial^2\Psi}{\partial y^2}-\delta^2\frac{\partial^2\Psi}{\partial x^2}\right)^2\}+\bar{b}\{2\delta^2\left(\frac{\partial^2\Psi}{\partial x\partial y}\right)^2 \\
&+\frac{1}{2}\left(\frac{\partial^2\Psi}{\partial y^2}-\delta^2\frac{\partial^2\Psi}{\partial x^2}\right)^2\}]],
\end{aligned}
\tag{3.17}
$$

$$
\begin{aligned}
S_{xy} &+ \lambda_1[\delta\left(\frac{\partial\Psi}{\partial y}\frac{\partial}{\partial x}-\frac{\partial\Psi}{\partial x}\frac{\partial}{\partial y}\right)S_{xy}+\frac{1}{2}\left(\frac{\partial^2\Psi}{\partial y^2}+\delta^2\frac{\partial^2\Psi}{\partial x^2}\right)(S_{xx}-S_{yy})+\frac{\tilde{c}}{2}(S_{xx}+S_{yy}) \\
&\times\left(\frac{\partial^2\Psi}{\partial y^2}-\delta^2\frac{\partial^2\Psi}{\partial x^2}\right)]+\tilde{a}\{\frac{S_{xx}}{2}+\frac{S_{yy}}{2}\left(\frac{\partial^2\Psi}{\partial y^2}-\delta^2\frac{\partial^2\Psi}{\partial x^2}\right)\}] \\
=& \ 2\left(\frac{\partial^2\Psi}{\partial y^2}-\delta^2\frac{\partial^2\Psi}{\partial x^2}\right)+\lambda_2[\delta\left(\frac{\partial\Psi}{\partial y}\frac{\partial}{\partial x}-\frac{\partial\Psi}{\partial x}\frac{\partial}{\partial y}\right)\left(\frac{\partial^2\Psi}{\partial y^2}-\delta^2\frac{\partial^2\Psi}{\partial x^2}\right) \\
&+\{\left(\frac{\partial^2\Psi}{\partial y^2}+\delta^2\frac{\partial^2\Psi}{\partial x^2}\right)\delta\frac{\partial^2\Psi}{\partial x\partial y}\}].
\end{aligned}
\tag{3.18}
$$

Note that in Eqs. $(3.11-3.18)$ δ, Re, G_r, B_r, N_b, N_t, θ and Φ denotes the wave number, the Reylonds number number, the local temperature Grashof number, the local nanoparticle Grashof number, the Brownian motion parameter, the thermophoresis parameter, the dimensionless temperature and nonoparticle phenomenon respectively. By adopting lubrication approximation Eqs. (3.12 - 3.18) take the form

$$
\frac{\partial p}{\partial x}=\frac{\partial S_{xy}}{\partial y}+G_r\theta+B_r\Phi,
\tag{3.19}
$$

$$
\frac{\partial p}{\partial y}=0,
\tag{3.20}
$$

$$
\frac{\partial^2\theta}{\partial y^2}+N_b\frac{\partial\theta}{\partial y}\frac{\partial\Phi}{\partial y}+N_t\left(\frac{\partial\theta}{\partial y}\right)^2=0,
\tag{3.21}
$$

$$
\frac{\partial^2\Phi}{\partial y^2}+\frac{N_t}{N_b}\left(\frac{\partial^2\theta}{\partial y^2}\right)=0,
\tag{3.22}
$$

35

where

$$S_{xy} = \frac{\frac{\partial^2 \Psi}{\partial y^2}\left(1 - \frac{\lambda_1 \lambda_2}{2}\lambda^*\left(\frac{\partial^2 \Psi}{\partial y^2}\right)^2\right)}{\left(1 - \frac{\lambda_1^2}{2}\lambda^*\left(\frac{\partial^2 \Psi}{\partial y^2}\right)^2\right)}, \tag{3.23}$$

in which

$$\lambda^* = \tilde{c}\tilde{b} + (\tilde{a} + \tilde{c} - 1)(\tilde{a} + \tilde{b} + 1). \tag{3.24}$$

Applying binomial expansion about λ^* on Eq. (3.23) and then using it in Eq. (3.19) we have

$$\frac{dp}{dx} = \frac{\partial}{\partial y}\left(\frac{\partial^2 \Psi}{\partial y^2} + \lambda^* \hat{A}\left(\frac{\partial^2 \Psi}{\partial y^2}\right)^3 + (\lambda^*)^2 \hat{B}\left(\frac{\partial^2 \Psi}{\partial y^2}\right)^5\right) + G_r \theta + B_r \Phi, \tag{3.25}$$

$$\hat{A} = \left(\frac{\lambda_1^2}{2} - \frac{\lambda_1 \lambda_2}{2}\right), \ \hat{B} = -\frac{\lambda_1^3 \lambda_2}{4}. \tag{3.26}$$

Through Eqs. (3.20) and (3.25) we can write

$$\frac{\partial^2}{\partial y^2}\left(\frac{\partial^2 \Psi}{\partial y^2} + \lambda^* \hat{A}\left(\frac{\partial^2 \Psi}{\partial y^2}\right)^3 + (\lambda^*)^2 \hat{B}\left(\frac{\partial^2 \Psi}{\partial y^2}\right)^5\right) + G_r \frac{\partial \theta}{\partial y} + B_r \frac{\partial \Phi}{\partial y} = 0. \tag{3.27}$$

The corresponding non-dimensional boundary conditions in the moving frame are given by

$$\Psi = \frac{F}{2}, \frac{\partial \Psi}{\partial y} = -1, \ at \ y = h_1 = 1 + a\cos x, \tag{3.28}$$

$$\Psi = -\frac{F}{2}, \frac{\partial \Psi}{\partial y} = -1, \ at \ y = h_2 = -d - b\cos\left(x + \bar{\phi}\right), \tag{3.29}$$

$$\theta = 0, \ at \ y = 1 + a\cos x, \ \theta = 1, \ at \ y = -d - b\cos\left(x + \bar{\phi}\right), \tag{3.30}$$

$$\Phi = 0, \ at \ y = 1 + a\cos x, \ \Phi = 1, \ at \ y = -d - b\cos\left(x + \bar{\phi}\right). \tag{3.31}$$

Here F is the flux in wave frame defined in Eq. (2.46) and $(\lambda^*, \hat{A}$ and $\hat{B})$ are material constants of the fluid.

3.2 Solution of the problem

By using Homotopy Perturbation Method the solutions of Eqs. (3.27), (3.21), (3.22) and (3.25) upto first order are given by

$$\Psi = K_{23} + K_{24}y + K_{25}y^2 + K_{26}y^3 + K_{29}y^4 + K_{30}y^5 + K_{27}y^6 + K_{28}y^7. \tag{3.32}$$

$$\theta = K_9 + K_{10}y + K_{11}y^2 + K_{12}y^3 + K_{13}y^4. \tag{3.33}$$

$$\Phi = K_1 + K_7 + (K_2 + K_8)\,y + K_{14}y^2. \tag{3.34}$$

$$\frac{dp}{dx} = (K_1 + K_7)\,B_r + G_r K_9 + 6(K_{27} + 12\hat{A}K_{25}^2 K_{26}\lambda^* + 80\hat{B}K_{25}^4 K_{26}(\lambda^*)^2. \tag{3.35}$$

Where the values of K's in above equations are given as follows:

$$K_1 = \frac{h_1}{h_1 - h_2}, \quad K_2 = \frac{1}{-h_1 + h_2}, \quad K_3 = -\frac{1}{2}K_2^2 h_1 h_2 (N_b + N_t), \quad K_4 = \frac{1}{2}K_2^2 (h_1 + h_2)(N_b + N_t),$$

$$K_5 = -\frac{1}{12L_2^4(N_b+N_t)^2} N_t \big(-K_4^4 + 6K_2^4 K_4^2 h_1 h_2 \left(N_b + N_t\right)^2 - 4K_2^6 K_4 h_1 h_2 (h_1 + h_2)\left(N_b + N_t\right)^3$$
$$+ K_2^8 h_1 h_2 \left(h_1^2 + h_1 h_2 + h_2^2\right) \left(N_b + N_t\right)^4\big),$$

$$K_6 = -\frac{1}{12L_2^2(N_b+N_t)} \big(N_t \left(2K_4 - K_2^2 (h_1 + h_2)(N_b + N_t)\right)\left(2K_4^2 - 2K_2^2 K_4 (h_1 + h_2)\right.$$
$$\times (N_b + (N_b + N_t)^2))N_t\big) + K_2^4 \left(h_1^2 + h_2^2\right),$$

$$K_7 = \frac{K_2^2 h_1 h_2 N_t (N_b + N_t)}{2N_b}, \quad K_8 = -\frac{K_2^2 (h_1 + h_2) N_t (N_b + N_t)}{2N_b},$$

$$K_9 = K_1 + K_3 + K_5 - \frac{K_4^4 N_t}{12K_2^4(N_b+N_t)^2}, \quad K_{10} = K_2 + K_4 + K_6 + \frac{K_4^3 N_t}{3K_2^2(N_b+N_t)}$$

$$K_{11} = -\big(\frac{K_2^2 N_b + K_2^2 N_t + K_4^2 N_t}{2}\big), \quad K_{12} = \frac{K_2^2 K_4 N_t (N_b + N_t)}{3}, \quad K_{13} = \frac{K_4^4 N_t (N_b + N_t)^2}{12},$$

$$K_{15} = -\frac{(h_1 + h_2)\big(2h_1 h_2(-h_1 + h_2) + F\big(h_1^2 - 4h_1 h_2 + h_2^2\big)\big)}{2(h_1 - h_2)^3}, \quad K_{16} = \frac{-h_1^3 - 3h_1(2F + h_1)h_2 + 3h_1 h_2^2 + h_2^3}{(h_1 - h_2)^3},$$

$$K_{17} = \frac{3(F + h_1 - h_2)(h_1 + h_2)}{(h_1 - h_2)^3}, \quad K_{14} = \frac{K_2^2 N_t (N_b + N_t)}{2N_b}, \quad K_{18} = \frac{-2(F + h_1 - h_2)}{(h_1 - h_2)^3},$$

37

$$K_{19} = \frac{1}{840}h_1^2 h_2^2(-35(B_r + G_r)K_2 + 144K_{18}^2\lambda^*(-21\hat{A}(5K_{17} + 6(h_1 + h_2)K_{18}) - 40\hat{B}(35K_{17}^3 + 126(h_1 +$$
$$K_{17}^2 K_{18} + 63\left(3h_1^2 + 4h_1 h_2 + 3h_2^2\right)K_{17}K_{18}^2 + 54(h_1 + h_2)\left(2h_1^2 + h_1 h_2 + 2h_2^2\right)K_{18}^3)\lambda^*)),$$

$$K_{20} = \frac{1}{420}h_1 h_2(35(h_1 + h_2)(B_r + G_r)K_2 + 72K_{18}^2\lambda^*(210A(h_1 + h_2)L_{17} + 63A\left(4h_1^2 + 7h_1 h_2 + 4h_2^2\right)K_1$$
$$+40\hat{B}(70(h_1 + h_2)K_{17}^3 + 63\left(4h_1^2 + 7h_1 h_2 + 4h_2^2\right)K_{18}K_{17}^2 + 378(h_1 + h_2)\left(h_1^2 + h_1 h_2 + h_2^2\right)K_{18}^2 I$$
$$27(8h_1^4 + 17h_1^3 h_2 + 20h_1^2 h_2^2 + 17h_1 h_2^3 + 8h_2^4)K_{18}^3)\lambda^*)),$$

$$K_{21} = -\frac{1}{24}(B_r + G_r)(h_1^2 + 4h_1 h_2 + h_2^2)K_2 - \frac{18}{5}(\hat{A}K_{18}^2(5(h_1^2 + 4h_1 h_2 + h_2^2)K_{17} + 6(h_1 + h_2)(h_1^2 + 4h_1 h_2$$
$$+h_2^2)K_{18}\lambda^* - \frac{48}{7}\hat{B}K_{18}^2(35(h_1^2 + 4h_1 h_2 + h_2^2)K_{17}^3 + 126(h_1 + h_2)(h_1^2 + 3h_1 h_2 + h_2^2)K_{17}^2 + 189$$
$$(h_1^2 + h_1 h_2 + h_2^2)(h_1^2 + 3h_1 h_2 + h_2^2)K_{18}^2 K_{17} + 54(h_1 + h_2)(2h_1^4 + 6h_1^3 h_2 + 5h_1^2 h_2^2 + 6h_1 h_2^3 +$$
$$2h_2^4)K_{18}^3)(\lambda^*)^2,$$

$$K_{22} = \frac{1}{12}(B_r + G_r)(h_1 + h_2)K_2 + \frac{18}{5}\hat{A}K_{18}^2(10(h_1 + h_2)K_{17} + 3\left(3h_1^2 + 4h_1 h_2 + 3h_2^2\right)K_{18})\lambda^* + \frac{48}{7}\hat{B}K_{18}^2$$
$$(h_1 + h_2)K_{17}^3 + 63\left(3h_1^2 + 4h_1 h_2 + 3h_2^2\right)K_{17}^2 K_{18} + 126(h_1 + h_2)(2h_1^2 + h_1 h_2 + 2h_2^2)K_{18}^2 K_{17} + 27$$
$$(5h_1^4 + 8h_1^3 h_2 + 9h_1^2 h_2^2 + 8h_1 h_2^3 + 5h_2^4)K_{18}^3)(\lambda^*)^2,$$

$$K_{23} = K_{15} + K_{19}, \quad K_{24} = K_{16} + K_{20}, \quad K_{25} = K_{17} + K_{21}, \quad K_{26} = K_{18} + K_{22}, \quad K_{27} = -432\hat{B}K_{18}^4 K_{17}(\lambda^*)^2,$$

$$K_{28} = -\frac{1296}{7}\hat{B}K_{18}^5(\lambda^*)^2, \quad K_{29} = -\frac{(B_r + G_r)K_2}{24} - 18\hat{A}K_{18}^2\lambda^* - 240\hat{B}K_{18}^2 K_{17}^3(\lambda^*)^2,$$

$$K_{30} = -\frac{54}{5}\hat{A}K_{18}^3\lambda^* - 432\hat{B}K_{18}^3 K_{17}^2(\lambda^*)^2.$$

3.3   Graphical results

The goal of the current section is to study and discuss the effects of various physical parameters such as B_r, G_r, N_t, N_b and material parameters λ^*, λ_1 and λ_2 that are involved in the flow regime on axial velocity $u(y)$, pressure gradient (dp/dx), pressure rise (ΔP_λ) and stream function (Ψ). The plots for velocity profile are parabolic in nature and are displayed in Figs.(3.1 − 3.5). In these, Fig. (3.1) depict that an increase in λ^* assist the velocity near the

wall of the channel and resist the velocity in the central part of the channel. Effects of B_r and G_r on velocity are shown in Figs. (3.2) and (3.3). These plots reflects that both of B_r and G_r intensify the velocity for $-1.5 < y < -0.25$ but for $-0.1 < y < 1.4$ the velocity decreases. Influence of relaxation time (λ_1) and retardation time (λ_2) on the velocity profile are discussed through Figs. (3.4) and (3.5). Opposite effect is observed on velocity for λ_1 and λ_2. Increase in the values of λ_1 assist the flow at the center of the channel whereas increase in λ_2 reduces the velocity near the channel's center. Plots in Figs. (3.6 − 3.12) are prepared to see the variation in pressure gradient (dp/dx) for different parameters of interest. Fig. (3.6) reveal that dp/dx decreases in the narrow part of the channel at $x = 3$ when the fluid parameter (λ^*) is increased. Furthermore pressure gradient is maximum when $\lambda^* = 0$ (Newtonian case). To see the influence of parameters B_r and G_r on dp/dx we prepared Figs. (3.7) and (3.8). These Figs. reveal that the pressure gradient is an increasing function for both B_r and G_r. Figs. (3.9) and (3.10) are displayed for the effect of λ_1 and λ_2 on dp/dx. These plots show that the pressure gradient enhances for large values of λ_1. However dp/dx decreases for an increase in λ_2. Figs. (3.11) and (3.12) indicate that pressure gradient is an increasing function of N_b and is a decreasing function of N_t.

The variations in pressure rise per wavelength (ΔP_λ) versus average flow rate (Θ) for distinct values of parameters involved in the flow problem are shown in Figs. (3.13 − 3.19). Figs. (3.13) and (3.17) show that pressure rise decreases in the peristaltic pumping region when λ^* and λ_2 are increased, whereas pressure rise increases in the peristaltic pumping region for large values of λ_1 (see Fig. 3.16). In addition to this Figs (3.14), (3.15) and (3.18) indicate that an increase in the values of parameters B_r, G_r and N_b boost up the pressure rise for all values of Θ. Impact of N_t on ΔP_λ is shown in Fig. (3.19). From the Fig. it is evident that effect of N_t on ΔP_λ is quite opposite to that of N_b.
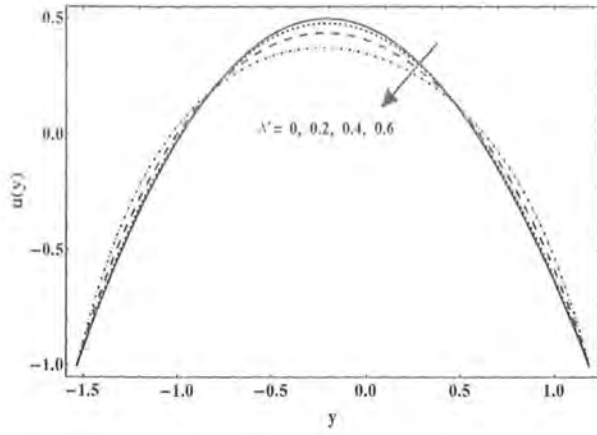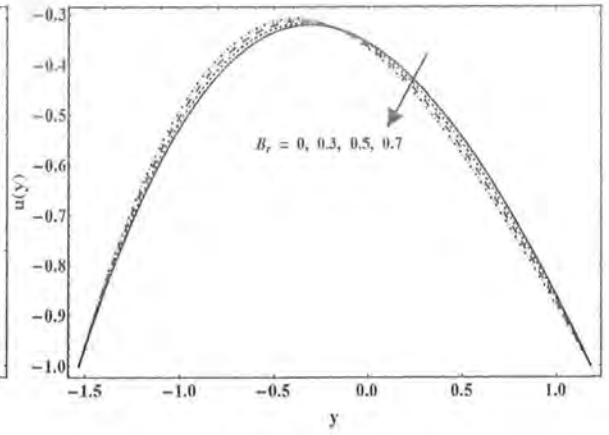
Fig. 3.1

Fig. 3.2

Figs. (3.1 - 3.2): Plots of velocity for λ^* with $B_r = 0.2$ and B_r with $\lambda^* = 0.1$, when $\Theta = 2$, $\lambda_1 = 0.7$, $a = 0.2$, $d = 2$, $x = 0.4$, $b = 1.2$, $\phi = \pi/2$, $\lambda_2 = 0.9$, $N_t = 0.7$, $N_b = 0.6$, $G_r = 0.3$,
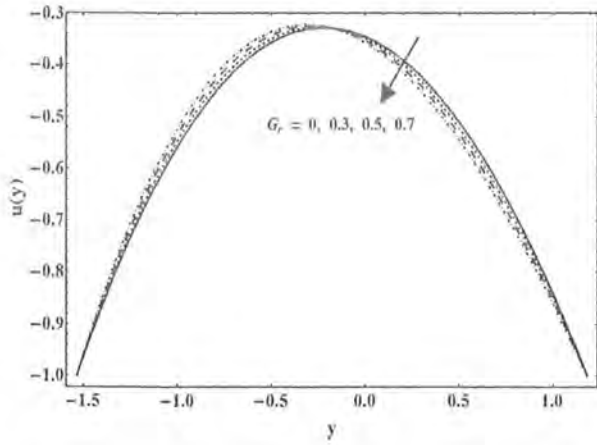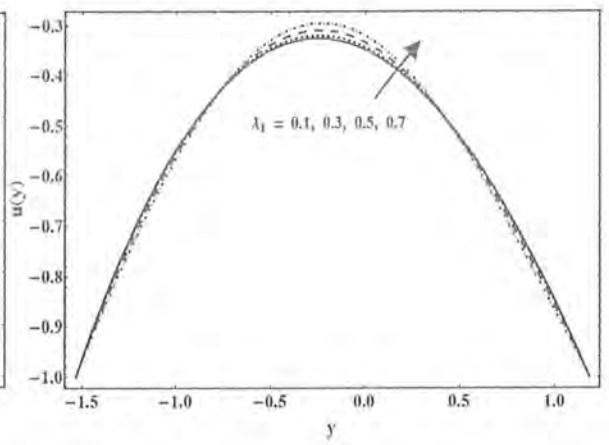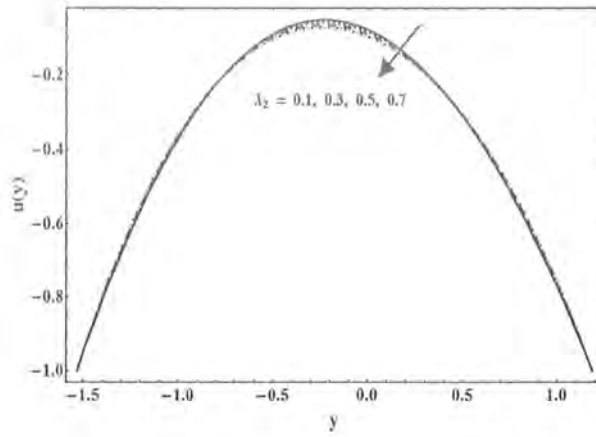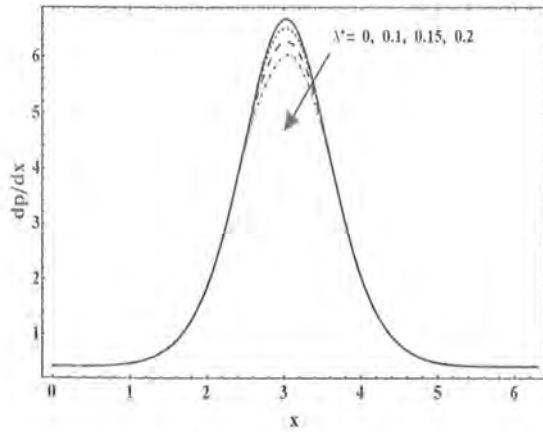

Fig. 3.3

Fig. 3.4

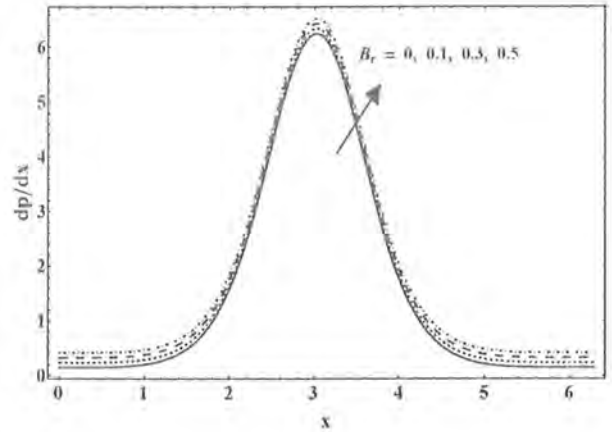Figs. (3.3 - 3.4): Plots of velocity for G_r with $\lambda_1 = 0.1$ and λ_1 with $G_r = 0.3$, when $\Theta = 2$, $\lambda^* = 0.1$, $a = 0.2$, $d = 2$, $x = 0.4$, $b = 1.2$, $\phi = \pi/2$, $\lambda_2 = 0.9$, $N_t = 0.7$, $N_b = 0.6$, $B_r = 0.2$.

Fig. 3.5

Fig. 3.5: Plots of velocity for λ_2 when $\Theta = 2$, $\lambda^* = 0.1$, $a = 0.2$, $d = 2$, $x = 0.4$, $b = 1.2$, $\phi = \pi/2$, $\lambda_1 = 0.7$, $N_t = 0.7$, $N_b = 0.6$, $G_r = 0.3$, $B_r = 0.2$.
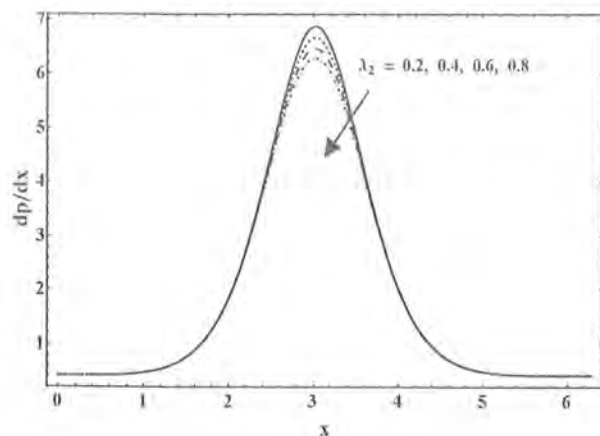

Fig. 3.6

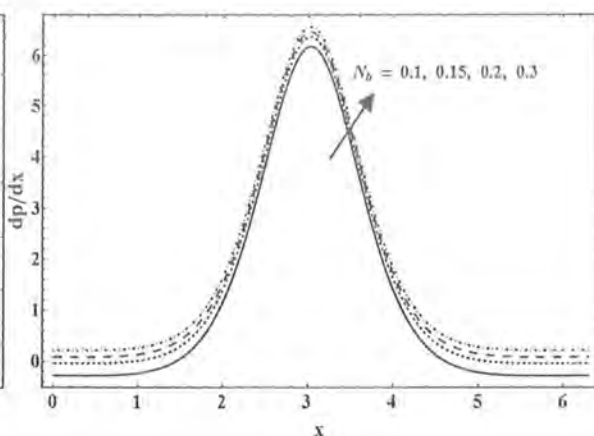Fig. 3.7

Figs. (3.6 - 3.7): Pressure gradient dp/dx for different values of λ^* with $B_r = 0.7$ and B_r with $\lambda^* = 0.1$, when $\Theta = 0.1$, $a = 0.7$, $d = 1.2$, $b = 0.3$, $\phi = 0.4$, $\lambda_1 = 0.8$, $\lambda_2 = 0.7$, $N_t = 0.3$, $N_b = 0.8$, $G_r = 0.8$.

41
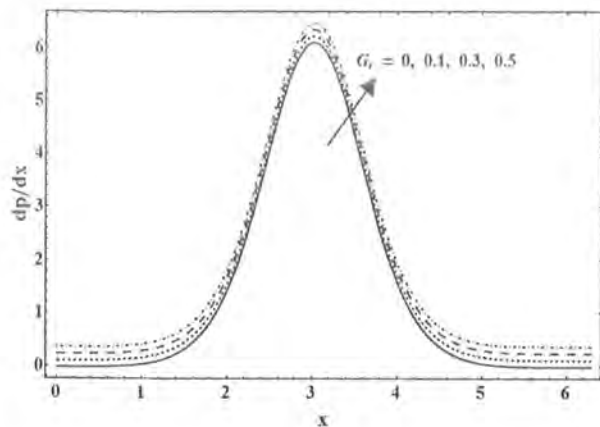
Fig. 3.8
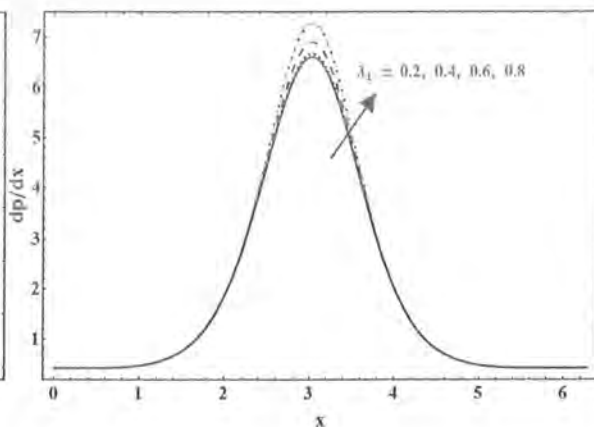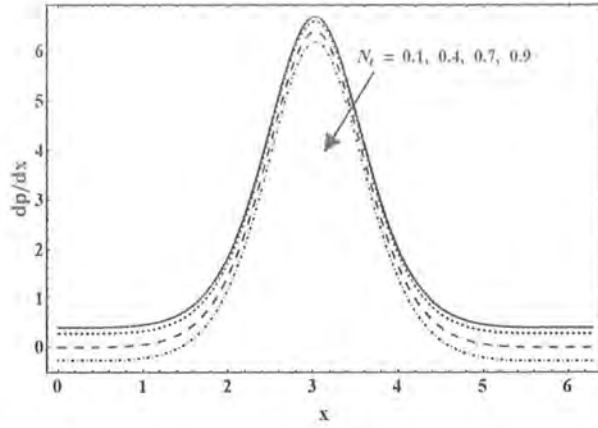

Fig. 3.9

Figs. (3.8 - 3.9): Pressure gradient dp/dx for different values of G_r with $\lambda_1 = 0.1$ and λ_1 with $G_r = 0.8$, when $\Theta = 0.1$, $a = 0.7$, $d = 1.2$, $b = 0.3$, $\phi = 0.4$, $\lambda_2 = 0.7$, $N_t = 0.3$, $N_b = 0.8$, $B_r = 0.2$.

Fig. 3.10

Fig. 3.11

Figs. (3.10 - 3.11): Pressure gradient dp/dx for different values of λ_2 with $N_b = 0.8$ and N_b with $\lambda_2 = 0.7$, when $\Theta = 0.1$, $a = 0.7$, $d = 1.2$, $b = 0.3$, $\phi = 0.4$, $\lambda^* = 0.1$, $\lambda_1 = 0.8$, $N_t = 0.3$, $G_r = 0.8$, $B_r = 0.2$.

Fig. 3.12

Fig. 3.12: Pressure gradient dp/dx for different values of N_t when $\Theta = 0.1$, $a = 0.7$, $d = 1.2$, $b = 0.3$, $\phi = 0.4$, $\lambda^* = 0.1$, $\lambda_1 = 0.8$, $\lambda_2 = 0.7$, $N_t = 0.3$, $G_r = 0.8$, $B_r = 0.2$.
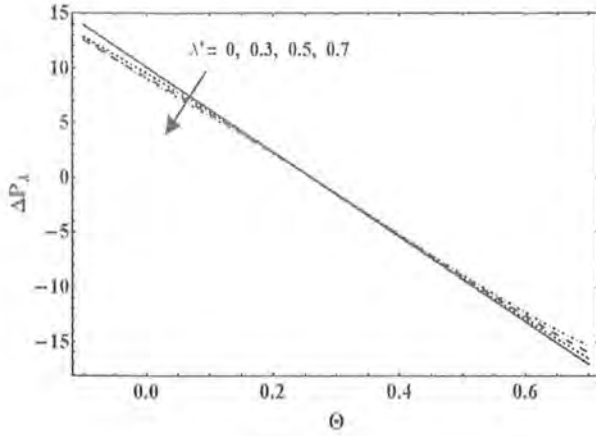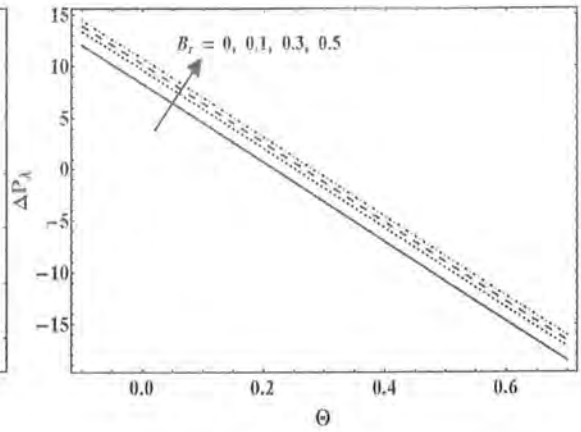

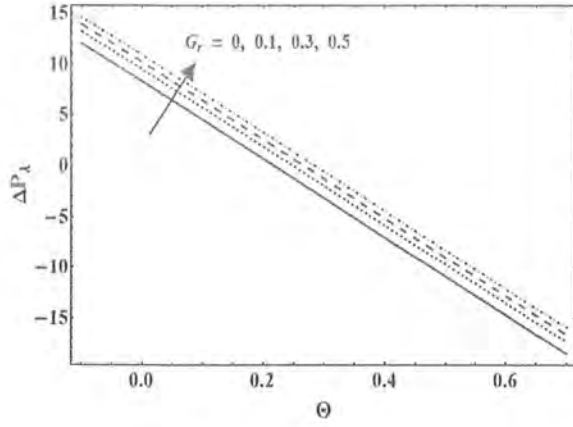
Fig. 3.13

Fig. 3.14

Figs. (3.13 - 3.14): Variations of ΔP_λ for different values of λ^* with $B_r = 0.2$ and B_r with $\lambda^* = 0.1$, when $a = 0.3$, $d = 0.4$, $b = 0.3$, $\phi = \pi/4$, $\lambda_1 = 0.5$, $\lambda_2 = 0.6$, $N_t = 0.3$, $N_b = 0.2$, $G_r = 0.2$.
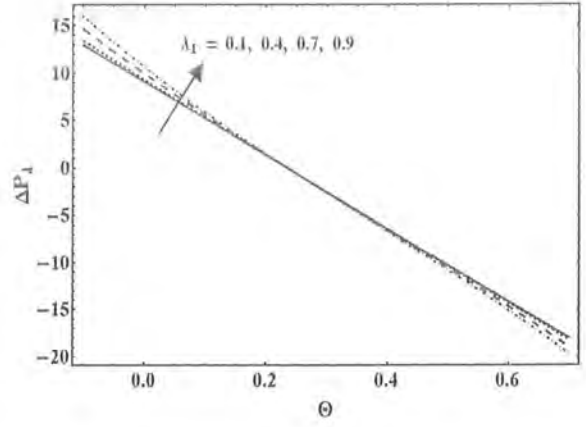
Fig. 3.15

Fig. 3.16

Figs. (3.15 - 3.16): Variations of ΔP_λ for different values of G_r with $\lambda_1 = 0.1$ and λ_1 with $G_r = 0.2$, when $a = 0.3$, $d = 0.4$, $b = 0.3$, $\phi = \pi/4$, $\lambda^* = 0.1$, $\lambda_2 = 0.6$, $N_t = 0.3$, $N_b = 0.2$, $B_r = 0.2$.
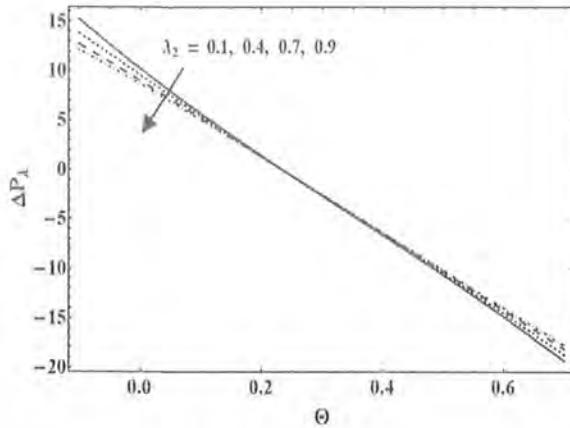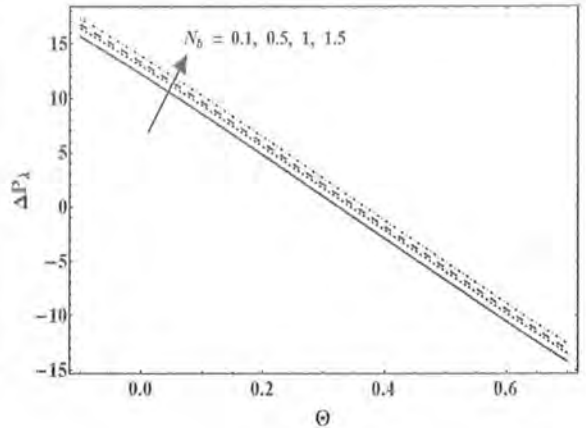

Fig. 3.17

Fig. 3.18

Figs. (3.17 - 3.18): Variations of ΔP_λ for different values of λ_2 with $N_b = 0.2$ and N_b with $\lambda_2 = 0.6$, when $a = 0.3$, $d = 0.4$, $b = 0.3$, $\phi = \pi/4$, $\lambda^* = 0.1$, $\lambda_1 = 0.5$, $N_t = 0.3$, $G_r = 0.2$, $B_r = 0.2$.
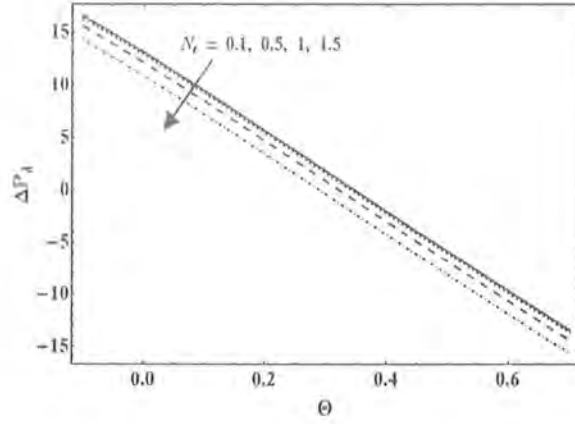
44

Fig. 3.19

Figs. 3.19: Deviation of ΔP_λ for distinct values of N_t when $a = 0.3$, $d = 0.4$, $b = 0.3$, $\phi = \pi/4$, $\lambda^* = 0.1$, $\lambda_1 = 0.5$, $\lambda_2 = 0.6$, $N_b = 0.2$, $G_r = 0.2$, $B_r = 0.2$.

3.3.1 Trapping

Trapping is an interesting phenomenon in peristalsis in which the stream lines in the wave frame of reference splits under certain conditions and enclose a bolus of fluid particles that is pulled ahead along the peristaltic wave with the same speed as the wave. Figs. $(3.20 - 3.24)$ are displayed for the influences of different parameters on the stream lines. The plots indicate that the size of bolus increases by increasing λ^*, B_r, G_r and λ_1 while the size of the bolus decreases by increasing λ_2.
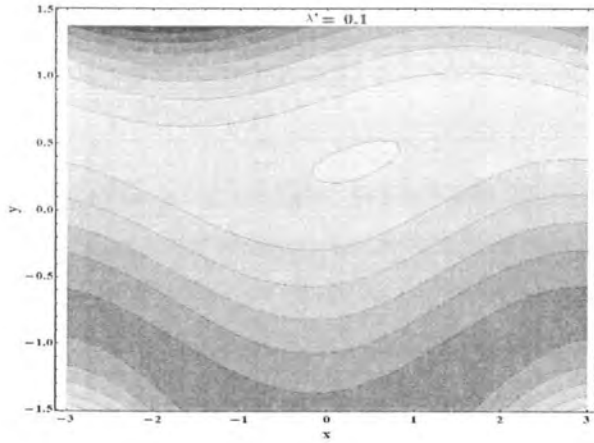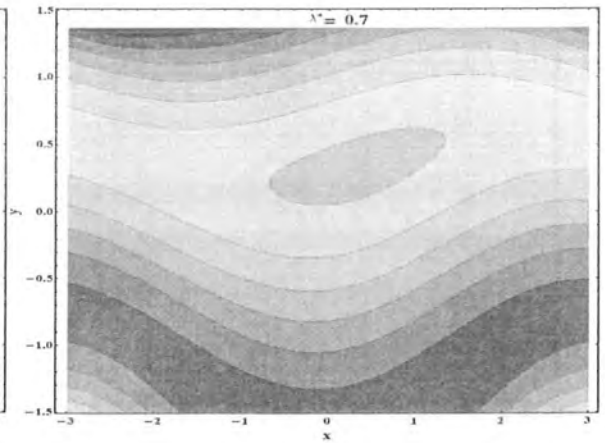
Fig. 3.20(a)   Fig. 3.20(b)

Fig. 3.20: Streamlines for $\lambda^* = 0.1$ (a) and $\lambda^* = 0.7$ (b), when $\Theta = 3.22$, $\lambda_1 = 0.6$, $a = 0.2$, $d = 1.6$, $b = 0.6$, $\phi = \pi/2$, $\lambda_2 = 0.1$, $N_t = 0.4$, $N_b = 0.3$, $B_r = 0.7$ $G_r = 0.7$.
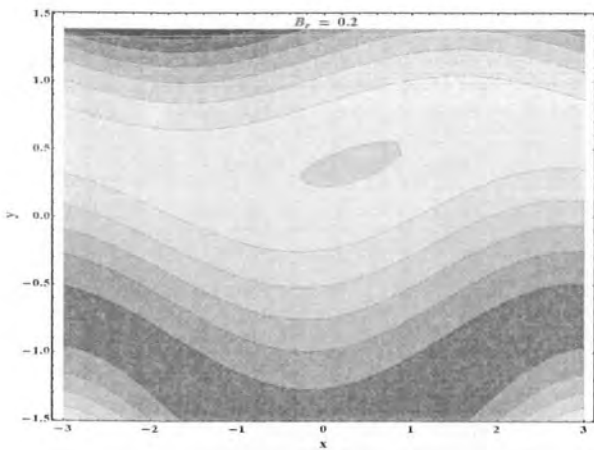

Fig. 3.21(a)   Fig. 3.21(b)

Fig. 3.21: Streamlines for $B_r = 0.2$ (a) and $B_r = 0.7$ (b), when $\Theta = 3.22$, $\lambda_1 = 0.6$, $a = 0.2$, $d = 1.6$, $b = 0.6$, $\phi = \pi/2$, $\lambda_2 = 0.1$, $\lambda^* = 0.1$, $N_t = 0.4$, $N_b = 0.3$, $G_r = 0.7$.

46

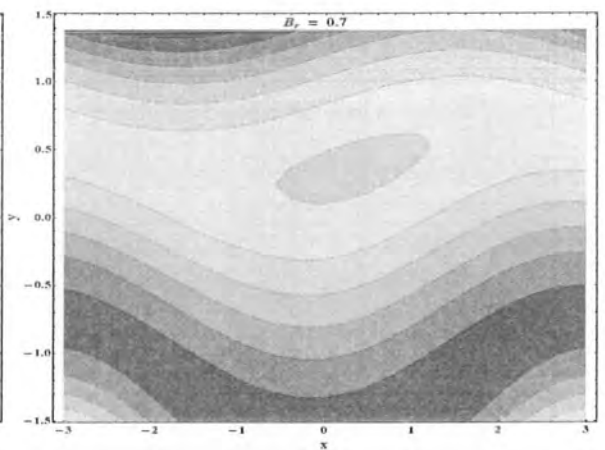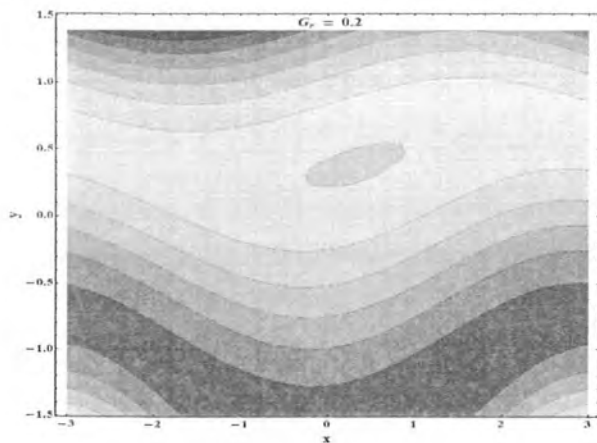Fig. 3.22(a)   Fig. 3.22(b)

Fig. 3.22: Streamlines for $G_r = 0.2$ (a) and $G_r = 0.7$ (b), when $\Theta = 3.22$, $\lambda_1 = 0.6$, $a = 0.2$, $d = 1.6$, $b = 0.6$, $\phi = \pi/2$, $\lambda_2 = 0.1$, $\lambda^* = 0.1$, $N_t = 0.4$, $N_b = 0.3$, $B_r = 0.7$.

Fig. 3.23(a)   Fig. 3.23(b)

Fig. 3.23: Streamlines for $\lambda_1 = 0.4$ (a) and $\lambda_1 = 0.7$ (b), when $\Theta = 3.22$, $a = 0.2$, $d = 1.6$, $b = 0.6$, $\phi = \pi/2$, $\lambda_2 = 0.1$, $\lambda^* = 0.1$, $N_t = 0.4$, $N_b = 0.3$, $B_r = 0.7$, $G_r = 0.7$.
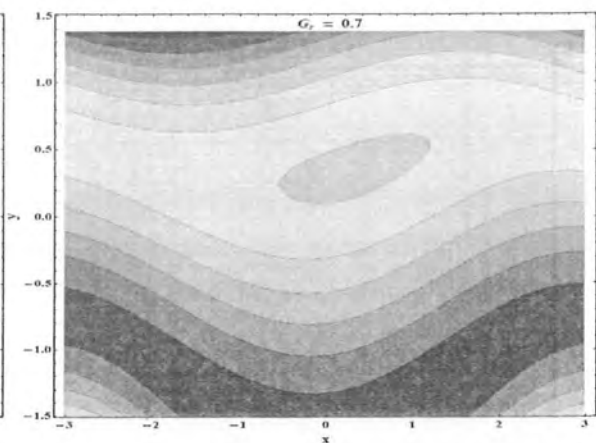
47

Fig. 3.24(a)   Fig. 3.24(b)

Fig. 3.24: Streamlines for $\lambda_2 = 0.1$ (a) and $\lambda_2 = 0.5$ (b), when $\Theta = 3.22$, $\lambda_1 = 0.6$, $a = 0.2$, $d = 1.6$, $b = 0.6$, $\phi = \pi/2$, $\lambda^* = 0.1$, $N_t = 0.4$, $N_b = 0.3$, $B_r = 0.7$ $G_r = 0.7$.
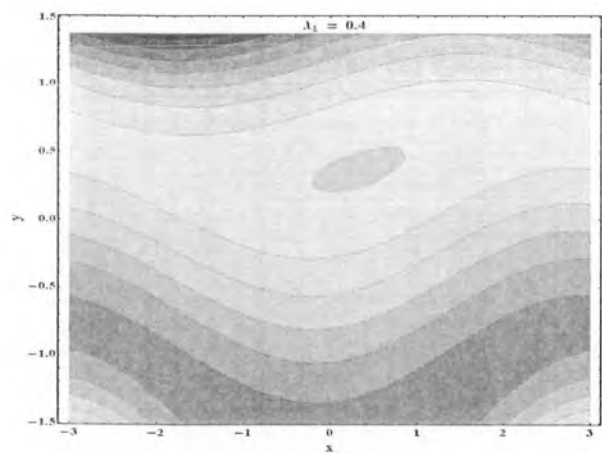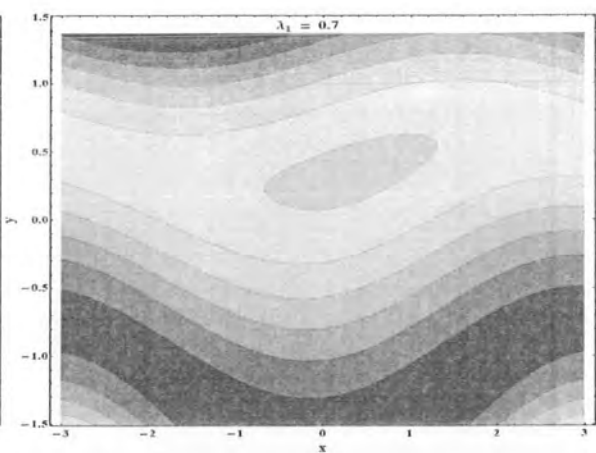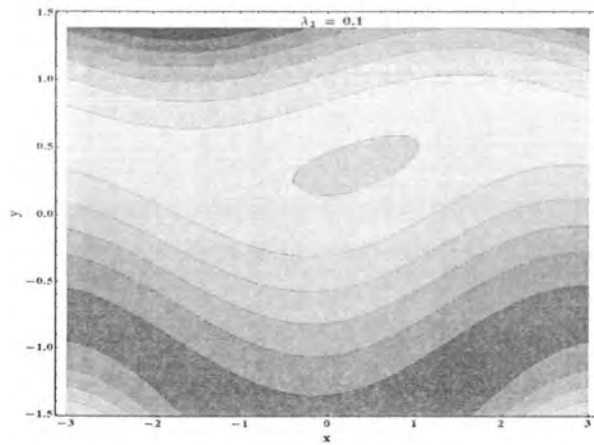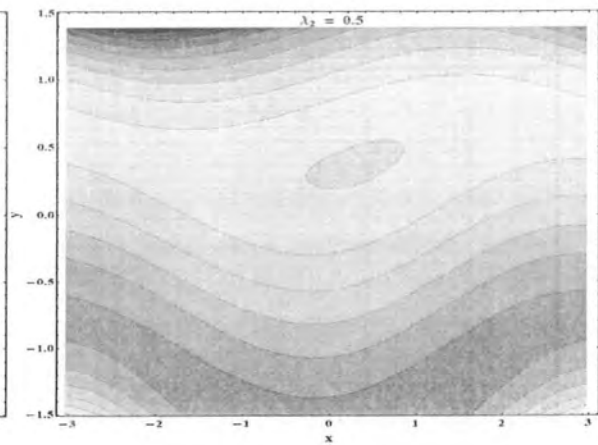
Chapter 4

Influence of slip on peristaltic flow of Powell-Eyring fluid in a symmetric channel

In this chapter we discussed the peristaltic transport of non-Newtonian fluid in a symmetric channel with partial slip effect. The non-Newtonian behavior of fluid is characterized by the constitutive equations of Powell-Eyring fluid. The motion is induced by a sinusoidal wave traveling along the flexible walls of channel. The flow analysis is analyzed in a wave frame of reference moving with the velocity of wave. The equations governing the flow are solved by adopting lubrication approach. Series solutions for the stream function and axial pressure gradient are obtained. Impact of slip and other emerging flow parameters is plotted and analyzed.

4.1   Mathematical formulation and modeling

We consider the flow of Powell-Eyring fluid in a symmetric channel of width $2d$. The flow is induced by a sinusoidal peristaltic wave of small amplitude that travels along the flexible wall of channel. Flow analysis is carried out in a Cartesian coordinate system in which $\overline{X}$-axis is taken along the central line of the channel and $\overline{Y}$-axis normal to it. The wall geometry due to

the infinite train of peristaltic wave can be written as:

$$\overline{H}\left(\overline{X},\bar{t}\right) = d + b\sin\frac{2\pi}{\lambda}\left(\overline{X} - c\bar{t}\right),\tag{4.1}$$

in which b is the wave amplitude, d represents the mean half width of the channel, λ is the wavelength, c is the velocity of the peristaltic wave and $\bar{t}$ is the time.

The basic equations governing the flow of an incompressible fluid in the absence of body forces are

$$\text{div}\,\bar{\mathbf{V}} = 0,\tag{4.2}$$

$$\rho_f\frac{d\bar{\mathbf{V}}}{d\bar{t}} = \text{div}\,\overline{\mathbf{T}},\tag{4.3}$$

where $d/d\bar{t}$ signifies the material derivative, ρ_f the density and $\bar{\mathbf{V}} = \{\bar{U}(\bar{X},\bar{Y},\bar{t}), \bar{V}(\bar{X},\bar{Y},\bar{t}), 0\}$ is the velocity of fluid. The expression of Cauchy stress tensor $\overline{\mathbf{T}}$ is

$$\overline{\mathbf{T}} = -\overline{P}\bar{\mathbf{I}} + \overline{\mathbf{S}}.\tag{4.4}$$

Here $\bar{p}$ is a pressure, $\bar{\mathbf{I}}$ the identity tensor and the extra stress tensor $\overline{\mathbf{S}}$ for a Powell-Eyring fluid is given by:

$$\overline{\mathbf{S}} = \mu\left(\boldsymbol{\nabla}\bar{\mathbf{V}}\right) + \frac{1}{\varpi}\sinh^{-1}\left(\frac{\boldsymbol{\nabla}\bar{\mathbf{V}}}{\zeta}\right),\tag{4.5}$$

where μ is the dynamic viscosity and ϖ and ζ are the material constants of Powell-Eyring fluid. For the stress components the function is approximated as

$$\sinh^{-1}\left(\frac{\boldsymbol{\nabla}\bar{\mathbf{V}}}{\zeta}\right) = \frac{\boldsymbol{\nabla}\bar{\mathbf{V}}}{\zeta} - \left(\frac{\boldsymbol{\nabla}\bar{\mathbf{V}}}{6\zeta}\right)^3 \text{ for } \left|\frac{\boldsymbol{\nabla}\bar{\mathbf{V}}}{\zeta}\right| << 1.\tag{4.6}$$

Equations (4.2) and (4.3) through Eqs. $(4.4 - 4.6)$ give

$$\overline{U},_{\overline{X}} + \overline{V},_{\overline{Y}} = 0,\tag{4.7}$$

$$\rho_f(\bar{U},_{\bar{t}} + \overline{U}\bar{U},_{\overline{X}} + \overline{V}\bar{U},_{\overline{Y}}) = -\bar{P},_{\overline{X}} + \overline{S}_{\overline{XX}},_{\bar{X}} + \overline{S}_{\overline{XY}},_{\bar{Y}},\tag{4.8}$$

$$\rho_f(\bar{V},_{\bar{t}} + \overline{U}\overline{V},_{\overline{X}} + \overline{V}\overline{V},_{\overline{Y}}) = -\bar{P},_{\overline{Y}} + \overline{S}_{\overline{YX}},_{\bar{X}} + \overline{S}_{\overline{YY}},_{\bar{Y}},\tag{4.9}$$

$$\overline{S}_{\overline{XX}} = 2\left(\mu + \frac{1}{\varpi\zeta}\right)\overline{U}_{,\overline{X}} - \frac{1}{3\varpi\zeta^3}\left[2(\overline{U}_{,\overline{X}})^3 + \overline{U}_{,\overline{X}}(\overline{U}_{,\overline{Y}} + \overline{V}_{,\overline{X}})^2 + 2\overline{U}_{,\overline{X}}(\overline{V}_{,\overline{Y}})^2\right], \qquad (4.10)$$

$$\overline{S}_{\overline{XY}} = 2\left(\mu + \frac{1}{\varpi\zeta}\right)(\overline{U}_{,\overline{Y}} + \overline{V}_{,\overline{X}}) - \frac{1}{6\varpi\zeta^3}\left[\begin{array}{c}\{2(\overline{U}_{,\overline{X}})^2 + (\overline{U}_{,\overline{Y}} + \overline{V}_{,\overline{X}})^2 \\ +2(\overline{V}_{,\overline{Y}})^2\}(\overline{U}_{,\overline{Y}} + \overline{V}_{,\overline{X}})\end{array}\right], \qquad (4.11)$$

$$\overline{S}_{\overline{YY}} = 2\left(\mu + \frac{1}{\varpi\zeta}\right)\overline{V}_{,\overline{Y}} - \frac{1}{3\varpi\zeta^3}\left[2\overline{V}_{,\overline{Y}}(\overline{U}_{,\overline{X}})^2 + \overline{V}_{,\overline{Y}}(\overline{U}_{,\overline{Y}} + \overline{V}_{,\overline{X}})^2 + 2(\overline{V}_{,\overline{Y}})^3\right], \qquad (4.12)$$

where the subscripts denote the partial derivatives. Note that in the fixed coordinate system $(\overline{X}, \overline{Y}, \overline{t})$, the motion is time-dependent. However in a coordinate system $(\overline{x}, \overline{y})$ moving with the wave speed c in the positive $\overline{x}$ direction the boundary shape is stationary. Defining the transformations

$$\overline{x} = \overline{X} - c\overline{t}, \ \overline{y} = \overline{Y}, \ \overline{u} = \overline{U} - c, \ \overline{v} = \overline{V}, \ \overline{p}(\overline{x}, \overline{y}) = \overline{P}(\overline{X}, \overline{Y}, \overline{t}) \qquad (4.13)$$

and introducing the dimensionless variables

$$x = \frac{2\pi\overline{x}}{\lambda}, \ y = \frac{\overline{y}}{d}, \ u = \frac{\overline{u}}{c}, \ v = \frac{\overline{v}}{c}, \ h(x) = \frac{\overline{H}(\overline{x})}{d}, \ p = \frac{2\pi d^2}{\lambda\mu c}\overline{p}, \ \delta = \frac{2\pi d}{\lambda},$$

$$S = \frac{d}{\mu c}\overline{S}, \quad \text{Re} = \frac{\rho_f c d}{\mu} \quad W = \frac{1}{\mu\varpi\zeta}, \quad A = \frac{W}{6}\left(\frac{c}{\zeta d}\right)^2, \qquad (4.14)$$

the resulting flow quantities in terms of stream function Ψ $\left(u = \frac{\partial\Psi}{\partial y}, v = -\delta\frac{\partial\Psi}{\partial x}\right)$ under lubrication approximations yield:

$$\frac{dp}{dx} = (1 + W)\frac{\partial^3\Psi}{\partial y^3} - A\frac{\partial}{\partial y}\left(\frac{\partial^2\Psi}{\partial y^2}\right)^3, \qquad (4.15)$$

$$S_{xy} = (1 + W)\frac{\partial^2\Psi}{\partial y^2} - A\left(\frac{\partial^2\Psi}{\partial y^2}\right)^3, \qquad (4.16)$$

$$(1 + W)\frac{\partial^4\Psi}{\partial y^4} = A\frac{\partial^2}{\partial y^2}\left(\frac{\partial^2\Psi}{\partial y^2}\right)^3, \qquad (4.17)$$

$$S_{xx} = S_{yy} = \frac{\partial p}{\partial y} = 0, \qquad (4.18)$$

where W and A are the material fluid parameters. Note that the continuity equation is identi-

51

cally satisfied and the shape of peristaltic wall $h(x)$ in dimensionless form is given by

$$h(x) = 1 + \phi \sin x, \tag{4.19}$$

in which $\phi \, (= b/d)$ is the amplitude ratio with $0 < \phi < 1$. For symmetric channel the flow rate in fixed frame is

$$\bar{Q} = \int_0^{\bar{h}} (\bar{u} + c) \, d\bar{y} = \int_0^{\bar{h}} \bar{u} d\bar{y} + \int_0^{\bar{h}} c d\bar{y} = q + c\bar{h}. \tag{4.20}$$

The average volume flow rate over one period $\left(\tilde{T} = \frac{\lambda}{c} \right)$ of the peristaltic wave is defined as follows:

$$
\begin{aligned}
Q &= \frac{1}{\tilde{T}} \int_0^{\tilde{T}} \bar{Q} d\bar{t} = \frac{1}{\tilde{T}} \int_0^{\tilde{T}} \left(q + c\bar{h} \right) d\bar{t} = q + cd. \\
\Theta &= F + 1.
\end{aligned}
\tag{4.21}
$$

In above equation $\Theta \left(= \frac{Q}{cd} \right)$ and $F \left(= \frac{q}{cd} \right)$ are the dimensionless flow rates in the fixed and wave frames, respectively. The relevant boundary conditions with respect to wave frame are

$$\Psi = 0, \qquad \frac{\partial^2 \Psi}{\partial y^2} = 0, \qquad at \ y = 0, \tag{4.22}$$

$$\frac{\partial \Psi}{\partial y} = -1 - \alpha \mathbf{S}_{xy}, \qquad \Psi = F, \qquad at \ y = h, \tag{4.23}$$

where α is the slip parameter, $\mathbf{S}_{xy}$ is the dimensionless shear stress and

$$F = \int_0^h \frac{\partial \Psi}{\partial y} dy = \Psi(h) - \Psi(0). \tag{4.24}$$

4.2 Development of series solution

Equations $(4.15) - (4.17)$ are non-linear and closed form solutions of these equations seem difficult. Therefore we will seek perturbation solution by considering fluid parameter A as a

perturbation parameter and expand Ψ, F and p in the forms:

$$\Psi = \Psi_0 + A\ \Psi_1 + A^2\Psi_2, \tag{4.25}$$

$$F = F_0 + A\ F_1 + A^2 F_2, \tag{4.26}$$

$$p = p_0 + A\ p_1 + A^2 p_2. \tag{4.27}$$

Using above relations and setting $F_0 = F - AF_1 - A^2F_2$, one has the following resulting expressions:

$$
\begin{aligned}
\Psi(y) \ = \ & \frac{y}{2h^2(h+3(1+W)\alpha)}(h^3 - hy^2 + F(-y^2 + 3h(h + 2(1+W)\alpha))) \\
& - (\frac{A}{20h^6(1+W)(h+3(1+W)\alpha)^4})27(F+h)^3(hy(h^2-y^2)^2 \\
& + 3y(1+W)(y^4 - h^4)\alpha) - (\frac{A^2}{700h^{10}(1+W)^2(h+3(1+W)\alpha)^7}) \\
& 243y(F+h)^5(h^2-y^2)(h^2(h^2-y^2)(37h^2+50y^2) \\
& + 3h(1+W)(113h^4 - 37h^2y^2 - 100y^4)\alpha - 450(1+W)^2 \\
& (h^4 + h^2y^2 + y^4)\alpha^2)),
\end{aligned}
$$

$$
\begin{aligned}
\frac{dp}{dx} \ = \ & -\frac{3(F+h)(1+W)}{h^2(h+3(1+W)\alpha)} + \frac{81A(F+h)^3}{5h^3(h+3(1+W)\alpha)^4} \\
& \frac{2187A^2(F+h)^5(4h+75(1+W)\alpha)}{175h^5(1+W)(h+3(1+W)\alpha)^7}.
\end{aligned}
$$

4.3 Graphical results

In this section we discuss the effect of emerging parameters on the flow. For this purpose, we divided the section into four subsections. In subsection one we displayed the effect of pertinent flow parameters on the velocity profile, subsection two presents the influence of flow parameters on the axial shear stress (S_{xy}). Plots in subsection three display the effect of pressure gradient $\left(\frac{dp}{dx}\right)$. Subsection four displays the effect for pressure rise (ΔP_λ) and finally effect of flow parameters on the trapping is analyzed in subsection five.

53

4.3.1 Velocity profile

In Fig. 4.1 a comparison between viscous fluid and non-Newtonian Powell-Eyring fluid is presented by neglecting the slip effect ($\alpha = 0$) through axial velocity. The plots reflect that the velocity for viscous fluid is greater than Powell-Eyring fluid at the center of channel. However the situation is opposite near the walls. Influence of α on the velocity is displayed in Fig. 4.2. It is found that by increasing α, the velocity of fluid at the central part of the channel decreases whereas it increases near the walls of the channel. Effect of fluid parameters (A) and (W) is presented in Figs. 4.3 and 4.4. The effect of these parameters on the flow is qualitatively opposite to each other. Increase in A decreases the velocity of the fluid at the central part of the channel while increase in W enhances the fluid velocity near the center of channel.
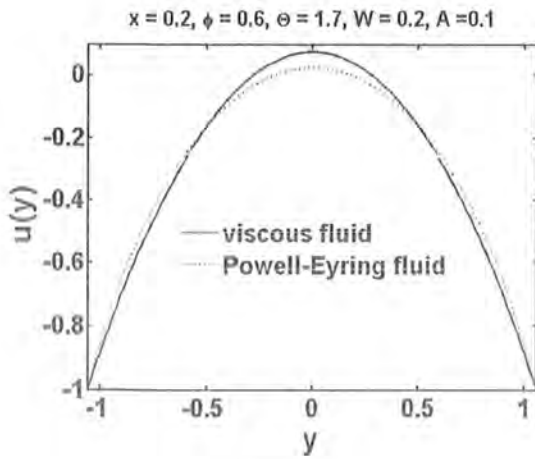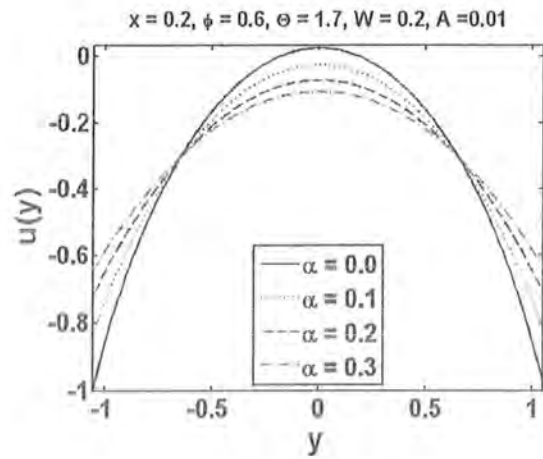

Fig. 4.1   Fig. 4.2

Fig. 4.1: Comparison of viscous and Powell-Erying fluids for $u(y)$. Fig. 4.2: Variation in $u(y)$ for different values of slip parameter (α).
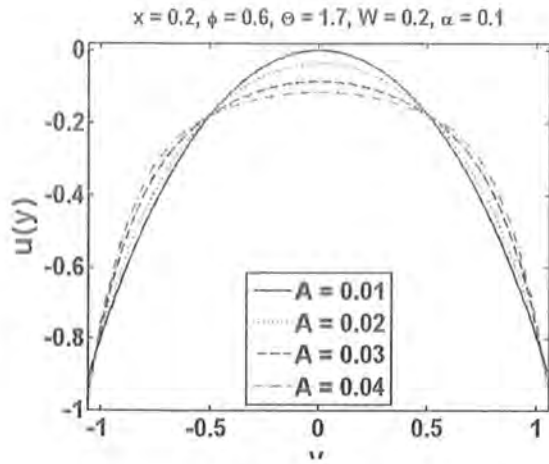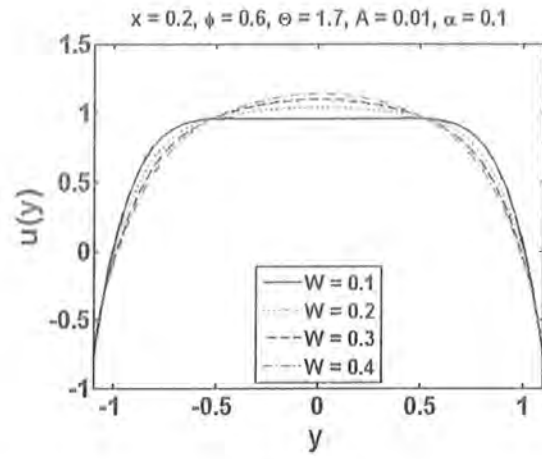
Fig. 4.3 | Fig. 4.4

Figs. (4.3 - 4.4) Variations in $u(y)$ for different values of fluid parameter (A) and (W).

4.3.2 Shear stress at the wall

In this subsection Figs. $(4.5) - (4.8)$ are displayed to analyze the effect of α, A, W and amplitude ratio ϕ on the axial shear stresses (S_{xy}) at the wall $y = h$. Fig. 4.5 reflects that by increasing slip parameter α the magnitude of shear stress decreases. Influence of fluid parameters A and W on shear stress are presented in Figs. 4.6 and 4.7. It is noted that effects of A and W are opposite to each other. Absolute value of stress decreases for an increase in A while the magnitude of shear stresses increases for increasing values of W. Impact of amplitude ratio ϕ on the shear stress is plotted in Fig. 4.8. The plots depict that by increasing ϕ the magnitude of the stresses decrease in the wider part of channel for $0 < x < \pi$ while the magnitude of shear stress enhances in the narrow part of the channel $\pi < x < 2\pi$.
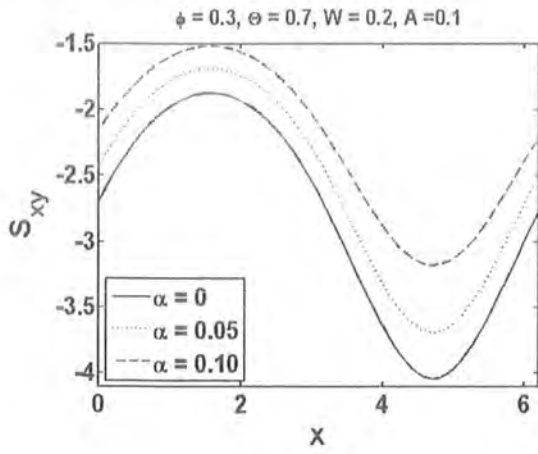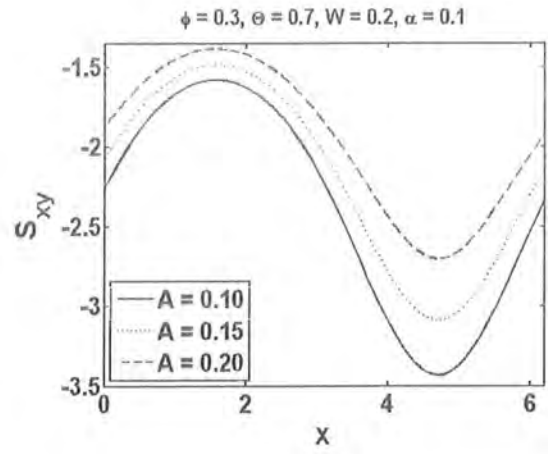
Fig. 4.5

Fig. 4.6

Figs. (4.5 - 4.6): Variations in shear stress (S_{xy}) for different values of slip parameter (α) and fluid parameter (A).
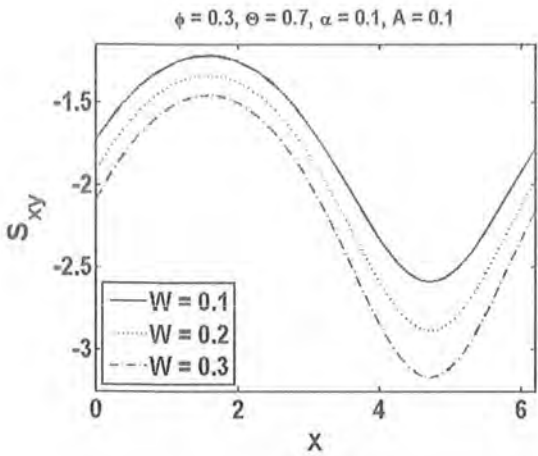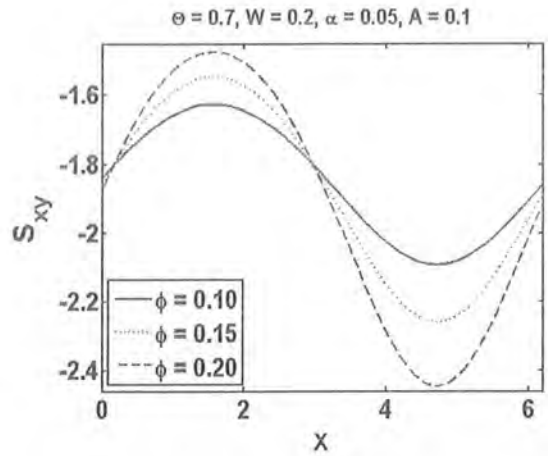

Fig. 4.7

Fig. 4.8

Figs. (4.7 - 4.8): Variations in shear stress (S_{xy}) for different values of fluid parameter (W) and amplitude ratio (ϕ).

4.3.3 Pressure gradient

This subsection analyze the influence of slip parameter (α), material parameters (A and W) and amplitude ratio (ϕ) on the dp/dx and are shown through Figs. $(4.9) - (4.13)$. These plots reflect that in the wider part of the channel ($0 < x < \pi$) the pressure gradient is relatively small and the flow can easily pass without imposition of large pressure gradient. However in narrow part of the channel ($\pi < x < 2\pi$) a much larger pressure gradient is required to maintain the same flux to pass through it. Fig. 4.9 presents a comparison between viscous and powell-Eyring fluids. A comparative study indicates that the magnitude of pressure gradient for Powell-Eyring fluid is greater than viscous fluid in the narrow part of the channel. Plot in Fig. 4.10 is prepared to illustrate the effect of α on the axial pressure gradient. It is observed that the magnitude of pressure gradient decreases by increasing α in the narrow part of the channel. Effect of material parameters A and W on pressure gradient are displayed in the Figs. 4.11 and 4.12. These plots depict that the effect of both parameters A and W are quite opposite i.e. by increasing A the pressure gradient decreases while the magnitude of the pressure gradient increases for larger W. Impact of amplitude ratio (ϕ) on pressure gradient is presented in Fig. 4.13. The plot shows that the magnitude of pressure gradient increases when ϕ enhances.
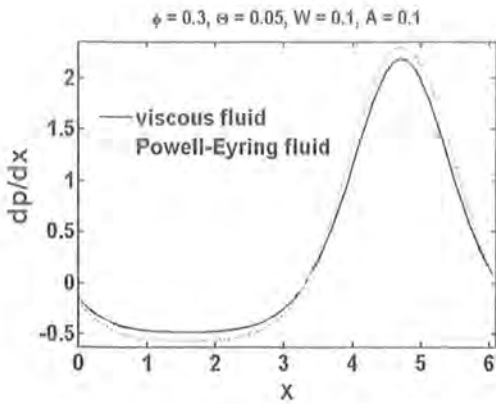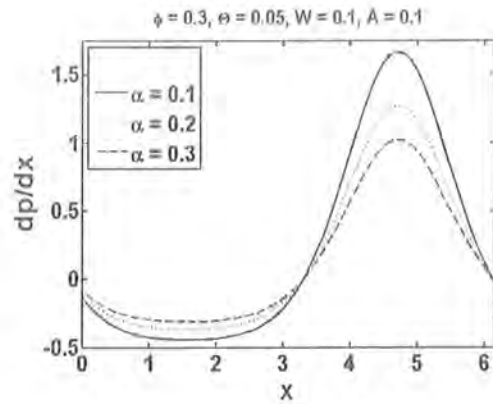

Fig. 4.9   Fig. 4.10

Fig. 4.9: Comparison of viscous and Powell-Erying fluids for dp/dx. Fig. 4.10: Variation in dp/dx for different values of slip parameter (α).

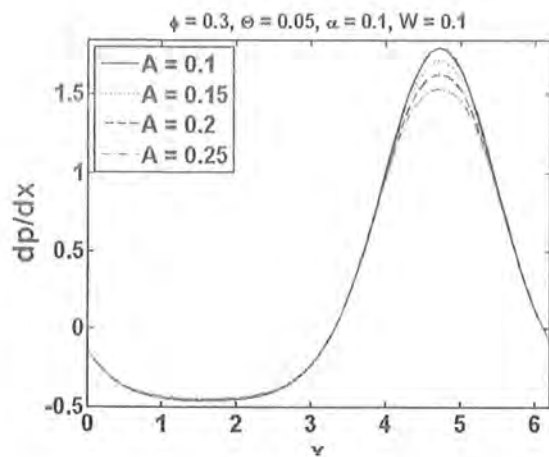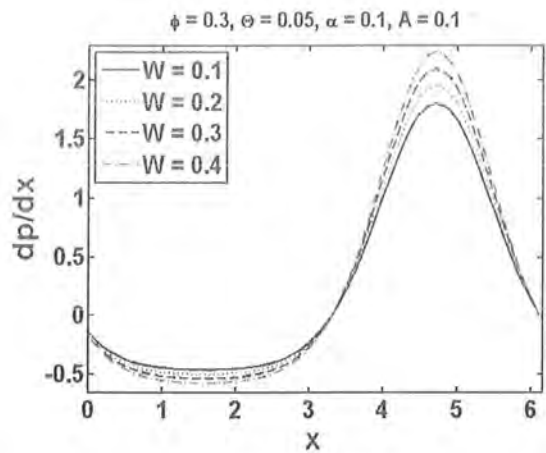Fig. 4.11

Fig. 4.12

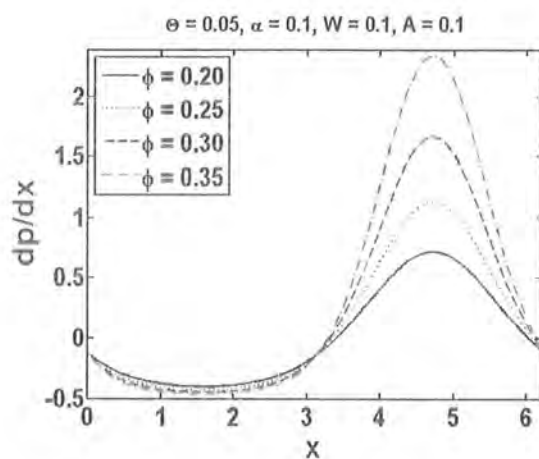Figs. (4.11 - 4.12): Variations in dp/dx for different values of fluid parameters (A) and (W)

Fig. 4.13

Fig. 4.13 Variation in dp/dx for different values of amplitude ratio (ϕ)

4.3.4 Pressure rise

Figs. (4.14) − (4.17) are displayed to examine the variation of dimensionless pressure rise (ΔP_λ) versus the time-average flux (Θ) for various values of pertinent flow parameters. For that numerical integration is performed through Eq. (4.15). The graphs are sectored so that the upper right-hand quadrant that is $\Theta > 0$ and $\Delta P_\lambda > 0$ represents the peristaltic pumping region while the lower left hand quardant for $\Theta > 0$ and $\Delta P_\lambda < 0$ is designated as augmented pumping region. These plots show a linear relation between ΔP_λ and Θ. Fig. 14 is prepared to analyze the effect of slip parameter (α) on ΔP_λ. It is noted that pressure rise decreases with an increase in α. Furthermore a comparison for viscous and Powell-Eyring fluids is also presented in Fig. 4.14. This Fig. shows that the value of pressure rise for Powell-Eyring fluid is greater than that of viscous fluid. Influence of material fluid parameters A and W on ΔP_λ are illustrated in Figs. 4.15 and 4.16. The behaviors of A and W on pressure rise are opposite to each other i.e. an increase in material parameter A decreases the pressure rise while pressure rise increases by increasing W in the peristaltic pumping region. Plot in Fig. 4.17 presents the effects of amplitude ratio (ϕ) on pressure rise. It is noted that an increase in ϕ enhances the pressure rise.
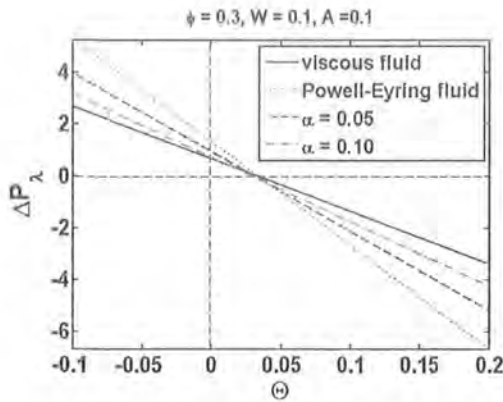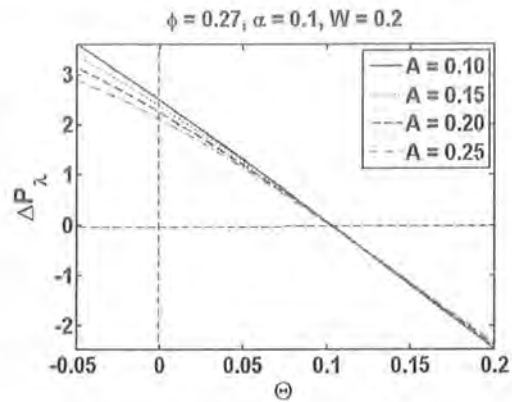

Fig. 4.14   Fig. 4.15

Fig. (4.14 - 4.15): Variations in ΔP_λ for different values of slip parameter (α) and fluid parameter (A).
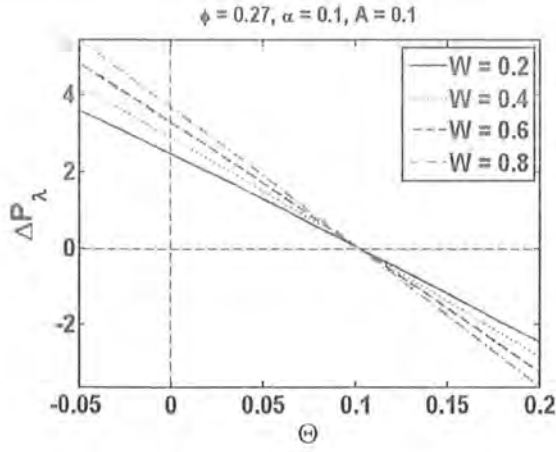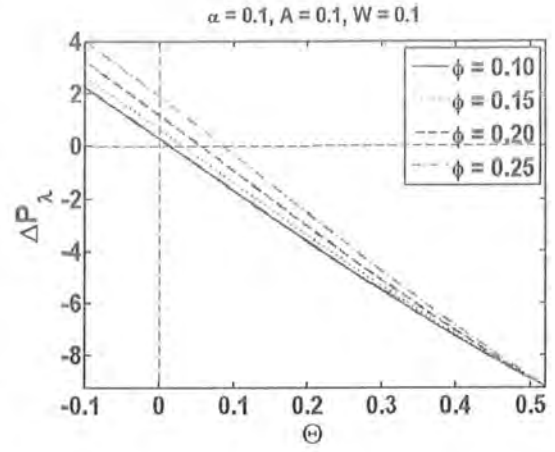
Fig. 4.16   Fig. 4.17

Fig. (4.16 - 4.17): Variations in ΔP_λ for different values of fluid parameter (W) and amplitude ratio (ϕ)

4.3.5 Trapping

The effect of slip parameter (α), material fluid parameters (A and W) and amplitude ratio (ϕ) on trapping can be seen through Figs. $(4.18) - (4.21)$. These plots depict that the size of the bolus increases with an increase in slip parameter α, material parameter W and amplitude ratio ϕ. However the size of the bolus decreases for increasing values of material parameter A.

$\phi=0.12$, $\theta=-0.26$, A=0.1, W=0.8

$\alpha = 0.05$ a

$\alpha = 0.1$ b
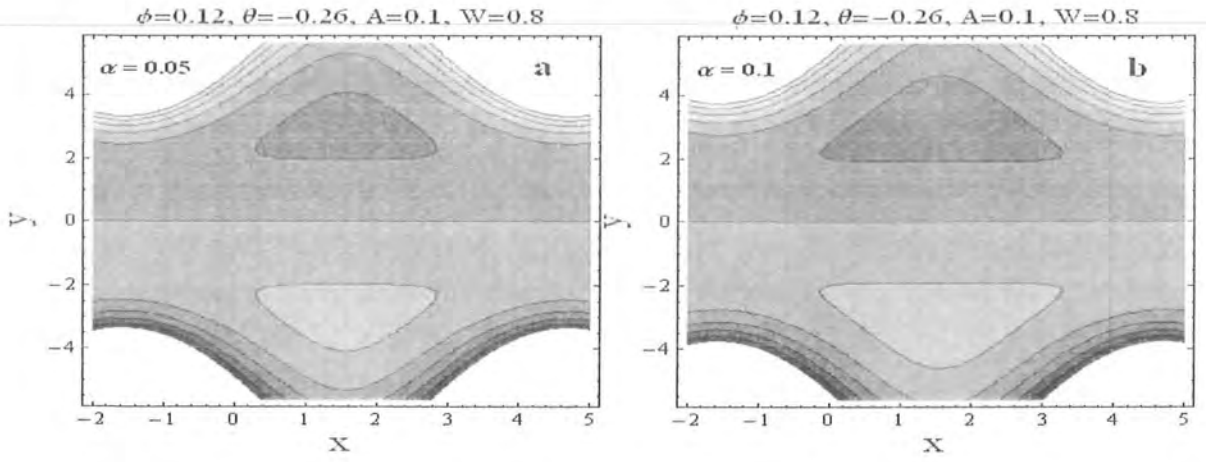
Fig. 4.18

Fig. 4.18(a, b): Plots of stream lines for different values of slip parameter (α).

$\phi=0.12$, $\theta=-0.26$, $\alpha=0.05$, W=0.8

A = 0.1   a

A = 0.3   b
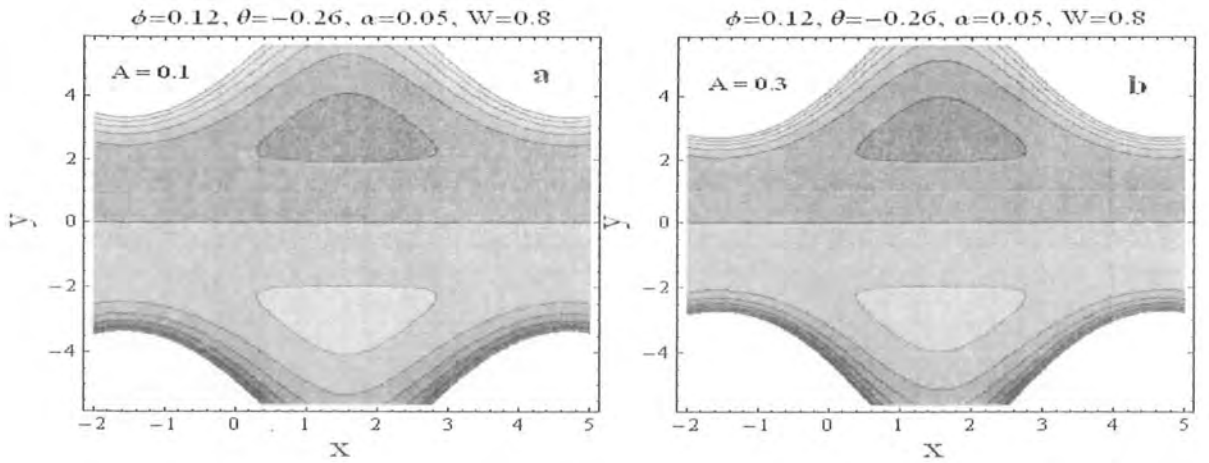
Fig. 4.19

Fig. 4.19(a, b): Plots of stream lines for different values of material fluid parameter (A).

61

$\phi=0.12,\ \theta=-0.26,\ a=0.05,\ A=0.1$

W = 0.2

a

$\phi=0.12,\ \theta=-0.26,\ a=0.05,\ A=0.1$

W = 0.8

b
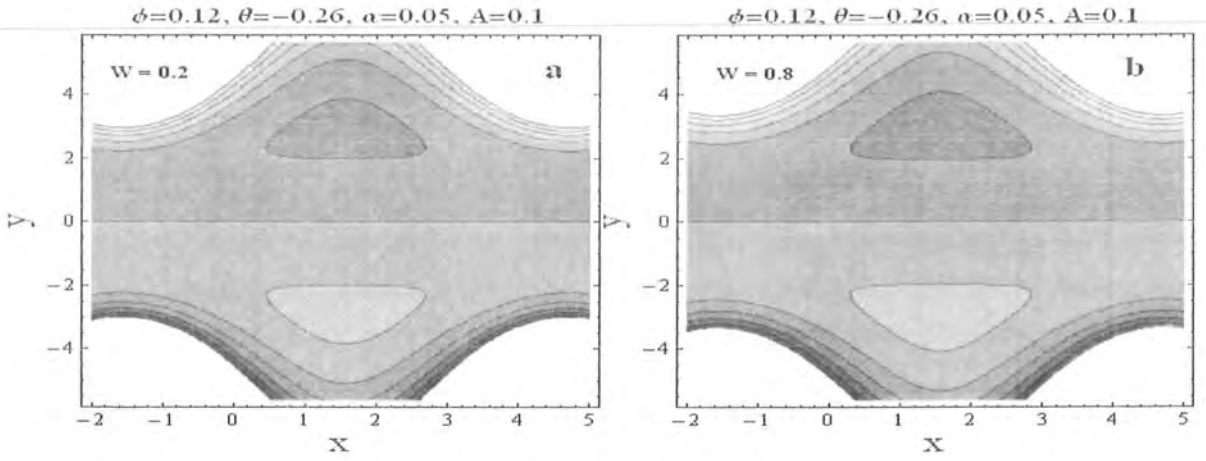
Fig. 4.20

Fig. 4.20(a, b): Plots of stream lines for different values of material fluid parameter (W).

$\theta=-0.26,\ a=0.05,\ A=0.1,\ W=0.8$

$\phi=0.1$

a

$\theta=-0.26,\ a=0.05,\ A=0.1,\ W=0.8$

$\phi=0.12$

b
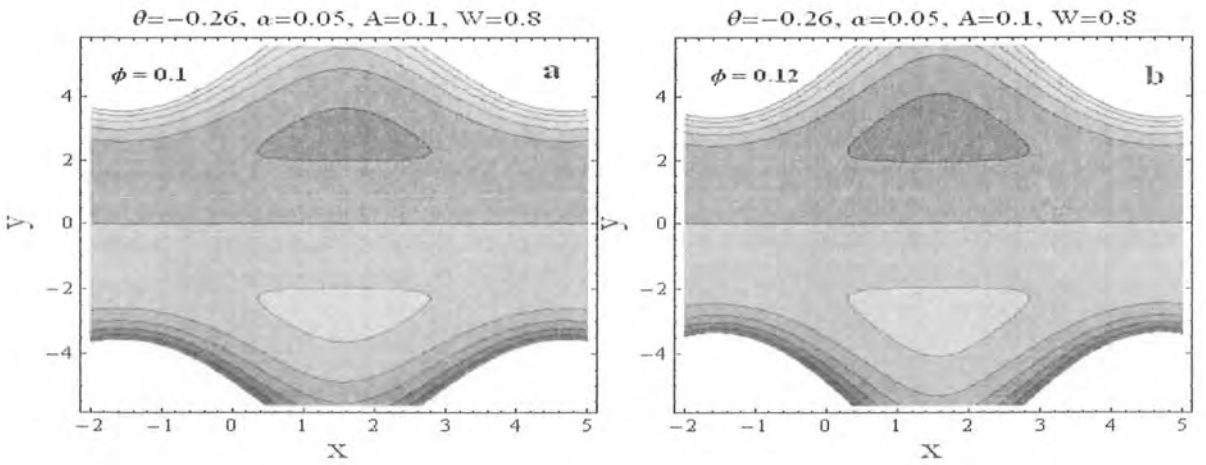
Fig. 4.21

Fig. 4.21(a, b): Plots of stream lines for different values of amplitude ratio (ϕ).

62

4.4 Concluding remarks

In the present study, we have examined the partial slip effect on peristaltic flow of Powell-Eyring fluid in a symmetric channel. The differential system is modeled and simplified by using the assumption of long wavelength approximation. The outcomes are discussed through graphs. We have the following main observations.

- The velocity decreases for the slip parameter (α) and fluid parameter (A) at the centre of the channel. However influence of fluid parameters (W) on the velocity profile is opposite to both α and A. The velocity profile shows an opposite behavior near the channel walls when compared with the centre of channel.

- Magnitude of axial shear stress decreases for slip parameter (α) and material parameter (A). However the magnitude of axial shear stress increases for material parameter (W).

- Pressure gradient decreases for slip parameter (α) and material parameter (A). However pressure gradient increases with an increase in fluid parameter (W) and amplitude ratio (ϕ).

- Pressure rise increases in peristaltic pumping region for an increase in slip parameter (α), material parameter (W) and amplitude ratio (ϕ). The effect of material parameter (A) is to decrease the pressure rise.

- The size of trapped bolus decreases for an increase in fluid parameter (A). However opposite effects are noted for slip parameter (α), fluid parameter (W) and amplitude ratio (ϕ) for the size of the trapped bolus.

Chapter 5

Effect of Hall current on peristaltic flow of Powell-Eyring fluid in a symmetric channel

Influence of Hall current on peristaltic transport of an electrically conducting non-Newtonian fluid in a channel is examined. Rheological properties of fluid are characterized through Powell-Eyring fluid. A sinusoidal wave propogates along the channel walls. Mathematical analysis is presented in a wave frame. Long wavelength theory is followed. Results of stream function and axial pressure gradient are obtained. Influence of rheological parameters, Hartman number and Hall parameter on the flow quantities of interest is plotted and analyzed.

5.1 Fundamental equations and modeling

We consider the flow of Powell-Eyring fluid in two-dimensional symmetric channel of width $2d$ with a sinusoidal peristaltic wave of small amplitude travelling along its flexible wall. The velocity of the wave is denoted by c. The Cartesian coordinate system is chosen in which $\overline{X}$-axis lies along the central line of the channel and $\overline{Y}$-axis normal to it. The wall geometry is therefore written as:

$$\overline{H}\left(\overline{X}, \overline{t}\right) = d + b \sin \frac{2\pi}{\lambda} \left(\overline{X} - c\overline{t}\right), \tag{5.1}$$

in which b represents the wave amplitude, λ is the wavelength and $\bar{t}$ is the time.

The basic equations that governing the flow of an incompressible fluid in the presence of an applied magnetic field can be written as:

$$\text{div } \bar{\mathbf{V}} = 0, \tag{5.2}$$

$$\rho_f \frac{d\bar{\mathbf{V}}}{d\bar{t}} = \text{div } \bar{\mathbf{T}} + \bar{\mathbf{J}} \times \bar{\mathbf{B}}, \tag{5.3}$$

where $d/d\bar{t}$ signifies the material derivative, ρ_f the density, $\bar{\mathbf{V}} = \{\bar{U}(\bar{X}, \bar{Y}, \bar{t}), \bar{V}(\bar{X}, \bar{Y}, \bar{t}), 0\}$ the velocity, $\bar{\mathbf{J}}$ the current density, $\bar{\mathbf{B}} = \mathbf{B}_0 + \mathbf{B}_1$ the total magnetic field, $\mathbf{B}_0$ the applied magnetic field and $\mathbf{B}_1$ the induced magnetic field. The expression of Cauchy stress tensor $\bar{\mathbf{T}}$ is defined in chapter 4 through Eqs. (4.4 - 4.6). Induced magnetic field is neglected by considering the magnetic Reynolds number to be very small. If the Hall term is retained in the generalized Ohm's law due to strong magnetic field, then the following expression is satisfied

$$\bar{\mathbf{J}} = \sigma(\bar{\mathbf{E}} + \bar{\mathbf{V}} \times \bar{\mathbf{B}}) - \frac{\alpha_e}{B_0}\left(\bar{\mathbf{J}} \times \bar{\mathbf{B}}\right), \tag{5.4}$$

where σ is the electrical conductivity, $\alpha_e = \left(\dfrac{\sigma B_0}{e n_e}\right)$ the Hall parameter, e the electric charge, n_e the number density of electrons and $\mathbf{E}$ the electric field. There is no applied voltage therefore electric field $\mathbf{E} = 0$ and Eq. (5.4) in component form reduces to

$$\bar{\mathbf{J}} \times \bar{\mathbf{B}} = -\sigma B_0^2 \gamma \left[\left(\bar{U} - \alpha_e \bar{V}\right)\hat{\imath} + \left(\bar{V} + \alpha_e \bar{U}\right)\hat{\jmath}\right], \quad \gamma = \frac{1}{1 + (\alpha_e)^2}, \tag{5.5}$$

where $\hat{\imath}$ and $\hat{\jmath}$ are the unit vectors parallel to $\bar{X}$ and $\bar{Y}$-axes respectively. Equations (5.2) and (5.3) through Eqs. $(4.4 - 4.6)$ and (5.5) gives the following scalar form of continuity and momentum equations:

$$\bar{U}_{,\overline{X}} + \bar{V}_{,\overline{Y}} = 0, \tag{5.6}$$

$$\rho_f(\bar{U}_{,\bar{t}} + \overline{U}\bar{U}_{,\overline{X}} + \overline{V}\bar{U}_{,\overline{Y}}) = -\bar{P}_{,\overline{X}} + \overline{S}_{\overline{XX},\overline{X}} + \overline{S}_{\overline{XY},\overline{Y}} - \sigma B_0^2 \gamma \left(\overline{U} - \alpha_e \overline{V}\right), \tag{5.7}$$

$$\rho_f(\bar{V}_{,\bar{t}} + \overline{U}\bar{V}_{,\overline{X}} + \overline{V}\bar{V}_{,\overline{Y}}) = -\bar{P}_{,\overline{Y}} + \overline{S}_{\overline{XY},\overline{X}} + \overline{S}_{\overline{YY},\overline{Y}} - \sigma B_0^2 \gamma \left(\overline{V} + \alpha_e \overline{U}\right), \tag{5.8}$$

$$\overline{S}_{\overline{XX}} = 2\left(\mu + \frac{1}{\varpi\zeta}\right)\bar{U}_{,\overline{X}} - \frac{1}{3\varpi\zeta^3}\left[2(\bar{U}_{,\overline{X}})^3 + \bar{U}_{,\overline{X}}(\bar{U}_{,\overline{Y}} + \bar{V}_{,\overline{X}})^2 + 2\bar{U}_{,\overline{X}}(\bar{V}_{,\overline{Y}})^2\right], \tag{5.9}$$

65

$$\overline{S}_{\overline{X}\overline{Y}} = 2\left(\mu + \frac{1}{\varpi\zeta}\right)\left(\overline{U}_{,\overline{Y}} + \overline{V}_{,\overline{X}}\right) - \frac{1}{6\varpi\zeta^3}\left[\begin{array}{c}\{2(\overline{U}_{,\overline{X}})^2 + (\overline{U}_{,\overline{Y}} + \overline{V}_{,\overline{X}})^2 \\ +2(\overline{V}_{,\overline{Y}})^2\}(\overline{U}_{,\overline{Y}} + \overline{V}_{,\overline{X}})\end{array}\right], \tag{5.10}$$

$$\overline{S}_{\overline{Y}\overline{Y}} = 2\left(\mu + \frac{1}{\varpi\zeta}\right)\overline{V}_{,\overline{Y}} - \frac{1}{3\varpi\zeta^3}\left[2\overline{V}_{,\overline{Y}}(\overline{U}_{,\overline{X}})^2 + \overline{V}_{,\overline{Y}}(\overline{U}_{,\overline{Y}} + \overline{V}_{,\overline{X}})^2 + 2(\overline{V}_{,\overline{Y}})^3\right], \tag{5.11}$$

where the subscripts denote the partial derivatives. Note that in the fixed coordinate system $\left(\overline{X}, \overline{Y}, \overline{t}\right)$, the motion is time-dependent. However the boundary shape is stationary in a co-ordinate system $(\overline{x}, \overline{y})$ moving with the wave speed c in the positive $\overline{x}$ direction. Defining the transformations

$$\overline{x} = \overline{X} - c\overline{t}, \qquad \overline{y} = \overline{Y}, \qquad \overline{u} = \overline{U} - c, \qquad \overline{v} = \overline{V} \tag{5.12}$$

and introducing the dimensionless variables as

$$x = \frac{2\pi\overline{x}}{\lambda}, \ y = \frac{\overline{y}}{d}, \ u = \frac{\overline{u}}{c}, \ v = \frac{\overline{v}}{c}, \ h = \frac{\overline{h}(\overline{x})}{d}, \ p = \frac{2\pi d^2}{\lambda\mu c}\overline{p}, \ \delta = \frac{2\pi d}{\lambda},$$

$$S = \frac{d}{\mu c}\overline{S}, \quad M = \sqrt{\frac{\sigma}{\mu}}B_0 d \quad \mathrm{Re} = \frac{\rho_f cd}{\mu} \quad W = \frac{1}{\mu\varpi\zeta}, \quad A = \frac{W}{6}\left(\frac{c}{\zeta d}\right)^2, \tag{5.13}$$

the resulting flow quantities in terms of stream function Ψ $\left(u = \frac{\partial\Psi}{\partial y}, v = -\delta\frac{\partial\Psi}{\partial x}\right)$ under lubrication approximations yield:

$$\frac{dp}{dx} = (1+W)\frac{\partial^3\Psi}{\partial y^3} - A\frac{\partial}{\partial y}\left(\frac{\partial^2\Psi}{\partial y^2}\right)^3 - M^2\gamma\left(\frac{\partial\Psi}{\partial y} + 1\right), \tag{5.14}$$

$$S_{xy} = (1+W)\frac{\partial^2\Psi}{\partial y^2} - A\left(\frac{\partial^2\Psi}{\partial y^2}\right)^3, \tag{5.15}$$

$$(1+W)\frac{\partial^4\Psi}{\partial y^4} = A\frac{\partial^2}{\partial y^2}\left(\frac{\partial^2\Psi}{\partial y^2}\right)^3 + M^2\gamma\frac{\partial^2\Psi}{\partial y^2}, \tag{5.16}$$

$$S_{xx} = S_{yy} = \frac{\partial p}{\partial y} = 0, \tag{5.17}$$

where W and A are the fluid parameters and M is the Hartman number. Note that the continuity equation is identically satisfied and the dimensionless shape of the peristaltic wall $h(x)$ is given by

$$h(x) = 1 + \phi\,\sin x, \tag{5.18}$$

66

in which $\phi \, (= b/d)$ is the amplitude ratio with $0 < \phi < 1$.

The relevant boundary conditions with respect to wave frame for symmetric channel are

$$\Psi = 0, \qquad \frac{\partial^2 \Psi}{\partial y^2} = 0, \qquad at \; y = 0, \tag{5.19}$$

$$\frac{\partial \Psi}{\partial y} = -1, \qquad \Psi = F, \qquad at \; y = h, \tag{5.20}$$

where

$$F = \Theta - 1. \tag{5.21}$$

5.2 Development of series solution

Equations (5.14) and (5.16) are non-linear and closed form solutions of these equations seem difficult. Therefore we will seek perturbation solution by considering fluid parameter A as a perturbation parameter and we expand Ψ, F and p in the forms:

$$\Psi \;\; = \;\; \Psi_0 + A \; \Psi_1 + O(A^2), \tag{5.22}$$

$$F \;\; = \;\; F_0 + A \; F_1 + O(A^2), \tag{5.23}$$

$$p \;\; = \;\; p_0 + A \; p_1 + O(A^2). \tag{5.24}$$

Using above relations and setting $F_0 = F - A \; F_1$ after calculating Ψ_0 and Ψ_1, one has the following resulting expressions upto first order.

$$
\begin{aligned}
\Psi(y) \;\; = \;\; & 1/32 C_1^4 \sqrt{1+W} (32 C_1^3 (FM\sqrt{1+W} y \sqrt{\gamma} \cosh[\tfrac{hM\sqrt{\gamma}}{\sqrt{1+W}}] + (1+W) y \sinh[\tfrac{hM\sqrt{\gamma}}{\sqrt{1+W}}] \\
& -F(1+W)\sinh[\tfrac{My\sqrt{\gamma}}{\sqrt{1+W}}] - h(1+W)\sinh[\tfrac{My\sqrt{\gamma}}{\sqrt{1+W}}]) + (1+W)^{-3/2} A(F+h)^3 M^4 \gamma^2 \\
& (-24hM^2 y\gamma - (1+W)\cosh[\tfrac{(h-3y)M\sqrt{\gamma}}{\sqrt{1+W}}] + 24hM^2(h+y)\gamma\cosh[\tfrac{(h-y)M\sqrt{\gamma}}{\sqrt{1+W}}] \\
& +(1+W)\cosh[\tfrac{(3h-y)M\sqrt{\gamma}}{\sqrt{1+W}}] - 12hM^2\gamma(h+y)\cosh[\tfrac{(h+y)M\sqrt{\gamma}}{\sqrt{1+W}}] - (1+W) \\
& (\cosh[\tfrac{(3h+y)M\sqrt{\gamma}}{\sqrt{1+W}}] - \cosh[\tfrac{(h+3y)M\sqrt{\gamma}}{\sqrt{1+W}}]) + 2M\sqrt{1+W} y\sqrt{\gamma}(8\sinh[\tfrac{2hM\sqrt{\gamma}}{\sqrt{1+W}}] \\
& -\sinh[\tfrac{2hM\sqrt{\gamma}}{\sqrt{1+W}}]) + M\sqrt{1+W}\sqrt{\gamma}(h\sinh[\tfrac{(h-3y)M\sqrt{\gamma}}{\sqrt{1+W}}] - 12y\sinh[\tfrac{(h-y)M\sqrt{\gamma}}{\sqrt{1+W}}] - 3h \\
& \sinh[\tfrac{(3h-y)M\sqrt{\gamma}}{\sqrt{1+W}}] - 12y\sinh[\tfrac{(h+y)M\sqrt{\gamma}}{\sqrt{1+W}}] + 3h\sinh[\tfrac{(3h+y)M\sqrt{\gamma}}{\sqrt{1+W}}] - h\sinh[\tfrac{(h+3y)M\sqrt{\gamma}}{\sqrt{1+W}}]))),
\end{aligned}
\tag{5.25}
$$

$$\frac{dp}{dx} = \frac{(F+h)M^3\gamma^{3/2}}{16C_1^4(1+W)^{5/2}}(-16h^3M^3(1+W)^{5/2}\gamma^{3/2}\cosh[\frac{hM\sqrt{\gamma}}{\sqrt{1+W}}] + 48h^2M^2(1+W)^3\gamma$$

$$\cosh^3[\frac{hM\sqrt{\gamma}}{\sqrt{1+W}}]\sinh[\frac{hM\sqrt{\gamma}}{\sqrt{1+W}}] + 16(1+W)^4\cosh[\frac{hM\sqrt{\gamma}}{\sqrt{1+W}}]\sinh^3[\frac{hM\sqrt{\gamma}}{\sqrt{1+W}}] - 8A(F+h)^2$$

$$M^4(1+W)\gamma^2\sinh[\frac{2hM\sqrt{\gamma}}{\sqrt{1+W}}] - 12hM(1+W)^{7/2}\gamma^{1/2}\sinh[\frac{2hM\sqrt{\gamma}}{\sqrt{1+W}}] + A(F+h)^2M^4\gamma^2$$

$$(12hM(1+W)^{1/2}\gamma^{1/2} + (1+W)\sinh[\frac{4hM\sqrt{\gamma}}{\sqrt{1+W}}])),$$

$$C_1 = hM\sqrt{\gamma}\cosh[\frac{hM\sqrt{\gamma}}{\sqrt{1+W}}] - \sqrt{1+W}\sinh[\frac{hM\sqrt{\gamma}}{\sqrt{1+W}}]. \tag{5.26}$$

It should be pointed out that results of applied magnetic field are recovered when Hall parameter $\alpha_e = 0$.

5.3 Graphical results

Our interest in this section is to discuss the effect of emerging parameters on the flow quantities. For this purpose, we divided this section into four subsections. In subsection one we displayed the effect of flow parameters on the velocity profile, subsection two presents the influence of flow parameters on the pressure gradient $\left(\frac{dp}{dx}\right)$, plots in subsection three display the effect for pressure rise and frictional forces and finally effect of flow parameters on the trapping is analyzed in subsection four.

5.3.1 Velocity profile

Figs. $5.1-5.4$ displayed the influence of fluid parameters (W, A), Hartman number M and Hall parameter α_e on the velocity field. In Figs. $5.1-5.2$ the velocity decreases by increasing the fluid parameter A and Hartman number M at the central part of channel. The influences of Hall parameter α_e and fluid parameter W on the velocity profile are presented in Figs. $5.3-5.4$. These Figs. show quite opposite behavior for α_e and W when compared with A and M. In these plots the velocity decreases near the wall and it increases at the central part of the channel. Furthermore by increasing Hartman number M the magnitude of Lorentz force increases which resists the flow causing a decrease in the velocity. However the increase in Hall parameter α_e assists the flow and has an opposite behavior to that of Hartman number M. Also by increasing the fluid parameter W the viscosity of the fluid decreases which give rise to an increase in the

fluid velocity as shown in Fig. 5.4. Thus the behavior of fluid parameters A and W are opposite to each other.
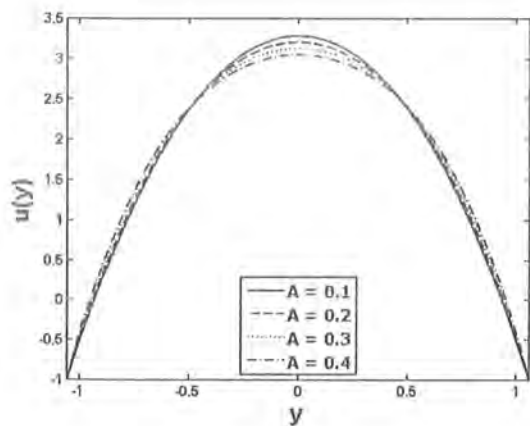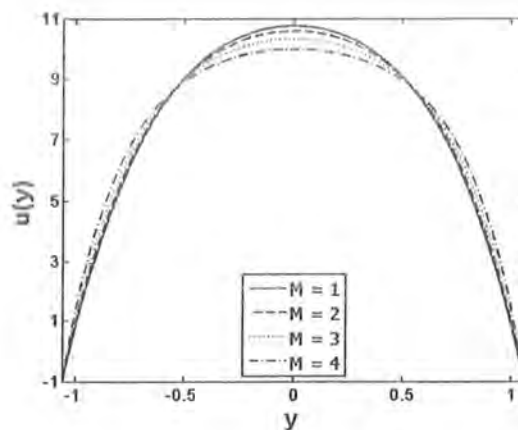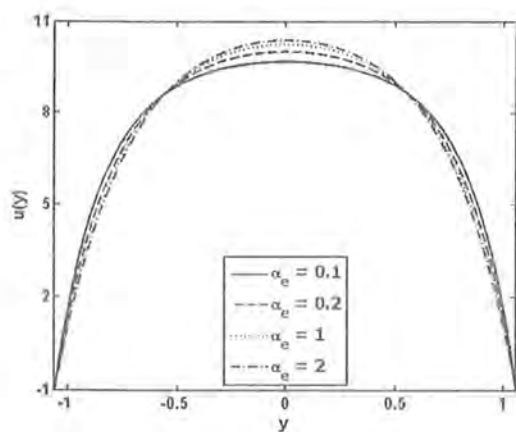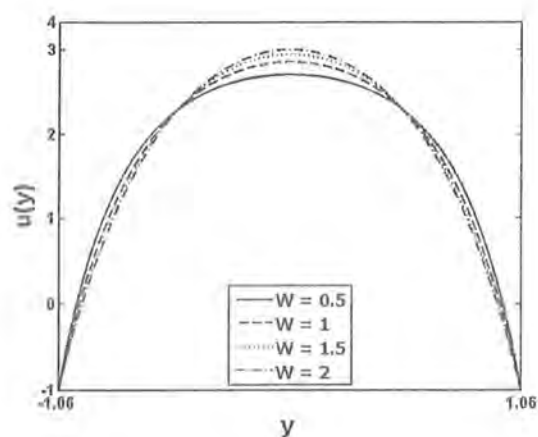
Fig. 5.1

Fig. 5.2

Fig. 5.3

Fig. 5.4

Figs. 5.1 - 5.4: Velocity profile for different values of flow parameters. Fig. 5.1; $W = 1.5$, $M = 2.8$, $\alpha_e = 0.5$, $\Theta = 0.35$, $\phi = 0.2$, $x = 0.3$, Fig 5.2; $A = 0.1$, $W = 1.5$, $\alpha_e = 0.5$, $\Theta = 0.35$, $\phi = 0.2$, $x = 0.3$, Fig. 5.3; $A = 0.1$, $W = 1.5$, $M = 2.8$, $\Theta = 0.35$, $\phi = 0.2$, $x = 0.3$, Fig. 5.4; $A = 0.1$, $M = 2.8$, $\alpha_e = 0.5$, $\Theta = 0.35$, $\phi = 0.2$, $x = 0.3$.

5.3.2 Pressure gradient

In this subsection, the influence of fluid parameters W and A, Hartman number M and Hall parameter α_e on dp/dx are presented through the plots in Figs. (5.5 − 5.8). These plots reflect that at $x = 1.5$, the pressure gradient is comparatively small and the flow can effortlessly pass without imposing larger pressure gradient. However at $x = 4.75$ a much larger pressure gradient is required to uphold the same flux to pass through it. Furthermore the magnitude of dp/dx decreases by increasing the value of each of the parameters A and α_e as shown in Figs. 5.5 and 5.6. Effects of Hartman number M and fluid parameter W on pressure gradient are displayed in Figs. 5.7 and 5.8. These Figs. indicate that dp/dx increases in magnitude with an increase in M and W.
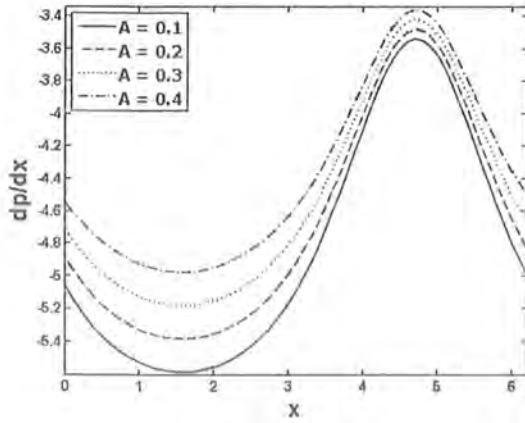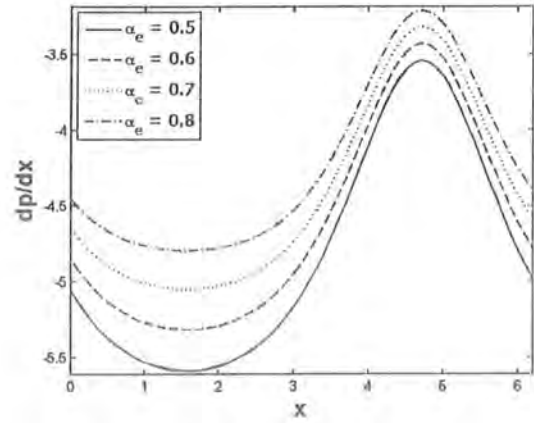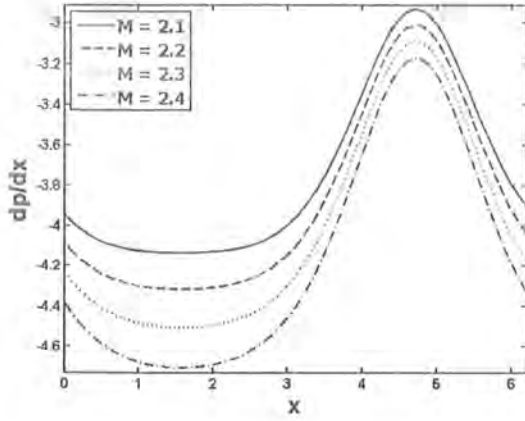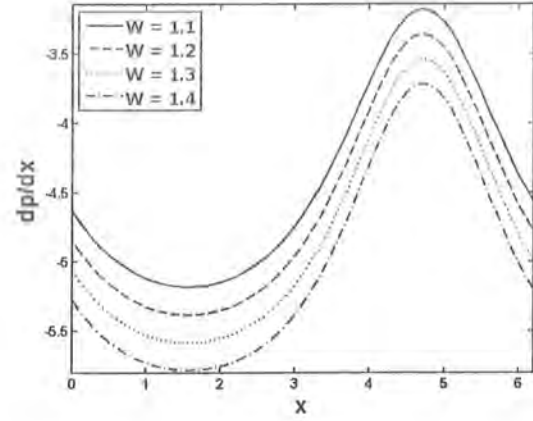

Fig. 5.5

Fig. 5.6

Fig. 5.7

Fig. 5.8

Figs. 5.5 - 5.8: Plots for variation in pressure gradient $\left(\frac{dp}{dx}\right)$ for different values of flow parameters. Fig. 5.5; $W = 1.5$, $M = 2.8$, $\alpha_e = 0.5$, $\Theta = 0.35$, $\phi = 0.2$, Fig. 5.6; $A = 0.1$, $W = 1.5$, $M = 2.8$, $\Theta = 0.35$, $\phi = 0.2$, Fig. 5.7; $A = 0.1$, $W = 1.5$, $\alpha_e = 0.5$, $\Theta = 0.35$, $\phi = 0.2$, Fig. 5.8; $A = 0.1$, $M = 2.8$, $\alpha_e = 0.5$, $\Theta = 0.35$, $\phi = 0.2$.

5.3.3 Pressure rise

Figs. (5.9 - 5.12) are displayed to analyze the deviation of pressure rise (ΔP_λ) versus the mean flow rate (Θ) for various values of pertinent flow parameters. Influence of fluid parameter A and Hartman number α_e on pressure rise are presented in the Figs. $(5.9 - 5.10)$. By increasing A and α_e, ΔP_λ decreases in the peristaltic pumping region $(\Theta > 0, \Delta P_\lambda > 0)$, whereas ΔP_λ increases in the augmented pumping region $(\Theta > 0, \Delta P_\lambda < 0)$. It is also noticed that the fluid parameter A has no influence on the free pumping. However, an increase in α_e leads to an increase in free pumping. The variation of ΔP_λ with Θ for distinct values of Hartman number M and fluid parameter W are presented in Fig. 5.11 and (5.12). Here maximum pressure against which the peristalsis works as a pump increases by increasing M and W in the peristaltic pumping region

72

whereas an opposite behavior is noticed in the co-pumping (augmented pumping) region.
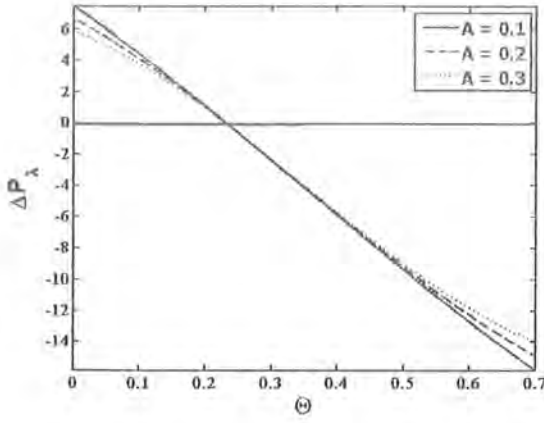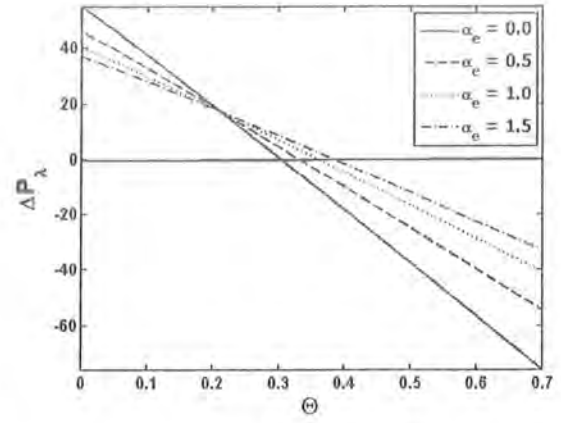

Fig. 5.9

Fig. 5.10
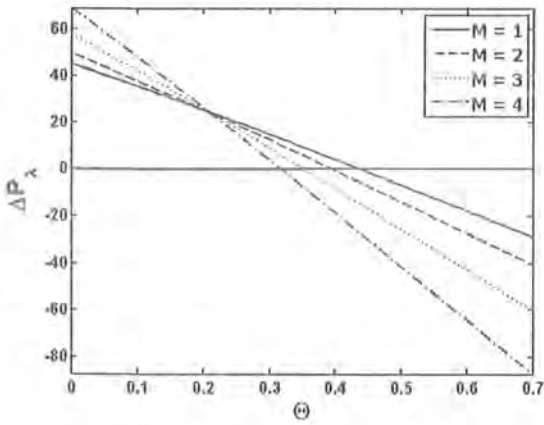

Fig. 5.11
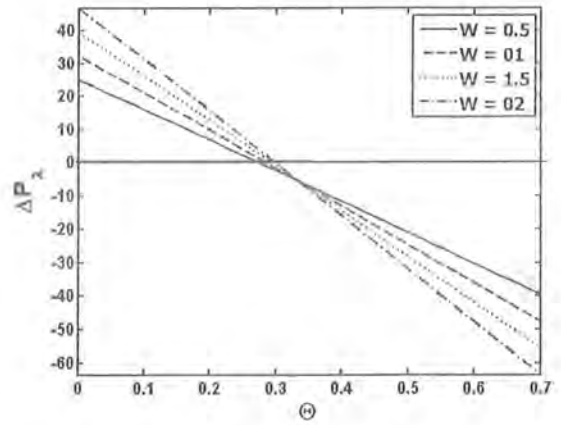

Fig. 5.12

Figs. 5.9 - 5.12: Plots for variation in pressure rise (ΔP) for different values of flow parameters. Fig. 5.9; $W = 1.5$, $M = 2.8$, $\alpha_e = 0.5$, $\phi = 0.45$, Fig. 5.10; $A = 0.1$, $W = 1.5$, $M = 2.8$, $\phi = 0.45$, Fig. 5.11; $A = 0.1$, $W = 1.5$, $\alpha_e = 0.5$, $\phi = 0.45$, Fig. 5.12; $A = 0.1$, $M = 2.8$, $\alpha_e = 0.5$, $\phi = 0.45$.

5.3.4 Trapping

The effect of Hartman number M, Hall parameter α_e and fluid parameters A and W on trapping can be seen through Figs. $(5.13 - 5.16)$. Figs. 5.13 and (5.14) illustrate that by magnifying the Hartman number M and A the size of bolus decreases and it vanishes for large values of M and A. Effect of α_e and W on the trapping are presented in the Figs. 5.15 and (5.16). The size of bolus in these plots increases for an increase in α_e and W.
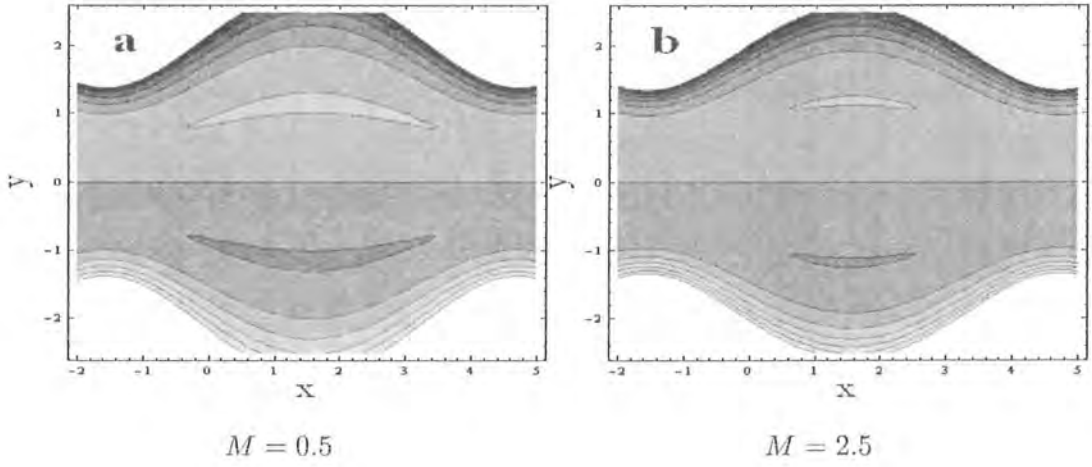

$$M = 0.5 \qquad\qquad\qquad M = 2.5$$

Fig. 5.13

Fig. 5.13(a, b): Plots of $\Psi(x,y)$ for distinct values of Hartman number (M) when $A = 0.1$, $W = 1.5$, $\alpha_e = 0.2$, $\Theta = 2.93$, $\phi = 0.37$.

$A = 0.1$ $A = 0.4$

Fig. 5.14
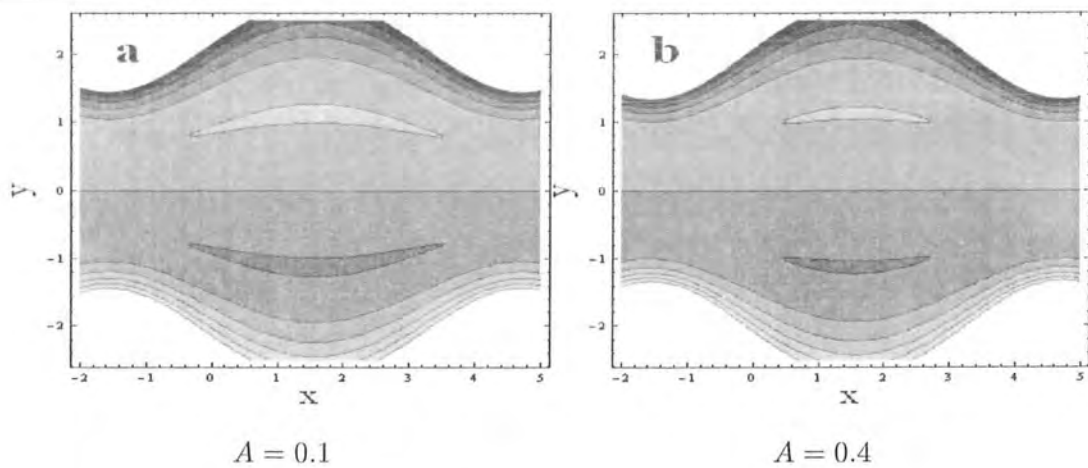
Fig. 5.14(a, b): Plots of $\Psi(x, y)$ for distinct values of fluid parameter (A) when $W = 1.5$, $M = 2.5$, $\alpha_e = 0.2$, $\Theta = 2.93$, $\phi = 0.37$.
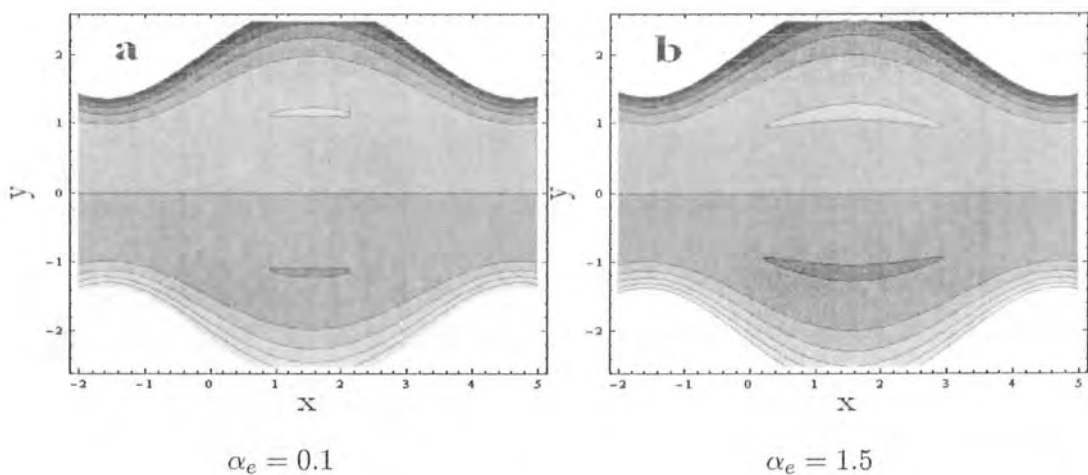

$\alpha_e = 0.1$ $\alpha_e = 1.5$

Fig. 5.15

Fig. 5.15(a, b): Plots of $\Psi(x, y)$ for different values of Hall parameter (α_e) when $A = 0.01$, $W = 1.5$, $M = 2.25$, $\Theta = 2.93$, $\phi = 0.37$.
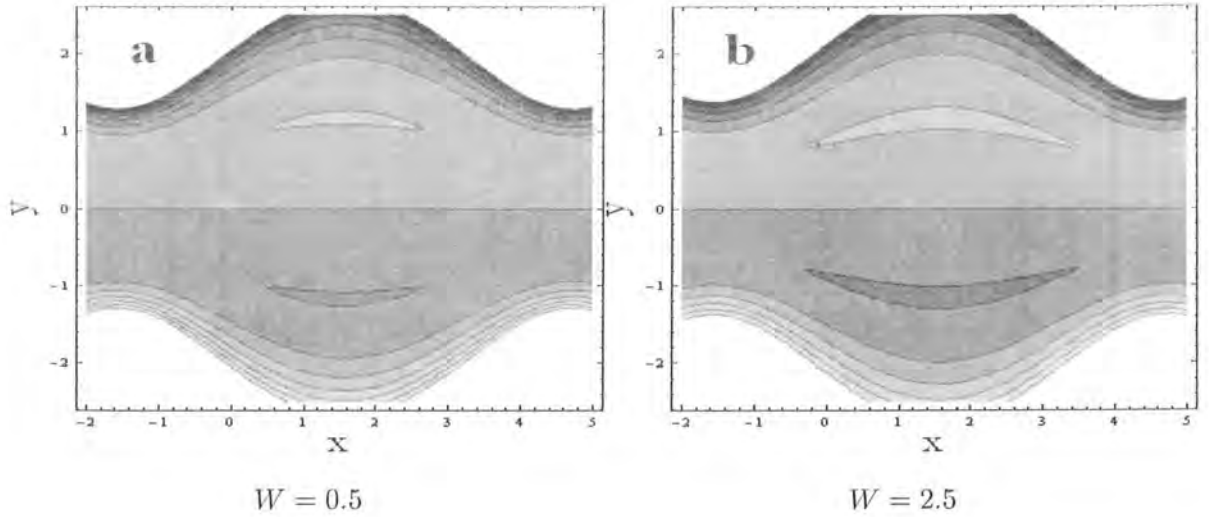
75

$W = 0.5$ $W = 2.5$

Fig. 5.16

Fig. 5.16(a, b): Plots of $\Psi(x, y)$ for different values of fluid parameter (W) when $A = 0.01$, $M = 2.5$, $\alpha_e = 0.2$, $\Theta = 2.93$, $\phi = 0.37$.

5.4   Conclusions

In the present chapter, we discussed the Hall effect on peristaltic motion of non-Newtonian fluid in a symmetric channel. The equations that governs the flow have been modeled and simplified under the assumption of long wavelength approximation. The outcomes of the analysis are discussed and presented through graphs. We have the following key observations:

- Effects of fluid parameter A and Hartman number M at the center of the channel are similar.

- Variations of W and α_e on the velocity are opposite to that of A and M.

- The velocity profile shows an opposite behavior near the channel walls when compared with the channel center.

- Pressure gradient decreases in magnitude for fluid parameter A and Hall parameter α_e. However dp/dx enhances for an increase in Hartman number M and fluid parameter W.

- Pressure rise decreases in peristaltic pumping region for an increase in A and $\overline{\alpha_e}$, whereas the effect of M and W is to increase the pressure rise.

- The size of bolus decreases for an increase in parameters A and M. However opposite effects are noted for α_e and W for the size of the trapped bolus.

Chapter 6

MHD peristaltic flow of third order fluid with Hall effects

Here a mathematical model is constructed to study the Hall effect for peristaltic flow of magnetohydrodynamic (MHD) third order fluid in a symmetric flow configuration. The governing equations of motion are simplified by employing the assumption of long wavelength approximation and considering small Reynolds number. Series solutions upto first order are obtained for the stream function, longitudinal velocity and pressure gradient. Numerical integration is carried out for the pressure rise and frictional forces. The influence of emerging parameters on the pressure rise, frictional forces, axial pressure gradient, velocity profile and trapping are discussed.

6.1 Formulation of problem

Let us consider the flow of an incompressible third grade fluid in a uniform channel of width $2d$. The fluid is conducted under the application of a transverse uniform magnetic field $\mathbf{B}_0$. The induced magnetic field is neglected under the assumption of small magnetic Reynolds number. Cartesian coordinate system is chosen in which $\overline{X}$-axis lies along the central line of channel whereas $\overline{Y}$-axis lies normal to it. We consider an infinite wave train travelling with velocity c along the walls of the symmetric channel. The wall geometry is defined as follows:

$$\bar{h}\left(\overline{X}, \bar{t}\right) = d + b \sin \frac{2\pi}{\lambda}\left(\overline{X} - c\bar{t}\right) \tag{6.1}$$

in which b represents the amplitude of wave, λ the wavelength and $\bar{t}$ the time. The equations of motion that governs the flow of MHD fluid are given by the following relations:

$$\operatorname{div} \overline{\mathbf{V}} = 0, \tag{6.2}$$

$$\rho_f \frac{d\overline{\mathbf{V}}}{d\bar{t}} = \operatorname{div} \overline{\mathbf{T}} + \mathbf{J} \times \mathbf{B}, \tag{6.3}$$

where $d/d\bar{t}$ signifies the material derivative, ρ_f the density, $\overline{\mathbf{V}}$ the velocity, $\mathbf{J}$ the current density and $\overline{\mathbf{T}}$ represents the Cauchy stress tensor respectively.

The expression of Cauchy stress tensor is

$$\overline{\mathbf{T}} = -\overline{P}\mathbf{I} + \overline{\mathbf{S}}. \tag{6.4}$$

The extra stress tensor $\overline{\mathbf{S}}$ for third order fluid is given by the relation

$$\overline{\mathbf{S}} = \left(\mu + \beta_3(tr\overline{\mathbf{A}}_1^2)\right)\overline{\mathbf{A}}_1 + \alpha_1\overline{\mathbf{A}}_2 + \alpha_2\overline{\mathbf{A}}_1^2 + \beta_1\overline{\mathbf{A}}_3 + \beta_2\left(\overline{\mathbf{A}}_1\overline{\mathbf{A}}_2 + \overline{\mathbf{A}}_2\overline{\mathbf{A}}_1\right), \tag{6.5}$$

where μ, $\alpha_i\,(i=1,2)$ and $\beta_j\,(j=1-3)$ represents the fluid constants. The Rivlin–Ericksen tensors $\overline{\mathbf{A}}_n$ are

$$\overline{\mathbf{A}}_1 = \left(\operatorname{grad}\overline{\mathbf{V}}\right) + \left(\operatorname{grad}\overline{\mathbf{V}}\right)^\top, \tag{6.6}$$

$$\overline{\mathbf{A}}_n = \frac{d}{dt}\overline{\mathbf{A}}_{n-1} + \overline{\mathbf{A}}_{n-1}\left(\operatorname{grad}\overline{\mathbf{V}}\right) + \left(\operatorname{grad}\overline{\mathbf{V}}\right)^\top\overline{\mathbf{A}}_{n-1}, \qquad n > 1, \tag{6.7}$$

where $\top$ indicates the transpose of the matrix. The velocity field is defined as

$$\overline{\mathbf{V}} = \left[\overline{U}\left(\overline{X},\overline{Y},\bar{t}\right), \overline{V}\left(\overline{X},\overline{Y},\bar{t}\right), 0\right]. \tag{6.8}$$

In above definition $\overline{U}$ and $\overline{V}$ are the velocity components parallel to the $\overline{X}$ and $\overline{Y}$-axes respectively. The generalized Ohm's law containing Hall terms due to strong magnetic field gives:

$$\mathbf{J} \times \mathbf{B} = -\sigma B_0^2 \gamma \left[\left(\overline{U} - \alpha_e\overline{V}\right)\hat{i} + \left(\overline{V} + \alpha_e\overline{U}\right)\hat{j}\right], \quad \gamma = \frac{1}{1+(\alpha_e)^2}. \tag{6.9}$$

79

Using Eqs. (6.4) − (6.9) in Eqs. (6.2) and (6.3) we have the following set of equations:

$$\frac{\partial \overline{U}}{\partial \bar{X}} + \frac{\partial \overline{V}}{\partial \bar{Y}} = 0, \tag{6.10}$$

$$\rho_f(\frac{\partial}{\partial \bar{t}} + \overline{U}\frac{\partial}{\partial \bar{X}} + \overline{V}\frac{\partial}{\partial \bar{Y}})\overline{U} = -\frac{\partial \bar{P}}{\partial \bar{X}} + \frac{\partial \overline{S}_{\overline{XX}}}{\partial \bar{X}} + \frac{\partial \overline{S}_{\overline{XY}}}{\partial \bar{Y}} - \sigma B_0^2 \gamma \left(\overline{U} - \alpha_e \overline{V} \right), \tag{6.11}$$

$$\rho_f(\frac{\partial}{\partial \bar{t}} + \overline{U}\frac{\partial}{\partial \bar{X}} + \overline{V}\frac{\partial}{\partial \bar{Y}})\overline{V} = -\frac{\partial \bar{P}}{\partial \bar{Y}} + \frac{\partial \overline{S}_{\overline{XY}}}{\partial \bar{X}} + \frac{\partial \overline{S}_{\overline{YY}}}{\partial \bar{Y}} - \sigma B_0^2 \gamma \left(\overline{V} + \alpha_e \overline{U} \right). \tag{6.12}$$

Expressions for $\overline{S}_{\overline{XX}}$, $\overline{S}_{\overline{XY}}$ and $\overline{S}_{\overline{YY}}$ can be found by using Eq. (6.5). Note that in the fixed coordinate system $\left(\overline{X},\overline{Y}\right)$, the motion is unsteady. However in a coordinate system $(\bar{x},\bar{y})$ moving with the wave speed c in positive $\bar{x}$ direction the boundary shape is stationary. Defining the transformations

$$\bar{x} = \bar{X} - c\bar{t}, \ \bar{y} = \bar{Y}, \ \bar{u} = \bar{U} - c, \ \bar{v} = \bar{V}, \ \bar{p}(\bar{x},\bar{y}) = \bar{P}\left(\bar{X},\bar{Y},\bar{t}\right), \tag{6.13}$$

and introducing the dimensionless variables by

$$
\begin{aligned}
x &= \frac{2\pi\bar{x}}{\lambda}, \quad y = \frac{\bar{y}}{d}, \quad u = \frac{\bar{u}}{c}, \quad v = \frac{\bar{v}}{c}, \quad h = \frac{\bar{h}}{d}, \quad \hat{\lambda}_1 = \frac{\alpha_1 c}{\mu d_1} \\
\hat{\lambda}_2 &= \frac{\alpha_2 c}{\mu d_1}, \quad \gamma_1 = \frac{\beta_1 c^2}{\mu d^2}, \quad \gamma_2 = \frac{\beta_2 c^2}{\mu d^2}, \quad \gamma_3 = \frac{\beta_3 c^2}{\mu d^2}, \quad p = \frac{2\pi d^2}{\lambda \mu c}\bar{p}, \\
S &= \frac{d}{\mu c}\overline{S}, \quad \Gamma = \gamma_2 + \gamma_3, \quad M = \sqrt{\frac{\sigma}{\mu}}B_0 d \quad \text{Re} = \frac{\rho_f dc}{\mu}, \quad \delta = \frac{2\pi d}{\lambda},
\end{aligned} \tag{6.14}
$$

the resulting flow Eqs. (6.11) and (6.12) in terms of the stream function Ψ $\left(u = \frac{\partial \Psi}{\partial y}, v = -\delta\frac{\partial \Psi}{\partial x}\right)$ under long wavelength approximation yield

$$\frac{dp}{dx} = \frac{\partial^3 \Psi}{\partial y^3} + 2\Gamma\frac{\partial}{\partial y}\left(\frac{\partial^2 \Psi}{\partial y^2}\right)^3 - M^2\gamma\left(\frac{\partial \Psi}{\partial y} + 1\right), \tag{6.15}$$

$$\frac{\partial p}{\partial y} = 0. \tag{6.16}$$

Eq. (6.16) implies that $p \neq p(y)$ so $p = p(x)$ only. Eliminating pressure by cross differentiation

of Eq. (6.15) and (6.16), one finds the compatibility equation in the form

$$\frac{\partial^4 \Psi}{\partial y^4} = -2\Gamma \frac{\partial^2}{\partial y^2} \left(\frac{\partial^2 \Psi}{\partial y^2} \right)^3 + M^2 \gamma \frac{\partial^2 \Psi}{\partial y^2}, \tag{6.17}$$

where Γ is the material parameter known as Deborah number and M is the Hartman number. The dimensionless shape of the wall $h(x)$ is given by

$$h(x) = 1 + \phi \sin x, \tag{6.18}$$

in which $\phi = (b/d)$ is the amplitude ratio and $0 < \phi < 1$. The relevant boundary conditions in the waveframe are

$$\Psi = 0, \qquad \frac{\partial^2 \Psi}{\partial y^2} = 0 \qquad at \ y = 0, \tag{6.19}$$

$$\frac{\partial \Psi}{\partial y} = -1, \qquad \Psi = F \qquad at \ y = h, \tag{6.20}$$

$$\Theta = F + 1. \tag{6.21}$$

In above equation Θ and F are the non-dimensional average flow rates in the fixed and wave frames respectively. The expressions of non-dimensional pressure rise per wavelength $(\triangle P_\lambda)$ and frictional forces (F_λ) are given by

$$\triangle P_\lambda = \int_0^{2\pi} \frac{dp}{dx} dx, \tag{6.22}$$

$$F_\lambda = \int_0^{2\pi} -h \frac{dp}{dx} dx. \tag{6.23}$$

6.2 Series solutions

The governing equations are non-linear. To find the solutions of these equations, we expanded the flow quantities in a power series of small parameter Γ as follows:

$$\Psi = \Psi_0 + \Gamma \, \Psi_1 + O(\Gamma^2), \tag{6.24}$$

$$F = F_0 + \Gamma \, F_1 + O(\Gamma^2), \tag{6.25}$$

$$p = p_0 + \Gamma \, p_1 + O(\Gamma^2). \tag{6.26}$$

The series solutions of Eqs. (6.15) and (6.17) by using Eqs. (6.25) − (6.27) along with Eqs. (6.22) and (6.23) upto first order expansion yields:

$$
\begin{aligned}
\Psi = {} & \tfrac{1}{32B^4h}\big(8y(4B^4F + 3h^2(F+h)^3M^6\gamma^3\Gamma) + h(F+h)^3M^4\gamma^2\Gamma\cosh[M(h-3y)\sqrt{\gamma}] \\
& -12h^2(F+h)^3M^6(h+y)\gamma^3\Gamma\cosh[M(h-y)\sqrt{\gamma}] + (F+h)(-h(F+h)^2M^4\gamma^2\Gamma \\
& \cosh[M(3h-y)\sqrt{\gamma}] + 12h^2(F+h)^2M^6(h-y)\gamma^3\Gamma\cosh[M(h+y)\sqrt{\gamma}] - 32B^3 \\
& y\sinh[My\sqrt{\gamma}] + h(32B^3\sinh[My\sqrt{\gamma}] + (F+h)^2M^4\gamma^2\Gamma(\cosh[M(3h+y)\sqrt{\gamma}] \\
& -\cosh[M(h+3y)\sqrt{\gamma}] + M\sqrt{\gamma}(4y(-7\cosh[hM\sqrt{\gamma}] + \cosh[3hM\sqrt{\gamma}] \\
& +6\cosh[My\sqrt{\gamma}])\sinh[hM\sqrt{\gamma}] + h(\sinh[M(h-3y)\sqrt{\gamma}] + 3\sinh[M(3h-y)\sqrt{\gamma}] \\
& -3\sinh[M(3h+y)\sqrt{\gamma}] + \sinh[M(h+3y)\sqrt{\gamma}])))))), \tag{6.27}
\end{aligned}
$$

$$
\begin{aligned}
dp/dx = {} & \tfrac{1}{16B^4}((F+h)M^3\gamma^{3/2}(6hM\sqrt{\gamma}(1 - h^2M^2\gamma - 2(F+h)^2M^4\gamma^2\Gamma) - 8h^3M^3\gamma^{3/2} \\
& \cosh[2hM\sqrt{\gamma}] - 2hM\sqrt{\gamma}(3 + h^2M^2\gamma)\cosh[4hM\sqrt{\gamma}] + 4(1 + 3h^2M^2\gamma \\
& +2(F+h)^2M^4\gamma^2\Gamma)\sinh[2hM\sqrt{\gamma}] - (-2 - 6h^2M^2\gamma + (F+h)^2M^4\gamma^2\Gamma) \\
& \sinh[4hM\sqrt{\gamma}])), \tag{6.28}
\end{aligned}
$$

where

$$B = -hM\sqrt{\gamma}\cosh[hM\sqrt{\gamma}] + \sinh[hM\sqrt{\gamma}].$$

82

6.3 Graphical results and discussion

The aim of this section is to discuss and analyze the effect of Hall parameter (α_e), Hartman number (M), Deborah number (Γ) and amplitude ratio (ϕ) on pressure rise per wavelength (ΔP_λ), friction force at the channel wall (F_λ), pressure gradient (dp/dx), longitudinal velocity (u) and trapping.

6.3.1 Pumping characteristics

This subsection describes the effects of parameters α_e, M, Γ and ϕ on ΔP_λ, F_λ and dp/dx. Figs. (6.1 - 6.4) are displayed to see the variations of pressure drop per wavelength (ΔP_λ) against the mean flow rate (Θ). Effect of Hall parameter (α_e) on pressure rise is presented in Fig. 6.1 which depicts that by increasing α_e the pumping rate in the peristaltic region decreases whereas it increases in the co-pumping region. Furthermore free pumping flux Θ_0 increases by increasing α_e. Plots in Fig. 6.2 display the influence of Hartman number (M) on pressure rise which illustrates that pumping rate increases in the peristaltic pumping region whilst it decreases in the co-pumping region when M is increased. Moreover the free pumping flux decreases for larger M. The influence of Deborah number (Γ) on pressure rise is presented in Fig. 6.3. It indicates that an increase of Γ results in an increase in the free pumping flux. Furthermore the pumping rate increases in the peristaltic pumping region and it decreases in the co-pumping region by increasing Γ. Effect of amplitude ratio (ϕ) on pressure rise is displayed in Fig. 6.4. It indicates that the pumping rate and free pumping flux increase for increasing values of ϕ. Also it is noted that the peristaltic pumping occurs for $\phi > 1$. In addition ΔP_λ decreases in the co-pumping region for larger ϕ. Effect of parameters α_e, M, Γ and ϕ on frictional forces are presented in Figs. (6.5 - 6.8) which shows quite opposite behavior in comparison with the plots displayed for pressure rise. Figs. (6.9 - 6.12) are prepared to see the variations of axial pressure gradient dp/dx for different values of α_e, M, Γ and ϕ. Here plots of dp/dx are sketched for one wavelength for $x \in [0, 2\pi]$. Fig. 6.9 depicts that the magnitude of pressure gradient decreases for larger values of α_e. Influence of parameters M and Γ on dp/dx are shown in the Figs. 6.10 and 6.11 respectively. Here increase in both M and Γ enhances the magnitude of pressure gradient. Effect of amplitude ratio ϕ on dp/dx is presented in Fig. 6.12. It shows

that by increasing ϕ the pressure gradient decreases for $0 < x < \pi$ whereas it increases when $\pi < x < 2\pi$.
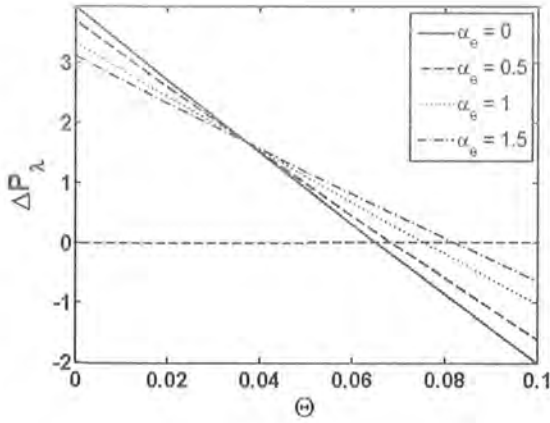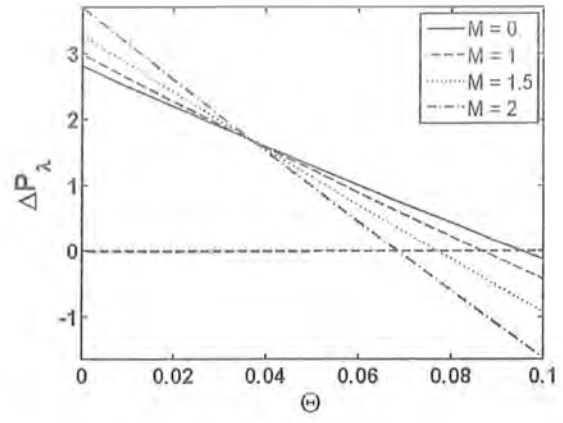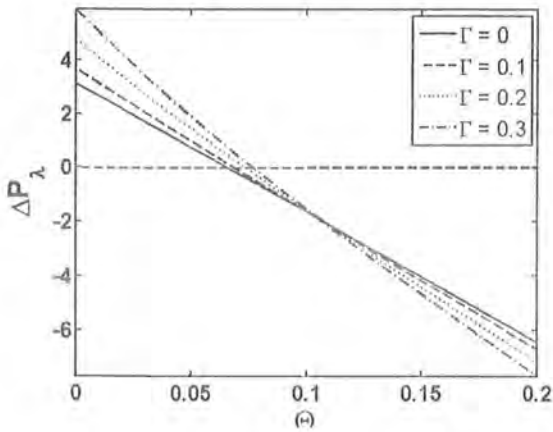
Fig. 6.1
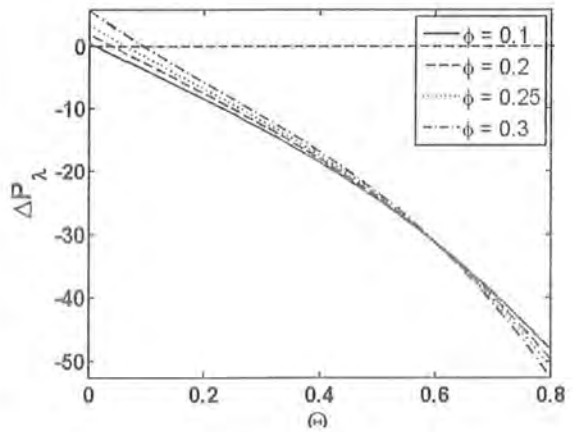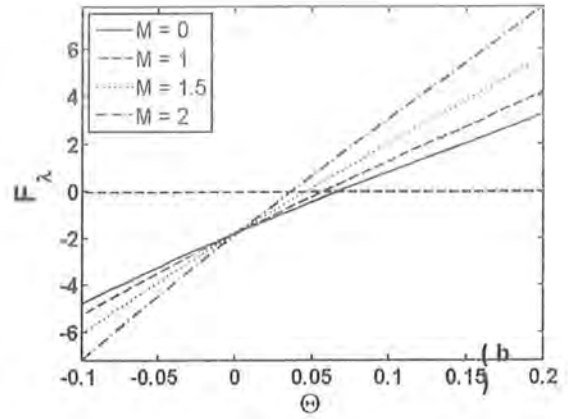

Fig. 6.2

Fig. 6.3

Fig. 6.4

Figs. (6.1 - 6.4): (ΔP_λ) versus average flow rate (Θ) for ddistinct values of Hall parameter (α_e), Hartman number (M), Deborah number (Γ) and amplitude ratio (ϕ). Fig. 6.1: $M = 2$, $\phi = 0.26$, $\Gamma = 0.1$, Fig. 6.2: $\alpha_e = 0.5$, $\phi = 0.26$, $\Gamma = 0.1$, Fig. 6.3: $M = 2$, $\phi = 0.26$, $\alpha_e = 0.5$, Fig. 6.4: $M = 2$, $\Gamma = 0.1$, $\alpha_e = 0.5$.
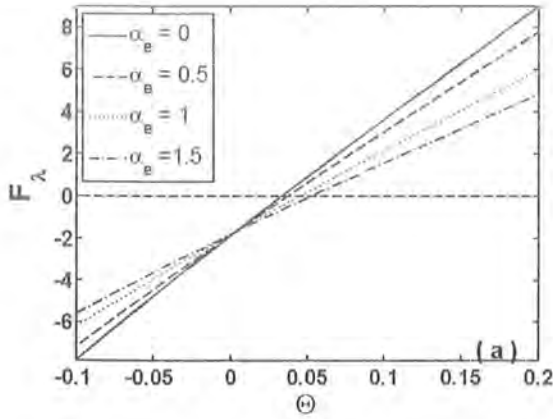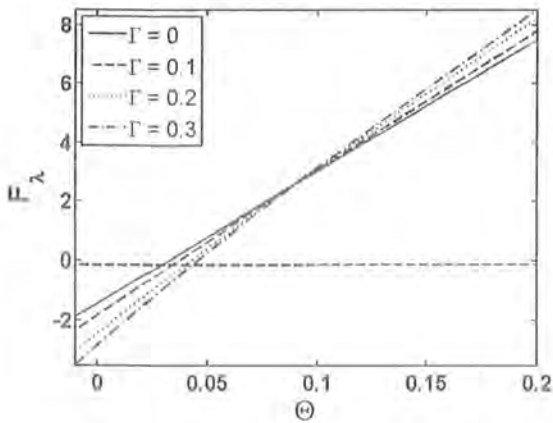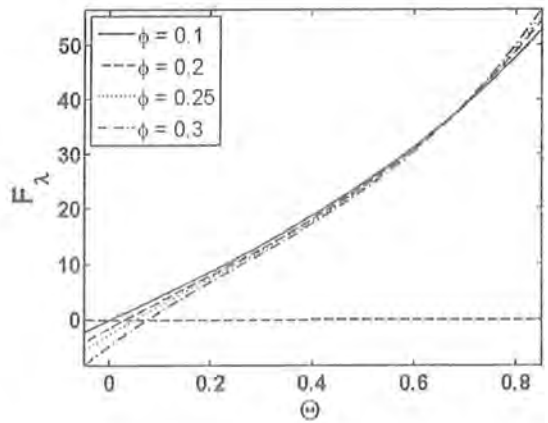
Fig. 6.5

Fig. 6.6

Fig. 6.7

Fig. 6.8

Figs. (6.5 - 6.8): F_λ versus average flow rate (Θ) for distinct values of Hall parameter (α_e), Hartman number (M), Deborah number (Γ) and amplitude ratio (ϕ). Fig. 6.5: $M = 2$, $\phi = 0.26$, $\Gamma = 0.1$, Fig. 6.6: $\alpha_e = 0.5$, $\phi = 0.26$, $\Gamma = 0.1$, Fig. 6.7: $M = 2$, $\phi = 0.26$, $\alpha_e = 0.5$, Fig. 6.8: $M = 2$, $\Gamma = 0.1$, $\alpha_e = 0.5$.
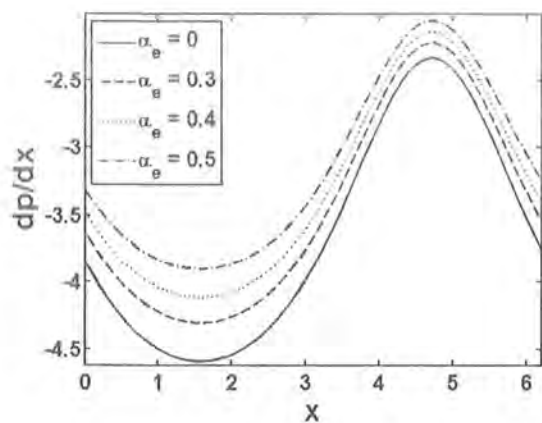
Fig. 6.9

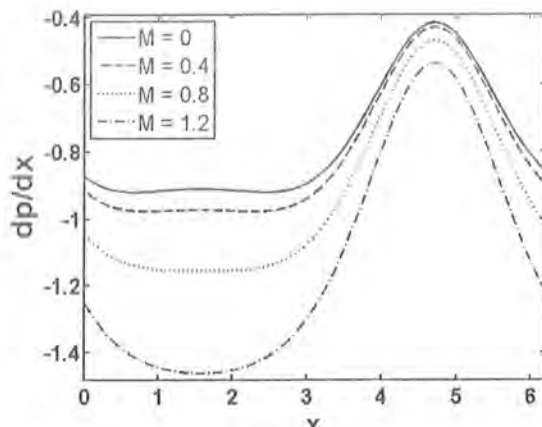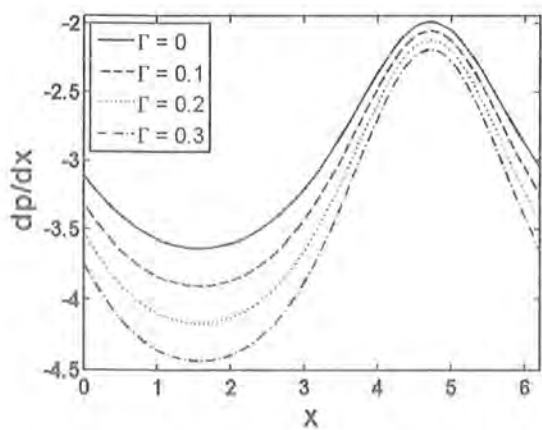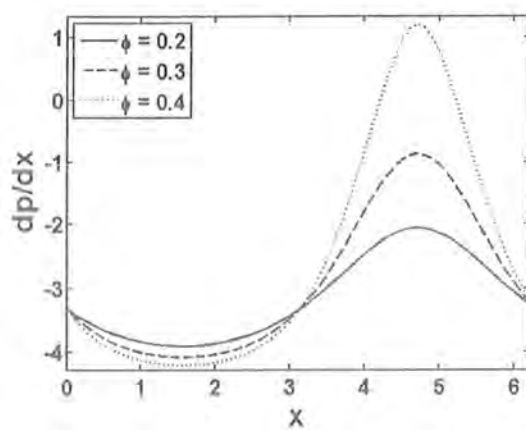Fig. 6.10

Fig. 6.11

Fig. 6.12

Figs. (6.9 - 6.12): dp/dx versus $x \in [0, 2\pi]$ for different values of Hall parameter (α_e), Hartman number (M), Deborah number (Γ) and amplitude ratio (ϕ). Fig. 6.9: $\Theta = 0.35$, $M = 2.5$, $\phi = 0.2$, $\Gamma = 0.1$, Fig. 6.10: $\Theta = 0.35$, $\alpha_e = 0.5$, $\phi = 0.2$, $\Gamma = 0.1$, Fig. 6.11: $\Theta = 0.35$, $M = 2.5$, $\phi = 0.2$, $\alpha_e = 0.5$, Fig. 6.12: $\Theta = 0.35$, $M = 2.5$, $\Gamma = 0.1$, $\alpha_e = 0.5$.

6.3.2 Axial velocity profile

Effects of parameters α_e, M and Γ on longitudinal velocity profile ($u(y)$) are presented in Figs. (6.13 - 6.15). Fig. 6.13 indicates that by increasing α_e the velocity ehnances at the central part of the channel whilst it reduces near the wall of channel. Fig. 6.14 is presented to analyze the impact of M on the velocity profile $u(y)$. It depicts that the impact of M on $u(y)$ is quite opposite to that of α_e. Here by increasing M the velocity decreases at the central part of the channel. This is due to fact that by increasing M the magnitude of magnetic flux B_0 increases which enhances the Lorentz force resisting the flow at the center of channel and hence the velocity decreases. Impact of Γ on velocity is displayed in Fig. 6.15. Here the velocity increases near the center of channel and it decreases near the walls when Γ increases.
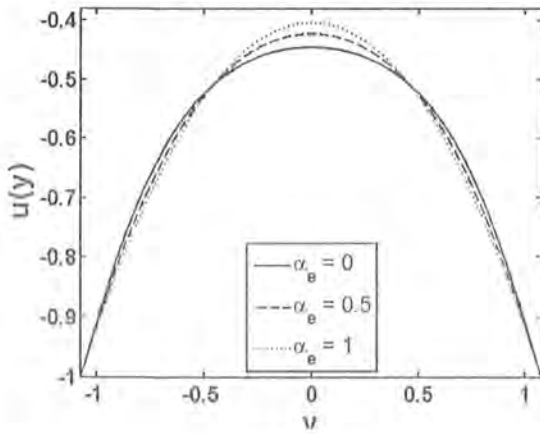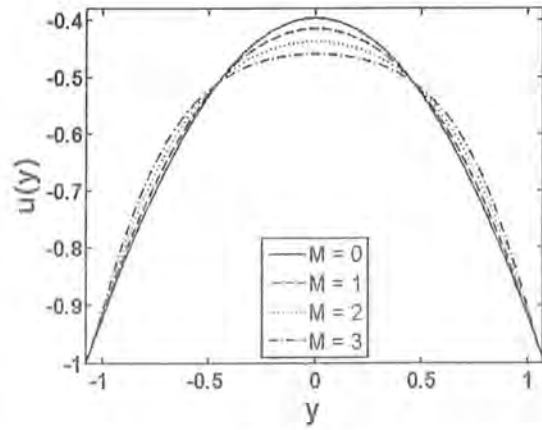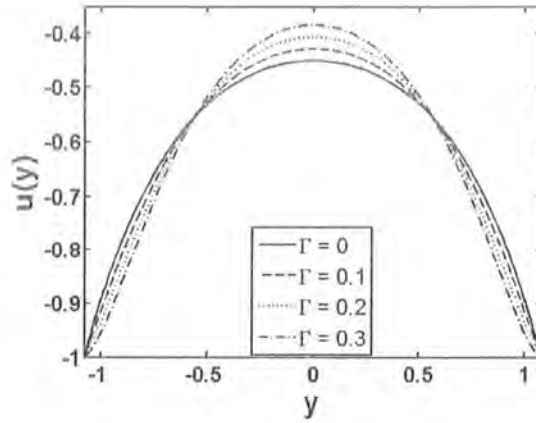

Fig. 6.13

Fig. 6.14

Fig. 6.15

Figs. (6.13 - 6.15): Velocity profile (u) versus y for distinct values of Hall parameter (α_e), Hartman number (M) and Deborah number (Γ). Fig. 6.13: $x = 0.2$, $\Theta = 0.35$, $M = 2.5$, $\phi = 0.4$, $\Gamma = 0.1$, Fig. 6.14: $x = 0.2$, $\Theta = 0.35$, $\alpha_e = 0.5$, $\phi = 0.4$, $\Gamma = 0.1$, Fig. 6.15: $x = 0.2$, $\Theta = 0.35$, $M = 2.5$, $\phi = 0.4$, $\alpha_e = 0.5$.

6.3.3 Trapping

The phenomenon in which the stream lines are circled under certain conditions to enclosed a bolus is known as trapping. This trapped bolus is pushed ahead along the peristaltic wave. Figs. $(6.16 - 6.19)$ are made to see the influences of Hall parameter α_e, Hartman number M, Deborah number Γ and amplitude ratio ϕ on trapping. In Figs. 6.16, 6.18 and 6.19 the size of trapped bolus increases when one of the α_e, Γ and ϕ is increased. However opposite behavior is noted with an increase in M (as shown in Fig. 6.17).
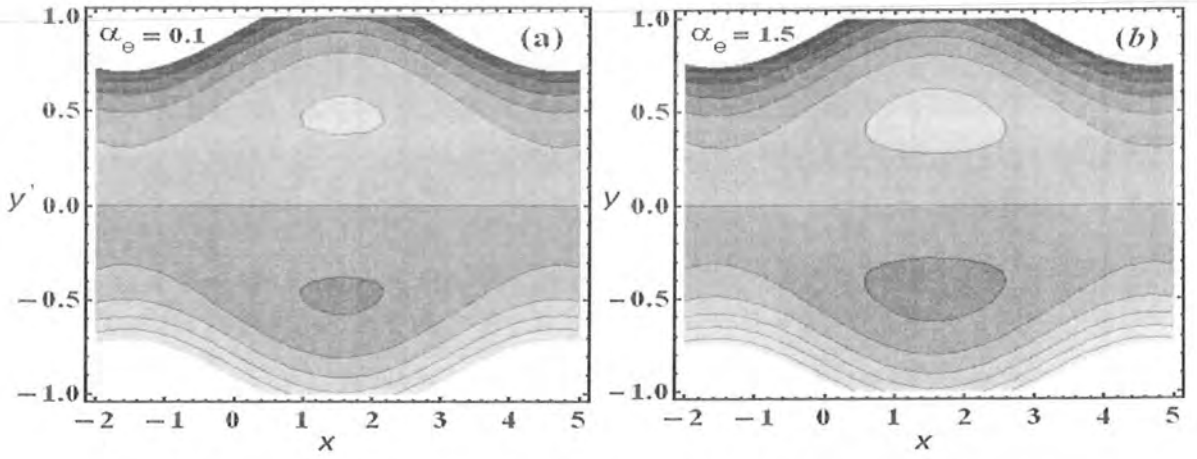
89

Fig. 6.16

Fig. 6.16 (a-b): Plots of $\Psi(x,y)$ for α_e. Other parameters are $\Theta = 0.715$, $M = 2.5$, $\phi = 0.2$, $\Gamma = 0.1$.

Fig. 6.17

Fig. 6.17 (a-b): Plots of $\Psi(x,y)$ for M. Other parameters are $\Theta = 0.715$, $\alpha_e = 0.5$, $\phi = 0.2$, $\Gamma = 0.1$.
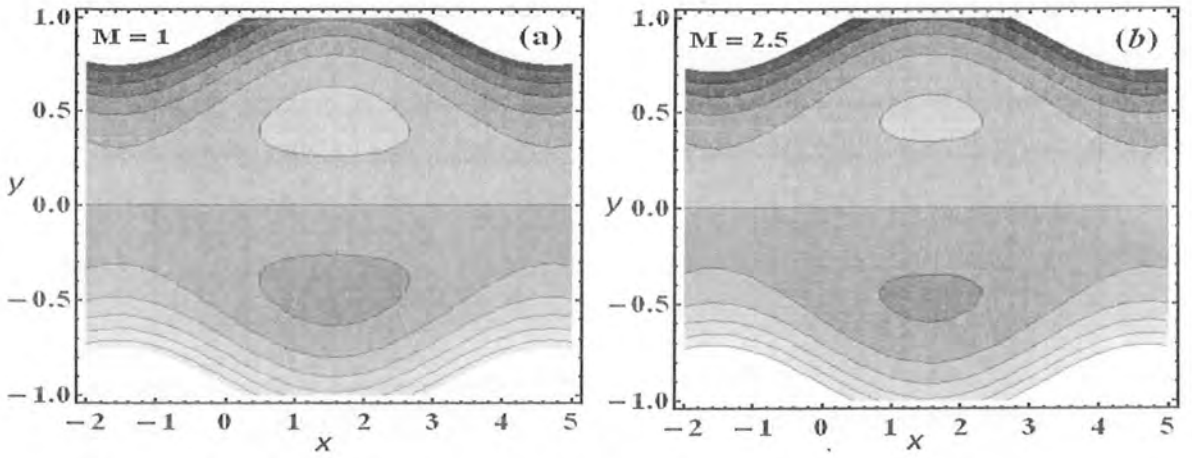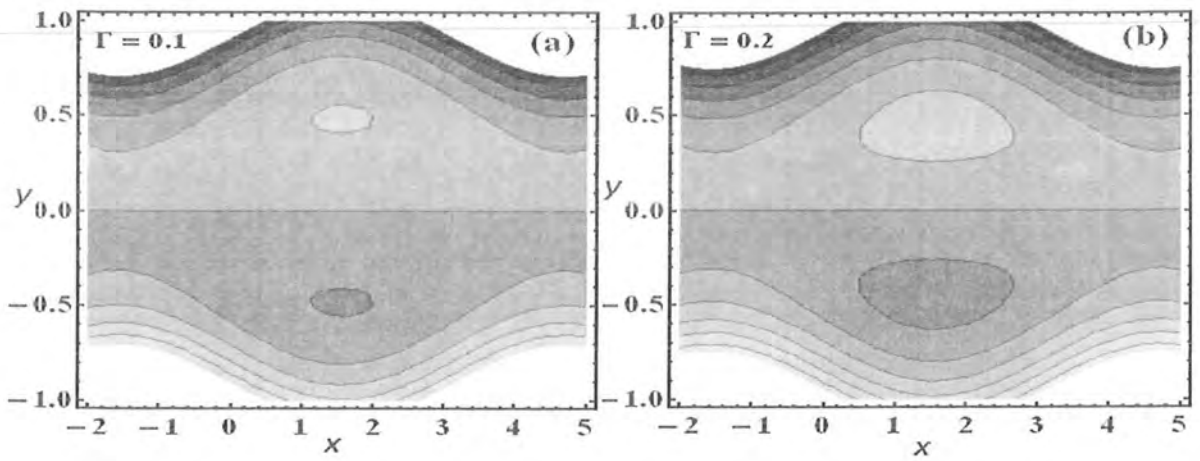
Fig. 6.18

Fig. 6.18 (a-b): Plots of $\Psi(x,y)$ for Γ. Other parameters are $\Theta = 0.715$, $\alpha_e = 0.5$, $\phi = 0.2$, $M = 3$.
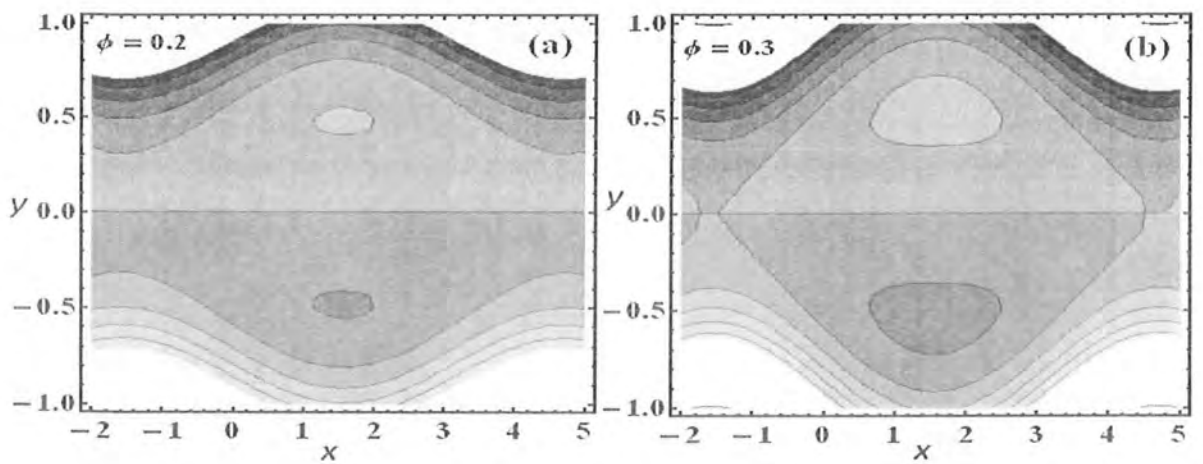
Fig. 6.19

Fig. 6.19: (a-b) Plots of $\Psi(x,y)$ for ϕ. Other parameters are $\Theta = 0.715$, $\alpha_e = 0.5$, $\Gamma = 0.1$, $M = 3$.

6.4   Concluding remarks

The presented study addressed the MHD flow of third order fluid in a symmetric channel. The following observations are worth mentioning:

- The pumping rate decreases in peristaltic pumping region by increasing α_e. However it increases for increasing values of M, Γ, and ϕ.

- Magnitude of dp/dx decreases for increasing values of α_e, whereas it increases for larger values of M and Γ.

- Effects of α_e and Γ on $u(y)$ are opposite to that of M. Furthermore $u(y)$ shows a reverse behavior at the central part of channel when compared it in the neighbourhood of the channel wall.

- Size of the bolus increases by increasing α_e, Γ, and ϕ whereas it decreases when M is enhanced.

Chapter 7

Peristaltic flow of hyperbolic tangent fluid with Hall and ion-slip effects

Effects of Hall and ion-slip currents on the peristaltic transport of an incompressible hyperbolic tangent fluid in a symmetric channel are investigated in this chapter. The flow caused is because of travelling wave along the channel walls. Long wavelength and low Reynolds number assumptions are employed in the problem formulation. Mathematical expressions for the stream functions and axial pressure gradient are constructed. Variations of physical parameters on the axial velocity, shear stress and axial pressure gradient are analyzed. Pumping and trapping phenomena are addressed.

7.1   Problem formulation

We examined the flow of an incompressible hyperbolic tangent fluid in an infinite two-dimensional channel of width $2d$. A sinusoidal wave of small amplitude travels along the channel walls with a constant speed c. The Cartesian coordinate system is chosen so that $\overline{X}$-axis lies along the central line of the channel and $\overline{Y}$-axis normal to it. The fluid is considered to be electrically conducting under the application of a transverse uniform magnetic field $(0,\ 0,\ B_0)$. The induced magnetic field is neglected under the assumption of low magnetic Reynolds number. The

93

geometry of walls satisfies the following relation:

$$\overline{H}\left(\overline{X}, \overline{t}\right) = d + b\cos\frac{2\pi}{\lambda}\left(\overline{X} - c\overline{t}\right),$$ (7.1)

in which b represents the amplitude of wave, λ is the wavelength and $\overline{t}$ is the time. The equations governing the MHD flow are

$$\operatorname{div}\overline{\mathbf{V}} = 0,$$ (7.2)

$$\rho_f\frac{d\overline{\mathbf{V}}}{d\overline{t}} = \operatorname{div}\overline{\mathbf{T}} + \mathbf{J}\times\mathbf{B},$$ (7.3)

where $d/d\overline{t}$ signifies the material derivative, ρ_f is the density, $\overline{\mathbf{V}}\left(= \left[\overline{U}, \overline{V}, 0\right]\right)$ the velocity and $\mathbf{J}$ the current density. Here $\overline{U}$ and $\overline{V}$ are the velocity components along $\overline{X}$ and $\overline{Y}$- axes respectively.

The Cauchy stress tensor $\overline{\mathbf{T}}$ for hyperbolic tangent fluid is given by

$$\overline{\mathbf{T}} = -\overline{P}\overline{I} + \overline{\mathbf{S}},$$ (7.4)

$$\overline{\mathbf{S}} = [\eta_\infty + (\eta_0 + \eta_\infty)\tanh(\mathring{\Gamma}\overline{\dot{\gamma}})^n]\overline{\mathbf{A}}_1,$$ (7.5)

$$\overline{\mathbf{A}}_1 = \left(\operatorname{grad}\overline{\mathbf{V}}\right) + \left(\operatorname{grad}\overline{\mathbf{V}}\right)^\top,$$ (7.6)

$$\overline{\dot{\gamma}} = \sqrt{\frac{1}{2}tr\left(\overline{\mathbf{A}}_1\right)^2}.$$ (7.7)

Here $\overline{P}$ is a pressure, $\overline{I}$ the identity tensor, $\overline{\mathbf{S}}$ the extra stress tensor, η_0 the zero shear rate viscosity, η_∞ the infinite shear rate viscosity, $\mathring{\Gamma}$ the time constant, n the power law index and $\overline{\mathbf{A}}_1$ the first Rivlin–Ericksen tensor. Under the assumptions of $\eta_\infty = 0$ and $\mathring{\Gamma}\overline{\dot{\gamma}} < 1$, Eq. (7.5) reduces to

$$\overline{\mathbf{S}} = \eta_0[1 + n(\mathring{\Gamma}\overline{\dot{\gamma}} - 1)]\overline{\mathbf{A}}_1.$$ (7.8)

The generalized Ohm's law in the presence of Hall and ion-slip effects is expressed by the relation:

$$\mathbf{J} = \sigma(\mathbf{E} + \mathbf{V}\times\mathbf{B}) - \frac{\alpha_e}{B_0}\left(\mathbf{J}\times\mathbf{B}\right) + \frac{\alpha_e\alpha_i}{B_0^2}[(\mathbf{J}\times\mathbf{B})\times\mathbf{B}],$$ (7.9)

in which σ is the electrical conductivity, $\alpha_e\left(= w_e\tau_e\right)$ the Hall parameter, $\alpha_i\left(= en_eB_0/(1 + n_e/n_a)\right)$

94

the ion-slip parameter, w_e the cyclotron frequency, τ_e the electron collision time, e the electric charge, n_e the number density of electrons, n_a the neutral particle density and $\mathbf{E}$ the electric field. The electric field here is negligible therefore from Eq. (7.9) we have

$$\mathbf{J} \times \mathbf{B} = -\frac{\sigma B_0^2}{((1 + \alpha_e \alpha_i)^2 + (\alpha_e)^2)} \left[\left((1 + \alpha_e \alpha_i)\overline{U} - \alpha_e \overline{V} \right), \ \left((1 + \alpha_e \alpha_i)\overline{V} + \alpha_e \overline{U} \right), \ 0 \right], \quad (7.10)$$

Using Eqs. $(7.4 - 7.8)$ and (7.10) in Eqs. (7.2) and (7.3) we have

$$\frac{\partial \overline{U}}{\partial \overline{X}} + \frac{\partial \overline{V}}{\partial \overline{Y}} = 0, \quad (7.11)$$

$$\rho_f \left(\frac{\partial}{\partial \overline{t}} + \overline{U}\frac{\partial}{\partial \overline{X}} + \overline{V}\frac{\partial}{\partial \overline{Y}} \right) \overline{U} = -\frac{\partial \overline{p}}{\partial \overline{X}} + \frac{\overline{S_{XX}}}{\partial \overline{X}} + \frac{\overline{S_{XY}}}{\partial \overline{Y}} - \sigma B_0^2 \left((1 + \alpha_e \alpha_i)\overline{U} - \alpha_e \overline{V} \right), \quad (7.12)$$

$$\rho_f \left(\frac{\partial}{\partial \overline{t}} + \overline{U}\frac{\partial}{\partial \overline{X}} + \overline{V}\frac{\partial}{\partial \overline{Y}} \right) \overline{V} = -\frac{\partial \overline{p}}{\partial \overline{Y}} + \frac{\overline{S_{YX}}}{\partial \overline{X}} + \frac{\overline{S_{YY}}}{\partial \overline{Y}} - \sigma B_0^2 \left((1 + \alpha_e \alpha_i)\overline{V} + \alpha_e \overline{U} \right), \quad (7.13)$$

$$\overline{S_{XX}} = 2\eta_0 \left[1 + n \left(\hat{\Gamma}\overline{\dot{\gamma}} - 1 \right) \right] \frac{\partial \overline{U}}{\partial \overline{X}}, \quad (7.14)$$

$$\overline{S_{XY}} = \eta_0 \left[1 + n \left(\hat{\Gamma}\overline{\dot{\gamma}} - 1 \right) \right] \left(\frac{\partial \overline{U}}{\partial \overline{Y}} + \frac{\partial \overline{V}}{\partial \overline{X}} \right), \quad (7.15)$$

$$\overline{S_{YY}} = 2\eta_0 \left[1 + n \left(\hat{\Gamma}\overline{\dot{\gamma}} - 1 \right) \right] \frac{\partial \overline{V}}{\partial \overline{Y}}, \quad (7.16)$$

$$\left(\overline{\dot{\gamma}} \right)^2 = 2 \left(\frac{\partial \overline{U}}{\partial \overline{X}} \right)^2 + \left(\frac{\partial \overline{U}}{\partial \overline{Y}} + \frac{\partial \overline{V}}{\partial \overline{X}} \right)^2 + 2 \left(\frac{\partial \overline{V}}{\partial \overline{Y}} \right)^2. \quad (7.17)$$

Note that in fixed frame with coordinates $(\overline{X}, \overline{Y})$, the motion is time-dependent. However in a coordinate system $(\overline{x}, \overline{y})$ moving with the wave speed c in positive $\overline{x}$ direction the boundary shape is stationary. Defining the transformations from the fixed frame of reference to the wave frame of reference $(\overline{x}, \overline{y})$ by

$$\overline{x} = \overline{X} - c\overline{t}, \ \overline{y} = \overline{Y}, \ \overline{u} = \overline{U} - c, \ \overline{v} = \overline{V}, \ \overline{p}(\overline{x}, \overline{y}) = \overline{P}(\overline{X}, \overline{Y}, \overline{t}) \quad (7.18)$$

and introducing the dimensionless variables

$$x = \frac{2\pi\bar{x}}{\lambda}, \; y = \frac{\bar{y}}{d}, \; u = \frac{\bar{u}}{c}, \; v = \frac{\bar{v}}{c}, \; h = \frac{\bar{h}(\bar{x})}{d}, \; \delta = \frac{2\pi d}{\lambda},$$

$$p = \frac{d^2}{\lambda\eta_0 c}\bar{p}(\bar{x}), \; S = \frac{d}{\eta_0 c}\bar{S}(\bar{x}), \; M = \sqrt{\frac{\sigma}{\eta_0}}B_0 d, \; \text{Re} = \frac{\rho_f dc}{\eta_0},$$

$$We = \frac{\tilde{\Gamma}c}{d}, \; \dot{\gamma} = \frac{\bar{\dot{\gamma}}d}{c}, \; N = \frac{M^2(1+\alpha_e\alpha_i)}{(\iota_e)^2 + (1+\alpha_e\alpha_i)^2}, \tag{7.19}$$

the flow Eqs. $(7.12 - 7.16)$ in terms of the stream function Ψ $\left(u = \frac{\partial\Psi}{\partial y}, v = -\delta\frac{\partial\Psi}{\partial x} \right)$ under lubrication approximation become

$$\frac{\partial p}{\partial x} = \frac{\partial S_{xy}}{\partial y} - N\left(\frac{\partial\Psi}{\partial y} + 1\right), \tag{7.20}$$

$$\frac{\partial^2}{\partial y^2}S_{xy} - N\frac{\partial^2}{\partial y^2}\Psi = 0, \tag{7.21}$$

$$S_{xy} = (1-n)\frac{\partial^2\Psi}{\partial y^2} + nWe\left(\frac{\partial^2\Psi}{\partial y^2}\right)^2, \tag{7.22}$$

$$S_{xx} = S_{yy} = \frac{\partial p}{\partial y} = 0. \tag{7.23}$$

The continuity equation (7.11) is identically satisfied. Moreover M, Re, δ and We are the Hartman, Reynolds, wave and Weissenberg numbers respectively. In this case $p \neq p(y)$ from Eq. (7.23).

The dimensionless shape of the peristaltic wall $h(x)$ is given by

$$h(x) = 1 + \phi \; \sin x, \tag{7.24}$$

in which $\phi = (b/d)$ is the amplitude ratio and $(0 < \phi < 1)$. The relevant dimensionless boundary conditions are:

$$\Psi = 0, \quad \frac{\partial^2\Psi}{\partial y^2} = 0, \quad at \; y = 0, \tag{7.25}$$

$$\frac{\partial\Psi}{\partial y} = -1, \quad \Psi = F, \quad at \; y = h, \tag{7.26}$$

96

where

$$F = \int_0^h \frac{\partial \Psi}{\partial y} dy = \Psi(h) - \Psi(0). \tag{7.27}$$

7.2 Perturbation solution

The governing Eqs. (7.20) and (7.21) are highly non-linear and exact solution of these equations seems difficult to compute. Therefore we are interested in calculating the series solution of the present problem. For that we apply perturbation technique and express the flow quantities in a series of the small parameter We as follows:

$$\Psi = \Psi_0 + We\,\Psi_1 + O(We^2), \tag{7.28}$$

$$F = F_0 + We\,F_1 + O(We^2), \tag{7.29}$$

$$p = p_0 + We\,p_1 + O(We^2). \tag{7.30}$$

Now solving Eqs. (7.20), (7.21), (7.25) and (7.26) through Eqs. (7.28) − (7.30) and then employing $F_0 = F - We\,F_1$ we get the solution expressions for stream function and pressure gradient as

$$\begin{aligned}
\Psi = {} & \tfrac{1}{C_1}(F\sqrt{N}y\cosh[h\sqrt{N}/\sqrt{1-n}] + \sqrt{1-n}(y\sinh[h\sqrt{N}/\sqrt{1-n}] \\
& -(F+h)\sinh[\sqrt{N}y/\sqrt{1-n}])) - \tfrac{1}{12C_1^2 C_2\sqrt{1-n}}((F+h)^2 nNWe(8\sqrt{N}y \\
& +\sqrt{N}((6h-9y)\cosh[h\sqrt{N}/\sqrt{1-n}] + y\cosh[3h\sqrt{N}/\sqrt{1-n}] \\
& +h(\cosh[\sqrt{N}(h-2y)/\sqrt{1-n}] - 8\cosh[\sqrt{N}(h-y)/\sqrt{1-n}] \\
& +2\cosh[\sqrt{N}(2h-y)/\sqrt{1-n}] - 2\cosh[\sqrt{N}(2h+y)/\sqrt{1-n}] \\
& +2\cosh[\sqrt{N}(h+2y)/\sqrt{1-n}])) - \sqrt{1-n}(6\sinh[h\sqrt{N}/\sqrt{1-n}] \\
& +\sinh[\sqrt{N}(h-2y)/\sqrt{1-n}] - 8\sinh[\sqrt{N}(h-y)/\sqrt{1-n}] \\
& +\sinh[\sqrt{N}(2h-y)/\sqrt{1-n}] - 6\sinh[\sqrt{N}y/\sqrt{1-n}] \\
& -\sinh[\sqrt{N}(2h+y)/\sqrt{1-n}] + \sinh[\sqrt{N}(h+2y)/\sqrt{1-n}]))),
\end{aligned}$$

97

$$dp/dx = \frac{\sqrt[2]{N^3}(F+h)}{3C_1^2 C_2 \sqrt{1-n}}(4(F+h)nNWe(2+\cosh[h\sqrt{N}/\sqrt{1-n}])\sinh[h\sqrt{N}/2\sqrt{1-n}]^4$$
$$-(3C_1^2 C_2 \sqrt{1-n})/(h\sqrt{N}+\sqrt{1-n}\tanh[h\sqrt{N}/\sqrt{1-n}])),$$

where

$$C_1 = h\sqrt{N}\cosh[h\sqrt{N}/\sqrt{1-n}] - \sqrt{1-n}\sinh[h\sqrt{N}/\sqrt{1-n}],$$

$$C_2 = h\sqrt{1-n}\sqrt{N}\cosh[h\sqrt{N}/\sqrt{1-n}] + (-1+n)\sinh[h\sqrt{N}/\sqrt{1-n}].$$

7.3 Graphical analysis and discussion

The aim of this section is to study the effects of various physical parameters on axial velocity (u), shear stress (S_{xy}), pressure gradient (dp/dx), pressure rise (ΔP_λ) and trapping.

7.3.1 Velocity profile

In this subsection Figs. (7.1 − 7.3) are prepared to see the influence of Hartmann number (M), Hall parameter (α_e) and ion-slip parameter (α_i) on the velocity. It is found from these Figs. that the plots of velocity versus y are parabolic in nature. Effect of Hartmann number (M) on the velocity profile is presented in Fig. (7.1). The plot shows that by increasing M the velocity decreases near center of the channel. Physically larger M increases the magnitude of magnetic flux B_0 in transverse direction to the fluid flow which enhances the magnitude of Lorntez force and hence velocity decreases. Figs. (7.2) and (7.3) show that the effect of α_e and α_i on the velocity are qualitatively similar. These parameters assist the flow by reducing the magnitude of magnetic flux and consequently the velocity of fluid increases by increasing both α_e and α_i. Also effect of α_e and α_i on velocity is opposite to that of M.
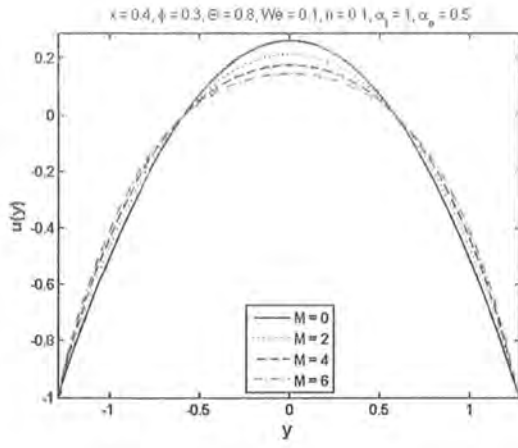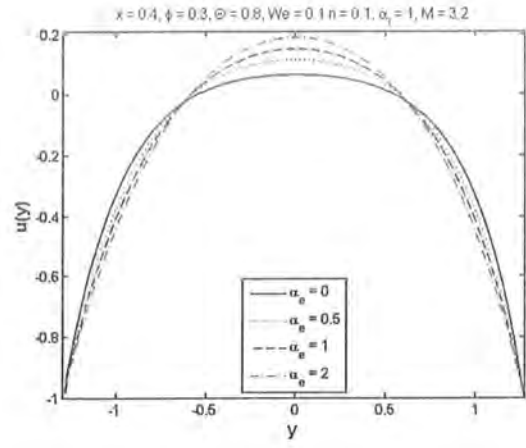
Fig. 7.1

Fig. 7.2
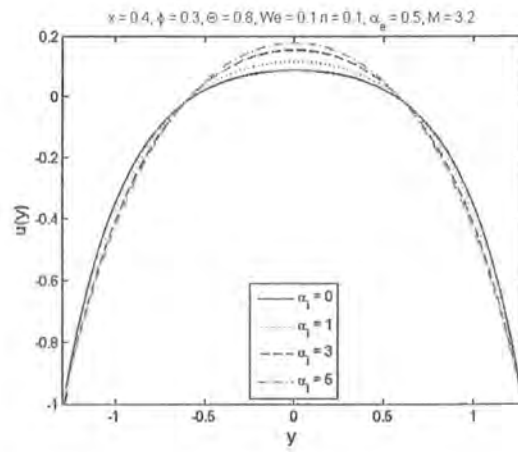

Fig. 7.3

Figs. (7.1 - 7.3): Plots of velocity for Hartmann number (M), Hall parameter (α_e), and ion-slip parameter (α_i).

7.3.2 Shear stress at the wall

Effects of Weissenberg number (We), Hartmann number (M), ion-slip parameter (α_i) and Hall parameter (α_e) on the shear stress (S_{xy}) are shown in the plots $(7.4 - 7.7)$ when $0 < x < 2\pi$. Fig. (7.4) indicates that the magnitude of stress S_{xy} increases when We increases. Influence of Hartmann number (M) on shear stress is presented in Fig. (7.5). Clearly larger values of M leads to an increase in the magnitude of S_{xy}. Fig. (7.6) illustrates that the magnitude of S_{xy} decreases by increasing the ion-slip parameter (α_i). Similar behavior is noted for the Hall parameter (α_e) in Fig. (7.7) where magnitude of shear stress S_{xy} decreases when α_e increases.
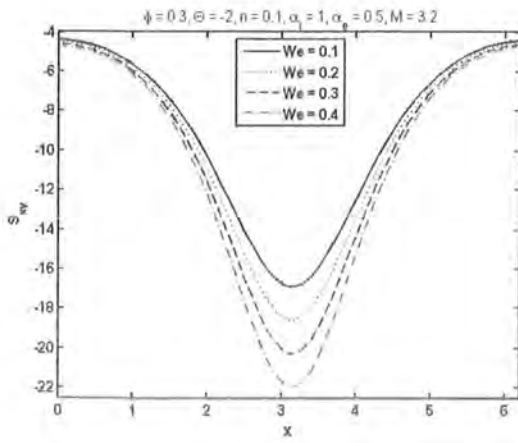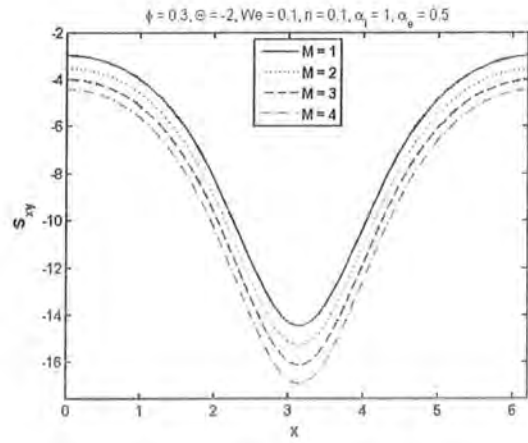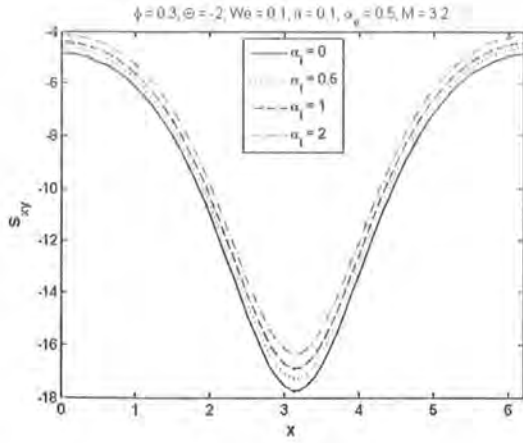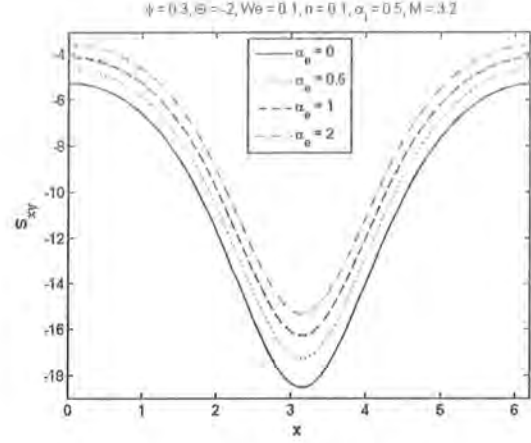

Fig. 7.4

Fig. 7.5

Fig. 7.6

Fig. 7.7

Figs. (7.4 - 7.7): Plots for shear stress for different values of Weissenberg number (We), Hartmann number (M), ion-slip parameter (α_i) and Hall parameter (α_e).

7.3.3 Pumping characteristics

This subsection portray the effect of pertinent parameters on the pressure gradient (dp/dx) and pressure rise per wavelength (ΔP_λ). Figs. $(7.8 - 7.12)$ are made to analyze the variation of dp/dx against the axial distance $x \in [0, 4\pi]$, for different values of Weissenberg number (We), power law index (n), Hartmann number (M), ion-slip parameter (α_i) and Hall parameter (α_e). Fig. (7.8) illustrates the influence of We on dp/dx. The Fig. depicts that an increase in We enhances the dp/dx in the narrow part of the channel. Effect of power law index (n) on dp/dx is presented in Fig. (7.9). The plot reveals that the dp/dx rises in the narrow part for larger values of n. Fig. (7.10) is displayed for the influence of Hartmann number (M) on dp/dx. Here pressure gradient increases when M is increased. Figs. (7.11) and (7.12) illustrate that effects of α_i and α_e on dp/dx are qualitatively similar. These Figs. indicate that the magnitude of dp/dx in the narrow part of the channel decreases when ion-slip (α_i) and Hall (α_e) parameters are increased. Moreover effect of M on dp/dx is quite opposite to the effects of α_i and α_e.
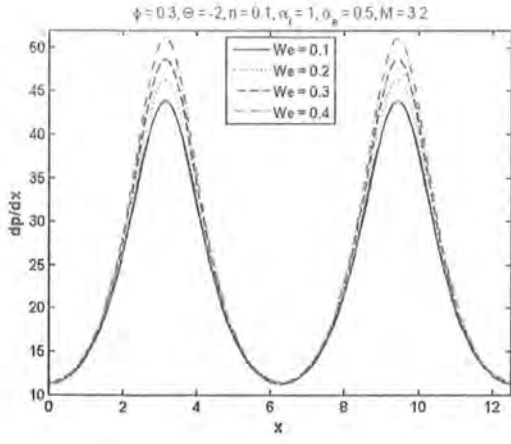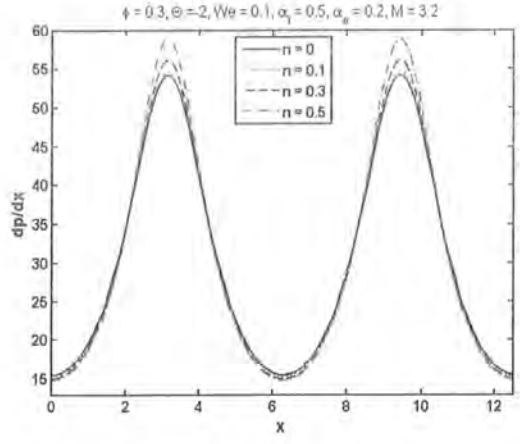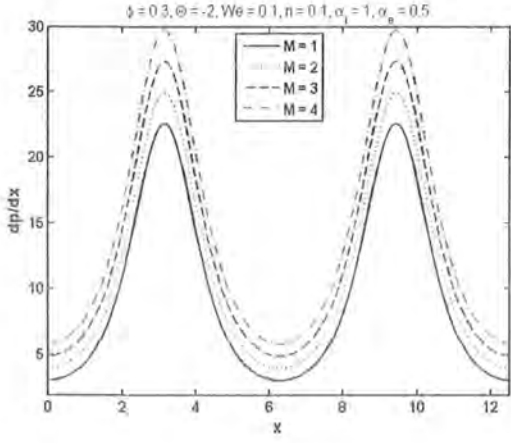
Fig. 7.8

Fig. 7.9

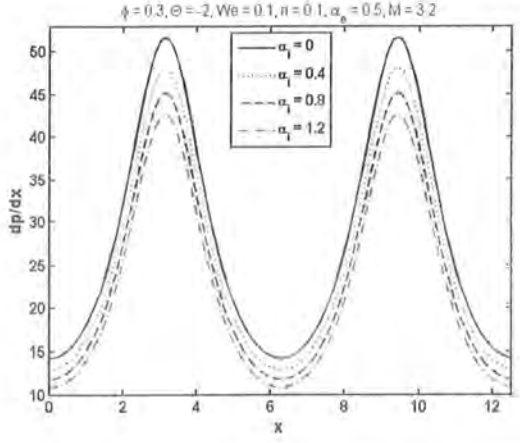Fig. 7.10

Fig. 7.11

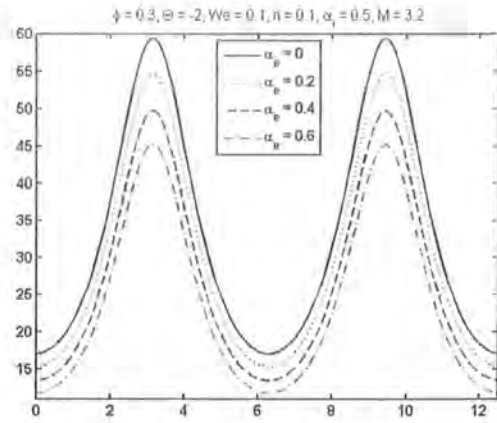$\phi = 0.3, \Theta = -2, We = 0.1, n = 0.1, \alpha_i = 0.5, M = 3.2$

Fig. 7.12

Figs. (7.8 - 7.12): Plots for pressure gradient for different values of Weissenberg number (We), fluid parameter (n), Hartmann number (M), ion-slip parameter (α_i) and Hall parameter (α_e).

Plots in Figs. (7.13 − 7.17) are made to analyze the variation in dimensionless pressure drop (ΔP_λ) versus the time-average flux Θ for different values of parameters We, n, M, α_i and α_e. All of these graphs are sectored such as the upper right hand quadrant (I) for $\theta > 0$ and $\Delta P_\lambda > 0$ denotes the pumping region and the region where $\Delta P_\lambda = 0$ is the free pumping region. Quadrant (II) where $\theta > 0$ and $\Delta P_\lambda < 0$ is designated as augmented pumping region and quadrant (IV) when $\theta < 0$ and $\Delta P_\lambda > 0$ as retrograde or backward pumping where the flow is opposite to the peristaltic motion. Fig. (7.13) discloses that an increase in the Weissenberg number (We) intensify the pressure rise. Furthermore for $We = 0$ corresponds to viscous case and has a linear relation between pressure rise (ΔP_λ) and flow rate (Θ). However non- linear relation is observed for $We > 0$. Fig. (7.14) is prepared to illustrate the effect of power law index (n) on pressure rise. We notice that ΔP_λ drops with an increase in n in the peristaltic pumping region. Fig. (7.15) presents the variation of ΔP_λ against Θ for different values of Hartmann number (M). It is found that when M is increased it enhances the pressure rise in the peristaltic pumping region while ΔP_λ decreases in the augmented pumping region. Also

103

the free pumping region decreases for increasing values of Hartmann number (M). To notice the effects of α_i and α_e on pressure rise (ΔP_λ) we prepared Figs. (7.16) and (7.17). These Figs. depict that by magnifying α_i and α_e the pressure rise decreases in the peristaltic pumping region. The free pumping region increases by increasing ion-slip and Hall parameters. The co-pumping region increases for increasing values of α_i and α_e. Furthermore $\alpha_e = 0$ in Fig. (7.17) corresponds to the case when Hall and ion-slip effects are absent. For $\alpha_e = 0$ the pressure rise enhances but the magnitude of ΔP_λ decreases in the presence of Hall and ion-slip parameters.
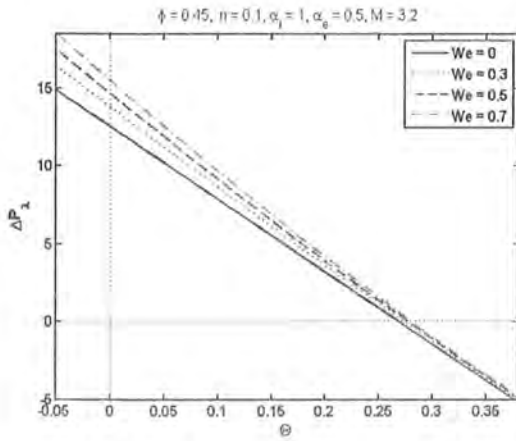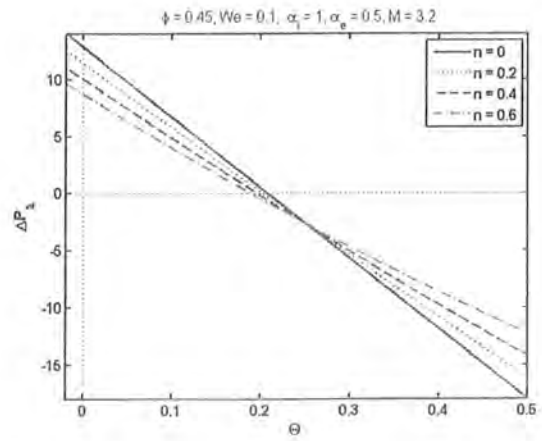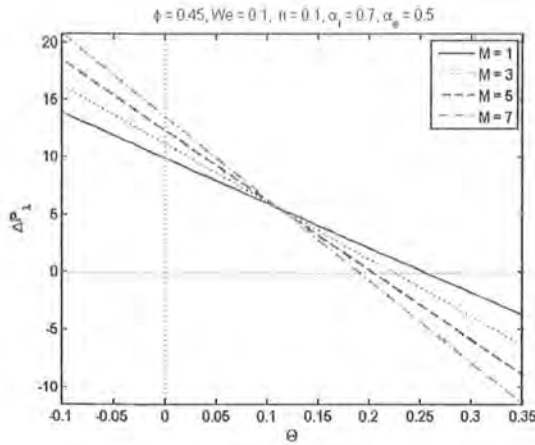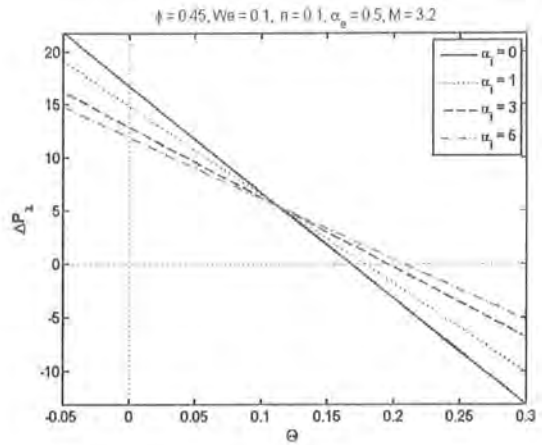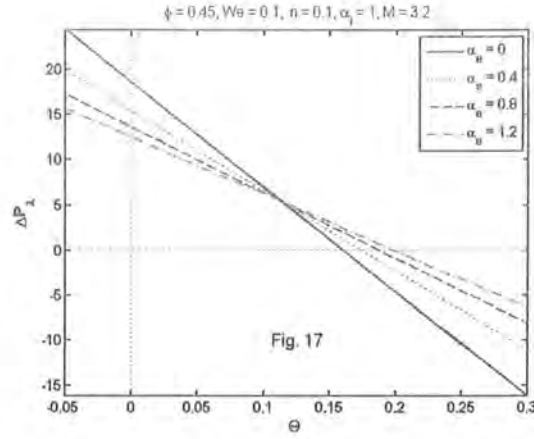

Fig. 7.13

Fig. 7.14

Fig. 7.15

Fig. 7.16

104

Fig. 7.17

Figs. (7.13 - 7.17): Plots for pressure rise for different values of Weissenberg number (We), fluid parameter (n), Hartmann number (M), ion-slip parameter (α_i) and Hall parameter (α_e).

7.3.4 Trapping

Fig. $(7.18 - 7.22)$ are displayed for the effects of Weissenberg number (We), power law index (n), Hartmann number (M), ion-slip parameter (α_i) and Hall parameter (α_e) on the trapping. In Figs. (7.18) and (7.19) the bolus size reduces in the upper part of the channel whereas it increases in the lower part of the channel when We and n are increased. Influence of Hartmann number on trapping is revealed in Fig. (7.20). It is noted that by increasing M the bolus size decreases and it vanishes for large M. Effects of parameters α_i and α_e on trapping are illustrated in Figs. (7.21) and (7.22). These plots depict that increasing values of α_i and α_e result in an increase in the size of bolus.

105

(a) $We = 0.1$

(b) $We = 0.4$
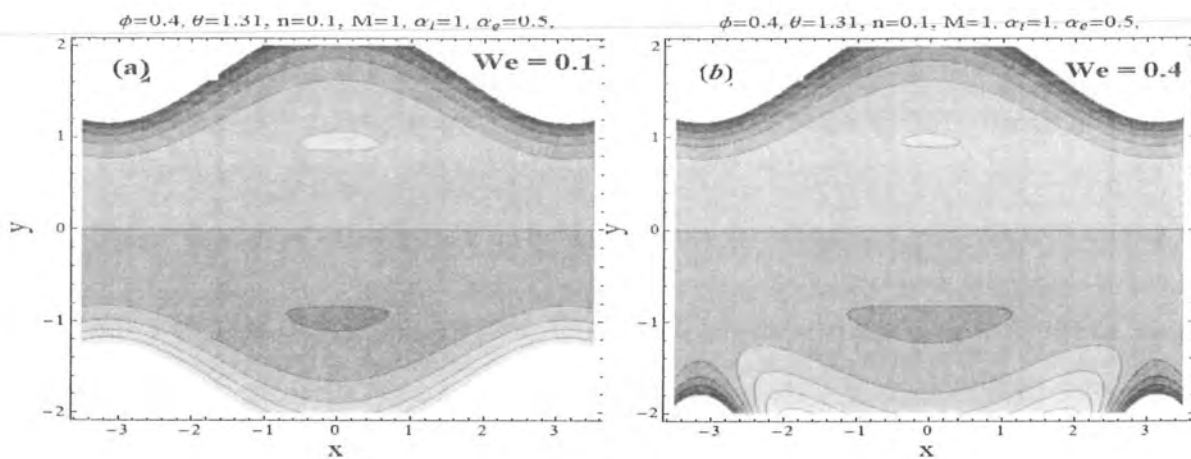
Fig. 7.18

Fig. 7.18 (a-b): Plots of $\Psi(x,y)$ for Weissenberg number (We).

(a) $n = 0$

(b) $n = 0.3$

Fig. 7.19

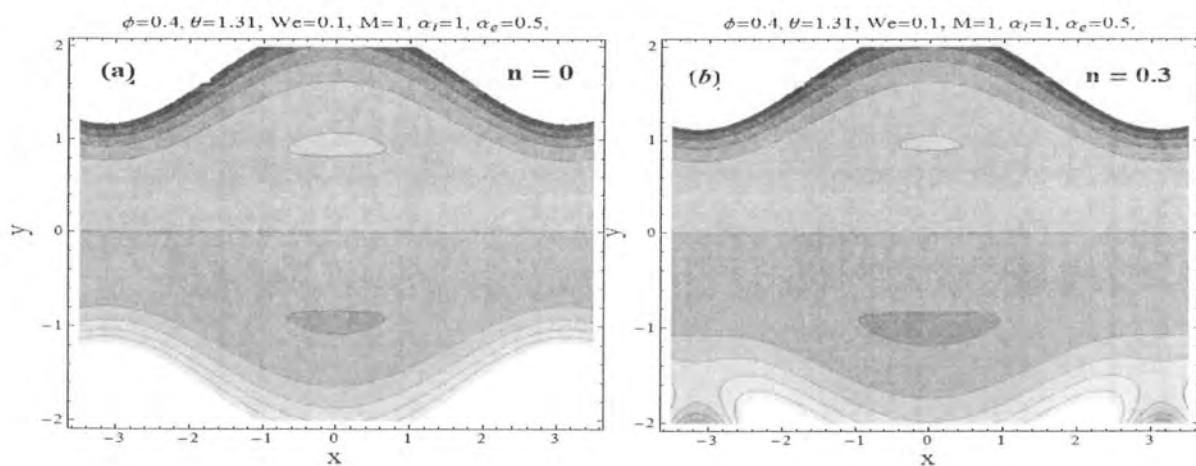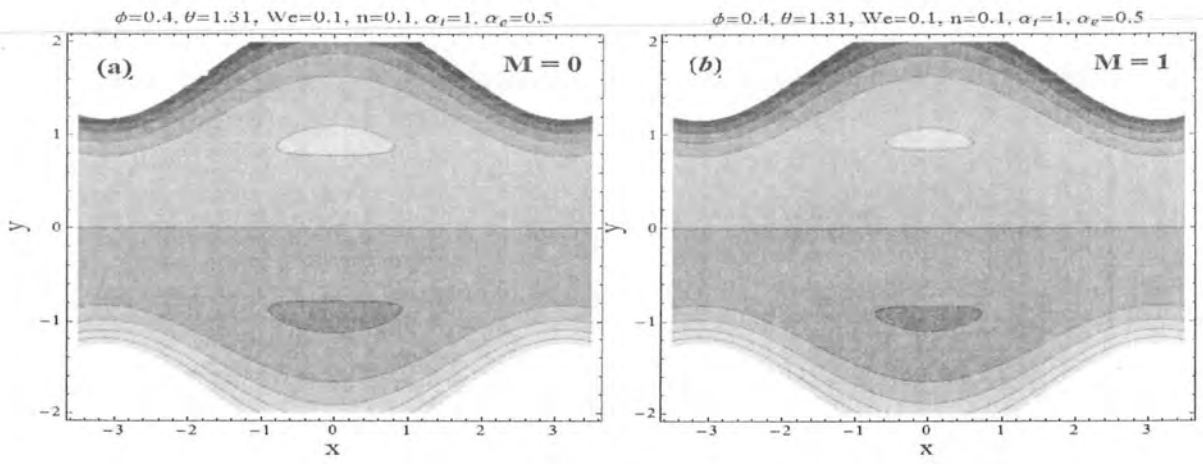Fig. 7.19 (a-b): Plots of $\Psi(x,y)$ for fluid parameter (n).

Fig. 7.20

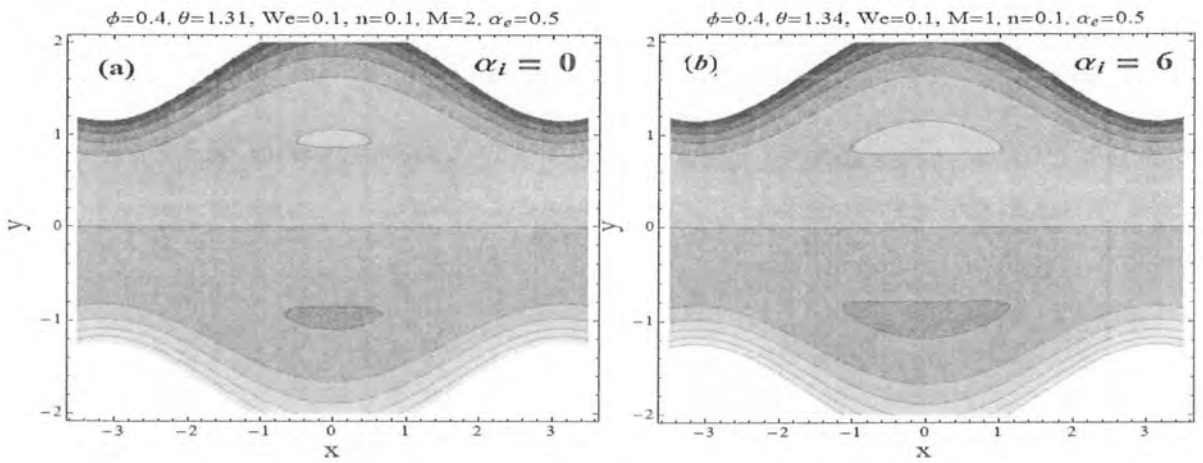Fig. 7.20 (a-b): Plots of $\Psi(x, y)$ for Hartmann number (M).

Fig. 7.21

Fig. 7.21 (a-b): Plots of $\Psi(x, y)$ for ion-slip parameter (α_i).
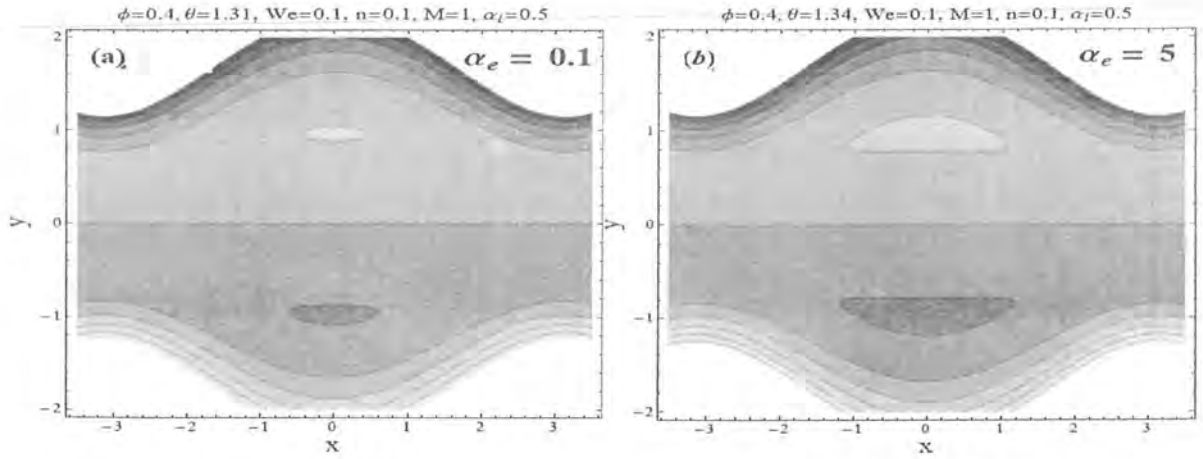
Fig. 7.22 (a-b): Plots of $\Psi(x,y)$ for Hall parameter (α_e).

7.4 Conclusions

In this study we examined the peristaltic transport of hyperbolic tangent fluid under the influence of Hall and ion-slip effects. The governing equations are first modeled and then solved by employing long wavelength and low Reynolds number approximations. Expressions for stream function and axial pressure gradient are obtained up to first order in We by using perturbation technique. Expression for pressure rise per wavelength is obtained through numerical integration. The key findings of the analysis are summarized as follows:

- The longitudinal velocity gives reverse behavior at the centre line and near the walls. Moreover velocity distribution is an increasing function of α_e and α_i. Whereas velocity decreases for increasing values of M at the center of channel.

- The magnitude of shear stress increases when the values of We and M are increased. However increase in α_e and α_i decreases the magnitude of shear stress.

- By increasing We, M and n pressure gradient intensify in the narrow part of the channel, while increasing α_e and α_i reduces the pressure gradient.

- We and M have opposite effects on pressure rise when compared with n, α_e and α_i.

- Due to an increase in We and n the size of the trapped bolus reduces in the upper half of the channel whereas it increases in the lower half of the channel.

- In the presence of α_e and α_i the size of the bolus increases. While opposite behavior is noted for magnetic parameter M.

Chapter 8

Influence of Joule heating in peristaltic flow of Williamson fluid with Hall and ion-slip effects

The objective of present chapter is to discuss the influences of Hall and ion-slip effects on peristaltic flow of non-Newtonian fluid in a symmetric channel. Viscous dissipation and Joule heating effects are also considered. The flow analysis is carried out in a frame moving with the velocity of the wave. Low Reynolds number and long wavelength approximations are adopted in the mathematical formulation. Series solutions for stream function, pressure gradient and temperature profile are constructed for small values of Weissenberg number (We). Variations of emerging physical parameters on the axial velocity, shear stress, pressure gradient and temperature are analyzed graphically. Pumping and trapping phenomena are also addressed.

8.1 Mathematical formulation

We investigate the magnetohydrodynamic (MHD) flow of an incompressible Williamson fluid in an infinite two-dimensional symmetric channel of width $2d$. A sinusoidal wave of small amplitude propagates along the channel walls with a constant speed c. The Cartesian coordinate system is chosen in such a way that $\overline{X}$-axis lies along the central line of the channel and $\overline{Y}$-axis normal to it. The fluid is electrically conducting under the application of a transverse uniform magnetic

field $(0, 0, \mathbf{B}_0)$. The induced magnetic field is neglected for small magnetic Reynolds number.

The geometry of walls satisfies the following expression:

$$\overline{H}\left(\overline{X}, \bar{t}\right) = d + b\cos\frac{2\pi}{\lambda}\left(\overline{X} - c\bar{t}\right),\tag{8.1}$$

in which b represents the wave amplitude, λ the wavelength and $\bar{t}$ the time.

The fundamental equations for the balances of mass, linear momentum and energy equation in the presence of viscous dissipation and Joule heating effects are expressed by the relations:

$$\boldsymbol{\nabla}\cdot\overline{\mathbf{V}} = 0,\tag{8.2}$$

$$\rho_f\frac{d\overline{\mathbf{V}}}{d\bar{t}} = -\mathrm{grad}\overline{P} - \boldsymbol{\nabla}\cdot\overline{\mathbf{S}} + \mathbf{J}\times\mathbf{B},\tag{8.3}$$

$$\rho_f\tilde{c}_p\frac{d\overline{T}}{d\bar{t}} = k\nabla^2\overline{T} + \overline{\mathbf{S}}\cdot\boldsymbol{\nabla}\overline{\mathbf{V}} + \frac{\mathbf{J}\cdot\mathbf{J}}{\sigma},\tag{8.4}$$

$$\mathbf{J} = \sigma(\mathbf{E} + \overline{\mathbf{V}}\times\mathbf{B}) - \frac{\alpha_e}{B_0}\left(\mathbf{J}\times\mathbf{B}\right) + \frac{\alpha_e\alpha_i}{B_0^2}[(\mathbf{J}\times\mathbf{B})\times\mathbf{B}],\tag{8.5}$$

$$\overline{\mathbf{V}} = \left(\overline{U}(\overline{X}, \overline{Y}, \bar{t}), \overline{V}(\overline{X}, \overline{Y}, \bar{t}), 0\right),\ \nabla^2 = \frac{\partial^2}{\partial\overline{X}^2} + \frac{\partial^2}{\partial\overline{Y}^2},\tag{8.6}$$

where $d/d\bar{t}$ signifies the material derivative, ρ_f the density, $\overline{\mathbf{V}}$ the velocity, $\overline{P}$ the pressure, $\overline{\mathbf{S}}$ the extra stress tensor, $\tilde{c}_p$ the specific heat, $\overline{T}$ the temperature, k the thermal conductivity, $\mathbf{J}$ the current density, σ the electrical conductivity, $\mathbf{B}$ the applied magnetic field, α_e and α_i are the Hall and ion-slip parameters.

Expression of stress tensor $\overline{\mathbf{S}}$ for Williamson fluid is given by

$$\overline{\mathbf{S}} = -[\eta_\infty + (\eta_0 - \eta_\infty)(1 - \hat{\Gamma}\bar{\gamma})^{-1}]\overline{\mathbf{A}}_1,\tag{8.7}$$

$$\overline{\mathbf{A}}_1 = \left(\mathrm{grad}\,\overline{\mathbf{V}}\right) + \left(\mathrm{grad}\,\overline{\mathbf{V}}\right)^\top,\tag{8.8}$$

$$\bar{\gamma} = \sqrt{\frac{1}{2}tr\left(\overline{\mathbf{A}}_1\right)^2}.\tag{8.9}$$

Here $\top$ represents the matrix transpose, η_∞ the infinite shear rate viscosity, η_0 the zero shear rate viscosity, $\hat{\Gamma}$ the time constant and $\overline{\mathbf{A}}_1$ the first Rivlin–Ericksen tensor. Note that when $\Gamma = 0$ Eq. (8.7) reduces to a viscous fluid. Under the assumptions of $\eta_\infty = 0$ and $\hat{\Gamma}\bar{\gamma} < 1$, Eq.

111

(8.7) reduces to

$$\overline{\mathbf{S}} = -\eta_0[1 + \Gamma\overline{\dot{\gamma}}]\overline{\mathbf{A}}_1. \tag{8.10}$$

There is no applied voltage therefore $\mathbf{E} = \mathbf{0}$ and with the use of Eq. (8.5) we have

$$\mathbf{J} \times \mathbf{B} = -\frac{\sigma B_0^2}{((1 + \alpha_e\alpha_i)^2 + (\alpha_e)^2)}\left[\left((1 + \alpha_e\alpha_i)\overline{U} - \alpha_e\overline{V}\right), \ \left((1 + \alpha_e\alpha_i)\overline{V} + \alpha_e\overline{U}\right), \ 0\right]. \tag{8.11}$$

Using Eqs. (8.6), (8.10) and (8.11) in Eqs. (8.2 - 8.4) the continuity, linear momentum and energy equations take the forms:

$$\frac{\partial\overline{U}}{\partial\overline{X}} + \frac{\partial\overline{V}}{\partial\overline{Y}} = 0, \tag{8.12}$$

$$\rho_f\left(\frac{\partial}{\partial\overline{t}} + \overline{U}\frac{\partial}{\partial\overline{X}} + \overline{V}\frac{\partial}{\partial\overline{Y}}\right)\overline{U} = -\frac{\partial\overline{p}}{\partial\overline{X}} + \frac{\overline{S}_{\overline{XX}}}{\partial\overline{X}} + \frac{\overline{S}_{\overline{XY}}}{\partial\overline{Y}}$$
$$-\frac{\sigma B_0^2}{((1 + \alpha_e\alpha_i)^2 + (\alpha_e)^2)}\left[(1 + \alpha_e\alpha_i)\overline{U} - \alpha_e\overline{V}\right], \tag{8.13}$$

$$\rho_f\left(\frac{\partial}{\partial\overline{t}} + \overline{U}\frac{\partial}{\partial\overline{X}} + \overline{V}\frac{\partial}{\partial\overline{Y}}\right)\overline{V} = -\frac{\partial\overline{p}}{\partial\overline{Y}} + \frac{\overline{S}_{\overline{YX}}}{\partial\overline{X}} + \frac{\overline{S}_{\overline{YY}}}{\partial\overline{Y}}$$
$$-\frac{\sigma B_0^2}{((1 + \alpha_e\alpha_i)^2 + (\alpha_e)^2)}\left[(1 + \alpha_e\alpha_i)\overline{V} + \alpha_e\overline{U}\right], \tag{8.14}$$

$$\overline{S}_{\overline{XX}} = -2\eta_0[1 + \hat{\Gamma}\overline{\dot{\gamma}}]\frac{\partial\overline{U}}{\partial\overline{X}}, \tag{8.15}$$

$$\overline{S}_{\overline{XY}} = -\eta_0[1 + \hat{\Gamma}\overline{\dot{\gamma}}]\left(\frac{\partial\overline{U}}{\partial\overline{Y}} + \frac{\partial\overline{V}}{\partial\overline{X}}\right), \tag{8.16}$$

$$\overline{S}_{\overline{YY}} = -2\eta_0[1 + \hat{\Gamma}\overline{\dot{\gamma}}]\frac{\partial\overline{V}}{\partial\overline{Y}}, \tag{8.17}$$

$$(\overline{\dot{\gamma}})^2 = 2\left(\frac{\partial\overline{U}}{\partial\overline{X}}\right)^2 + \left(\frac{\partial\overline{U}}{\partial\overline{Y}} + \frac{\partial\overline{V}}{\partial\overline{X}}\right)^2 + 2\left(\frac{\partial\overline{V}}{\partial\overline{Y}}\right)^2, \tag{8.18}$$

$$\rho\tilde{c}_p\left(\frac{\partial}{\partial\overline{t}} + \overline{U}\frac{\partial}{\partial\overline{X}} + \overline{V}\frac{\partial}{\partial\overline{Y}}\right)\overline{T} = k\left(\frac{\partial^2\overline{T}}{\partial\overline{X}^2} + \frac{\partial^2\overline{T}}{\partial\overline{Y}^2}\right) + \overline{S}_{\overline{XX}}\frac{\partial\overline{U}}{\partial\overline{X}} + \overline{S}_{\overline{XY}}\left(\frac{\partial\overline{U}}{\partial\overline{Y}} + \frac{\partial\overline{V}}{\partial\overline{X}}\right)$$
$$+\overline{S}_{\overline{YY}}\frac{\partial\overline{V}}{\partial\overline{Y}} + \frac{N}{A}\left(\overline{U}^2 + \overline{V}^2\right). \tag{8.19}$$

Note that the flow is unsteady in the fixed frame with coordinates $(\overline{X}, \overline{Y}, \overline{t})$. We now introducing a coordinate system $(\overline{x}, \overline{y})$ moving with the wave speed c in the positive $\overline{x}$ direction in which the boundary shape is stationary. The coordinates and velocities in the fixed and wave frames are related by the transformations:

$$\overline{x} = \overline{X} - c\overline{t}, \ \overline{y} = \overline{Y}, \ \overline{u} = \overline{U} - c, \ \overline{v} = \overline{V}, \ \overline{p}(\overline{x}, \overline{y}) = \overline{P}(\overline{X}, \overline{Y}, \overline{t})$$

Defining dimensionless variables by

$$
\begin{aligned}
x &= \frac{2\pi\overline{x}}{\lambda}, \ y = \frac{\overline{y}}{d}, \ u = \frac{\overline{u}}{c}, \ v = \frac{\overline{v}}{c}, \ h = \frac{\overline{h}}{d}, \ p = \frac{d^2}{\lambda\eta_0 c}\overline{p}, \ S = \frac{d}{\eta_0 c}\overline{S}, \ \dot{\gamma} = \frac{\overline{\dot{\gamma}}d}{c}, \\
M &= \sqrt{\frac{\sigma}{\eta_0}}B_0 d, \ \mathrm{Re} = \frac{\rho_f dc}{\eta_0}, \ \theta = \frac{\overline{T} - T_0}{T_1 - T_0}, \ \delta = \frac{2\pi d}{\lambda}, \ We = \frac{\Gamma c}{d}, \\
N &= \frac{M^2 \tilde{A}}{(\alpha_e)^2 + (A)^2}, \ \tilde{A} = 1 + \alpha_e \alpha_i, \ \mathrm{Pr} = \frac{\eta_0 \tilde{c}_p}{k}, \ Ec = \frac{c^2}{\tilde{c}_p(T_1 - T_0)},
\end{aligned}
\tag{8.20}
$$

the flow Eqs. (8.13 - 8.19) in terms of stream function Ψ $\left(u = \dfrac{\partial\Psi}{\partial y}, v = -\delta\dfrac{\partial\Psi}{\partial x}\right)$ under the assumptions of long wavelength and low Reynolds number approximations become

$$\frac{dp}{dx} = -\frac{\partial S_{xy}}{\partial y} - N\left(\frac{\partial\Psi}{\partial y} + 1\right), \tag{8.21}$$

$$S_{xy} = -(1 + We\ \dot{\gamma})\dot{\gamma}, \ \text{and} \ \dot{\gamma} = \frac{\partial^2\Psi}{\partial y^2}, \tag{8.22}$$

$$S_{xx} = S_{yy} = \frac{\partial p}{\partial y} = 0, \tag{8.23}$$

$$\frac{\partial^2\theta}{\partial y^2} + \mathrm{Pr}\ Ec\left[(S_{xy}\ \dot{\gamma}) + \frac{N}{A}\left(\frac{\partial\Psi}{\partial y} + 1\right)^2\right] = 0. \tag{8.24}$$

The continuity equation (8.12) is identically satisfied. Moreover M, Re, δ, We, Pr and Ec denote respectively the Hartman, Reynolds, wave, Weissenberg, Prandtl and Eckert numbers. Eq. (8.24) implies that $p \neq p(y)$ therefore $p = p(x)$ only and $\dfrac{\partial p}{\partial x} = \dfrac{dp}{dx}$. To eliminate pressure we cross differentiate Eqs (8.22) and (8.24) and obtained the following expression

$$\frac{\partial^2}{\partial y^2}\left[\left(1 + We\ \frac{\partial^2\Psi}{\partial y^2}\right)\frac{\partial^2\Psi}{\partial y^2}\right] - N\frac{\partial^2\Psi}{\partial y^2} = 0. \tag{8.25}$$

113

The non-dimensional shape of the peristaltic wall $h(x)$ is given by

$$h(x) = 1 + \phi \, \cos x, \tag{8.26}$$

in which $\phi = (b/d)$ is the amplitude ratio and $(0 < \phi < 1)$. The relevant dimensionless boundary conditions in wave frame are:

$$\Psi = 0, \qquad \frac{\partial^2 \Psi}{\partial y^2} = 0, \qquad \theta = 0, \qquad at \ y = 0, \tag{8.27}$$

$$\frac{\partial \Psi}{\partial y} = -1, \qquad \Psi = F, \qquad \theta = 1, \qquad at \ y = h, \tag{8.28}$$

where

$$F = \int_0^h \frac{\partial \Psi}{\partial y} dy = \Psi(h) - \Psi(0). \tag{8.29}$$

The non-dimensional pressure rise per wavelength $(\triangle P_\lambda)$ and heat transfer coefficient Z are

$$\triangle P_\lambda = \int_0^{2\pi} \frac{dp}{dx} dx, \tag{8.30}$$

$$Z = \left[\frac{\partial h}{\partial x} \left(\left. \frac{\partial \theta}{\partial y} \right|_{y=h} \right) \right]. \tag{8.31}$$

8.2   Series solutions

The governing equations are highly non-linear and exact solutions of these equations seem difficult to compute. Therefore we are interested in calculating the series solutions and express the flow quantities in a series of the small parameter We as follows:

$$\Psi = \Psi_0 + We \ \Psi_1 + We^2 \ \Psi_2 + O(We^3), \tag{8.32}$$

$$F = F_0 + We \ F_1 + We^2 \ F_2 + O(We^3), \tag{8.33}$$

$$p = p_0 + We \ p_1 + We^2 \ p_2 + O(We^3). \tag{8.34}$$

Using Eqs. (8.33) - (8.35) in the Eqs. (8.22), (8.25), (8.26), (8.28) and (8.29) and then solving the resulting zeroth, first and second order systems, we get the solution expressions for the

114

stream function (Ψ), pressure gradient (dp/dx) and temperature (θ) as follows:

$$
\begin{aligned}
\Psi &= 1/3N(3N(C_3 + C_4 y + We(C_7 + C_{11}We + C_8 y + C_{12}Wey)) + (3(C_2 \\
&\quad + We(C_5 + C_6 + (C_9 + C_{10})We)) + 12C_1^2 C_2 We^2(-5 + 2\sqrt{N}y) \\
&\quad + C_1(3 - 2C_2^2 We^2(5 + 2\sqrt{N}y)))\cosh[\sqrt{N}y] - We(C_1^2 + C_2^2 + 2(C_1 C_5 \\
&\quad + C_2 C_6)We)\cosh[2\sqrt{N}y] + (C_1^3 + C_2^3)We^2\cosh[3\sqrt{N}y] + 3(3C_1 \\
&\quad - 10(C_1^2 C_2 - C_1 C_2^2)We^2 + 3C_9 We^2 - 3(C_2 + We(C_6 - C_5 + C_{10})We)) \\
&\quad + 4C_1 C_2(C_1 + C_2)\sqrt{N}We^2 y)\sinh[\sqrt{N}y] + We(C_2^2 - C_1^2 - 2(C_1 C_5 \\
&\quad - C_2 C_6)We\sinh[2\sqrt{N}y] + (C_1^3 - C_2^3)We^2\sinh[3\sqrt{N}y]),
\end{aligned}
\tag{8.35}
$$

$$
dp/dx = -N((1 + C_4) + C_8 We + C_{12}We^2), \tag{8.36}
$$

$$
\begin{aligned}
\theta &= -1/2700AN(675(-4AC_{13}N - 4AC_{14}Ny - 4C_1 C_2 N Ec\Pr y^2 + 4C_4 N^2 Ec\Pr y^2 \\
&\quad + 2C_4^2 N^2 Ec\Pr y^2 + 8(C_1 - C_2)(1 + C_4)Ec\sqrt{N}\Pr\cosh[\sqrt{N}y] + (C_1^2 \\
&\quad + C_2^2)Ec\Pr\cosh[2\sqrt{N}y] + 8C_1 Ec\sqrt{N}\Pr\sinh[\sqrt{N}y] + C_1^2 Ec\Pr\sinh[2\sqrt{N}y] \\
&\quad - C_2^2 Ec\Pr\sinh[2\sqrt{N}y]) + 2Ec\Pr We(-1350C_2 C_5 Ny^2 + 900(15AC_1^3 C_2^2 \\
&\quad + C_1^2 C_2(-2 + 15AC_2^2) + 6Ec\Pr We^2(-1750C_3 C_7 Ny^2 + 350(15AC_2^3 C_1^3 \\
&\quad + 4C_1 C_2(C_1 - C_2)\sqrt{N}Wey)\sinh[3\sqrt{N}y] + We(5 + 2\sqrt{N}y)))\cosh[3\sqrt{N}y])), \quad (8.37)
\end{aligned}
$$

where the values of $C_l(l = 1 - 14)$ can be calculated through algebraic computations easily.

8.3 Graphical analysis and discussion

This section interprets the graphical results in order to analyze the quantitative effects of Hall parameter (α_e), ion-slip parameter (α_i), Wessienberg number (We), Hartman number (M), Prandtl number ($\Pr$) and Eckert number (Ec) on pressure rise (ΔP_λ), pressure gradient (dp/dx), shear stress (S_{xy}), axial velocity (u), temperature (θ) and trapping.

8.3.1 Pumping analysis

This subsection analyzes the variation in dimensionless pressure drop (ΔP_λ) versus the time-average flux Θ and pressure gradient (dp/dx) against the axial distance $x \in [0, 2\pi]$ for different values of parameters M, We, α_e and α_i and are represented through figs. $(8.1 - 8.8)$. Fig. (8.1) discloses that larger M intensify the pressure rise in the peristaltic pumping region but after a critical value of Θ that is $\Theta = 0.08$ the pressure rise decreases when M is increased. However the behavior remains the same in the free and augmented pumping regions. Influence of We on ΔP_λ is shown in Fig. (8.2). It depicts that by increasing We the pumping rate increases only in the augmented pumping region. Figs. (8.3) and (8.4) are prepared to illustrate the effects of α_e and α_i on pressure rise (ΔP_λ). These Figs. reveal that by increasing α_e and α_i the pumping rate decreases in the peristaltic pumping region. However after $\Theta = 0.08$ the pressure drop increases in free and co-pumping regions for increasing values of α_e and α_i. Moreover the pressure rise is maximum for the case when $\alpha_e = 0$. Fig. (8.5) illustrates the influence of M on dp/dx. This Fig. depicts that an increase in M enhances the magnitude of pressure gradient. Effect of We on dp/dx is presented in Fig. (8.6). The plot reveals that the magnitude of pressure gradient decreases in the narrow part of channel for larger values of We. Figs. (8.7) and (8.8) are displayed for the influences of α_e and α_i on dp/dx. These Figs. indicate that the dp/dx decreases in magnitude when α_e and α_i are increased. Moreover impact of M on dp/dx is quite opposite to that of α_i and α_e. Moreover these plots reflect that in the wider part of the channel at $x = 0$ and $x = 2\pi$, dp/dx is comparatively small and the flow can easily pass without imposition of large pressure gradient. However in narrow part of channel at $x = \pi$ a much large pressure gradient is required to uphold the same flux to pass through it.
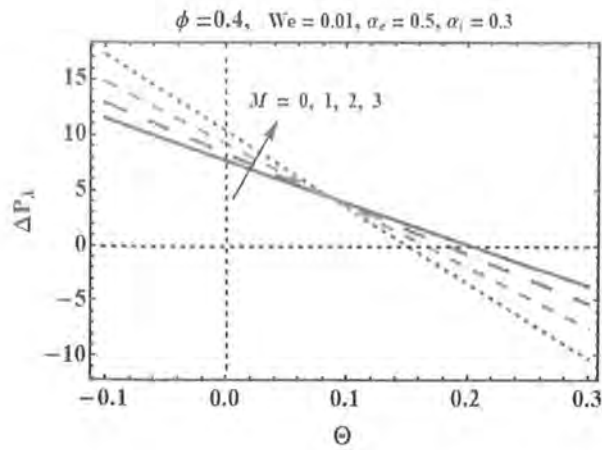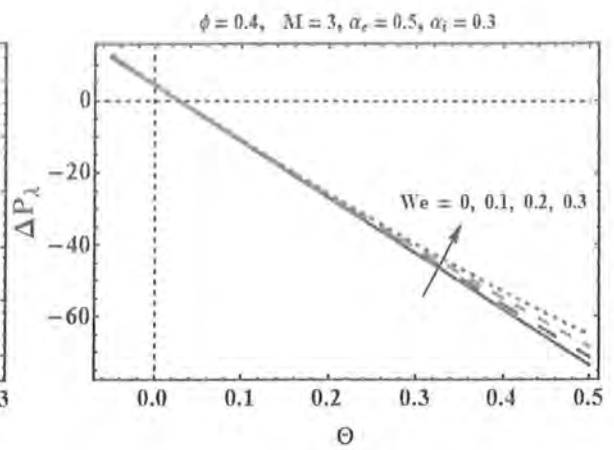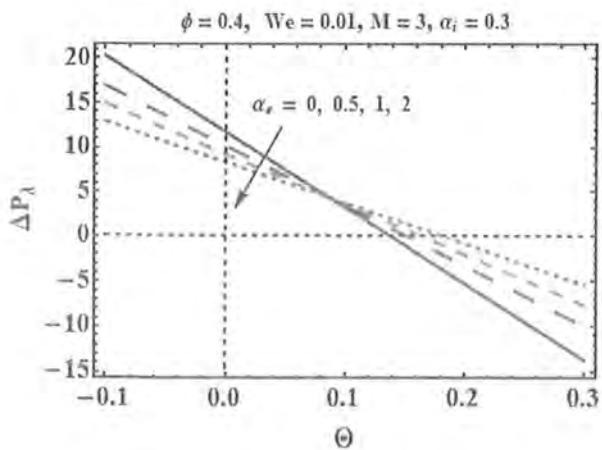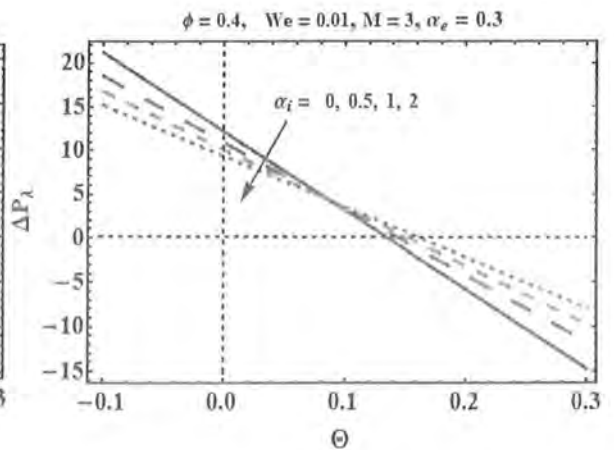
Fig. 8.1

Fig. 8.2

Fig. 8.3

Fig. 8.4

Figs. (8.1 - 8.4): Variation in pressure drop (ΔP_λ) versus average flow rate (Θ) for distinct values of Hartman number (M), Wessienberg number (We), Hall parameter (α_e) and ion-slip parameter (α_i).

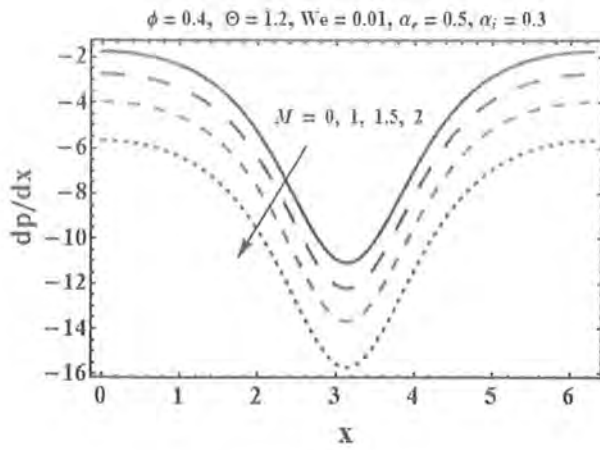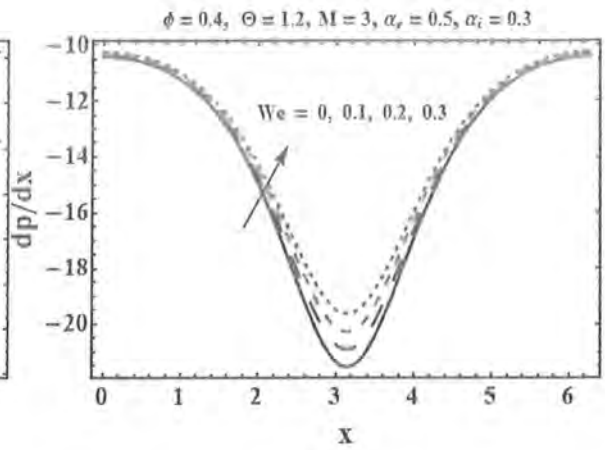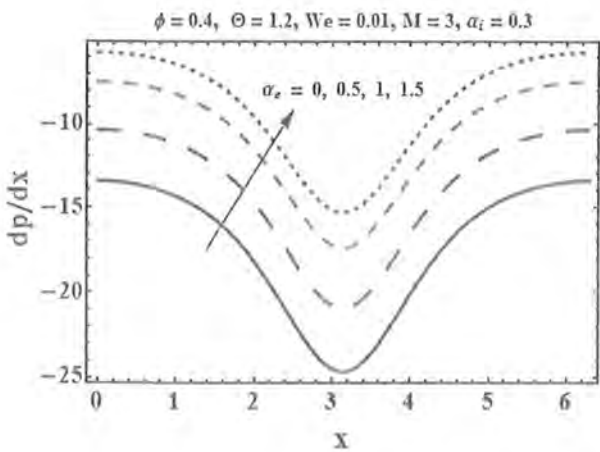$\phi = 0.4, \ \Theta = 1.2, \ We = 0.01, \ \alpha_e = 0.5, \ \alpha_i = 0.3$

$M = 0, \ 1, \ 1.5, \ 2$

Fig. 8.5

$\phi = 0.4, \ \Theta = 1.2, \ M = 3, \ \alpha_e = 0.5, \ \alpha_i = 0.3$

$We = 0, \ 0.1, \ 0.2, \ 0.3$

Fig. 8.6

$\phi = 0.4, \ \Theta = 1.2, \ We = 0.01, \ M = 3, \ \alpha_i = 0.3$

$\alpha_e = 0, \ 0.5, \ 1, \ 1.5$

Fig. 8.7

$\phi = 0.4, \ \Theta = 1.2, \ We = 0.01, \ M = 3, \ \alpha_e = 0.5$

$\alpha_i = 0, \ 0.5, \ 1, \ 2$
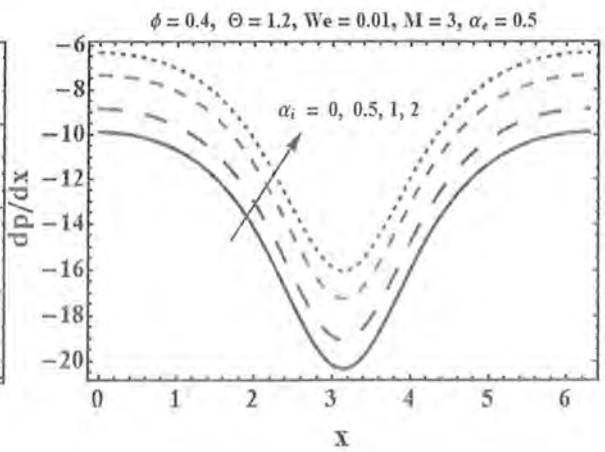
Fig. 8.8

Figs. (8.5 - 8.8): Variation in dp/dx versus axial distance (x) for distinct values of Hartman number (M), Wessienberg number (We), Hall parameter (α_e) and ion-slip parameter (α_i).

118

8.3.2 Shear stress at the upper wall

In Figs. $(8.9 - 8.12)$ the variations in shear stress (S_{xy}) against $x \in [0, 2\pi]$ have been portrayed for distinct values of flow parameters M, We, α_e and α_i. Fig. (8.9) illustrates that for large values of M the shear stress at the upper wall increases. However it is noted that from Figs. $(8.10 - 8.12)$ that the effects of We, α_e and α_i on shear stress are quite opposite to that of M. Here by increasing We, α_e and α_i the shear stress decreases.
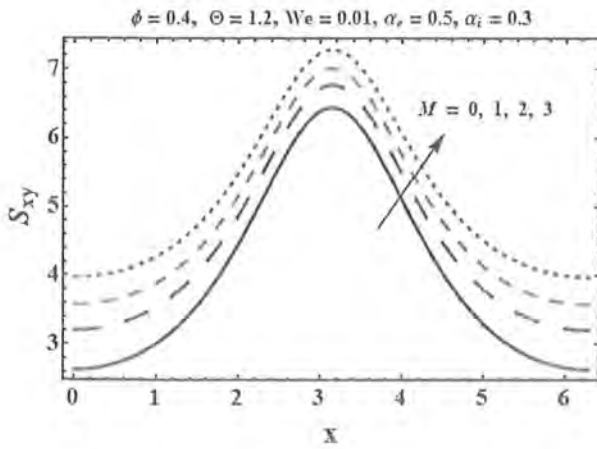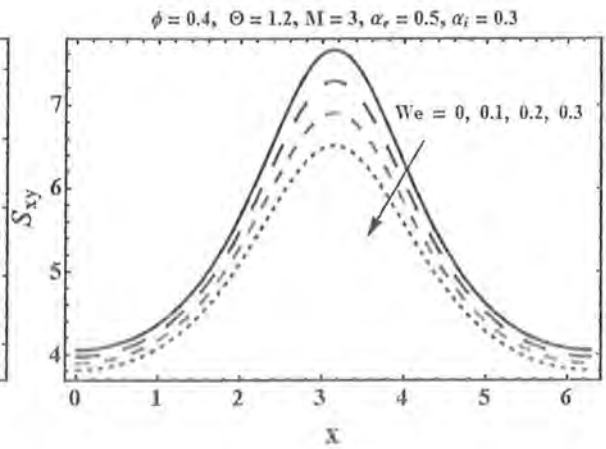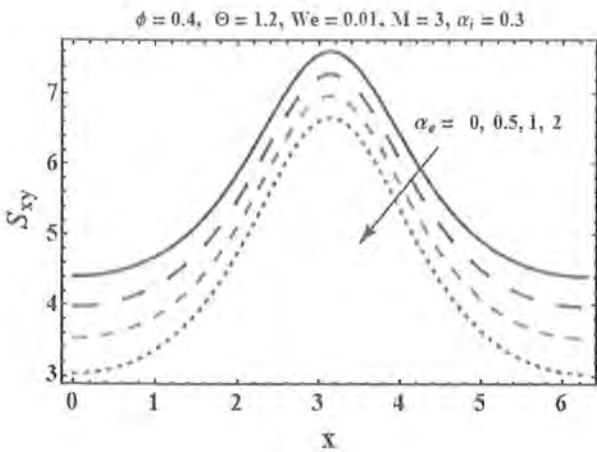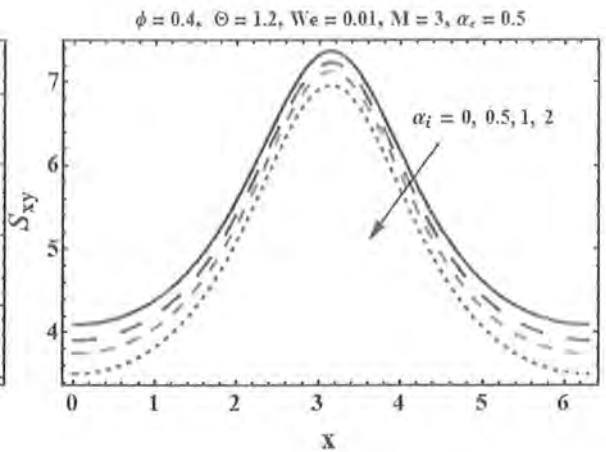

Fig. 8.9

Fig. 8.10

Fig. 8.11

Fig. 8.12

Figs. (8.9 - 8.12): Variation in shear stress (S_{xy}) against axial distance (x) for Hartman number (M), Wessienberg number (We), Hall parameter (α_e) and ion-slip parameter (α_i).

8.3.3   Velocity profile

In this subsection the Figs. (8.13 − 8.15) are prepared to see the influences of Hartman number (M), Hall parameter (α_e) and ion-slip parameter (α_i) on the velocity. It is found from these Figs. that the plots of velocity versus y are parabolic in nature and have opposite behavior near the walls when compared with center of the channel. impact of M on the velocity profile is presented in Fig. (8.13). The plot shows that by increasing M the velocity decreases near center of the channel. Physically larger M increases the magnitude of magnetic flux B_0 in transverse direction to the fluid flow which enhances the magnitude of Lorentz force and hence the velocity decreases. Figs. (8.14) and (8.15) show that the effects of α_e and α_i on the velocity are qualitatively similar. However their effects are opposite to that of M. These parameters assist the flow by reducing the magnitude of magnetic flux and consequently the velocity of fluid increases near the center of the channel by increasing each α_e and α_i.
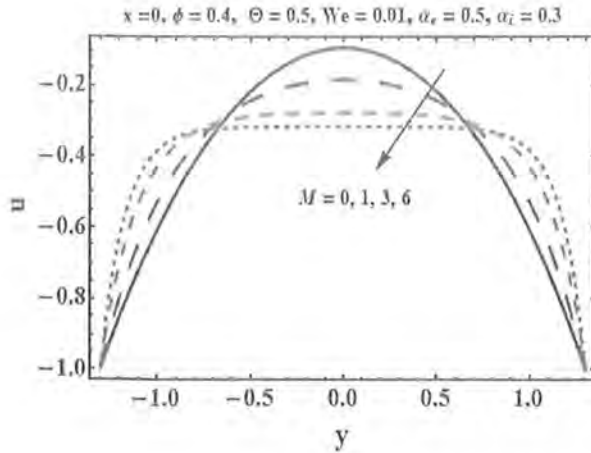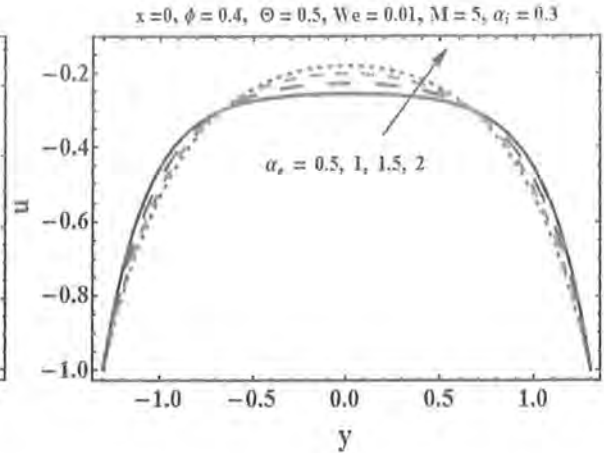

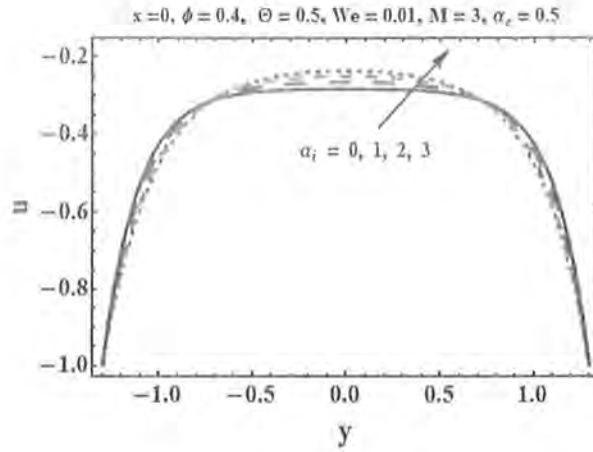Fig. 8.13   Fig. 8.14

Fig. 8.15

Figs. (8.13 - 8.15): Variation in longitudinal velocity (u) against (y) for Hartman number (M), Hall parameter (α_e) and ion-slip parameter (α_i).

8.3.4 Temperature profile

In this subsection the Figs. ($8.16 - 8.20$) are displayed in order to capture the impacts of M, α_e, α_i, Ec and Pr on temperature profile (θ) versus y. Fig. (8.16) is presented to see the influence of M on θ. It depicts that the temperature increases by increasing M. The velocity also decreases when M is increased due to which the friction between the fluid particles increases and hence the temperature rises. Effects of α_e and α_i on temperature are shown in the Figs. (8.17) and (8.18). These Figs. illustrate that the temperature is a decreasing function of both α_e and α_i. The consequences of an increase in Ec on temperature (θ) is visualized in Fig. (8.19). It is observed that an increase in Ec intensify the temperature profile. It is because of the the fact that with an increase in Eckert number the viscous dissipation increases and generates more heat. This leads to enhance the fluid temperature. Also $Ec = 0$ corresponds to the case in which viscous dissipation effects are absent. Similar effect is noted for the parameter Pr on temperature profile as shown in Fig. (8.20) where the temperature of the fluid increases for
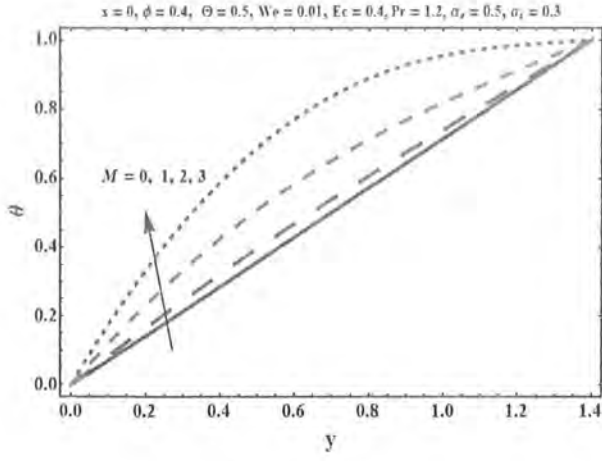
larger values of Pr due to the strong viscous dissipation effects.
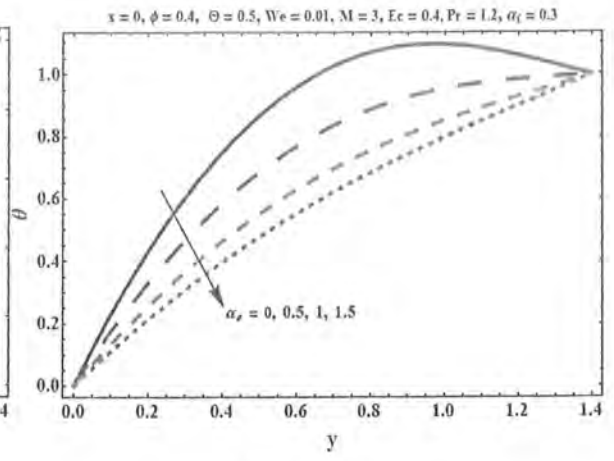

Fig. 8.16

Fig. 8.17

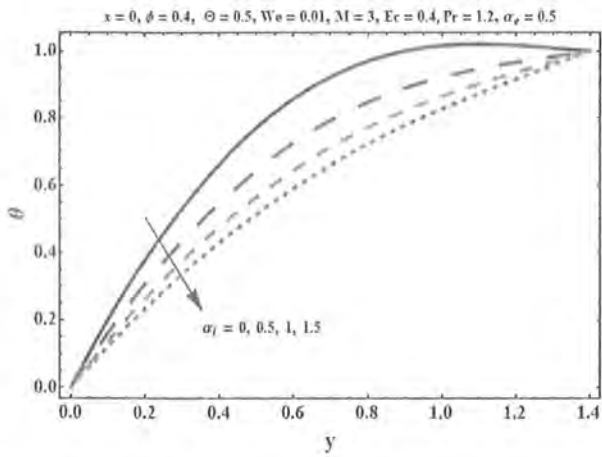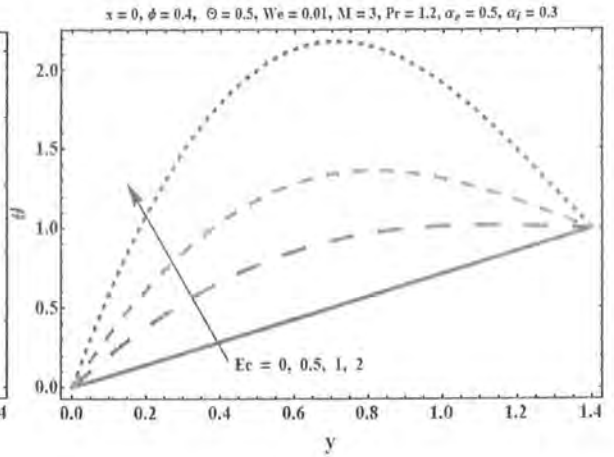

Fig. 8.18

Fig. 8.19
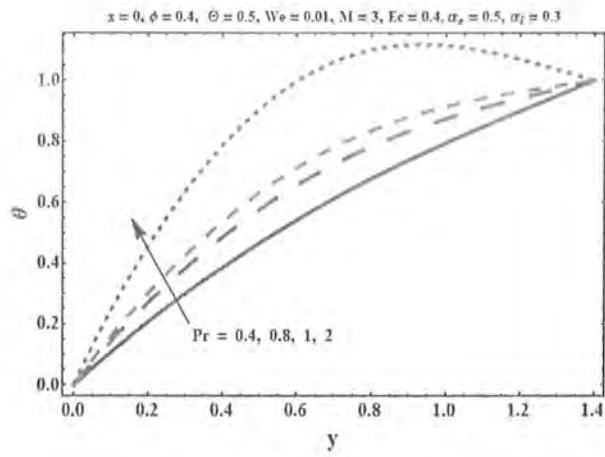
Fig. 8.20

Figs. (8.16 - 8.20): Variation in temperature (θ) against axial distance (x) for distinct values of Hartman number (M), Hall parameter (α_e), ion-slip parameter (α_i), Eckert number (Ec) and Prandtl number (Pr).

Figs. (8.21 − 8.26) are sketched to notice the effects of parameters M, α_e, α_i, We, $\Pr$ and Ec on heat transfer coefficient (Z). Figs. (8.21), (8.22), (8.25) and (8.26) indicate that the magnitude of heat transfer coefficient enhances when the values of parameters M, We, $\Pr$ and Ec are increased. However Figs. (8.23) and (8.24) depict that the magnitude of heat transfer coefficient decreases when α_e and α_i are increased.
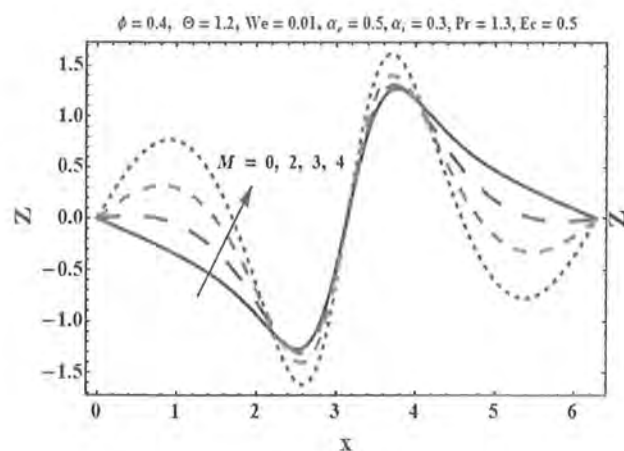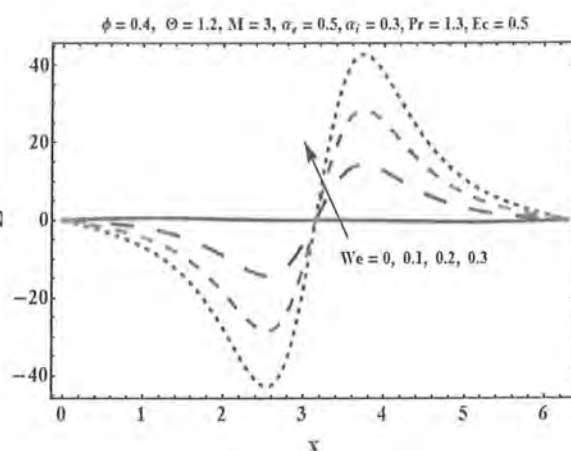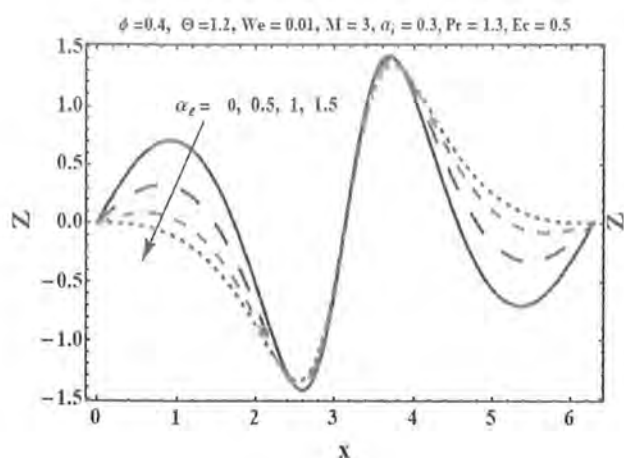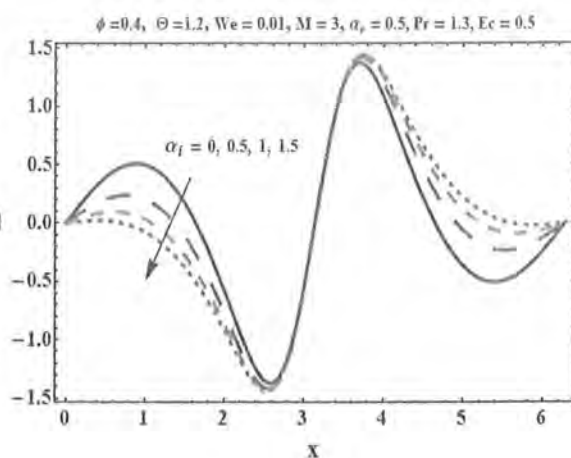

Fig. 8.21

Fig. 8.22

Fig. 8.23

Fig. 8.24

124

$\phi = 0.4, \ \Theta = 1.2, \ We = 0.01, \ M = 3, \ \alpha_e = 0.5, \ \alpha_i = 0.3, \ Ec = 0.5$

$Pr = 0.5, \ 1, \ 1.5, \ 2$

Fig. 8.25

$\phi = 0.4, \ \Theta = 1.2, \ We = 0.01, \ M = 3, \ \alpha_e = 0.5, \ \alpha_i = 0.3, \ Pr = 1.3$

$Ec = 0.2, \ 0.4, \ 0.6, \ 0.8$
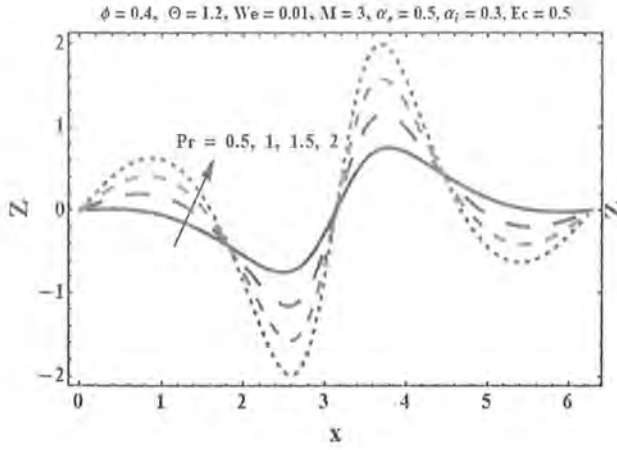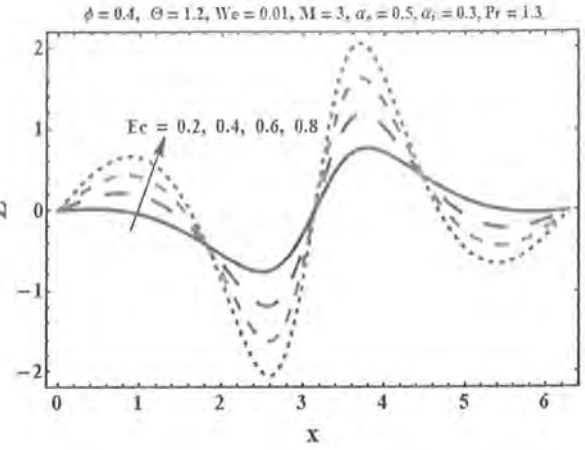
Fig. 8.26

Figs. (8.21 - 8.26): Variation in heat transfer coefficient (Z) against axial distance (x) for Hartman number (M), Wessienberg number (We), Hall parameter (α_e), ion-slip parameter (α_i), Prandtl number (Pr) and Eckert number (Ec).

8.3.5 Trapping

Fig. $(8.27 - 8.30)$ are displayed for the effects of Weissenberg number (We), Hatrman number (M), Hall parameter (α_e) and ion-slip parameter (α_i) on the trapping. In Figs. (2.27) and (2.28) the size of bolus decreases for larger values of We and M. Effects of parameters α_e and α_i on trapping are illustrated in Figs. (8.29) and (8.30). These plots depict that increasing values of α_i and α_e result in an increase of the size of trapped bolus.

125

Fig. 8.27

Fig. 8.27: Plots for $\Psi(x, y)$ for Wessienberg number (We).

Fig. 8.28

Fig. 2.28: Plots for $\Psi(x, y)$ for Hartman number (M).

126
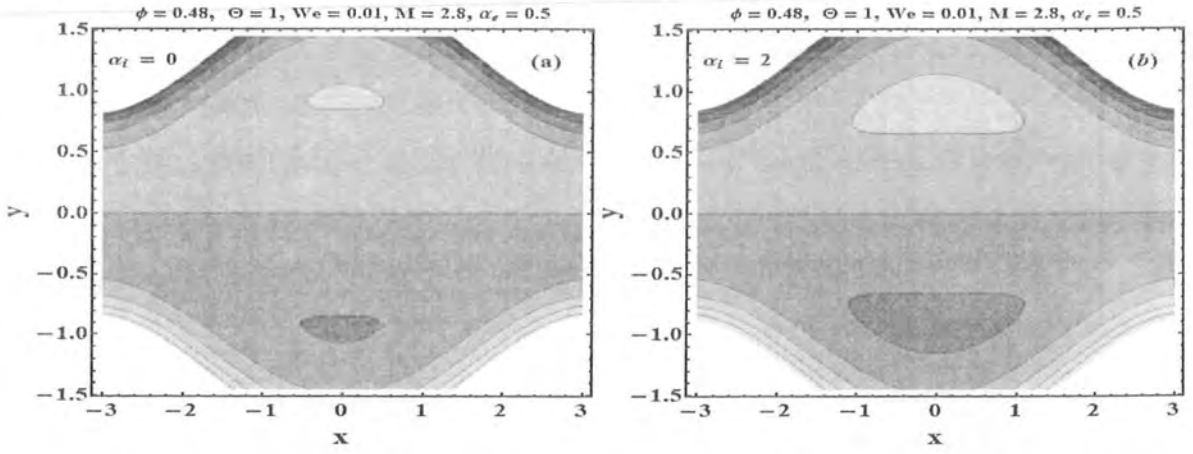
Fig. 8.29

Fig. 8.29: Plots for $\Psi(x,y)$ for Hall parameter (α_i).
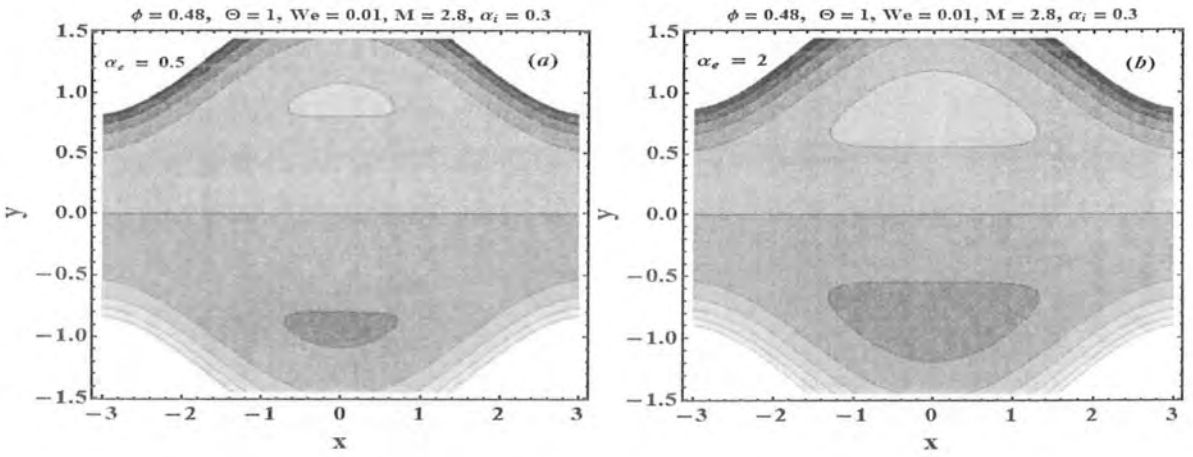
Fig. 8.30

Fig. 8.30: Plots for $\Psi(x,y)$ for ion-slip parameter (α_e).
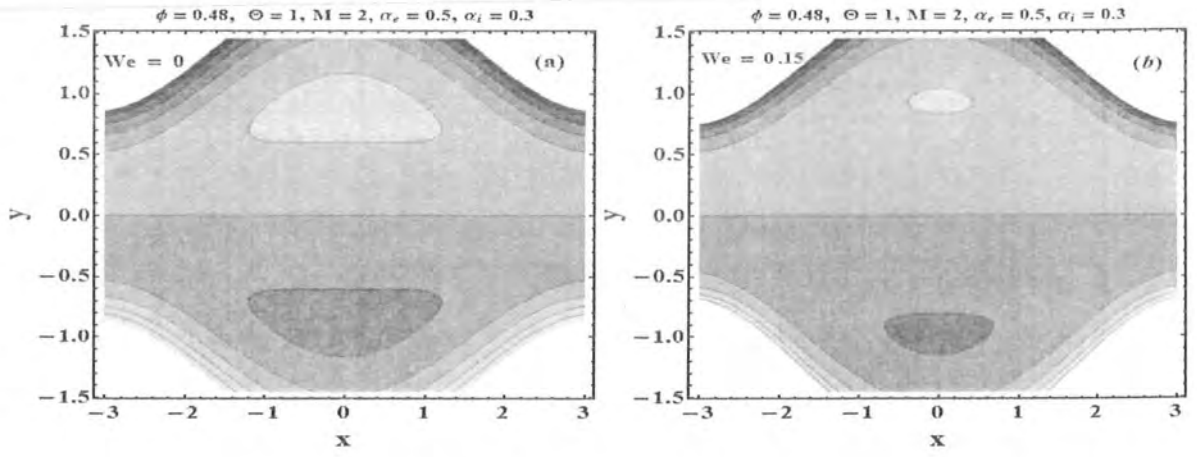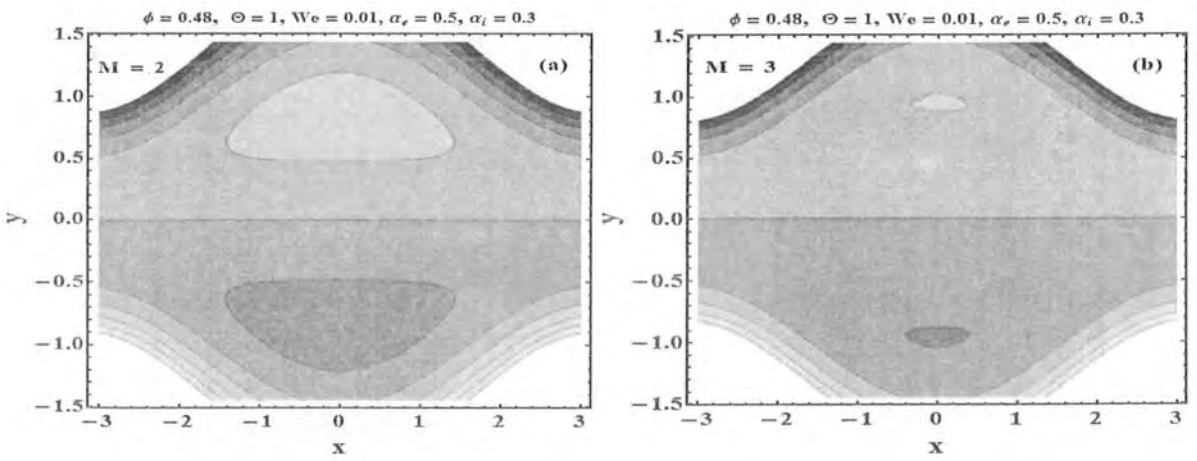
8.4 Conclusions

In this chapter we analyzed the heat transfer analysis on peristaltic flow of Williamson fluid in a symmetric channel when Hall and ion-slip effects are present. Effect of Joule heating and viscous dissipation are also retained. The key findings of present study can be listed below.

- Pressure rise increases in peristaltic pumping region for large values of M, whereas it decreases for the increase in α_e and α_i.

- Magnitude of dp/dx decreases by increasing We, α_e and α_i and it increases via larger M.

- Increase in parameters We, α_e and α_i decreases the shear stress at the wall while shear stress increases when M is increased.

- Longitudinal velocity gives reverse behavior at the center line and near the walls. Moreover effects of α_e and α_i on velocity distribution are quite opposite to that of M .

- Temperature is increasing function of parameters M, Ec, and Pr. However the temperature decreases for α_e and α_i.

- Due to increase in We and M the size of bolus decreases. However the bolus size increases for larger values of α_e and α_i.

Chapter 9

Effects of Hall and ion-slip currents in peristaltic flow of Phan-Thein-Tannar (PTT) fluid with Joule heating and viscous dissipation

The influences of Hall and ion-slip on peristaltic transport of Phan-Thein-Tannar fluid in a symmetric channel is discussed in this chapter. Viscous dissipation and Joule heating effects are also considered. The flow analysis is carried out in a wave frame of reference moving with the velocity of the wave. Low Reynolds number and long wavelength approximations are employed in the mathematical formulation. Series solutions for stream function, pressure gradient and temperature profile are constructed for small values of Weissenberg number (We). Impact of physical parameters on the axial velocity, pressure gradient and temperature are analyzed graphically. Pumping and trapping phenomena are also examined. The results show that the axial velocity increases by increasing the Hall and ion-slip parameters.

9.1 Development of mathematical model

We examined the MHD flow of an incompressible, electrically conducting PTT fluid in an infinite two-dimensional channel of uniform width $2d$. A sinusoidal wave of small amplitude and constant speed c propagates along the channel walls. Cartesian coordinate system is choosen such that $\overline{X}$-axis lies along the central line of the channel and $\overline{Y}$-axis normal to it. A uniform magnetic field of strength $\mathbf{B_0}$ is applied in the transverse direction $(0, 0, \mathbf{B_0})$ and the induced magnetic field is neglected for low magnetic Reynolds number.

The geometry of walls satisfies the following expression:

$$\overline{H}\left(\overline{X}, \bar{t}\right) = d + b \cos \frac{2\pi}{\lambda} \left(\overline{X} - c\bar{t}\right), \tag{9.1}$$

in which b represents the wave amplitude, λ the wavelength and $\bar{t}$ the time.

The velocity for the two-dimensional flow is

$$\overline{\mathbf{V}} = \left[\overline{U}(\overline{X}, \overline{Y}, \bar{t}), \overline{V}(\overline{X}, \overline{Y}, \bar{t}), 0\right]. \tag{9.2}$$

The fundamental equations governing the MHD flow are;

(i). the continuity equation

$$\boldsymbol{\nabla} \cdot \overline{\mathbf{V}} = 0, \tag{9.3}$$

(ii). the linear momentum equation in the presence of Lorentz force

$$\rho_f \frac{d\overline{\mathbf{V}}}{d\bar{t}} = \boldsymbol{\nabla} \cdot \bar{\mathbf{T}} + \mathbf{J} \times \mathbf{B}, \tag{9.4}$$

$$\bar{\mathbf{T}} = -\bar{P}\bar{\mathbf{I}} + \bar{\mathbf{S}}, \tag{9.5}$$

(iii). the energy equation in the presence of viscous dissipation and Joule heating effects:

$$\rho_f \tilde{c}_p \frac{d\overline{T}}{d\bar{t}} = k\nabla^2 \overline{T} + \bar{\mathbf{S}} \cdot \boldsymbol{\nabla} \overline{\mathbf{V}} + \frac{\mathbf{J} \cdot \mathbf{J}}{\sigma}, \quad \nabla^2 = \frac{\partial^2}{\partial \overline{X}^2} + \frac{\partial^2}{\partial \overline{Y}^2}, \tag{9.6}$$

where $d/d\bar{t}$ signifies the material derivative, ρ_f the density, $\bar{p}$ the pressure, $\bar{\mathbf{I}}$ the identity tensor, $\bar{\mathbf{T}}$ the Cauchy stress tensor, $\overline{\mathbf{S}}$ the extra stress tensor, $\tilde{c}_p$ the specific heat, $\overline{T}$ the temperature,

k the thermal conductivity, $\mathbf{J}$ the current density and σ the electrical conductivity.

The generalized Ohm's law in the presence of Hall and ion-slip effects is

$$\mathbf{J} = \sigma (\mathbf{E} + \overline{\mathbf{V}} \times \mathbf{B}) - \frac{\alpha_e}{B_0} (\mathbf{J} \times \mathbf{B}) + \frac{\alpha_e \alpha_i}{B_0^2} [(\mathbf{J} \times \mathbf{B}) \times \mathbf{B}], \tag{9.7}$$

in which $\alpha_e \, (= w_e \tau_e)$ denotes the Hall parameter, $\alpha_i \, (= e n_e B_0 / (1 + n_e / n_a))$ the ion-slip parameter, w_e the cyclotron frequency, τ_e the electron collision time, e the electric charge, n_e the number density of electrons, n_a the neutral particle density and $\mathbf{E}$ the electric field.

Expression of extra stress tensor $\overline{\mathbf{S}}$ for the Phan-Thein-Tanner (PTT) model is given by

$$\bar{f}\overline{\mathbf{S}} + \lambda_1 \overline{\mathbf{S}}^{\nabla} = \mu \overline{\mathbf{A}}_1, \tag{9.8}$$

$$\overline{\mathbf{S}}^{\nabla} = \frac{d\overline{\mathbf{S}}}{d\bar{t}} - \overline{\mathbf{S}} \cdot \left(\operatorname{grad} \overline{\mathbf{V}} \right)^{\top} - \left(\operatorname{grad} \overline{\mathbf{V}} \right) \cdot \overline{\mathbf{S}}, \tag{9.9}$$

$$\overline{\mathbf{A}}_1 = \left(\operatorname{grad} \overline{\mathbf{V}} \right) + \left(\operatorname{grad} \overline{\mathbf{V}} \right)^{*}. \tag{9.10}$$

The function $\bar{f}$ in linearized PTT model is

$$\bar{f} = 1 + \frac{\varepsilon \lambda_1}{\mu} tr \left(\overline{\mathbf{S}} \right). \tag{9.11}$$

Here μ is the dynamic viscosity, λ_1 the relaxation time, $\varepsilon \in [0, 1]$ the model parameter, $\overline{\mathbf{S}}^{\nabla}$ represents Oldroyd's upper-convected derivative, tr the trace. Note that the PTT model reduce to upper convected Maxwell (UCM) model when $\varepsilon = 0$. There is no applied voltage therefore we take $\mathbf{E} = \mathbf{0}$ and with the use of Eq. (9.7) we have

$$\mathbf{J} \times \mathbf{B} = -\frac{\sigma B_0^2}{(1 + \alpha_e \alpha_i)^2 + (\alpha_e)^2} \left[\left((1 + \alpha_e \alpha_i)\overline{U} - \alpha_e \overline{V} \right), \; \left((1 + \alpha_e \alpha_i)\overline{V} + \alpha_e \overline{U} \right), \; 0 \right]. \tag{9.12}$$

Making use of Eqs. (9.8 - 9.12) in Eqs. (9.3) and (9.4) the continuity, momentum and energy equations take the forms:

$$\frac{\partial \overline{U}}{\partial \overline{X}} + \frac{\partial \overline{V}}{\partial \overline{Y}} = 0, \tag{9.13}$$

$$\rho_f \left(\frac{\partial}{\partial \bar{t}} + \overline{U} \frac{\partial}{\partial \overline{X}} + \overline{V} \frac{\partial}{\partial \overline{Y}} \right) \overline{U} = -\frac{\partial \overline{P}}{\partial \overline{X}} + \frac{\partial \overline{S}_{\overline{XX}}}{\partial \overline{X}} + \frac{\partial \overline{S}_{\overline{XY}}}{\partial \overline{Y}} - \sigma B_0^2 \left[(1 + \alpha_e \alpha_i)\overline{U} - \alpha_e \overline{V} \right], \tag{9.14}$$

131

$$\rho_f \left(\frac{\partial}{\partial \overline{t}} + \overline{U} \frac{\partial}{\partial \overline{X}} + \overline{V} \frac{\partial}{\partial \overline{Y}} \right) \overline{V} = -\frac{\partial \overline{p}}{\partial \overline{Y}} + \frac{\overline{S}_{YX}}{\partial \overline{X}} + \frac{\overline{S}_{YY}}{\partial \overline{Y}} - \sigma B_0^2 \left[(1 + \alpha_e \alpha_i) \overline{V} + \alpha_e \overline{U} \right], \quad (9.15)$$

$$f \overline{S}_{XX} + \lambda_1 \left(\frac{\partial \overline{S}_{XX}}{\partial \overline{t}} + \overline{U} \frac{\partial \overline{S}_{XX}}{\partial \overline{X}} + \overline{V} \frac{\partial \overline{S}_{XX}}{\partial \overline{Y}} - 2 \frac{\partial \overline{U}}{\partial \overline{X}} \overline{S}_{XX} - 2 \frac{\partial \overline{U}}{\partial \overline{Y}} \overline{S}_{XY} \right) = 2\mu \frac{\partial \overline{U}}{\partial \overline{X}}, \quad (9.16)$$

$$f \overline{S}_{XY} + \lambda_1 \left(\frac{\partial \overline{S}_{XY}}{\partial \overline{t}} + \overline{U} \frac{\partial \overline{S}_{XY}}{\partial \overline{X}} + \overline{V} \frac{\partial \overline{S}_{XY}}{\partial \overline{Y}} - \frac{\partial \overline{V}}{\partial \overline{X}} \overline{S}_{XX} - \frac{\partial \overline{V}}{\partial \overline{Y}} \overline{S}_{XY} - \frac{\partial \overline{U}}{\partial \overline{X}} \overline{S}_{XY} - \frac{\partial \overline{U}}{\partial \overline{Y}} \overline{S}_{YY} \right)$$
$$= \mu \left(\frac{\partial \overline{U}}{\partial \overline{Y}} + \frac{\partial \overline{V}}{\partial \overline{X}} \right), \quad (9.17)$$

$$f \overline{S}_{YY} + \lambda_1 \left(\frac{\partial \overline{S}_{YY}}{\partial \overline{t}} + \overline{U} \frac{\partial \overline{S}_{YY}}{\partial \overline{X}} + \overline{V} \frac{\partial \overline{S}_{YY}}{\partial \overline{Y}} - 2 \frac{\partial \overline{V}}{\partial \overline{X}} \overline{S}_{YX} - 2 \frac{\partial \overline{V}}{\partial \overline{Y}} \overline{S}_{YY} \right) = 2\mu \frac{\partial \overline{V}}{\partial \overline{Y}}, \quad (9.18)$$

$$f = 1 + \frac{\varepsilon \lambda_1}{\mu} \left(\overline{S}_{XX} + \overline{S}_{YY} \right), \quad (9.19)$$

$$\rho_f \tilde{c}_p \left(\frac{\partial}{\partial \overline{t}} + \overline{U} \frac{\partial}{\partial \overline{X}} + \overline{V} \frac{\partial}{\partial \overline{Y}} \right) \overline{T} = k \left(\frac{\partial^2 \overline{T}}{\partial \overline{X}^2} + \frac{\partial^2 \overline{T}}{\partial \overline{Y}^2} \right) + \overline{S}_{XX} \frac{\partial \overline{U}}{\partial \overline{X}} + \overline{S}_{XY} \left(\frac{\partial \overline{U}}{\partial \overline{Y}} + \frac{\partial \overline{V}}{\partial \overline{X}} \right)$$
$$+ \overline{S}_{YY} \frac{\partial \overline{V}}{\partial \overline{Y}} + \frac{N}{A} \left(\overline{U}^2 + \overline{V}^2 \right). \quad (9.20)$$

Note that the flow is unsteady in the fixed frame with coordinates $\left(\overline{X}, \overline{Y}, \overline{t} \right)$. We now introduce a coordinate system $(\overline{x}, \overline{y})$ moving with the wave speed c in the positive $\overline{x}$ direction in which the boundary shape is stationary. The coordinates and velocities in the fixed and wave frames are related by the transformations:

$$\overline{x} = \overline{X} - c\overline{t}, \ \overline{y} = \overline{Y}, \ \overline{u} = \overline{U} - c, \ \overline{v} = \overline{V}, \ \overline{p}(\overline{x}, \overline{y}) = \overline{P} \left(\overline{X}, \overline{Y}, \overline{t} \right). \quad (9.21)$$

Defining the dimensionless quantities by

$$x = \frac{2\pi \overline{x}}{\lambda}, \ y = \frac{\overline{y}}{d}, \ u = \frac{\overline{u}}{c}, \ v = \frac{\overline{v}}{c}, \ h = \frac{\overline{h}}{d}, \ p = \frac{d^2}{\lambda \mu c} \overline{p}, \ \mathbf{S} = \frac{d}{\mu c} \overline{\mathbf{S}},$$

$$M = \sqrt{\frac{\sigma}{\mu}} B_0 d, \ \mathrm{Re} = \frac{\rho_f d c}{\mu}, \ \theta = \frac{\overline{T} - T_0}{T_1 - T_0}, \ \delta = \frac{2\pi d}{\lambda}, \ We = \frac{\lambda_1 c}{d},$$

$$N = \frac{M^2 A}{(\alpha_e)^2 + (A)^2}, \ A = 1 + \alpha_e \alpha_i, \ Br = \frac{\mu c^2}{k(T_1 - T_0)}, \quad (9.22)$$

in which M, Re, δ, We, and Br denote respectively the Hartman, Reynolds, wave, Weissenberg, and Brikman numbers. Introducing the stream function Ψ $\left(u = \dfrac{\partial \Psi}{\partial y}, v = -\delta \dfrac{\partial \Psi}{\partial x}\right)$ the continuity equation (9.13) is identically satisfied. By adopting long wavelength and low Reynolds number approximations Eqs. (9.14) - (9.20) in terms of stream function Ψ yield:

$$\frac{dp}{dx} = \frac{\partial S_{xy}}{\partial y} - N\left(\frac{\partial \Psi}{\partial y} + 1\right), \tag{9.23}$$

$$\frac{\partial p}{\partial y} = 0, \tag{9.24}$$

$$f S_{xx} = 2We\frac{\partial^2 \Psi}{\partial y^2} S_{xy}, \tag{9.25}$$

$$f S_{yy} = 0, \tag{9.26}$$

$$f S_{xy} = -We\frac{\partial^2 \Psi}{\partial y^2} S_{yy} + \frac{\partial^2 \Psi}{\partial y^2}, \tag{9.27}$$

$$f = 1 + \varepsilon We\left(S_{xx} + S_{yy}\right). \tag{9.28}$$

$$\frac{\partial^2 \theta}{\partial y^2} + Br\left[\left(S_{xy}\,\frac{\partial^2 \Psi}{\partial y^2}\right) + \frac{N}{A}\left(\frac{\partial \Psi}{\partial y} + 1\right)^2\right] = 0. \tag{9.29}$$

Eq. (9.24) implies that $p \neq p(y)$ therefore $p = p(x)$ only and $\dfrac{\partial p}{\partial x} = \dfrac{dp}{dx}$. The non-dimensional shape of the peristaltic wall $h(x)$ is given by

$$h(x) = 1 + \phi\cos(x), \tag{9.30}$$

in which $\phi = (b/d)$ is the amplitude ratio and $(0 < \phi < 1)$. The volume flow rates in fixed and wave frame are given by

$$\Theta = F + 1, \tag{9.31}$$

where

$$F = \int_0^h \frac{\partial \Psi}{\partial y} dy. \tag{9.32}$$

133

9.2 Solution of the problem

We integrate Eq. (9.23) subjected to the boundary condition $S_{xy} = 0$ at $y = 0$ that gives

$$S_{xy} = y\frac{dp}{dx} + N\left(\Psi + y\right). \tag{9.33}$$

With the aid of Eqs. (9.25) and (9.27) one can write

$$S_{xx} = 2WeS_{xy}^2, \tag{9.34}$$

using Eqs. (9.26) and (9.36) in Eq. (9.28) we get

$$f = 1 + 2 \in We^2 S_{xy}^2. \tag{9.35}$$

Finally From Eqs. (9.27), (9.35) and (9.37) we have the relation

$$\frac{\partial^2 \Psi}{\partial y^2} = y\frac{dp}{dx} + N\left(\Psi + y\right) + 2\varepsilon We^2 \left(y\frac{dp}{dx} + N\left(\Psi + y\right)\right)^3. \tag{9.36}$$

The relevant dimensionless boundary conditions in waveframe are:

$$\Psi = 0, \qquad \frac{\partial^2 \Psi}{\partial y^2} = 0, \qquad \theta = 0, \qquad at\ y = 0, \tag{9.37}$$

$$\frac{\partial \Psi}{\partial y} = -1, \qquad \Psi = F, \qquad \theta = 1, \qquad at\ y = h. \tag{9.38}$$

9.2.1 Series solutions

The governing Eq. (9.38) is highly non-linear and its exact solution seems difficult to compute. Therefore we are interested in calculating the series solution and thus expand the flow quantities in a series for small Wessenberg number (We) as follows:

$$\Psi = \Psi_0 + We^2\ \Psi_2 + O(We)^4, \tag{9.39}$$

$$F = F_0 + We^2\ F_2 + O(We)^4, \tag{9.40}$$

$$p = p_0 + We^2\ p_2 + O(We)^4. \tag{9.41}$$

134

Using Eqs. (42)-(44) in the Eqs. (23), (38), (39) and (40) and then solving the resulting zeroth and second order systems by comparing the coefficients of like powers of We^2, we get the solution expressions for the stream function (Ψ), pressure gradient (dp/dx) and temperature (θ) as follows:

$$
\begin{aligned}
\Psi ={}& 1/4h(4(C_1 + C_2 + F)y + 4We(C_7 + C_{11}We + C_8 y + C_{12}Wey)) \\
&+ We(C_5 + C_6 + (C_9 + C_{10})We)) + 12C_1^2 C_2 We^2(-5 + 2\sqrt{N}y) \\
&+ C_1(3 - 2C_2^2 We^2(5 + 2\sqrt{N}y))) \cosh[\sqrt{N}y] - We(C_1^2 + C_2^2 + 2(C_1 C_5 \\
&+ C_2 C_6)We)\cosh[2\sqrt{N}y] + (C_1^3 + C_2^3)We^2 \cosh[3\sqrt{N}y] + 3(3C_1 \\
&- 10(C_1^2 C_2 - C_1 C_2^2)We^2 + 3C_9 We^2 - 3(C_2 + We(C_6 - C_5 + C_{10})We)) \\
&+ 4C_1 C_2(C_1 + C_2)\sqrt{N}We^2 y)\sinh[\sqrt{N}y] + We(C_2^2 - C_1^2 - 2(C_1 C_5 \\
&- C_2 C_6)We\sinh[2\sqrt{N}y] + (C_1^3 - C_2^3)We^2 \sinh[3\sqrt{N}y]),
\end{aligned} \tag{9.42}
$$

$$
dp/dx = -N((1 + C_4) + C_8 We + C_{12}We^2), \tag{9.43}
$$

$$
\begin{aligned}
\theta ={}& -1/2700AN(675(-4AC_{13}N - 4AC_{14}Ny - 4C_1 C_2 N Ec \Pr y^2 + 4C_4 N^2 Ec \Pr y^2 \\
&+ 2C_4^2 N^2 Ec \Pr y^2 + 8(C_1 - C_2)(1 + C_4)Ec\sqrt{N}\Pr \cosh[\sqrt{N}y] + (C_1^2 \\
&+ C_2^2)Ec \Pr \cosh[2\sqrt{N}y] + 8C_1 Ec\sqrt{N}\Pr \sinh[\sqrt{N}y] + C_1^2 Ec \Pr \sinh[2\sqrt{N}y] \\
&- C_2^2 Ec \Pr \sinh[2\sqrt{N}y]) + 2Ec \Pr We(-1350C_2 C_5 Ny^2 + 900(15AC_1^3 C_2^2 \\
&+ C_1^2 C_2(-2 + 15AC_2^2) + 6Ec \Pr We^2(-1750C_3 C_7 Ny^2 + 350(15AC_2^3 C_1^3 \\
&+ 4C_1 C_2(C_1 - C_2)\sqrt{N}Wey)\sinh[3\sqrt{N}y] + We(5 + 2\sqrt{N}y)))\cosh[3\sqrt{N}y])),
\end{aligned} \tag{9.44}
$$

where the values of $C_l(l = 1 - 14)$ can be calculated through algebraic computations easily.

9.3 Graphical results and discussion

This section interprets the graphical results in order to analyze the qualitative effects of Hall parameter (α_e), ion-slip parameter (α_i), Wessienberg number (We), Hartman number (M), and Brinkman number (Br) on axial velocity $(u(y))$, pressure rise (ΔP_λ), pressure gradient

(dp/dx), temperature (θ) and trapping.

9.3.1 Velocity profile

In this subsection Figs. $(9.1) - (9.4)$ are prepared to see the influences of parameters α_e, α_i, M, and We on the axial velocity. These Figs. show that the plots of velocity versus the transverse displacement (y) are non-linear, parabolic in nature and have opposite behavior near the walls when compared with centre of the channel. Effects of α_e and α_i on the velocity are captured in Figs. (9.1) and (9.2). These Figs. depicts that each of α_e and α_i assist the flow at the center of the channel and hence the velocity increases with an increase in α_e and α_i. Moreover α_e has grater effect than α_i on velocity profile. To notice the effect of M on velocity we prepared Fig. (9.3) shows that by increasing M the velocity decreases at the center of the channel. Physically it is true because an increase in M enhances the magnitude of Lorentz force that act as a resistive agent and hence the velocity decreases. Fig. (9.4) illustrates the effects of viscoelastic parameter We on velocity. It is revealed that by increasing We the viscosity of the fluid increases that cause a decrease in the velocity. Also it is seen that effect of M on velocity is quite opposite to both α_e and α_i.
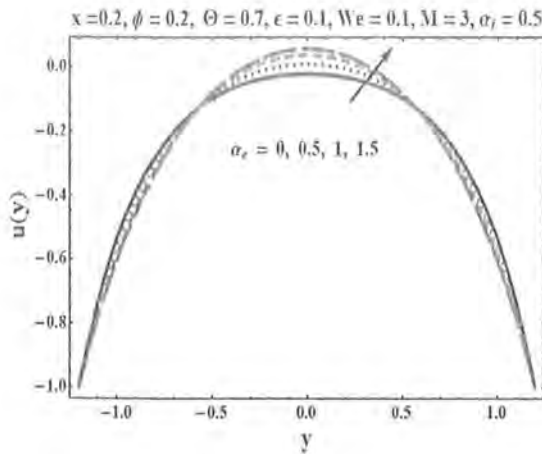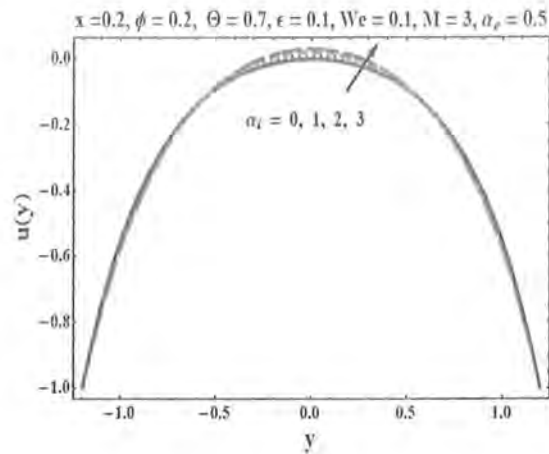

Fig. 9.1: Effect of α_e on u(y)
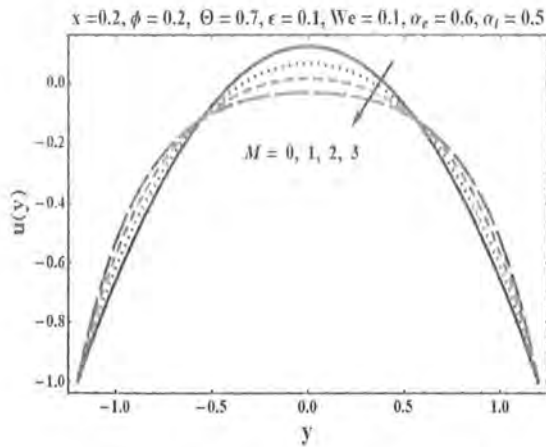

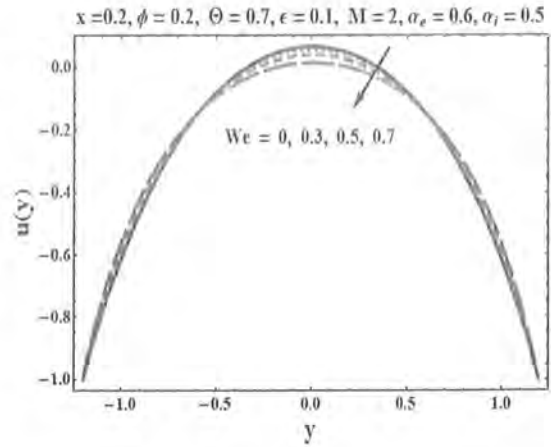Fig. 9.2: Effect of α_i on u(y)

Fig. 9.3: Effect of M on u(y)

Fig. 9.4: Effect of We on u(y)

9.3.2 Pumping analysis

In this subsection Figs. (9.5) − (9.12) disclose the variation in dimensionless pressure drop (ΔP_λ) and pressure gradient (dp/dx) for different values of α_e, α_i, M and We. Figs. (9.5) and (9.6) are sketched to illustrate the effects of α_e and α_i on pressure rise (ΔP_λ). These Figs. depicts that an increase in α_e and α_i decreases the pumping rate in the peristaltic pumping region. However after a critical value of Θ that is $\Theta = 0.08$ the pressure drop increases in free and augmented pumping region for an increasing values of α_e and α_i. Moreover for $\alpha_e = 0$ the pressure rise is maximum. Fig. (9.7) discloses that when M is increased it intensify the pressure rise in the peristaltic pumping region but after $\Theta = 0.08$ the pressure rise decreases. However the behavior remains the same in the free and augmented pumping regions. Influence of We on ΔP_λ is shown in Fig. (9.8) which reveals that an increase in We reduces the pumping rate in the peristaltic and free pumping regions however it has no effect in the augmented pumping
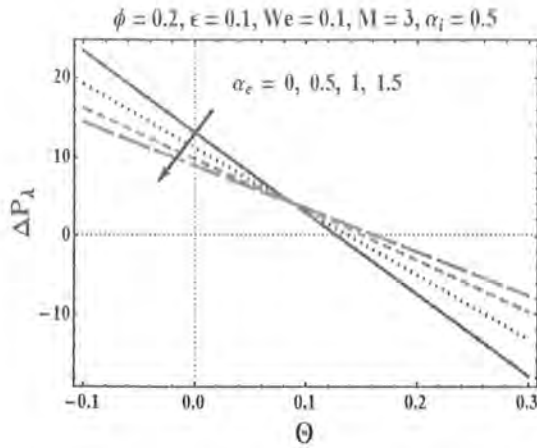
region.

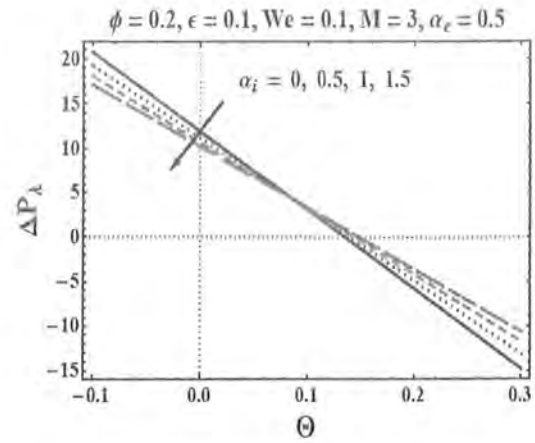Fig. 9.5: Effect of α_e on ΔP_λ
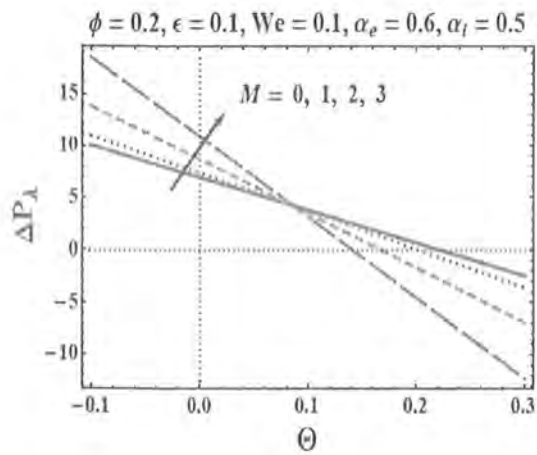

Fig. 9.6: Effect of α_i on ΔP_λ

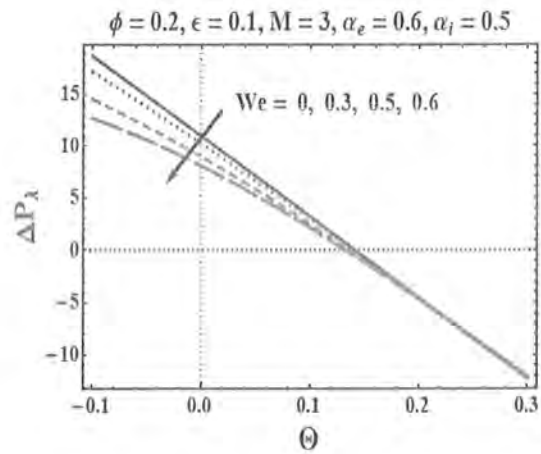Fig. 9.7: Effect of M on ΔP_λ

Fig. 9.8: Effect of We on ΔP_λ

Figs. $(9.9) - (9.12)$ are constructed to analyze the variation in pressure gradient (dp/dx) against the axial distance $x \in [0, 2\pi]$, for different values of parameters α_e, α_i, M and We. Figs. (9.9), (9.10) and (9.12) are displayed for the influences of α_e, α_i and We on dp/dx. These Figs. indicate that the magnitude of pressure gradient decreases when α_e, α_i and We are increased. However opposite effect is observed for parameter M as shown in Fig. (9.12) where an increase

138

in M enhances the magnitude of pressure gradient. Moreover these plots reflect that the effects of parameters are more prominent in the wider part of the channel at $x = 0$ and $x = 2\pi$ when compared with the narrow part of channel at $x = \pi$.
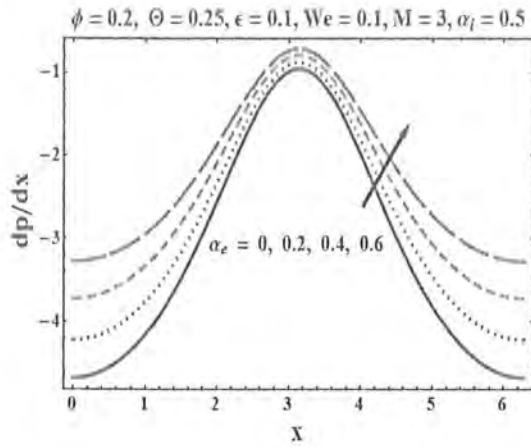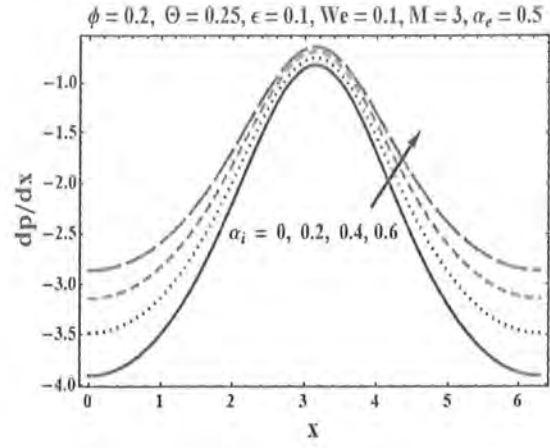

Fig. 9.9: Effect of α_e on dp/dx
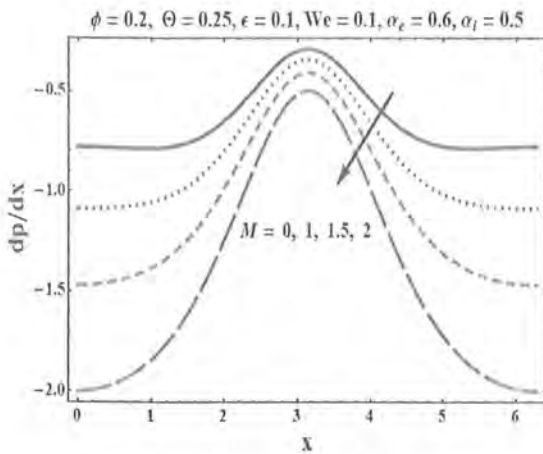

Fig. 9.10: Effect of α_i on dp/dx

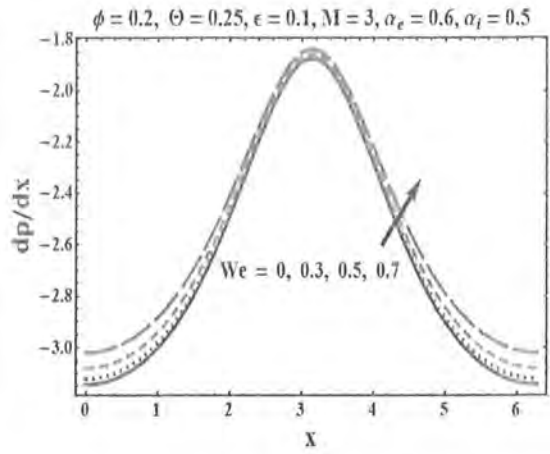Fig. 9.11: Effect of M on dp/dx

Fig. 9.12: Effect of We on dp/dx

9.3.3 Temperature profile

Figs. $(9.13) - (9.19)$ are presented to capture the impacts of parameters α_e, α_i, M, We and Br on temperature profile $(\theta(y))$ versus y. In Fig. (9.14) and (9.16) we have neglected the effect of

joule heating. Fig. (9.13) and (9.14) are prepared to see the influence of α_e on $\theta(y)$. From these Figs. it is noticed that in the absence of joule heating the temperature increases by increasing α_e. However the effect is quite opposite when joule heating effects are taken into account. In such a case the temperature of the fluid decreases by increasing α_e. Figs. (9.15) and (9.16) illustrates the impact of parameter M on $\theta(y)$. It is noted that effect of M on temperature is opposite to that of α_e. The effect of α_i and We on $\theta(y)$ are similar to α_e [See Figs. (9.17) and (9.18)]. The consequences of an increase in Br on temperature (θ) is visualized in Fig. (9.19). It is seen that an increase in Br intensify the temperature profile. It is because of the fact that with an increase in Br the viscous dissipation increases and generates more heat that leads to enhance the fluid temperature.
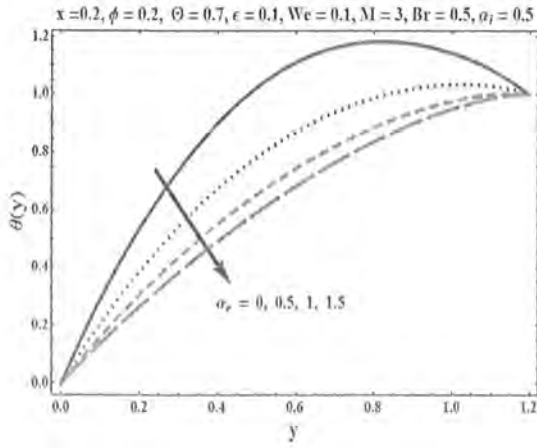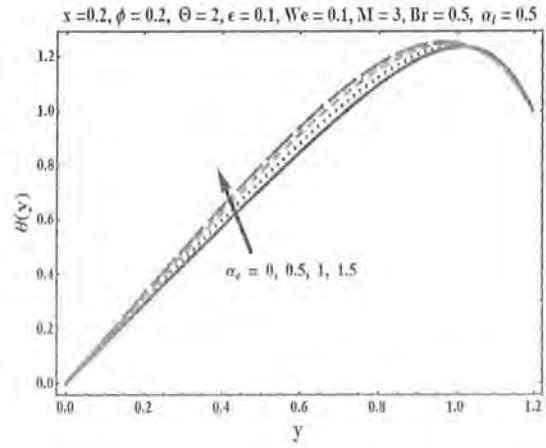

Fig. 9.13: Effect of α_e on $\theta(y)$ Fig. 9.14: Effect of α_i on $\theta(y)$
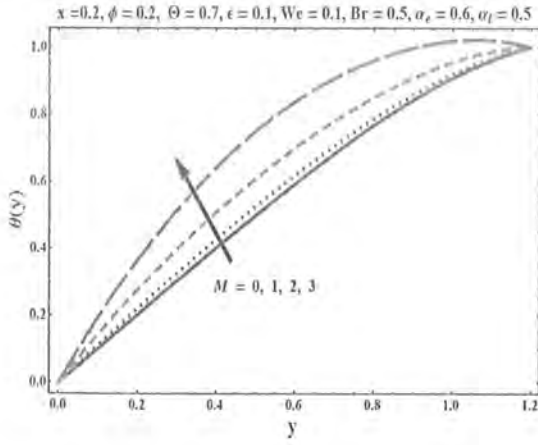
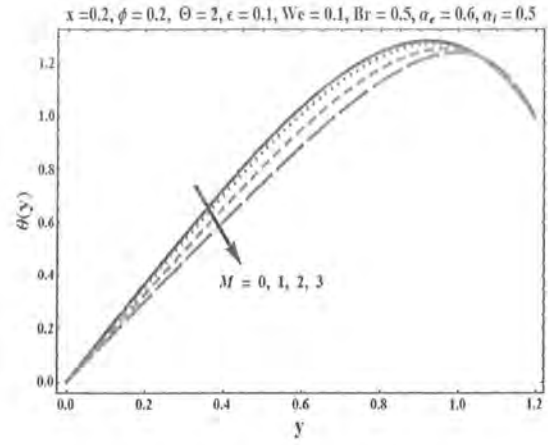Fig. 9.15: Effect of M on $\theta(y)$

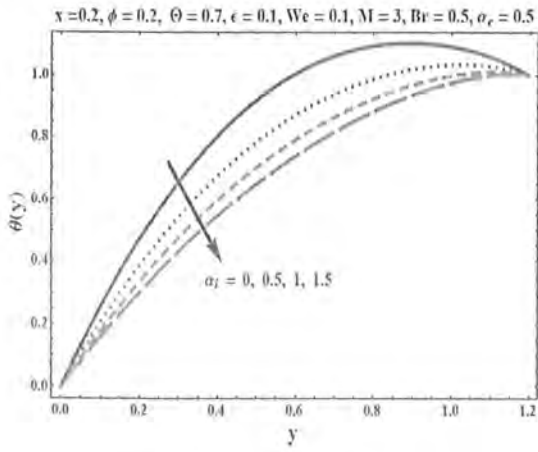Fig. 9.16: Effect of M on $\theta(y)$

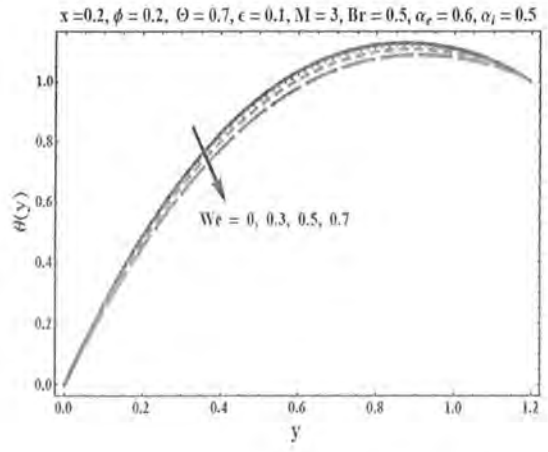Fig. 9.17: Effect of α_i on $\theta(y)$

Fig. 9.18: Effect of We on $\theta(y)$
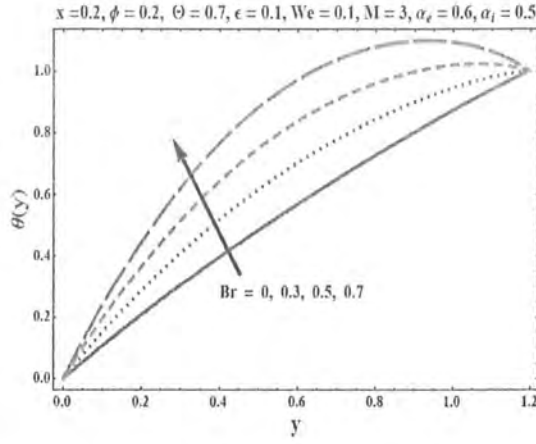
Fig. 9.19: Effect of Br on $\theta(y)$

9.3.4 Trapping

Figs. $(9.20) - (9.22)$ are displayed for the effects of Weissenberg number (We), Hartman number (M) and Hall parameter (α_e) on the trapping. In Figs. (9.20) and (9.21) the bolus decreases and it vanishes for larger values of We and M. Effects of parameters α_e on trapping are illustrated in Figs. (9.22). The plot depicts that increasing values of α_e result in an increase of the size of trapped bolus.

Fig. 9.20

142

Fig. 20 (a-b): Stream lines for different values of Wessienberg number (We).

Fig. 9.21

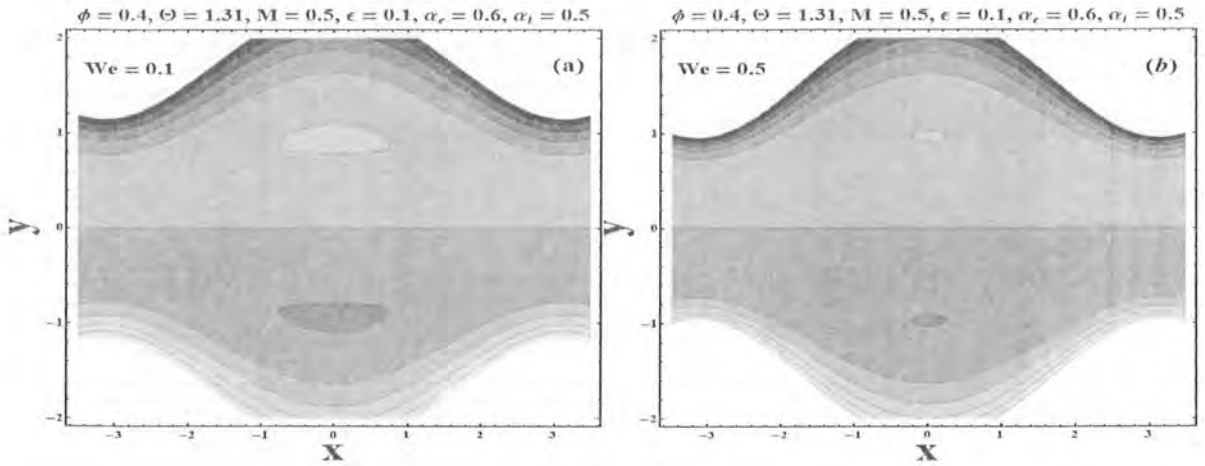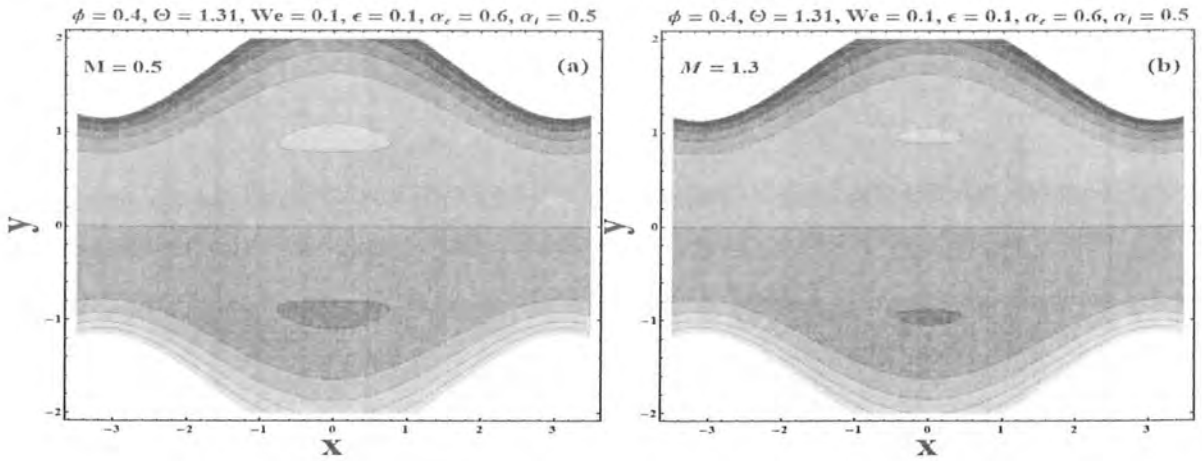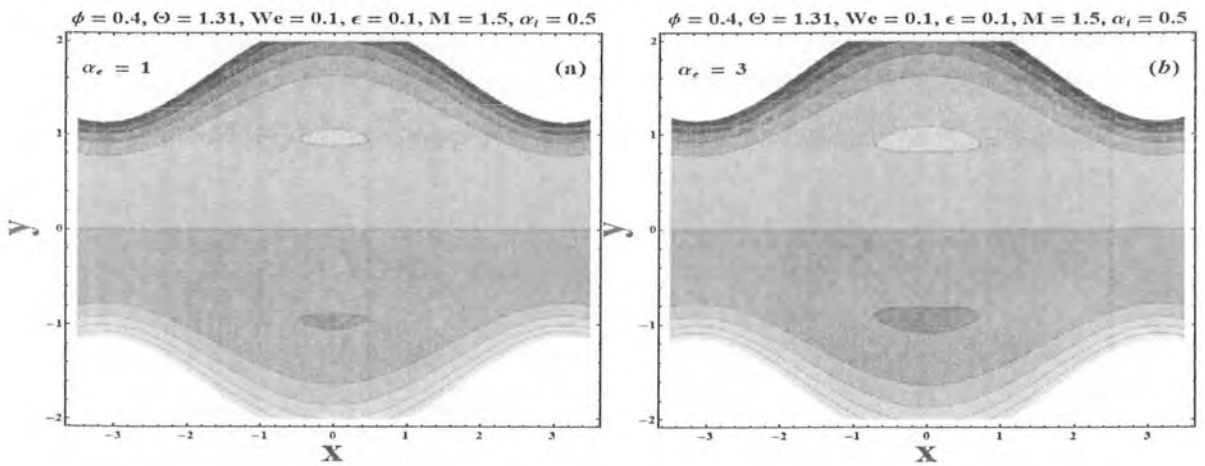Fig. 21 (a-b): Stream lines for different values of Hatrman number (M).

Fig. 9.22

Fig. 22 (a-b): Stream lines for different values of Hall parameter (α_e).

9.4 Conclusions

We analyzed the heat transfer analysis on peristaltic flow of PTT fluid in a symmetric channel when Hall and ion-slip effects are present. Effect of Joule heating and viscous dissipation are

also retained. The main observations are listed below.

- Longitudinal velocity gives reverse behavior at the center line and near the walls. Moreover effects of α_e and α_i on velocity distribution are quite opposite to that of M and We.

- Pressure rise increases in peristaltic pumping region for large values of M, whereas it decreases for the increase in α_e, α_i and We.

- Magnitude of pressure gradient decreases by increasing α_e, α_i and We and its magnitude increases via larger M.

- In presence of Joule heating effects, temperature is increasing function of parameters M and Br. However the temperature decreases for α_e, α_i and We.

- Due to increase in We and M the size of bolus decreases. However the bolus size increases for larger values of α_e.

Chapter 10

Hall and ion-slip effects on peristaltic transport of Prandtl fluid in an inclined channel

In this chapter we investigate the peristaltic flow of Prandtl fluid in an inclined asymmetric channel. Hall and ion-slip effects are considered. Asymmetry in the channel is created by considering the peristaltic waves along the walls with different amplitudes and phases. The flow analysis is carried out in a wave frame of reference moving with the velocity of the wave. Series solutions for the stream function and pressure gradient have been computed under long wavelength and low Reynolds number assumptions. The flow quantities have been examined graphically for various emerging parameters.

10.1   Mathematical modeling

We consider the peristaltic flow of an electrically conducting incompressible Prandtl fluid in an infinite two-dimensional asymmetric channel of width $d_1 + d_2$. A constant magnetic field is applied. Both the magnetic field and channel are inclined. The channel walls are inclined at an angle ξ_2 to the horizontal while the magnetic field is inclined at an angle ξ_1 to the channel walls. A sinusoidal wave of constant speed c propagating along the channel walls induces the flow. We take Cartesian coordinate system in such a way that $\overline{X}$-axis lies along the central

line of the channel and $\overline{Y}$-axis normal to it. The induced magnetic field is neglected for small magnetic Reynolds number.
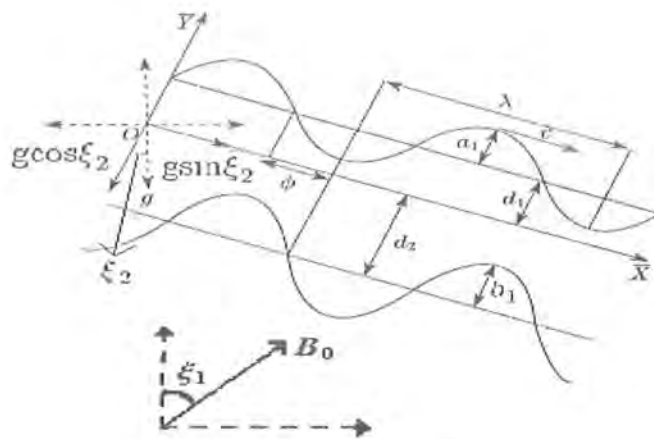
Geometry of the problem

The geometry of walls satisfies the following relations

$$\bar{Y} \;=\; \bar{H}_1 = d_1 + a_1 \cos\left(\frac{2\pi}{\lambda}\left(\bar{X} - c\bar{t}\right)\right), \tag{10.1}$$

$$\bar{Y} \;=\; \bar{H}_2 = -d_2 - b_1 \cos\left(\frac{2\pi}{\lambda}\left(\bar{X} - c\bar{t}\right) + \tilde{\phi}\right). \tag{10.2}$$

Here a_1 and b_1 show the waves amplitudes, λ is the wave length, $d_1 + d_2$ the channel width, c the wave speed, t the time and the phase difference $\tilde{\phi}$ ranges $0 \leq \tilde{\phi} \leq \pi$.

The governing equations for the MHD flow of Prandtl fluid in the presence of gravity effects are expressed by the relations:

$$\boldsymbol{\nabla}{\cdot}\overline{\mathbf{V}} = 0, \tag{10.3}$$

$$\rho_f \frac{d\overline{\mathbf{V}}}{d\bar{t}} = -\boldsymbol{\nabla}\overline{P} + \boldsymbol{\nabla}{\cdot}\overline{\mathbf{S}} + \mathbf{J}\times\mathbf{B} + \rho\mathbf{g}, \tag{10.4}$$

$$\overline{\mathbf{V}} = \left(\overline{U}(\overline{X},\overline{Y},\bar{t}), \overline{V}(\overline{X},\overline{Y},\bar{t}), 0\right), \tag{10.5}$$

where $d/d\bar{t}$ signifies the material derivative, ρ_f the density, $\overline{\mathbf{V}}$ the velocity, $\overline{p}$ the pressure, $\overline{\mathbf{S}}$ the extra stress tensor, $\mathbf{J}$ the current density and $\mathbf{g}$ the acceleration due to gravity.

146

The Ohm's law in the presence of Hall and ion-slip effects is

$$\mathbf{J} = \sigma(\mathbf{E} + \overline{\mathbf{V}} \times \mathbf{B}) - \frac{\alpha_e}{B_0}(\mathbf{J} \times \mathbf{B}) + \frac{\alpha_e \alpha_i}{B_0^2}[(\mathbf{J} \times \mathbf{B}) \times \mathbf{B}], \tag{10.6}$$

in which α_e denotes the Hall parameter, α_i the ion-slip parameter and $\mathbf{E}$ the electric field.

The constitutive equation for the expression of extra stress tensor $\overline{\mathbf{S}}$ for Prandtl fluid is given by:

$$\overline{\mathbf{S}} = \frac{\tilde{A}\sin^{-1}\left(\frac{1}{\tilde{C}}\left[\left(\frac{\partial \bar{U}}{\partial \overline{Y}}\right)^2 + \left(\frac{\partial \bar{V}}{\partial \overline{X}}\right)^2\right]^{\frac{1}{2}}\right)}{\left[\left(\frac{\partial \bar{U}}{\partial \overline{Y}}\right)^2 + \left(\frac{\partial \bar{V}}{\partial \overline{X}}\right)^2\right]^{\frac{1}{2}}}\overline{\mathbf{A}}_1, \tag{10.7}$$

$$\overline{\mathbf{A}}_1 = \left(\text{grad}\,\overline{\mathbf{V}}\right) + \left(\text{grad}\,\overline{\mathbf{V}}\right)^{\top}. \tag{10.8}$$

Here $\tilde{A}$ and $\tilde{C}$ are the material constants of Prandtl fluid model. There is no applied voltage therefore $\mathbf{E} = \mathbf{0}$ and through Eq. (10.6) we have

$$\mathbf{J} \times \mathbf{B} = \frac{-\sigma B_0^2}{((1+\alpha_e\alpha_i)^2 + \alpha_e^2)}\left\{\begin{array}{l}\left((1+\alpha_e\alpha_i)\overline{U}\cos^2(\xi_1) - \alpha_e\overline{V}\cos(\xi_1)\sin(\xi_1)\right), \\ \left((1+\alpha_e\alpha_i)\overline{V}\sin^2(\xi_1) + \alpha_e\overline{U}\cos(\xi_1)\sin(\xi_1)\right), \ 0 \end{array}\right\}. \tag{10.9}$$

Using Eqs. (10.5) and (10.9) in Eqs. (10.3), (10.4) and (10.7) we have the following relations:

$$\frac{\partial \overline{U}}{\partial \overline{X}} + \frac{\partial \overline{V}}{\partial \overline{Y}} = 0, \tag{10.10}$$

$$\rho_f\left(\frac{\partial}{\partial \bar{t}} + \overline{U}\frac{\partial}{\partial \overline{X}} + \overline{V}\frac{\partial}{\partial \overline{Y}}\right)\overline{U} = -\frac{\partial \overline{P}}{\partial \overline{X}} - \frac{\overline{S}_{\overline{XX}}}{\partial \overline{X}} - \frac{\overline{S}_{\overline{XY}}}{\partial \overline{Y}} - \frac{\sigma B_0^2}{((1+\alpha_e\alpha_i)^2+\alpha_e^2)}\cos(\xi_1)\left[(1+\alpha_e\alpha_i)\overline{U}\cos(\xi_1)\right.$$
$$\left. -\alpha_e\overline{V}\sin(\xi_1)\right] + \rho g\sin(\xi_2), \tag{10.11}$$

$$\rho_f\left(\frac{\partial}{\partial \bar{t}} + \overline{U}\frac{\partial}{\partial \overline{X}} + \overline{V}\frac{\partial}{\partial \overline{Y}}\right)\overline{V} = -\frac{\partial \overline{P}}{\partial \overline{Y}} - \frac{\overline{S}_{\overline{YX}}}{\partial \overline{X}} - \frac{\overline{S}_{\overline{YY}}}{\partial \overline{Y}} - \frac{\sigma B_0^2}{((1+\alpha_e\alpha_i)^2+\alpha_e^2)}\sin(\xi_1)\left[(1+\alpha_e\alpha_i)\overline{V}\sin(\xi_1)\right.$$
$$\left. +\alpha_e\overline{U}\cos(\xi_1)\right] - \rho g\cos(\xi_2), \tag{10.12}$$

147

$$\overline{S}_{\overline{XX}} = \frac{\tilde{A}\sin^{-1}\left(\frac{1}{\tilde{C}}\left[\left(\frac{\partial \bar{U}}{\partial \bar{Y}}\right)^2 + \left(\frac{\partial \bar{V}}{\partial \bar{X}}\right)^2\right]^{\frac{1}{2}}\right)}{\left[\left(\frac{\partial \bar{U}}{\partial \bar{Y}}\right)^2 + \left(\frac{\partial \bar{V}}{\partial \bar{X}}\right)^2\right]^{\frac{1}{2}}}\frac{\partial \overline{U}}{\partial \overline{X}}, \tag{10.13}$$

$$\overline{S}_{\overline{XY}} = \frac{\tilde{A}\sin^{-1}\left(\frac{1}{\tilde{C}}\left[\left(\frac{\partial \bar{U}}{\partial \bar{Y}}\right)^2 + \left(\frac{\partial \bar{V}}{\partial \bar{X}}\right)^2\right]^{\frac{1}{2}}\right)}{\left[\left(\frac{\partial \bar{U}}{\partial \bar{Y}}\right)^2 + \left(\frac{\partial \bar{V}}{\partial \bar{X}}\right)^2\right]^{\frac{1}{2}}}\left(\frac{\partial \overline{U}}{\partial \overline{Y}} + \frac{\partial \overline{V}}{\partial \overline{X}}\right), \tag{10.14}$$

$$\overline{S}_{\overline{YY}} = \frac{\tilde{A}\sin^{-1}\left(\frac{1}{\tilde{C}}\left[\left(\frac{\partial \bar{U}}{\partial \bar{Y}}\right)^2 + \left(\frac{\partial \bar{V}}{\partial \bar{X}}\right)^2\right]^{\frac{1}{2}}\right)}{\left[\left(\frac{\partial \bar{U}}{\partial \bar{Y}}\right)^2 + \left(\frac{\partial \bar{V}}{\partial \bar{X}}\right)^2\right]^{\frac{1}{2}}}\frac{\partial \overline{V}}{\partial \overline{Y}}. \tag{10.15}$$

Following Shapiro et al. [2] we introduce the transformations from fixed frame to wave frame by

$$\bar{x} = \bar{X} - c\bar{t}, \ \bar{y} = \bar{Y}, \ \bar{u} = \bar{U} - c, \ \bar{v} = \bar{V}, \ \bar{p}(\bar{x}) = \bar{P}\left(\bar{X}, \bar{t}\right).$$

Introducing the dimensionless quantities as

$$
\begin{aligned}
x &= \frac{2\pi\bar{x}}{\lambda}, \ y = \frac{\bar{y}}{d_1}, \ u = \frac{\bar{u}}{c}, \ v = \frac{\bar{v}}{c}, \ \delta = \frac{2\pi d_1}{\lambda}, \ d = \frac{d_2}{d_1}, \ a = \frac{a_1}{d_1}, \\
p &= \frac{2\pi d_1^2 \bar{p}}{\mu c \lambda}, \ h_1 = \frac{\bar{H}_1}{d_1}, \ h_2 = \frac{\bar{H}_2}{d_2}, \ \mathrm{Re} = \frac{\rho_f c d_1}{\mu}, \ b = \frac{a_2}{d_1}, \ S = \frac{\bar{S} d_1}{\mu c}, \\
\hat{\alpha} &= \frac{\bar{A}}{\tilde{C}\mu}, \ \hat{\beta} = \frac{\hat{\alpha} c^2}{d_1^2}, \ Fr = \frac{c^2}{d_1 g}, \ N^2 = \frac{M^2\left(1 + \alpha_e \alpha_i\right)}{(\alpha_e)^2 + (1 + \alpha_e \alpha_i)^2},
\end{aligned} \tag{10.16}
$$

where Re, M, Fr and δ are the Reynolds, Hartman, Froude and wave number respectively. The flow quantities in terms of stream function Ψ ($u = \frac{\partial \Psi}{\partial y}$ and $v = -\delta\frac{\partial \Psi}{\partial x}$) are given by

$$
\begin{aligned}
\mathrm{Re}\,\delta\left[\frac{\partial \Psi}{\partial y}\frac{\partial}{\partial x} - \delta\frac{\partial \Psi}{\partial x}\frac{\partial}{\partial y}\right]\frac{\partial \Psi}{\partial y} &= -\frac{\partial p}{\partial x} + \delta\frac{\partial S_{xx}}{\partial x} - N^2\cos(\xi_1)[(\frac{\partial \Psi}{\partial y} + 1)\cos(\xi_1) \\
&\quad + \delta\frac{\partial \Psi}{\partial x}\sin(\xi_1)] + \frac{\mathrm{Re}}{Fr}\sin(\xi_2) + \frac{\partial S_{xy}}{\partial y},
\end{aligned} \tag{10.17}
$$

148

$$\mathrm{Re}\,\delta^4\left[\delta\frac{\partial\Psi}{\partial x}\frac{\partial}{\partial y}-\frac{\partial\Psi}{\partial y}\frac{\partial}{\partial x}\right]\frac{\partial\Psi}{\partial x}\ =\ -\frac{\partial p}{\partial y}+\delta^2\frac{\partial S_{xy}}{\partial x}+\delta N^2\sin(\xi_1)[(\frac{\partial\Psi}{\partial y}+1)\cos(\xi_1)$$

$$+\delta\frac{\partial\Psi}{\partial x}\sin(\xi_1)]-\frac{\delta\,\mathrm{Re}}{Fr}\cos(\xi_2)+\delta\frac{\partial S_{yy}}{\partial y},\qquad(10.18)$$

$$S_{xx}=2\delta\left[\hat{\alpha}+\frac{\hat{\beta}}{6}\left(\left(\frac{\partial^2\Psi}{\partial y^2}\right)^2+\delta^4\left(\frac{\partial^2\Psi}{\partial x^2}\right)^2\right)\right]\frac{\partial}{\partial x}\left(\frac{\partial\Psi}{\partial y}\right),\qquad(10.19)$$

$$S_{xy}=\left[\hat{\alpha}+\frac{\hat{\beta}}{6}\left(\left(\frac{\partial^2\Psi}{\partial y^2}\right)^2+\delta^4\left(\frac{\partial^2\Psi}{\partial x^2}\right)^2\right)\right]\left(\frac{\partial^2\Psi}{\partial y^2}-\delta\frac{\partial^2\Psi}{\partial x^2}\right),\qquad(10.20)$$

$$S_{yy}=-2\delta\left[\hat{\alpha}+\frac{\hat{\beta}}{6}\left(\left(\frac{\partial^2\Psi}{\partial y^2}\right)^2+\delta^4\left(\frac{\partial^2\Psi}{\partial x^2}\right)^2\right)\right]\frac{\partial}{\partial y}\left(\frac{\partial\Psi}{\partial x}\right).\qquad(10.21)$$

The continuity Eq. (10.10) is identically satisfied and under the assumptions of long wavelength and low Reynolds number the Eqs.(10.11 - 10.15) take the form

$$\frac{dp}{dx}=\frac{\partial S_{xy}}{\partial y}-N^2\cos(\xi_1)[(\frac{\partial\Psi}{\partial y}+1)\cos(\xi_1)]+\frac{\mathrm{Re}}{Fr}\sin(\xi_2),\qquad(10.22)$$

$$\frac{\partial p}{\partial y}=0,\qquad(10.23)$$

$$S_{xx}=0=S_{yy},$$

$$S_{xy}=\left[\hat{\alpha}+\frac{\hat{\beta}}{6}\left(\frac{\partial^2\Psi}{\partial y^2}\right)^2\right]\left(\frac{\partial^2\Psi}{\partial y^2}\right).\qquad(10.24)$$

The average volume flow rate of the peristaltic wave is defined as follows:

$$\Theta=F+1+d,\qquad(10.25)$$

with

$$F=\int_{h_1}^{h_2}\frac{\partial\Psi}{\partial y}dy=\Psi(h_2)-\Psi(h_1).\qquad(10.26)$$

The appropriate dimensionless boundary conditions can be written in the forms:

$$\Psi\ =\ \frac{F}{2},\ \frac{\partial\Psi}{\partial y}=-1,\ at\ y=h_1=1+a\cos x,\qquad(10.27)$$

$$\Psi\ =\ -\frac{F}{2},\ \frac{\partial\Psi}{\partial y}=-1,\ at\ y=h_2=-d-b\cos\left(x+\bar{\phi}\right),\qquad(10.28)$$

149

Here F is the flux in wave frame and $a, b, \tilde{\phi}$ and d satisfy

$$a^2 + b^2 + 2ab\cos\tilde{\phi} \le (1+d)^2.$$

10.2 Series solutions

The governing Eqs. are highly non-linear and exact solution of these equations seems difficult to compute. Therefore we are interested in calculating the series solutions and thus expand the flow quantities in a series of the small parameter $\hat{\beta}$ as follows:

$$\Psi = \Psi_0 + \hat{\beta}\,\Psi_1 + O(\hat{\beta}^2), \tag{10.29}$$

$$F = F_0 + \hat{\beta}\,F_1 + O(\hat{\beta}^2), \tag{10.30}$$

$$p = p_0 + \hat{\beta}\,p_1 + O(\hat{\beta}^2). \tag{10.31}$$

Using Eqs. (10.29)-(10.31) in the Eqs. (10.22), (10.24), (10.27) and (10.28) and then solving the resulting zeroth and first order systems, we get the solution expressions for the stream function (Ψ) and pressure gradient (dp/dx) as follows:

$$
\begin{aligned}
\Psi ={}& -1/E_1(C_3 E_1 + (A_1 + E_1 - E_2)y - \sqrt{E_1\alpha}((C_1 - C_2)\cosh[\sqrt{E_1/\alpha}y] \\
& (C_1 + C_2)\sinh[\sqrt{E_1/\alpha}y]) + \beta(C_6 + 1/48 E_1\alpha^{5/2}(-48 A_2 y\alpha^{5/2} \\
& -(C_1^3\alpha - C_2^3)E_1^{3/2}\cosh[3\sqrt{E_1/\alpha}y] + 6(-8C_5\sqrt{E_1}\alpha^3 + C_1 C_2^2(2E_1^2 y\sqrt{\alpha} \\
& +3E_1^{3/2}\alpha)) - (\cosh[\sqrt{E_1/\alpha}y] - \sinh[\sqrt{E_1/\alpha}y]) + 6(8C_4\sqrt{E_1}\alpha^3 \\
& +C_1^2 C_2(2E_1^2 y\sqrt{\alpha} - +3E_1^{3/2}\alpha))(\cosh[\sqrt{E_1/\alpha}y] + \sinh[\sqrt{E_1/\alpha}y]) \\
& -(C_1^3 - C_2^3)E_1^{3/2}\alpha\sinh[3\sqrt{E_1/\alpha}y])),
\end{aligned}
$$

$$dp/dx = A_1 + \beta A_2,$$

where

$$E_1 = N^2\cos^2[\xi_1] \text{ and } E_2 = (\mathrm{Re}/F_r)\sin[\xi_2].$$

150

The values of $C_l(l = 1 - 6)$ and $A_i(i = 1, 2)$ can be calculated through algebraic computations easily.

10.3 Graphical results and discussion

This section describes the effects of emerging parameters on the velocity $u(y)$, pressure gradient (dp/dx), and pressure rise (ΔP_λ). Figs. (10.1) $-$ (10.6) are constructed to see the influences of ξ_1 (angle of inclination of magnetic field), Hatrman number (M), ion-slip parameter (α_i), Hall parameter (α_e) and material parameter $\left(\hat{\beta}\right)$ on the axial velocity. It is found that the plots of velocity versus y are parabolic in nature and have opposite behavior near the walls when compared with center of the channel. Figs. (10.1) and (10.2) illustrate the effect of ξ_1 on $u(y)$ when the channel is asymmetric and symmetric. These Figs. depict that by increasing angle of inclination of magnetic field (ξ_1) the velocity of the fluid increases near the center of the channel and it decreases near the walls of the channel. Moreover the fluid velocity is greater in symmetric channel when compared with asymmetric channel. Effect of Hartman number (M) on the velocity profile is presented in Fig. (10.3). The plot shows that by increasing M the velocity of the fluid reduces near the center of the channel. Physically it is true because larger M increases the magnitude of magnetic flux B_0 which enhances the Lorentz force and as a result the velocity decreases. Figs. (10.4) and (10.5) show that the effects of ion-slip parameter (α_i) and Hall parameter (α_e) on the velocity are qualitatively similar and their effects are opposite to that of M. Both α_i and α_e assist the flow by reducing the magnitude of magnetic flux and hence the velocity of fluid enhances near the center of the channel by increasing each α_e and α_i. Furthermore impact of α_e on velocity is greater than α_i. To notice the effect of material parameter $\left(\hat{\beta}\right)$ on velocity we prepared Fig. (10.6). It shows that by increasing $\hat{\beta}$ the velocity increases at the center of the channel.

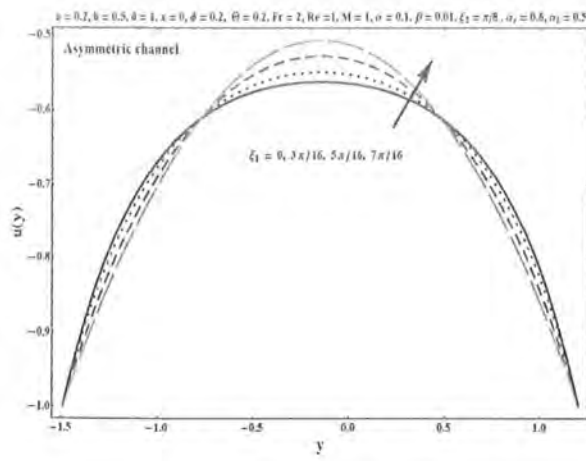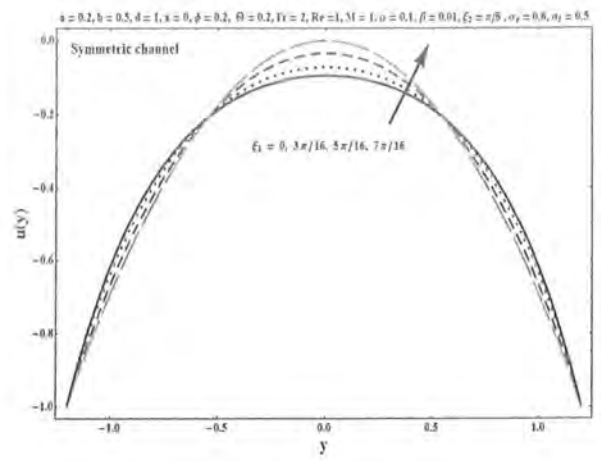Fig. 10.1: Variation of $u(y)$ with ξ_1

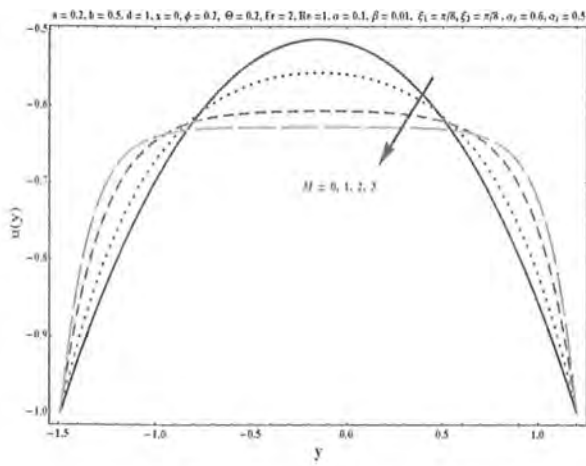Fig. 10.2: Variation of $u(y)$ with ξ_1
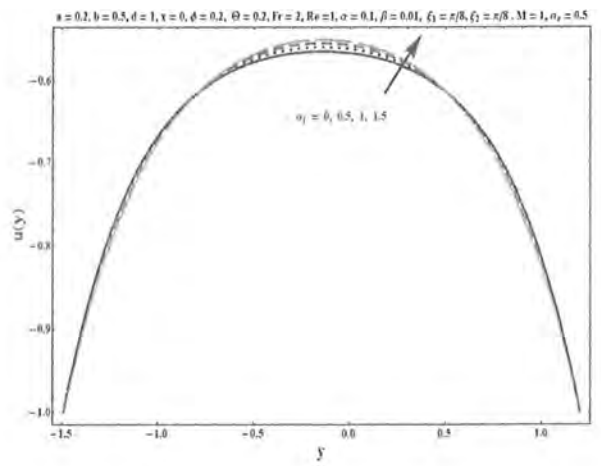

Fig. 10.3.Variation of $u(y)$ with M

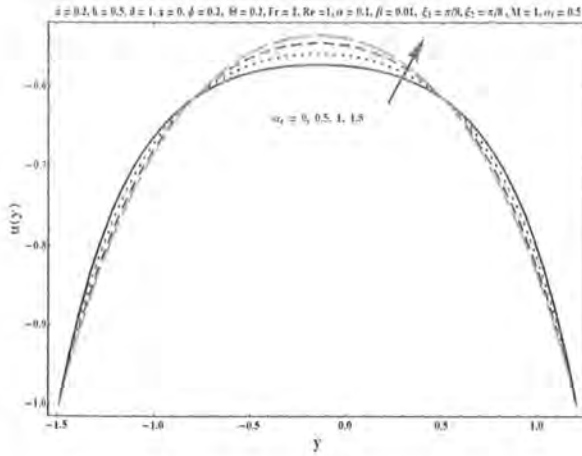Fig. 10.4: Variation of $u(y)$ with ξ_2

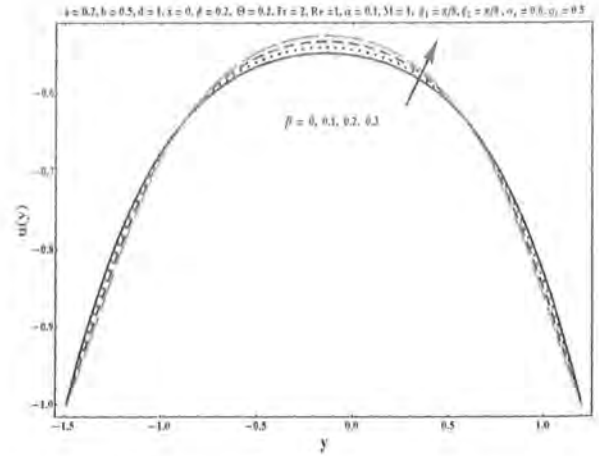Fig. 10.5: Variation of $u(y)$ with α_e

Fig. 10.6: Variation of $u(y)$ with $\hat{\beta}$

Figs. $(10.7 - 10.14)$ are constructed to analyze the variation in pressure gradient (dp/dx) against the axial distance $x \in [0, 2\pi]$, for different values of parameters ξ_2 (angle of inclination of the channel), ξ_1, M, α_e, α_i and β. Figs. (10.7) and (10.8) are displayed to see the influence of angle of inclination of the channel (ξ_2) for both asymmetric and symmetric channels. It is observed that by increasing the angle of inclination the pressure gradient increases in the whole region. Furthermore the magnitude of (dp/dx) is greater in asymmetric channel when compared with symmetric channel. To notice the effect of parameter ξ_1 (angle of inclination of magnetic field) on dp/dx we presented Figs. (10.9) and (10.10). These plots reveal that dp/dx decreases in the narrow part of channel and it increases in the wider part of the channel for larger values of ξ_1 in both asymmetric and symmetric channels. However in symmetric channel the pressure gradient is less when compared with an asymmetric channel. Fig. (10.11) is displayed for the influence of M on dp/dx which indicates that pressure gradient is an increasing function of M in the narrow part of the channel. However opposite effect is observed for parameter M in the wider part where an increase in M decreases the pressure gradient. Figs. (10.12) and (10.13) are made to analyze the change in pressure gradient (dp/dx) for different values of parameters α_e and α_i. These Figs. illustrate that effects of α_e and α_i on pressure gradient are opposite to that of M. Both α_e and α_i decrease/increase dp/dx in the narrow/wider part of the channel. Influence of material parameter $\hat{\beta}$ on dp/dx is presented in Fig. (10.14). The plot reveals that the pressure gradient increases in the narrow part of channel for larger values of $\hat{\beta}$.
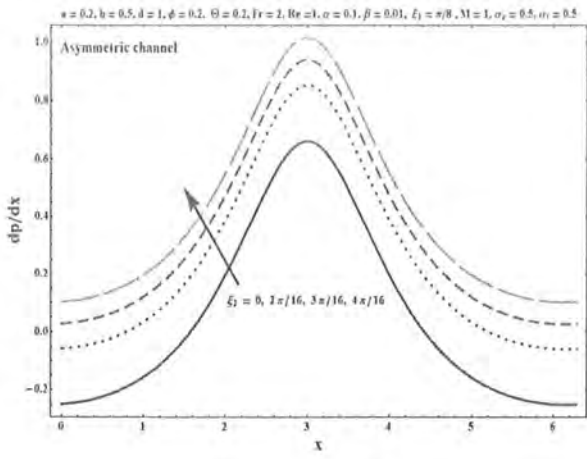
153

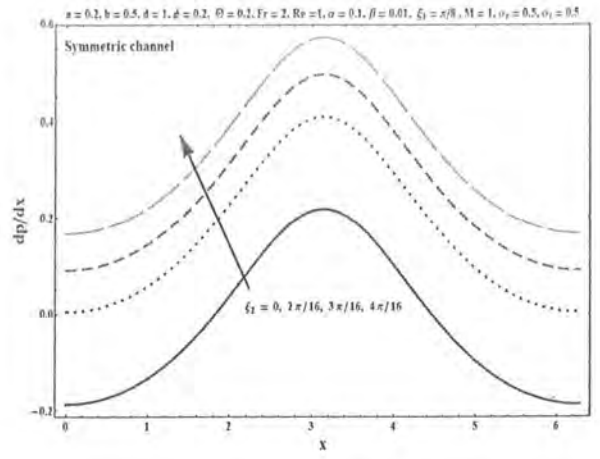Fig. 10.7: Variation of $\frac{dp}{dx}$ for with ξ_2

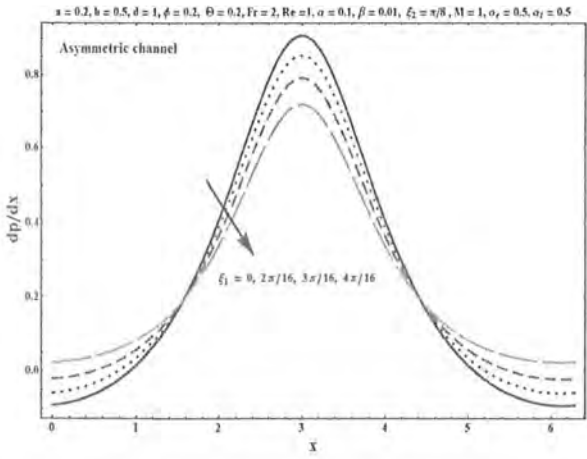Fig. 10.8: Variation of $\frac{dp}{dx}$ with ξ_2

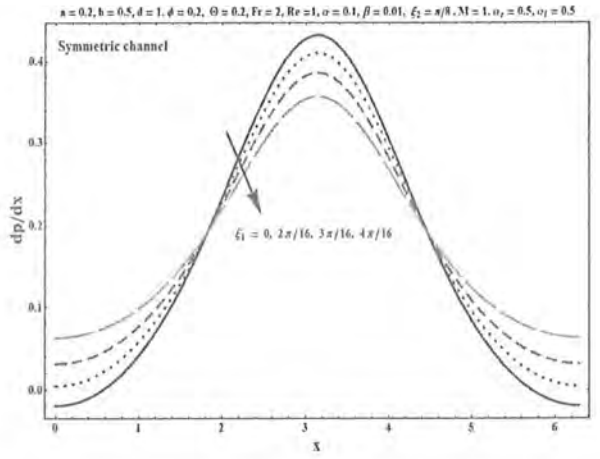Fig. 10.9: Variation of $\frac{dp}{dx}$ with ξ_1

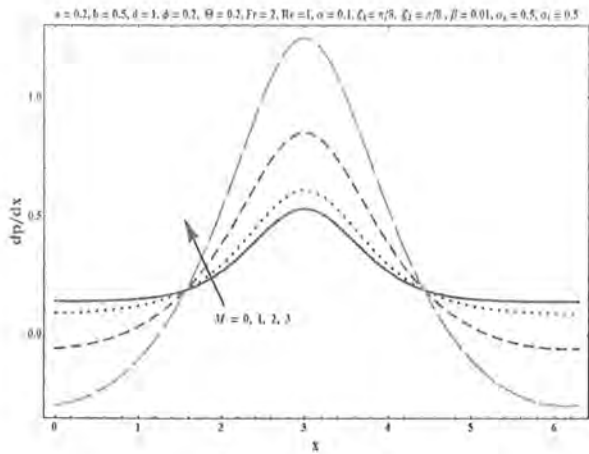Fig. 10.10: Variation of $\frac{dp}{dx}$ with ξ_1

154

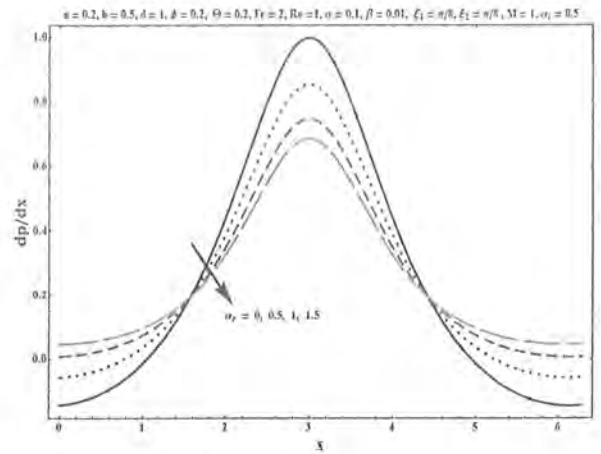Fig. 10.11: Variation of $\frac{dp}{dx}$ with M

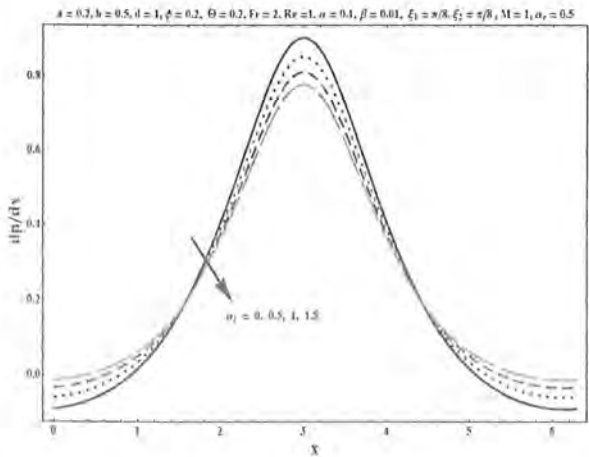Fig. 10.12: Variation of $\frac{dp}{dx}$ with α_e

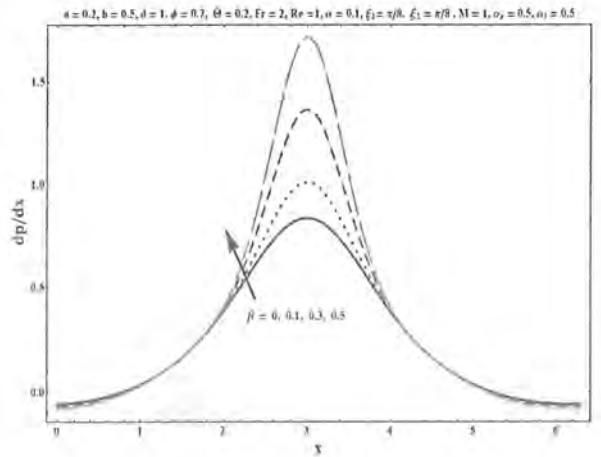

Fig. 10.13: Variation of $\frac{dp}{dx}$ with α_i

Fig. 10.14: Variation of $\frac{dp}{dx}$ with $\hat{\beta}$

Figs. (10.15) − (10.22) disclose the variation in dimensionless pressure drop (ΔP_λ) versus the time-average flux Θ for different values of ξ_1, ξ_2, M, α_e, α_i, and β. Figs. (10.15) and (10.16) are presented for the influence of ξ_2 on ΔP_λ for asymmetric and symmetric channels. It is noted that by increasing ξ_2 the pressure rise per wavelength increases in the whole region. Moreover pressure rise is larger in asymmetric channel. Effect of ξ_1 on ΔP_λ is shown in Figs. (10.17) and (10.18). These Figs. depict that increasing ξ_1 decreases the pumping rate in the pumping region. However after a critical value of Θ the pressure drop increases in the free and

155

augmented pumping regions. Moreover in asymmetric channel the pressure rise is large when compared with symmetric channel. Furthermore ΔP_λ is maximum when $\xi_1 = 0$ i.e. (when direction of magnetic field is perpendicular to channel walls). Fig. (10.19) discloses that an increase in M intensify the pressure rise in the peristaltic pumping region. Figs. (10.20) and (10.21) are prepared to illustrate the effects of α_e and α_i on pressure rise (ΔP_λ). These Figs. reveal that by increasing α_e and α_i the pumping rate decreases in the pumping region but after a critical value of Θ the pressure drop increases. Moreover the pressure rise is maximum for the case when $\alpha_e = 0$. Also it is observed that effects of both α_e and α_i are opposite to that of M. Influence of $\mathring{\beta}$ on ΔP_λ is shown in Fig. (10.22). It depicts that by increasing $\mathring{\beta}$ the pumping rate increases in the peristaltic pumping region and it decreases in the augmented pumping region. Also it is noted that free pumping region is independent of $\mathring{\beta}$.
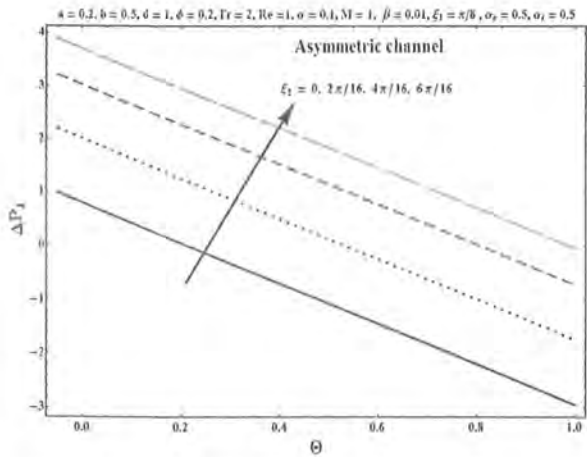

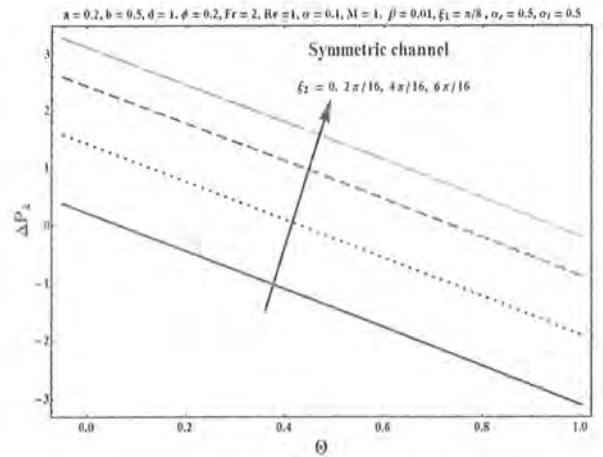Fig. 10.15: Variation of ΔP_λ with ξ_2 Fig. 10.16: Variation of ΔP_λ with ξ_2
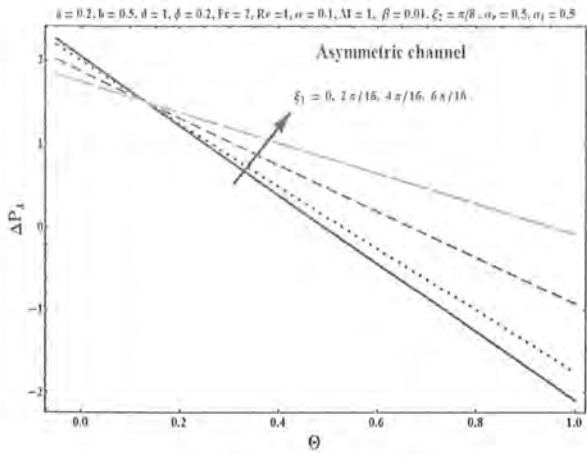
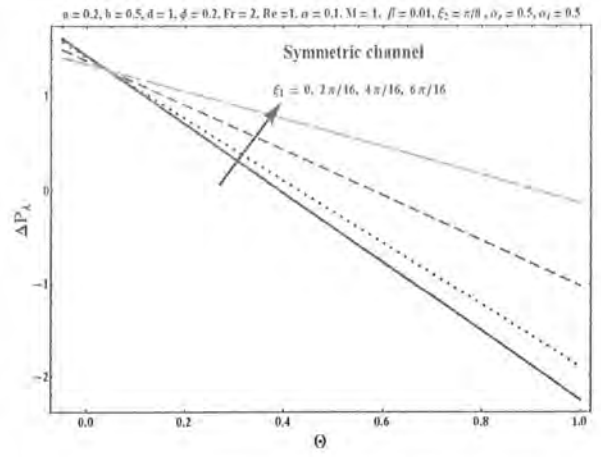Fig. 10.17: Variation of ΔP_λ with ξ_1

Fig. 10.18: Variation of ΔP_λ with ξ_1
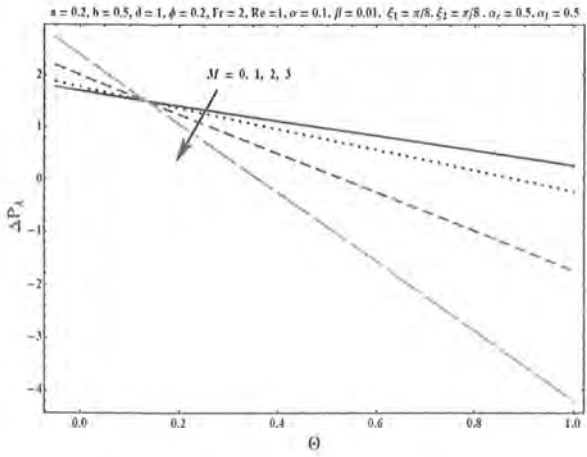
Fig. 10.19: Variation of ΔP_λ with M
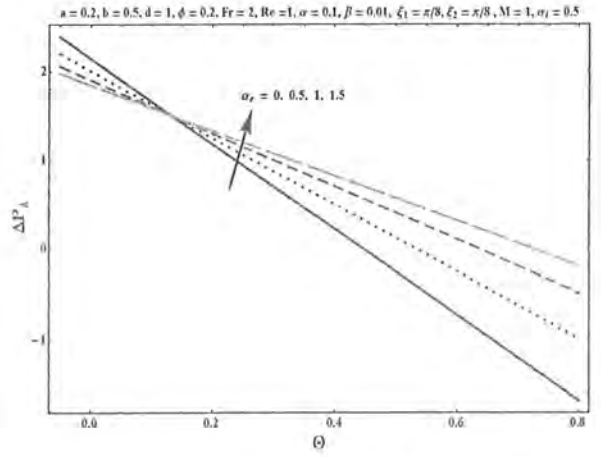
Fig. 10.20: Variation of ΔP_λ with α_e
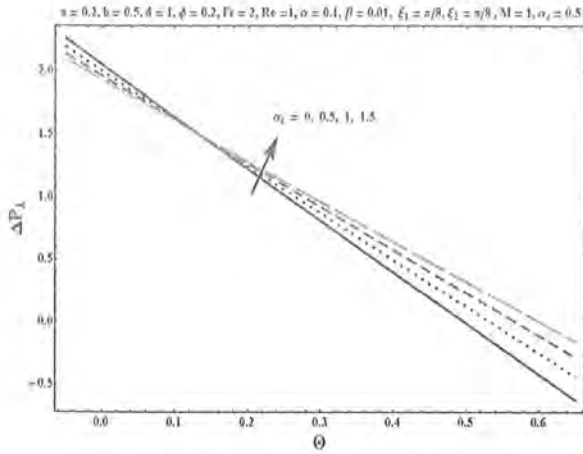
Fig. 10.21: Variation of ΔP_λ with α_i
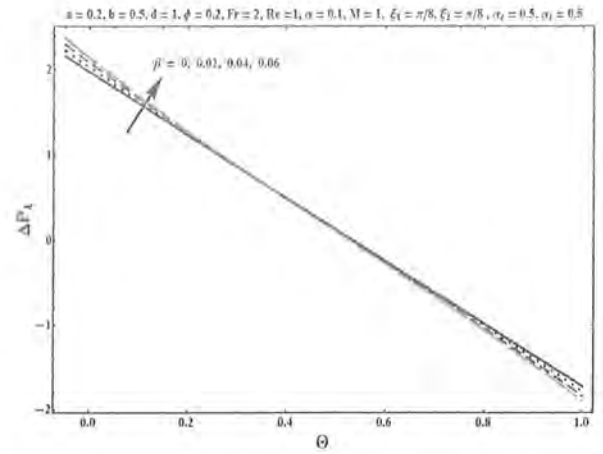
Fig. 10.22: Variation of ΔP_λ with $\hat{\beta}$

10.4 Key observations

The following points through this study are worthmentioning.

- The velocity of fluid is an increasing function of parameters ξ_1, α_e and $\hat{\beta}$ while it is a decreasing function of M. In symmetric channel the velocity is greater than asymmetric channel.

- Pressure gradient increases in both asymmetric and symmetric channels by increasing the inclination of the channel. Moreover pressure gradient decreases at the center of the channel when ξ_1, α_e and α_i are increased. The pressure gradient enhances for the increase in the parameters M and $\hat{\beta}$. Furthermore magnitude of dp/dx in asymmetric channel is larger than symmetric channel.

- Pressure rise per wavelength increases for increase in ξ_2, M and $\hat{\beta}$. However it decreases when parameters ξ_1, α_e and α_i are increased. The value of pressure rise is large in an asymmetric channel when compared with symmetric channel.

Bibliography

[1] T. W. Latham, Fluid motion in a peristaltic pump, MS. Thesis, M. I. T. Cambridge, (1966).

[2] A. H. Shapiro, Pumping and retrograde diffusion in peristaltic wave,"Proceedings. Workshop on ureteral reflux in children". National Academy of Science (Natural Research Council) (1967) 109.

[3] C. Barton and S. Raynor, Peristaltic flow in tubes, Bull. Math. Biophys., 30 (1968) 663.

[4] A. H. Shapiro, M. Y. Jaffrin and S. L. Weinberg, Peristaltic pumping with long wave lengths at low Reynolds numbers, J. Fluid Mech., 37 (1969) 799.

[5] F. Yin and Y. C. Fung, Peristaltic wave in circular cylindrical tubes, J. Appl. Mech., 36 (1969) 579.

[6] H. S. Lew, Y. C. Fung and C. B. Lowensteinm, Peristaltic carrying and mixing of chyme in the small intestine, J. Biomech., 4 (1971) 297.

[7] H. S. Lew and Y. C. Fung, A study on the low Reynolds number flow in a valved vessel, J. Biomech., 4 (1971) 85.

[8] M. Y. Jaffrin, Inertia and streamline curvature effects in peristaltic pumping, Int. J. Eng. Sci., 11 (1973) 681.

[9] M. Y. Jaffrin and A. H. Shapiro, Peristaltic pumping, Ann. Rev. Fluid Mech., 3 (1971) 13.

[10] T. K. Mittra and S. N. Prasad, Interaction of peristaltic motion with Poiseuille flow, Bull. Math. Biol., 36 (1974) 127.

[11] R. E. Smelser, W. J. Shack and T. J. Lardner, The swimming of spermatozoa in an active channel, J. Biomech., 7 (1974) 349.

[12] M. J. Manton, Long wavelength peristaltic pumping at low Reynolds number, J. Fluid Mech., 68 (1975) 467.

[13] S. Takabatake and K. Ayukawa, Numerical Analysis of two dimensional peristaltic flow, J. Fluid Mech., 122 (1982) 439.

[14] S. Takabatake, K. Ayukawa and A. Mori, Peristaltic pumping in circular tubes: A numerical study of fluid transport and its efficiency, J. Fluid Mech., 193 (1988) 267.

[15] K. De Vries, E. A. Lyons, J. Ballaed, C. S. Levi and D. J. Lindsay, Contractions of the inner third of the myometrium, Am J. Obstetrics Gynecol, 102 (1990) 679.

[16] O. Eytan, A. J. Jaffa, J. H. Toov, E. Dalach and D. Elad, Dynamics of the intra-uterine fluid-wall interface, Annals of Biomed. Eng., 27 (1999) 372.

[17] O. Eytan and D. Elad, Analysis of intrauterine fluid motion induced by uterine contractions, Bull. Math. Bio., 61 (1999) 221.

[18] M. Mishra and A. R. Rao, Peristaltic transport of a Newtonian fluid in an asymmetric channel, Z. Angew. Math. Phys., 54 (2004) 532.

[19] A. R Rao and M. Mishra, Nonlinear and curvature effects on peristaltic flow of viscous fluid in an asymmetric channel, Acta Mech., 168 (2004) 35.

[20] Kh. S. Mekheimer, Peritaltic transport of a Newtonian fluid through a uniform and non-uniform annulus, Arab. J. Sci. Eng., 30 (2005) 69.

[21] P. Chaturani and R. P. Samy, A study of non-Newtonian aspect of blood flow through stenosed arteries and its application in arterial diseases, J. Biorheology, (1985) 521.

[22] K. K. Raju and R. Devanathan, Peristaltic motion of a non-Newtonian fluid, Rheol. Acta, 11 (1972) 170.

[23] G. Radhakrishnemacharya, Long wavelength approximation to peristaltic motion of a power-law fluid, Rheol. Acta, 21 (1982) 30.

[24] M. W. Johnson and D. Segalman, A model for viscoelastic fluid behavior which allows non-affine deformation, J. Non-Newtonian Fluid Mech., 2 (1977) 255.

[25] N. P. Thien and R. I. Tanner, A new constitutive equation derived from network theory, J. Non-Newtonian fluid Mech., 2 (1977) 353.

[26] P. Thien, A nonlinear network viscoelastic model, J. Rheol., 22 (1978) 259.

[27] L. M. Srivastava and V. P. Srivastava, Peristaltic transport of a non-Newtonian fluid: Applications to the vas deferens and small intestine, Ann. Biomed. Eng., 13 (1985) 137.

[28] A. M. Siddiqui and W. H. Schwarz, Peristaltic motion of a third order fluid in a planar channel, Rheol. Acta, 32 (1993) 47.

[29] A. M. Siddiqui and W. H. Schwarz, Peristaltic flow of a second order fluid in tubes, J. Non-Newtonian Fluid Mech., 53 (1994) 257.

[30] E. F. E. Shehawey and K. S. Mekheimer, Couple-stresses in peristaltic transport of fluids, J. Physics D: Appl. Phys., 27 (1994) 1163.

[31] D. Tsiklauri and I. Beresnev, Non-Newtonian effects in the peristaltic flow of a Maxwell fluid, Phys. Rev. E, 64 (2001) 036303.

[32] T. Hayat, Y. Wang, A. M. Siddiqui and K. Hutter, Peristaltic flow of Johnson-Segalman fluid in a planar channel, Math. Prob. Eng., 1 (2003) 1.

[33] T. Hayat, Y. Wang, K. Hutter, S. Asghar and A. M. Siddiqui, Peristaltic transport of an Oldroyd-B fluid in a planar channel, Math. Prob. Eng., 4 (2004) 347.

[34] K. Vajravelu, S. Sreenadh and V. R. Babu, Peristaltic transport of a Herschel-Bulkley fluid in an inclined tube, Int. J. Nonlinear Mech., 40 (2005) 83.

[35] T. Hayat, N. Ali and S. Asghar, Peristaltic motion of a Burger's fluid in a planar channel, Appl. Math. Comput., 186 (2007) 309.

[36] M. H. Haroun, Effect of Deborah number and phase difference on peristaltic transport of a third-order fluid in an asymmetric channel, Comm. Nonlinear Sci. Numer. Simul., 12 (2007) 1464.

[37] T. T. Nguyen, M. Pham and N. S. Goo, Development of a peristaltic micropump for bio-medical applications based on Mini LIPCA, J. Bionic Eng., 5 (2008) 126.

[38] N. Ali, M. Sajid and T. Hayat, Long wavelength flow analysis in a curved channel, Z. Naturforch., 65a (2010) 191.

[39] T. Hayat and M. Javed, Exact solution to peristaltic transport of power-law fluid in asymmetric channel with compliant walls, Appl. Math. Mech., 31 (2010) 1231.

[40] S. Maiti and J. C. Misra, Peristaltic transport of a couple stress fluid: Some applications to hemodynamics, J. Mech. Med. Biol., 12 (2012) ID 1250048 (21 pages).

[41] S. Nadeem, N. S. Akbar, T. Hayat and A. A. Hendi, Peristaltic flow of Walter's B fluid in endoscope, Appl. Math. Mech., 32 (2012) 689.

[42] T. R. Rao and D. R. V. P. Rao, Peristaltic flow of a couple stress fluid through a porous medium in a channel at low Reynolds number, Int. J. Appl. Math., Mech. 8 (2012) 97.

[43] K. Yazdanpanh-Ardakani and H. Niroomand-Oscuii, New approach in modeling peristaltic transport of non-Newtonian fluid, J. Mech. Med. Biol., 13 (2013) DOI:10.1142/S0219519413500528.

[44] T. Hayat, S. Noreen, N. Ali and S. Abbasbanday, Peristaltic motion of Phan-Thein-Tanner fluid in a planar channel, Numer. Meth. Partial Diff. Eqs., 28 (2012) 737.

[45] A. Kalantari, K. Sadeghy and S. Sadeqi, Peristaltic flow of non-Newtonian fluids through curved channels: A numerical study, Ann. Transac. Nordic Rheo. Soc., 21 (2013) 163.

[46] P. Hari Prabakaran, A. Kavitha, R. Saravana, R. H. Reddy and S. Sreenadh, Peritaltic transport of a fourth grade fluid between porous walls with suction and injection, Int. J. Pure Appl. Math., 86 (2013) 293.

[47] R. Ellahi, A. Riaz and S. Nadeem, Three dimensional peristaltic flow of Williamson fluid in a rectangular duct, Indian J. Phys., 87 (2013) 1275.

[48] K. Vajravelu, G. Radhakrishnamacharya and V. R. Murty, Peristaltic flow and heat transfer in a vertical annulus with long wave approximation, Int. J. Nonlinear Mech., 42 (2007) 754.

162

[49] S. Srinivas and M. Kothandapani, Peristaltic transport in an asymmetric channel with heat transfer-A note, Int. Commun. Heat Mass Transfer, 34 (2008) 514.

[50] T. Hayat, M. U. Qureshi and Q. Hussain, Effect of heat transfer on the peristaltic flow of an electrically conducting fluid in a porous space, Appl. Math. Model., 33 (2009) 1862.

[51] S. Nadeem and N. S. Akbar, Influence of heat transfer on peristaltic flow of Jhonson-Segalman fluid in a non-uniform tube, Int. J. Heat Mass Transfer 36 (2009) 1050.

[52] S. Nadeem and N. S. Akbar, Effects of temperature dependent viscosity on peristaltic flow of a Jeffrey six constant fluid in a non-uniform vertical tube, Comm. Nonlinear Sci. Numer. Simul. 15 (2010) 3950.

[53] S. Nadeem, N. S. Akbar, N. Bibi and S. Ashiq, Influence of heat and mass transfer on peristaltic flow of a third order fluid in a diverging tube, Comm. Nonlinear Sci. Numer. Simul. 15 (2010) 2916.

[54] Kh. S. Mekheimer, S. Z. A. Husseny and Y. Abd Elmaboud, Effects of heat transfer and space porosity on peristaltic flow in a vertical asymmetric channel, Numer. Methods Partial Diff. Eqs., 26 (2010) 747.

[55] C. Vasudev, U. R. Rao, M. V. S. Reddy and G. P. Rao, Effect of heat transfer on peristaltic transport of a Newtonian fluid through a porous medium in an asymmetric vertical channel, Europ. J. Scientific Research, 44 (2010) 79.

[56] A. M. Sobh, S. S. Al Azab and H. H. Madi, Heat transfer in peristaltic flow of viscoelastic fluid in an asymmetric channel, Appl. Math. Sci., 4 (2010) 1583.

[57] T. Hayat, Q. Hussain, M. U. Qureshi, N. Ali and A. A. Hendi, Influence of slip condition on the peristaltic transport in an asymmetric channel with heat transfer: An exact solution, Int. J. Numer. Meth. Fluids, 67 (2011) 1944.

[58] S. Srinivas, R. Gayathri and M. Kothandapani, Mixed convective heat and mass transfer in an asymmetric channel with peristalsis, Comm. Nonlinear Sci. Numer. Simul., 16 (2011) 1845.

[59] S. Srinivas, R. Muthuraj and J. Sakina, A note on the influence of heat and mass transfer on a peristaltic flow of a viscous fluid in a vertical asymmetric channel with wall slip, Chem. Ind. Chem. Eng. Quart., 18 (2012) 483.

[60] T. Hayat, S. Hina, and A. A. Hendi, Heat and mass transfer effects on peristaltic flow of an Oldroyd-B fluid in a channel with compliant walls, Heat Trans. Asian Res., 41 (2012) 63.

[61] T. Hayat, S. Hina and A. A. Hendi, Slip effects on peristaltic transport of a Maxwell fluid with heat and mass transfer, J. Mech. Med. Biol. 12 (2012) DOI:10.1142/S0219519412004375.

[62] D. Tripathi, A mathematical model for swallowing of food bolus through the esophagus under the influence of heat transfer, Int. J. Thermal Sci., 51 (2012) 91.

[63] R. Ellahi, M. Mubashir Bhatti and K. Vafai, Effects of heat and mass transfer on peristaltic flow in a non-uniform rectangular duct, Int. J. Heat and Mass Trans., 71 (2014) 706.

[64] S. U. S. Choi, Enhancing thermal conductivity of fluids with nano particles, Developments and Applications of Non-Newtonian Flows, ASME, 66 (1995) 99.

[65] K. Khanafer, K. Vafai, M. Lightstone, Buoyancy-driven heat transfer enhancement in a two-dimensional enclosure utilizing nanofluids, Int. J. Heat and Mass Transfer., 46 (2003) 3639.

[66] J. Buongiorno, Convective transport in nanofluids, ASME J. Heat transfer, 128(2006)240.

[67] K. Sadik and A. Pramuanjaroenkij, Review of convective heat transfer enhancement with nanofluids, Int. J. Heat and Mass Trans., 52 (2009) 3187.

[68] S. Nadeem and N. S. Akbar, Endoscopic effects on peristaltic flow of a nanofluid, Commun. Theor. Phys., 56 (2011) 761.

[69] Adi T. Utomoa, Heiko Pothb, Phillip T. Robbinsa, Andrzej W. Paceka, Experimental and theoretical studies of thermal conductivity, viscosity and heat transfer coefficient of titania and alumina nano fluids, Int. J. Heat and Mass Trans., 55 (2012) 777.

[70] M. Mustafa, S. Hina, T. Hayat and A. Alsaedi, Influence of wall properties on the peristaltic flow of a nanofluid: Analytical and numerical solutions, Int. J. Heat and Mass Trans., 55 (2012) 4871.

[71] R. Ellahi, S. Aziz and A. Zeeshan, Non-Newtonian nanofluid flow through a porous medium between two coaxial cylinders with heat transfer and variable viscosity, J. Porous Media, 16 (2013) 205.

[72] M. Mustafa, S. Hina, T. Hayat and A. Alsaedi, Slip effects on the peristaltic motion of nanofluid in a channel with wall properties, ASME J. Heat Transfer, 135 (2013) ID 041701 (7 pages).

[73] Kh.S. Mekheimer, Peristaltic flow of blood under effect of a magnetic field in a non-uniform channels, Appl. Math. Comp., 153 (2004) 763.

[74] A. Yıldırım and S. A. Sezer, Effects of partial slip on the peristaltic flow of a MHD Newtonian fluid in an asymmetric channel, Math. Comput. Model, 52 (2010) 618.

[75] T. Hayat and S. Hina, The influence of wall properties on the MHD peristaltic flow of a Maxwell fluid with heat and mass transfer, Nonlinear Anal. RWA, 11 (2010) 3155.

[76] T. Hayat, Y. Khan, N. Ali and Kh.S. Mekheimer, Effect of an induced magnetic field on the peristaltic flow of a third order fluid, Numer. Meth. Partial Diff. Eqs., 26 (2010) 345-360.

[77] S. Srinivas and R. Muthuraj, Effects of chemical reaction and space porosity on MHD mixed convective flow in a vertical asymmetric channel with peristalsis, Math. Comput. Model, 54 (2011) 1213.

[78] Y. Abd elmaboud, Influence of induced magnetic field on peristaltic flow in an annulus, Commun. Nonlinear Sci. Numer. Simulat., 17 (2012) 685.

[79] K. Vajravelu, S. Sreenadh and R. Saravana, Combined influence of velocity slip, temperature and concentration jump conditions on MHD peristaltic transport of a Carreau fluid in a non-uniform channel, Appl. Math. Comp., 225 (2013) 656.

[80] L. K. Saha, M. A. Hossain and R. S. R. Gorla, Effect of Hall current on the MHD laminar natural convection flow from a vertical permeable flat plate with uniform surface temperature, Int. J. Therm. Sci., 46 (2007) 790.

[81] T. Hayat, N. Ali and S. Asghar, Hall effects on peristaltic flow of a Maxwell fluid in a porous medium, Phys. Lett. A, 363 (2007) 397.

[82] T. Hayat and M. Nawaz, Hall and ion-slip effects on three-dimensional flow of a second grade fluid, Int. J. Numer. Meth. Fluids, 66 (2011) 183.

[83] N. S. Gad, Effect of Hall currents on interaction of pulsatile and peristaltic transport induced flows of a particle–fluid suspension, Appl. Math. Comp., 27 (2011) 4313.

[84] Kh. Nowar, E. Abo-Eldahab and E. Barakat, peristaltic pumping of Johnson-Segalman fluid in an asymmetric channel under the effect of Hall and ion-slip currents, J. Appl. Comp. Math., 1 (2012) 1.

[85] S. R. El Koumy, El S. I. Barakat and S. I. Abdelsalam, Hall and porous boundaries effects on peristaltic transport through porous medium of a Maxwell Model, Trans. Porous Med., 94 (2012) 643.